SYNTHESIS AND CHARACTERIZATION OF CADMIUM SELENIDE (CdSe) AND LEAD SULPHUR SELENIDE ($PbS_{1-x}Se_x$) THIN FILMS BY CHEMICAL BATH DEPOSITION METHOD

BY

Fekadu Gashaw Hone (Hons.) MSc.

A Thesis submitted to the Department of Physics, Kwame Nkrumah University of Science and Technology in partial fulfillment of the requirements for the degree

of

DOCTOR OF PHILOSOPHY

(Solid State Physics)

College of Science

January 2015

DECLARATION

I hereby declare that this submission is my own work towards the PhD and that, to the best of my knowledge, it contains no material previously published by another person nor material which has been accepted for the award of any other degree of the University, except where due acknowledgment has been made in the text.

Fekadu Gashaw Hone	……	……
Student	Signature	Date

Certified by:

Prof. Robert Kwame Nkum	……	……
Supervisor	Signature	Date
Dr. Francis Kofi Ampong	……	……
Supervisor	Signature	Date
Prof. Francis Boakye	……	……
Supervisor	Signature	Date
Prof. S. K. Danuor	……	……...
Head of Department	Signature	Date

ACKNOWLEDGEMENT

First and foremost, thank you God! The challenge was too much during the course of this work but you gave me the strength, courage and patience. I will forever be thankful. I would like to express my deepest gratitude to my supervisor, Prof. Francis Boakye. His guidance, support and valuable suggestions over the past years were helpful. Especially I am always thankful for your guidance during my thesis write up. I also wish to thank my research supervisor Prof. Robert Nkum whose door was always open to my academic and office related issues. Dr. Kofi Ampong`s valuable advice and patience during my study made it possible for me to complete this work. I would like to thank Prof S. K. Danuor, being the head of the department; he was kind enough to provide me all the facilities available at the department. I acknowledge with thanks Intra-ACP program which gave me a partial scholarship for this work. I am also thankful to host institution Intra-ACP program coordinators.

I express my appreciation to the department of Physics, University of Ghana for allowing me to carry out XRD measurements. I wish to thank Dr. Martine and Elena from University of Ghana who helped me during my XRD measurement. I am grateful to my friend Girma Hailu from Uppsal University for sparing his valuable time in taking EDX and SEM measurements of my samples; without his support and encouragements I could not have finished this work. I am also thankful to Dr. Mesfin Kebede from South Africa for his willingness and valuable time to taking SEM and EDX measurements for some of my samples. I am thankful to all teaching and technical staffs of Department of Physics of KNUST for their help and cooperation. I would also like to present my sincere thanks to my laboratory colleagues Tizazu Abza, Isaac Nkrumah, Mark Paal, Charles and Bernice for their kind friendship, help and useful cooperation. I would

like to thank all Ethiopian students in KNUST for their support in various aspects including academic research and merrier life inside and outside campus. Yibelital I thank you for everything you did for me.

I thank every member of my family for being always a source of inspiration. Finally, I am indebted to my wife and life partner, Firhiwot Tilahun, for her unconditional love, patience and encouragement that made possible my whole dedication toward the present study. Very special thanks to W/r Getenesh Gebire and the whole family, I will never forget your devotion for taking care of my kids in the absence of me and my wife. My lovely children, Edom and Leul have given me happiness whatever, wherever and whenever!!

ABSTRACT

Cadmium selenide (CdSe) and lead sulphur selenide ($PbS_{1-x}Se_x$) thin films have been successfully deposited by chemical bath deposition technique (CBD). The films were characterized by powder X-ray diffraction, scanning electron microscopy, energy dispersive X-ray analysis and optical absorption spectrophotometer. Cadmium selenide thin films were deposited from chemical bath containing cadmium acetate, tartaric acid, ammonia and sodium selenosulphate, at a bath temperature of 85 ^{0}C. The films were annealed in air for 1 hour at 350 ^{0}C. The as-deposited films were redishe while the annealed films were dark grey in color. The films were smooth, well adherent and specularly reflective. For the as-deposited films, the XRD analysis revealed a uniform cubic phase of CdSe nanocrystalline thin film with preferred orientation along the (111) plane. The SEM micrographs showed that the film surface was composed of spherically shaped grains. The elemental analyses of the films confirmed that the atomic percentage of Cd:Se is very close to one, indicating that the synthesized thin films were in the desired stoichiometric ratio. The effects of annealing on structural, morphological and optical properties of CdSe thin films were studied. From the XRD analysis it was observed that the annealed CdSe thin film consisted mainly of the cubic CdSe phase. After annealing a new peak appeared at 67.1^0 and a slight shift in peak positions towards smaller 2θ angles was observed. The average crystallite sizes were found to increase from 40 Å to 45 Å whereas dislocation density and microstrain decreased after annealing. Texture coefficent result revealed that the crystallites were oriented along the (111) plane for both as-deposited and annealed CdSe thin films. Optical studies revealed that the as-deposited sample have direct band transition whose value decreased from 1.86 eV to 1.74 eV after annealing. The variation of optical band gap was due to the change in the crystallite size. $PbS_{1-x}Se_x$ nanocrystalline thin films were

synthesized by CBD technique for the entire compositional range of ($0 \leq x \leq 1$). The thin films were deposited from baths containing lead acetate, thiourea, sodium hydroxide, ammonia and sodium selenosulphate, at a bath temperature of 90 ^{0}C. The XRD analyses revealed that all the $PbS_{1-x}Se_x$ thin films were polycrystalline in nature with the diffraction peaks indexed to the face centered cubic structure. The XRD analyses showed that addition of selenium (Se) in PbS shifted the peak positions slightly towards smaller 2θ angles and modified the peaks intensity. The XRD studies also showed that varying the concentration of Se in $PbS_{1-x}Se_x$ thin films strongly influenced the preferred orientations of the crystallites as well as structural parameters such as average crystallite size, d-spacing and crystal lattice parameter. The average crystallite size was found to increase with Se concentration. The lattice parameter a (Å) and inter planer distance d (Å) increased linearly with the gradual addition of Se in PbS_{1-x} Se_x thin films, this result is consistent with Vegard's law and supports the formation of a continuous series of solid solution. The EDX analyses confirmed that the films were consistent with the formation of binary and ternary compounds of $PbS_{1-x}Se_x$ on silica glass slide. In addition, it was observed that the molar percentages of selenium in the as-deposited $PbS_{1-x}Se_x$ thin films had a good correlation with the calculated molar percentages of Se in $PbS_{1-x}Se_x$ chemical baths. The SEM micrographs of all the films showed uniform surface morphology over the entire glass substrate without defects like cracks, peeling or pinholes. The films showed a gradual increase in absorbance as Se concentration increases. The optical band gap, calculated from optical absorption of ternary $PbS_{1-x}Se_x$ samples decreased almost linearly from 1.32 eV to 1.08 eV as Se concentration increased. This linear variation with Se composition revealed that the optical band gap of the $PbS_{1-x}Se_x$ thin films can be controlled in an optimal region for photovoltaic absorbance as well as for other optoelectronic devices.

Table of Contents

APPENDIX

LIST OF TABLES

LIST OF FIGURES

ACRONYMS AND SYMBOLS

A	Absorbance
Å	Angstrom
α	Absorbance coefficients
CB	Conduction Band
CBD	Chemical Bath Deposition
Cd	Cadmium
CdSe	Cadmium Selenide
$CdS_{1-x}Se_x$	Cadmium Sulpher Selenide
CdTe	Cadmium Telluried
$Cd_{1-x}Pb_xS$	Cadmium Lead Sulphied
$Cd_{1-x}Pb_xSe$	Cadmium Lead Selenide
$Cd_{1-x}Zn_xS$	Cdmium Zinc Sulphied
$Cd_{1-x}Zn_xSe$	Cadmium Zinc Selenide
CdS	Cadmium Sulphied
CGS	Copper Gallium Selenide
CIGS	Copper Indium Gallium Selenide
CVD	Chemical Vapor Deposition
DOS	Density of States
EDX	Energy Dispersive X-ray analysis
Eg	Optical band gap
eV	Electron Volt
fcc	Face centered cubic
FTIR	Fourier Transformed Infrared spectroscopy
FWHM	Full Width at Half Maximum
h	Planck constant
hr	hour
I	Intensity
IR	Infrared
JCPDS	Joint Committee for Powder Diffraction Standards
k	Wave vector, Extinction coefficient

kV	Kilovolt
Ksp	Solubility Product
λ	Wavelength
M	Molar concentration
MBE	Molecular Beam Epitaxy
min	Minuet
Na_2SeSO_3	Sodium selenosulphite
nm	Nanometer
NH_3	Ammonia
NIR	Near Infrared
Pb	Lead
PbS	Lead Sulphied
PbSe	Lead Selenide
$PbS_{1-x}Se_x$	Lead Sulphur Selenide
PCEs	Power Conversion Efficiencies
PL	Photoluminescence
PV	Photovoltaic
QDs	Quantum Dots
S	Sulphur
Se	Selenium
Si	Silicon
SEM	Scanning Electron Microscopy
T	Transmittance
TC	Texture coefficient
θ	Theta
UV	Ultraviolet
ν	Photon frequency
μm	Micrometer
VB	Valence band
VIS	Visible Spectrum
XRD	X-ray Diffraction

Chapter 1

1. INTRODUCTION

The provision of clean and sustainable energy supplies to satisfy our ever growing needs is one of the most critical challenges currently facing mankind. It is becoming increasingly clear that the traditional ways in which we have satisfied our large and growing appetite for energy to heat our homes, power our industries and fuel our transportation systems are no longer sustainable (Randolph *et al.*, 2008). At the present time our primary energy sources are dominated by non-renewable fossil fuels, with nearly 80% of global energy demand supplied from crude oil, natural gas, and coal (Fanchi, 2004; Randolph and Masters, 2008). Also, energy production by burning fuel produces hazardous pollutants, such as oxides of sulfur and nitrogen, hydrocarbons and most significantly, carbon monoxide. Thus, traditional fossil energy resources are not only rapidly depleting, but also contribute to unpredictable and possibly irreversible climate changes in the near future (Trykozko, 1997). These and other factors have prompted scientists and researchers all over the world to look for alternative sources of energy.

Renewable energy sources seem to provide an optional solution to the global energy problem. Due to their sustainable nature, renewable energy technologies are capable of preserving resources, ensuring the security and diversity of the energy supply and providing energy services virtually without any environmental impact. A more sustainable pattern of energy supply and end-use for the future will inevitably lead to the need for greater utilization of renewable energy sources, such as solar, wind and biomass energy as well as geothermal energy which many people consider to be sustainable, at least for the foreseeable future (Krylova *et al.*, 2014). Many

assessments have shown that there is certainly enough primary energy available from renewable sources to supply all of our energy needs (Evans, 2007). Among renewable energy sources, solar energy is an exciting alternative to fossil fuels (Yafei *et al.*, 2012). Solar energy is the most abundant, inexhaustible and clean of all the renewable energy resources till date. The power from the sun intercepted by the earth is about 1.8×10^{11} MW, which is many times larger than the present rate of all the energy consumption (Parida *et al.*, 2011). There is no doubt that the natural energy flows that are driven by the sun represent a vast resource; sufficient both to replace the fuels and to meet the expected future increased demand for energy. Therefore, solar energy is perhaps the most popular choice in this regard. It is almost inexhaustible, non-polluting source of power, as it does not have any dangerous by-products harmful to the environment, and distributed all over the globe (Kemell *et al.*, 2005). It is for this reason that intense efforts are being made in many parts of the world to make more extensive use of solar energy to meet our growing energy needs.

Solar energy was the first energy source used by mankind. The initial use was limited to drying things and heating caused by direct contact. In modern times, solar energy has been a power source since the early 1950s, but is not widespread due to technological issues (Richard *et al.*, 1983; Sze, 1981). Given the continued dominance of fossil fuels, world CO_2 emissions are expected to increase more rapidly than the energy consumption (2.1% per year on average). In 2030, world CO_2 emissions are expected more than twice the level of 1990 (Commission, 2003). Currently, the world energy consumption is 10 terawatts (TW) per year, and by 2050, it is projected to be about 30 TW. The world will need about 20 TW of non-CO_2 energy to stabilize CO_2 in the atmosphere by mid-century (Cyrus *et al.*, 2009; Razykov *et al.*, 2011). Figure 1.1

shows the history and projections for the world marketed energy consumption from1990 to 2035. The same report also states that world GDP rises by an average of 3.2 percent per year from 2007 to 2035 which results in world energy demand increase by 49 percent, or 1.4 percent per year (Cyrus *et al.*, 2009).

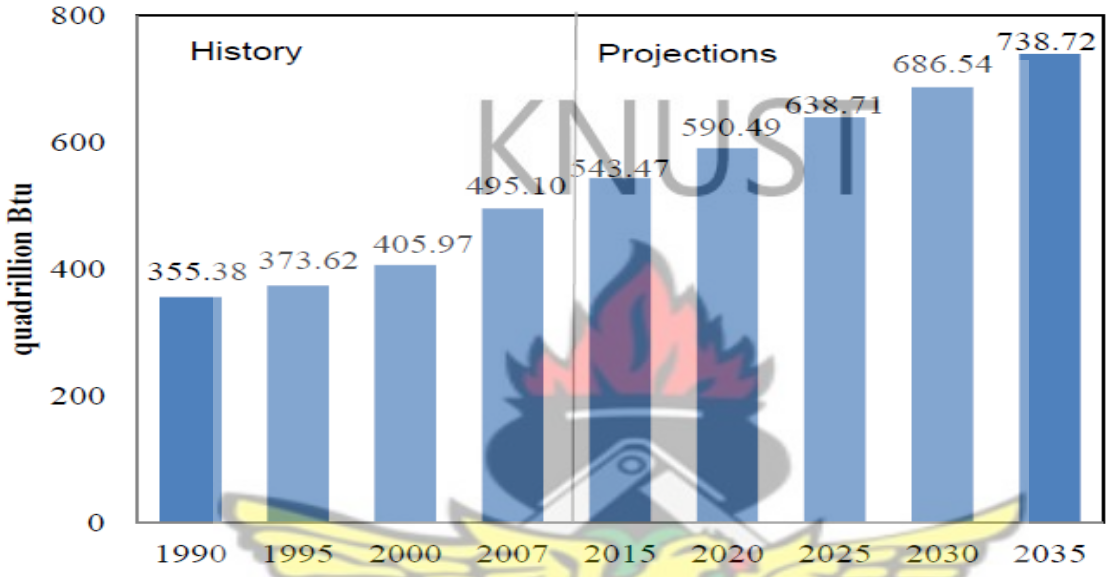

Figure 1.1: World marketed energy consumption from 1990 to 2035 (Munteha, 2011)

It is also estimated that by 2100, solar energy will account for 80% of the total energy produced around the world (Aberle, 2007; Nelson, 2007). Hence, it is not surprising a lot of solar energy related researches are being conducted all round the world.

1.1 SEMICONDUCTOR MATERIALS

Semiconductors are a group of materials either inorganic or organic compounds having electrical conductivities intermediate between metals and insulators. It is significant that the conductivity of these materials can be varied over orders of magnitude by changes in temperature, optical

excitation and impurity content. This variability of electrical properties makes the semiconductor materials natural choices for electronic device fabrications.

Two general classifications of semiconductors are elemental and compound semiconductors. The elemental semiconductor materials are found in group IV of the periodic table and the compound semiconductor materials, most of which are formed from special combinations of group III and group V elements. Semiconductors can also be formed from combinations of group II and group VI elements. The column IV semiconductors, silicon and germanium, are called elemental semiconductors because they are composed of single species of atoms.

The elemental semiconductor Ge was widely used in the early days for the development of transistors and diodes. Silicon is now used in majority of transistors, rectifiers and integrated circuits. In addition to the elemental materials, compounds formed from elements in column III and column V, as well as certain combinations from II and VI, and from IV, make up the compound semiconductors. The two-element (binary) III—V compounds such as GaP, GaAs, and InP are common in light-emitting diodes (LEDs). The three-element (ternary) compounds such as PbS_{1-x} Se_x, GaAsP and four-element (quaternary) compounds such as $In_{1-x}Ga_{1-x}As_yP_{1-y}$ can be grown to provide added flexibility in choosing material properties for specific device applications (Streetman *et al.*, 2006) (see Table-1).

One of the most important characteristics of a semiconductor, which distinguishes it from metals and insulators, is its energy band gap. This property determines among other things the wavelengths of light that can be absorbed or emitted by the semiconductor. For example, the band gap of GaAs is about 1.43 eV, which corresponds to light wavelengths in the near infrared

(Tyagi *et al.*, 2013). In contrast, GaP has a band gap of about 2.3 eV, corresponding to wavelengths in the green portion of the spectrum.

Table 1-1: Common binary and ternary semiconductors

Periodic table Group	**Binary compounds**	**Ternary compound**
II-VI	CdS, CdSe, CdTe, ZnS, ZnSe, ZnTe	$Hg_{1-x}Cd_xTe$, $Cd_{1-x}Zn_xTe$, $ZnS_{1-x}Se_x$, $Cd_{1-x}Zn_xS$, $Cd_{1-x}Zn_xSe$
III-V	GaP, GaAs, GaSb, InP, InAs, InSb	
IV-VI	PbS, PbSe, PbTe	$Pb_{1-x}Sn_xTe$, $Pb_{1-x}Sn_xSe$, $PbS_{1-x}Se_x$
IV-IV	SiC, $Si_{1-x}Ge_x$	
V-VI	Bi_2Te_3	
I-III-VI_2 or II-VI-V_2 Chalcopyrite	$AgGaS_2$, $AgGaSe_2$	$CuInS_2$, $CuInSe_2$

The electronic and optical properties of semiconductor materials are strongly affected by impurities, which may be added in precisely controlled amounts. Such impurities are used to vary the conductivities of semiconductors over wide ranges. This process of controlled addition of impurities is called doping (Streetman and Banerjee, 2006).

An organic semiconductor is an organic compound that possesses similar properties to inorganic semiconductors with hole and electron conduction layer and a band gap (Horowitz, 1990). Conduction mechanisms for organic semiconductor are mainly through tunneling. Like inorganic semiconductors, organic semiconductors can be doped in order to change its conductivity. Recently, organic semiconductors have been used as active elements in optoelectronic devices such as organic light emitting diodes (OLED), organic solar cells and organic field effect transistors (OFET). There are many advantages of using organic

semiconductors, such as easy fabrication, mechanical flexibility and low cost. Organic semiconductors offer the ability to fabricate electronic device at lower temperature and over large areas on various flexible substrates such as plastic and paper. However, inorganic semiconductors have charge carrier mobilities nearly three order of magnitude higher than those of typical organic semiconductors. As a result of this limitation, organic semiconductors are not suitable for use in electronic applications that require very high switching speeds (Mascaro *et al.*, 2001).

1.2 SEMICONDUCTOR SOLAR CELLS

Semiconductors derive their great importance from the fact that their electrical conductivity can be greatly altered via an external stimulus (voltage, photon flux, etc), making semiconductors critical parts of many different kinds of electrical circuits and optical applications. The physical phenomenon responsible for converting light to electricity, the photovoltaic effect, was first observed in 1839 by a French physicist, Edmund Becquerel (Lynn, 2010; Razykov *et al.*, 2011). Becquerel noted a voltage appeared when one of two identical electrodes in a weak conducting solution was illuminated. The PV effect was first studied in solids, such as selenium, in the 1870s. In the 1880s, selenium photovoltaic cells were built that exhibited 1% - 2% efficiency in converting light to electricity. A major step forward in solar cell technology came in the 1940s and early 1950s when a method called the Czochralski (CZ) method was developed for producing highly pure crystalline silicon. In 1954, work at Bell Telephone Laboratories resulted in a silicon photovoltaic cell with a 4% efficiency (Lynn, 2010). Bell Labs soon bettered this to a 6% and then 11% efficiency, heralding an entirely new era of power producing cells. Subsequently, a cadmium sulphide thin film solar cell was developed by Reynolds. Currently,

solar cells are used for various device configurations and employing single crystal, polycrystal and amorphous thin film structures (Hersch *et al.*, 1982; Sze, 1981). Polycrystalline thin film solar cells based on copper indium diselenide ($CuInSe_2$) and its alloys and cadmium telluride (CdTe) appear to be the most promising candidates for large scale application of photovoltaic energy conversion (Asim *et al.*, 2012).

Solar cells at present furnish the most important long duration power supply. As the worldwide energy demand increases, conventional energy resources, such as fossil fuels, will be exhausted in the not too distance future. Therefore, we must develop and use alternative energy resources, especially our only long term natural resource, the sun. Solar cell is consider a major candidate for obtaining energy from the sun, since it can provide nearly permanent power at low operating cost and is virtually free of pollution. Recently, research and development of low cost, flat panel solar cells, thin films devices, concentrator systems and many innovative concepts have increased. In the near future, the costs of small solar power modular units and solar power plants will be economically feasible for large scale use of solar energy (Colinge *et al.*, 2002; Richard and Hu, 1983).

1.3 CURRENT MARKET TRENDS FOR SOLAR CELLS

The photovoltaics (PV) industry is booming, with very high rates (30 – 40%), annually similar to that of the telecommunication and computer sectors. Also the world wide installed capacity of the solar photovoltaic power has increased from 331 MW in the year 2001 to 16.7 GW in 2010 (Razykov *et al.*, 2011). It is predicted by report on the solar photovoltaic electricity empowering the world that PV will deliver about 345 GW around 4% by 2020 and 1081 GW by 2030 (Tyagi

et al., 2013). The drivers for this industry are rising energy cost, increased subsidies by governments, energy security and environmental concerns and technology development. This explosive growth has been driven by rapidly increasing fossil fuel prices, an almost universal acceptance of the link between global warming and human activity, the growing realization of a gap between the increasing global demand for energy and the ability to supply (Aberle, 2007; Karim, 2007; Price *et al.*, 2010). The evolution of their production capacity is represented in the Figure 1.2 below. The production capacity of CdTe and CIGS solar cells is limited by the materials used for the photovoltaic cells, and high temperature processing (Stolle *et al.*, 2013) while that of dye-sensitized solar cells is limited by the materials used for electrodes. Solar photovoltaics have great promise for a low carbon future but remain expensive relative to other technologies (Cyrus *et al.*, 2009). The high cost of crystalline silicon wafers (up to 40-50% of the cost of a finished module) has led the industry to look for cheaper materials to produce solar cells. Second generation PV materials have been developed to address energy requirements and production costs. Alternative manufacturing techniques such as vapour deposition or electroplating are advantageous since they reduce high temperature processing significantly.

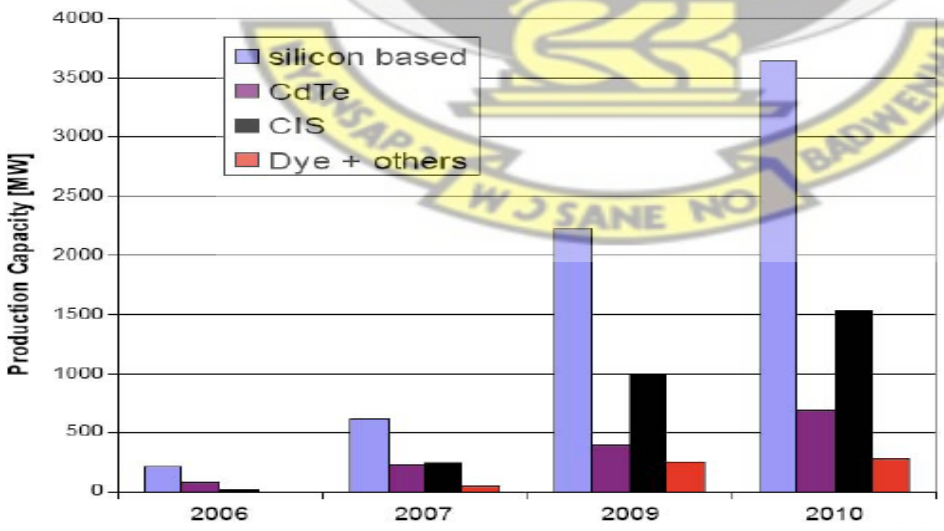

Figure 1.2: Production capacity of different generation of solar cells (Dragoman *et al.*, 2010)

The most successful second generation materials are amorphous and micro-morphous silicon, cadmium telluride (CdTe) and the chalcopyrite family $Cu(In_x,Ga_{1-x})(S_y,Se_{1-y})_2$. These materials are applied as a thin film onto a supporting substrate such as glass, ceramics, stainless steel, or even polyimide thus reducing material costs and final weight. Additionally, the pay-back time of Si-based solar cells is on the scale of 2-3 years, and therefore, 10% of the expected lifetime of a Si-solar module is lost (Araoz, 2009). Thin film solar cells are less demanding and have the potential to achieve payback times of one year (Johnston, 2012; Knapp *et al.*, 2000).

Recently research and development efforts shifted gradually towards two other polycrystalline thin film material systems: copper indium diselenide ($CuInSe_2$) and cadmium telluride (CdTe) based solar cells. During the past twenty years, these research and development efforts resulted in conversion efficiency improvements from 6% to 17% for $CuInSe_2$ based and from 8% to 16% for CdTe based small area laboratory devices. As a result, these materials systems are being considered seriously as the basis of PV module technologies for terrestrial power generation (Eser *et al.*, 1997). Greatly increased penetration of photovoltaics into global energy markets requires an expansion in attention from designs of high performance to those that can deliver significantly lower cost per kilowatt-hour (Cyrus *et al.*, 2009).

Wafer based silicon solar cells is still the main technology and had around 80% market shares in 2009, but thin film solar cells are continuously increasing their share since 2005. Back then, production of thin film solar modules reached for the first time more than 100 MW per annum. Since then, the Compound Annual Growth Rate (CAGR) of thin film solar module production was even beyond that of the overall industry, increasing the market share of thin film products

from 6% in 2005 to about 16% in 2008 and 16% – 34% in 2012 (Jager-Waldau, 2011; Price and Margolis, 2010) see Figure 1.3.

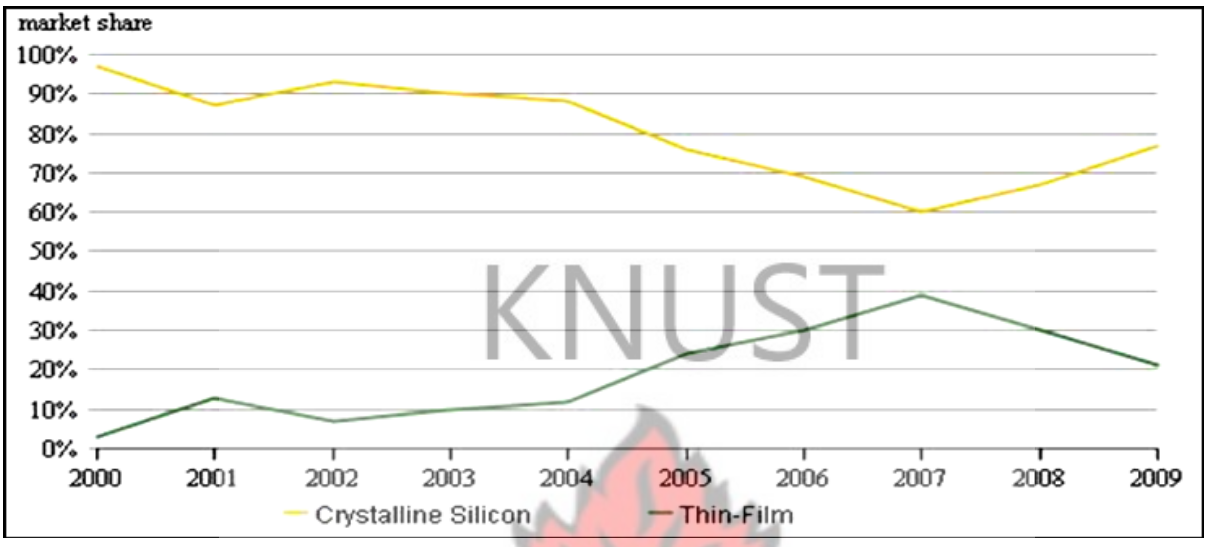

Figure 1.3: Market share change of crystalline silicon and thin film solar cells (Munteha, 2011)

Concentrator solar cells have also started to increase their market share. Although crystalline Silicon, CdTe, CIGS and concentrated solar cell market is growing steadily, there are still fundamental problems for the current technologies which prevents them contributing world energy production in large scale (Asim *et al.*, 2012).

1.4 CADMIUM SELENIDE AND LEAD SULPHUR SELENIDE THIN FILMS

Within the last decade, there has been much interest in the growth and characterization of binary and ternary semiconductor compounds. The compound cadmium selenide (CdSe) is one of the elements of the groups II–VI having wide range of applications. The knowledge of various properties of CdSe films has widely contributed to the phenomenal growth of their applications in scientific, technological and industrial applications. Usually CdSe is an n-type material and

they are of interest due to their applications as photoconductors, solar cells, optoelectronic and microelectronic devices (Moholkar *et al.*, 2006; Velumani *et al.*, 2003). The bulk CdSe has an energy band gap of 1.74 eV but the band gap can vary to 2.44 eV due to size quantization of CdSe nanoparticles (Nair *et al.*, 1998). CdSe is a uniaxial crystalline material and there are three main documented structures of CdSe, a hexagonal wurtzite structure, a cubic zinc blende structure known as sphalerite and the rock salt. Only the wurtzite and the sphalerite exist at atmospheric pressures. The wurtzite is the most stable form since the sphalerite also converts to wurtzite at high temperatures (Zakharov *et al.*, 1995). Although most researchers have reported hexagonal structure with the c axis oriented normal to the substrate surface (Velumania *et al.*, 1998) there are several studies indicating the cubic structure for the CdSe polycrystalline thin films.

The ternary semiconductor thin films are considered to be an important technological material due to their prime applications in various optical and electronic devices. The IV-VI semiconductors present one of the rare naturally occurring semiconductors hence the name "lead salts" for the IV-VI semiconductors (Al-Fawade *et al.*, 2013). The ternary lead chalcogenide compound, lead sulphur selenide thin film is considered as one of the important semiconductors with a narrow band gap showing potential applications in various optoelectronic devices. In the case of $PbS_{1-x}Se_x$, the crystal structure and the band gap can be tailored by changing the concentration of S and Se, so that the visible solar energy can be suitably harnessed for maximum conversion to electrical energy. $PbS_{1-x}Se_x$ alloys as bulks and films at room temperature appears as polycrystalline of face center cubic (Nasir *et al.*, 2013).

In recent years, there has been considerable interest in lead chalcogenides and their alloys due to their demanding applications as detectors of infrared radiation, photoresistors, lasers, solar cells, optoelectronic devices, thermoelectric devices, and more recently, as infrared emitters and solar control coatings (Sushil *et al.*, 2003).

1.5 RESEARCH OBJECTIVES

Due to wide range of applications the nanocrystalline chalcogenide thin films gains attention among researchers. For the present work binary and ternary nanocrystalline CdSe and $PbS_{1-x}Se_x$ thin films have been synthesized by chemical bath deposition method for PV application. The reason for selecting CBD method as compared to other methods; CBD is uniquely suited for deposition of a uniform film over large substrates of complex geometries. Furthermore, film formation is truly a deposition of compound rather than a co-deposition of separate elements. The chemical bath deposition is inexpensive technology process at low deposition temperatures.

Silicon based solar cell has several disadvantages for solar cell applications with high production cost and its band gap is not in the optimum ranges of photovoltaic materials based on theoretical conversion efficiency. Although organic semiconductor materials are very much photosensitive but their shorter diffusion length of minority carrier, low optical energy band gap and big molecular size are the problems to make high efficient solar cells. Inorganic materials maybe best used in solar application. Inorganic CdSe and $PbS_{1-x}Se_x$ thin films which are the materials selected for the present work, possess several exceptional material properties, which make them potentially well suited for solar cell applications. Their band gaps can be easily tuned around the optimum for solar energy conversion. Both films have high absorption coefficient and

photosensitive properties, which are suitable for solar cells. Keeping this in mind, the main objectives of this research work are:

I. **To synthesize CdSe and $PbS_{1-x}Se_x$ thin films using chemical bath deposition.**

There are various factors that influence the deposition process in chemical bath deposition technique. However, deposition of good quality thin film for various applications is possible by controlling the pH of the solution, bath temperature and reagent concentrations which can affect physical and compositional properties of the thin film. If those parameters are not carefully selected, they can produce wrong results. Thus, it is important to carry out several investigations to get the desired optimum conditions for the synthesis of both CdSe and $PbS_{1-x}Se_x$ thin films.

II. **To investigate structural, elemental, morphological and optical properties of CdSe and $PbS_{1-x}Se_x$ thin films.**

The internal structure and properties of thin films are very sensitive to the deposition parameters. Each new set of deposition parameters could affect the micro-structural characteristics such as crystal structure, morphology etc. The purpose of characterization is to investigate the relationship between the structure of materials at atomic or molecular scales and their macroscopic properties. This is very important for device applications. In the present study, characterization techniques such as, X-ray diffractometer, UV/Visible spectrophotometer, Scanning electron microscope and Energy dispersive X-ray analysis will be used to investigate the optical, elemental, structural and morphological properties of the samples.

III. To study the effect of annealing on structural, morphological and optical properties of nanocrystalline CdSe thin film deposited under condition I.

Annealing leads to significant changes in structural, electrical and optical properties of chemically deposited semiconductor thin films. Annealing semiconductor thin films will enhance their characteristics for different applications, including solar cell study. This is because annealing is assumed to enhance grain size and eliminate grain boundaries between them. In the present work well controlled rate of heating and cooling will be applied to anneal CdSe thin film to investigate the effect of annealing on its structural, morphological and optical properties.

A lot of research work has been carried on the synthesis and characterization of CdSe thin films using the CBD technique. In most of these reports, the deposition was carried out using complexing agents such as triethylamine, sodium hydroxide, ammonia and trisodium citrate. There are very few available reports on the use of tartaric acid as a complexing agent for the deposition of CBD CdSe thin films. In this thesis, the chemical bath deposition method used to synthesis CdSe thin films uses tartaric acid as a complexing agent, at a bath temperature of 85 ^{0}C, a pH of 9.5 and a deposition time of ninety minutes. To the best of my knowledge, this is also the first time cadmium acetate is being used as the source of cadmium ions in combination with tartaric acid as complexing agent for the chemical bath deposition of CdSe thin films.

The second compound, $PbS_{1-x}Se_x$ thin films have been synthesized using physical deposition techniques. There are very few reports on the deposition of this ternary material using CBD technique. In this work, reports on the synthesis and characterization of $PbS_{1-x}Se_x$, thin films

deposited by the CBD technique are well established. To the best of my knowledge, the deposition conditions such as, the concentrations of precursors and combination of reactants, bath temperature, and pH of the bath solution for the synthesis of ternary $PbS_{1-x}Se_x$ thin films is being used for the first time in this work.

1.6 JUSTIFICATION OF THE RESEARCH

The rapid growth of the world economy as well as the Earth's population puts a strict requirement toward the new way and methods for inexpensive and environmental friendly energy generation. Renewable energy sources, such as solar energy have attracted significant amount of attention (Krylova *et al.*, 2014). Current trends suggest that solar energy will play an important role in future energy production (Kaelin *et al*., 2004). Every day, the sun shines a huge amount of energy which is generated through a process of nuclear fusion. Even the sun radiates more energy in one second than people have practiced since the beginning of time. It has been noted that the technical potential of solar energy all over the world is many times larger than the current total primary energy demanded (Abdin *et al.*, 2013).

Photovoltaic (PV) devices convert sunlight directly to electricity. Since solar energy is plentiful and freely available, PV electricity has obvious economic, environmental and societal benefits, yet its high cost compared to fossil fuels has limited its use. Cheaper and more efficient PV devices are required (Stolle *et al.*, 2013). Silicon has been and remains the traditional solar cell material of choice. Although silicon is a highly abundant material, it requires an energy intensive process to purify and crystallize. Furthermore, installations of silicon cells require heavy glass

protection plates, which reduce residential applications (Udai *et al.*, 2010). Recently, commercial interest is beginning to shift towards thin film solar cells (Graham-Rowe, 2007). Thin film solar cells are basically thin layers of semiconductor materials applied to a solid backing material. Thin films greatly reduce the amount of semiconductor material required for each cell when compared to silicon wafers and hence lowers the cost of production of photovoltaic cells (Parida *et al.*, 2011). One approach to low cost of PV electricity is to deposit the light absorbing semiconductor layer using cheaper deposition techniques like chemical bath deposition (Parida *et al.*, 2011). Thin film semiconductor compounds, especially CdSe, lead chalcogenide and their alloys have drawn a lot of attention due to their technological importance and future prospects in various electronic and optoelectronic devices (Alvi *et al.*, 2013). All solar cells require a light absorbing material which is present within the cell structure to absorb/ harvest photons and generate free electrons via the photovoltaic effect. CdSe and PbS_{1-x} Se_x are the most promising semiconductors for the absorber layer of thin film solar cells.

Narrow band gap semiconductors are of interest for photovoltaic solar energy conversion as they can absorb the "IR tail" of the solar spectrum, which is not absorbed by commonly used PV materials. The use of such absorbers in semiconductor sensitized solar cells allows the integration of low cost device configurations and broad spectral response, which may also be utilized in IR and Near-IR (NIR) (Mohamed, 2014). Lead chalcogenides and their ternary compounds have band gaps that are too low, but the large Bohr radius of excitons in PbSe, PbS and ternary $PbS_{1-x}Se_x$ compounds make them strongly quantum confined in crystallites. The ability to tune the optical properties of $PbS_{1-x}Se_x$ nanocrystals by varying Se /S concentration is especially useful in device constructions requiring semiconductors with a range of band gaps.

This possibility for optical band gap variation in $PbS_{1-x}Se_x$ thin films presents the opportunity for the design of solar cells absorber (Barrios-Salgado *et al.*, 2011).

The key condition for high power conversion efficiency is that the photoactive (absorber) layer should have a narrow band gap (around 1–2 eV) to absorb photons with a wide range of energies, most especially, in that portion of the solar irradiance with high intensity (Calnan, 2014). The optical band gap of $PbS_{1-x}Se_x$ thin films can be control in an optimal region for photovoltaic application. Such kind of fine tunable band gap properties of ternary $PbS_{1-x}Se_x$ thin films make them appropriate material for solar cell absorber. The low band gap values exhibited by CdSe nanocrystal thin film together with high absorbance in the VIS region also make the film ideal for use as absorber material for solar cell application.

1.7 STRUCTURE OF THE THESIS

The thesis is structured in seven chapters. The first chapter deals with a general introduction to solar cells. It starts with current energy crisis and suggests an optional solution to the global energy problem. Moreover, brief histories of semiconductor solar cells are also discussed. Later, common physical properties and applications of CdSe and $PbS_{1-x}Se_x$ thin films are explained. The reason for characterization and annealing also mentioned in this chapter. The chapter ends by stating objectives of the present work, justification of the present study and describes how the thesis is organized.

The second chapter introduces thin film materials and their different deposition techniques. Historical development and basic principles of the chemical bath deposition technique is explained in some detail, which is followed by discussing important conditions for film

formation and various factors which affect chemical bath deposition technique. The crystal structure of CdSe and $PbS_{1-x}Se_x$ semiconductor thin films are also presented, the chapter ends by presenting an exhaustive review on CdSe thin film deposited by chemical bath deposition method and $PbS_{1-x}Se_x$ thin films deposited by chemical and physical deposition techniques.

The third chapter mainly deals with physics of semiconductor theories which are relevant to the present work. The basic theories of different electron models and the concept of allowed and forbidden energy bands in a single solid crystal are discussed in some detail. Finally size quantization of CdSe and PbSe compounds are presented. Characterizations of thin films are discussed in the fourth chapter.

The fifth chapter deals with the synthesis, deposition and characterization of cadmium selenide thin films by chemical bath deposition method. The effects of annealing on the structural, morphological and optical parameters of CdSe thin films are also discussed. Data obtained from analytical techniques are also presented in graphical format and explained.

The sixth chapter explains the details of preparation and characterization of ternary $PbS_{1-x}Se_x$ thin films. Data obtained from analytical techniques such as XRD, SEM, EDX and UV/VIS spectrophotometer are presented in graphical format and discussed. General conclusions and suggestion for future work are given in chapter seven.

Chapter 2

2. LITERATURE REVIEW

This chapter introduces the general aspects of thin films and some selected physical and chemical deposition techniques, followed by discussing and reviewing historical developments of the chemical bath deposition technique. The basic principle of chemical bath deposition and concept of solubility product are also discussed. The structural and physical properties of (Cd, Pb) (S, Se) chalcogenide thin films are also presented. In addition, a review of CdSe and $PbS_{1-x}Se_x$ semiconductor thin films are presented in some detail.

2.1 THIN FILM MATERIALS

The definition given by Chopra *et al.* provides a good starting point and also yields a criterion to discriminate the term 'thin film' from 'thick film' (Poortmans *et al.*, 2006). They define a thin film as a material created by the random nucleation and growth processes of individually condensing / reacting atomic / ionic / molecular species on a substrate. The structural, chemical, metallurgical and physical properties of such materials are strongly dependent on a number of deposition parameters and thickness. Thin films encompass a considerable thickness range, varying from few nanometers to tens of micrometers and thus are best defined in terms of 'birth processes' rather than thickness. The atomistic random nucleation and growth processes give new exotic properties to thin film materials (Paulson *et al.*, 2004). These properties can be controlled and reproduced by precisely modulating a range of deposition parameters (Chopra, 1969). The thin film is a traditional well-established material technology. However, thin film technology is still being developed on a daily basis since it is a key in the twenty first century

development of new materials such as nanometer materials and/or a man-made super lattices (Wasa *et al.*, 2004).

Thin film studies have directly or indirectly advanced many new areas of research in solid state physics and chemistry which are based on phenomena uniquely characteristic of the thickness, geometry, and structure of the film (West, 2003).

Thin films have very interesting properties that are quite different from those of the bulk materials which they are made of. As the film becomes thinner, the surface properties become more important than the bulk. The other cause of interest is the miniaturization of elements such as electronic resistors, thin film transistors and capacitors. This is because of the fact that their properties depend on a number of interrelated parameters and also the deposition technique. The thin films are characterized by the thickness, crystalline orientation and multilayer aspects. Electronic semiconductor devices and optical coating are the main applications benefiting from thin films constrictions (Nain *et al.*, 2010). The following important steps are expected in the formation of thin films:

i. The formation of thin films from any deposition techniques starts with a random nucleation process followed by further nucleation and growth stages.

ii. The concept of nucleation in solution is that the clusters of molecules formed undergo rapid decomposition and particles combine to grow up to a certain thickness of the film.

iii. Depending upon deposition conditions such as bath temperature, stirring rate, pH, solution concentration etc the film growth can take place by ion-by-ion condensation of materials or by adsorption of colloidal particles from the solution on the substrate

iv. The characterstics of the thin films such as film structure, defects and stress depends on the deposition conditions at nucleation stage.

v. The deposition condition is also responsible for the crystal phase and crystal orientation of the films (Pawar *et al.,* 2011; Sakharam *et al.,* 2000).

The growth process thus may be summarized as consisting of a statistical process of nucleation, surface-diffusion controlled growth of the three-dimensional nuclei and formation of a network structure and its subsequent filling to give a continuous film. Depending on the thermodynamic parameters of the deposit and the substrate surface, the initial nucleation and growth stages may be described as *(a)* island type, called Volmer-Weber type, *(b)* layer type, called Frank-van der Merwe type, and *(c)* mixed type, called Stranski-Krastanov type. This is illustrated in Figure 2.1.

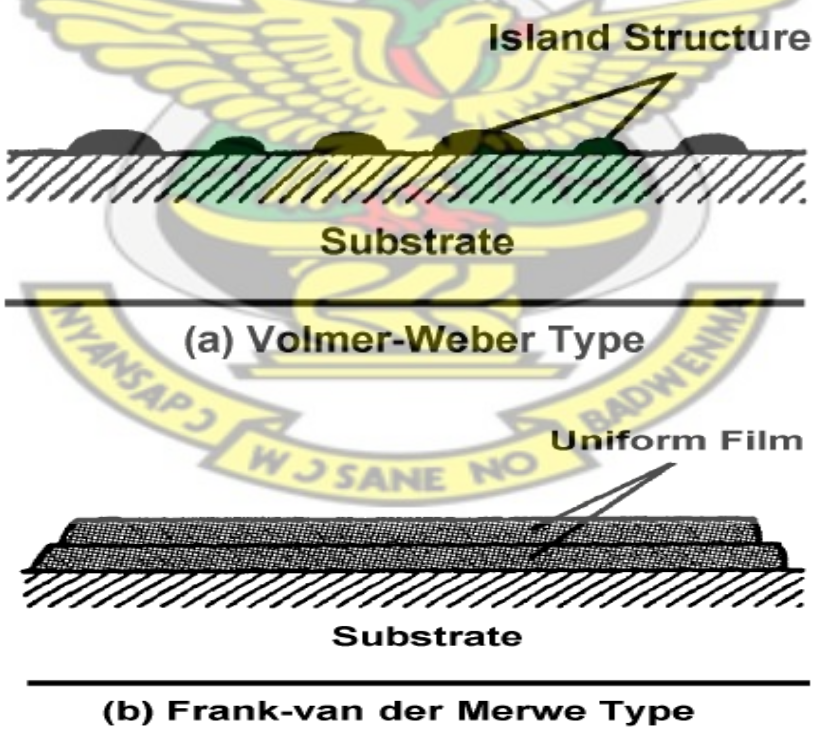

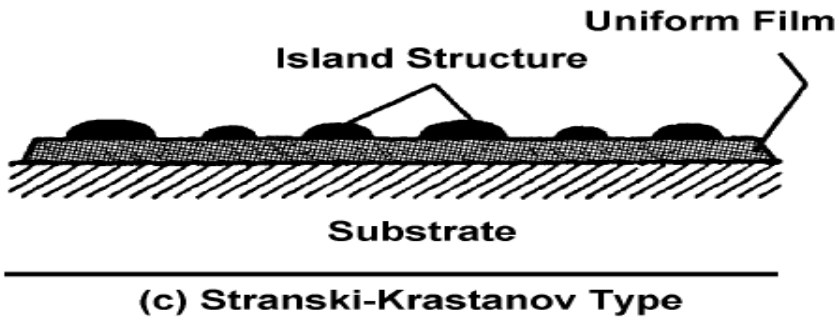

Figure 2.1: Three modes of thin film growth processes (Wasa *et al.*, 2004)

In almost all practical cases, the growth takes place by island formation (Wasa *et al.*, 2004). The growth process and nucleation of thin film will be discussed in detail in the next sections. The structural and physical properties of thin films depend on the deposition processes and the thin film solar cells have different configurations: *p-n* junctions, heterojunctions or *p-i-n* structures, depending on the material parameters. Some of the advantages of thin films are listed below:

i. There are many deposition techniques for thin films from the same material
ii. The structure of the films can vary from amorphous to micro/nanocrystalline, depending on the substrate and the technique and parameters of deposition
iii. Can be deposited on many substrates of different forms and surfaces
iv. Doping and alloys/compounds in different proportions can be obtained due to relaxation of the solubility conditions
v. The grain limits and the surfaces can be passivated with suitably chosen materials
vi. Several types of electronic junctions can be fabricated: single junction, in tandem, etc

vii. It is possible to fabricate materials with desired and/or graded energy gaps/ compositions/lattice constants/reflection coefficients

viii. The surfaces and interfaces can be modified to obtain suitable diffusion barriers at interfaces/electric fields

2.2 THIN FILM DEPOSITION TECHNIQUES

During the last few decades, a number of experimental techniques have been developed for the preparation of thin films of different types of materials, mainly due to the increase in the application of thin films. Vacuum evaporation, various sputtering techniques, spray pyrolysis, electrodeposition, ion beam assisted coating, molecular beam epitaxy and chemical bath deposition are the prominent techniques developed during the last fifty years (Das *et al.*, 1983). Each technique has its own advantages and limitations. The properties of the thin film depend on its structure and composition, which in turn mainly depend on the method of preparation and variation of the parameters of the technique. A better fundamental understanding of materials leads to expanded applications and new designs of devices that incorporate these materials (Seshan, 2002). Thin films can be fabricated in various ways. The techniques can be divided into physical methods (Top-down approach) and chemical (Bottom-up approach) methods as listed in Table 2.1 (George, 1992; Toda *et al.*, 2011).

In physical methods, the film material is moved from a target source with some form of energy to the substrate. This method is widely used in compound thin films. Under physical methods we have vacuum evaporation and sputtering, where the deposition has been transferred to gaseous state either by evaporation or an impact process.

Table 2-1: Classification of thin film deposition techniques

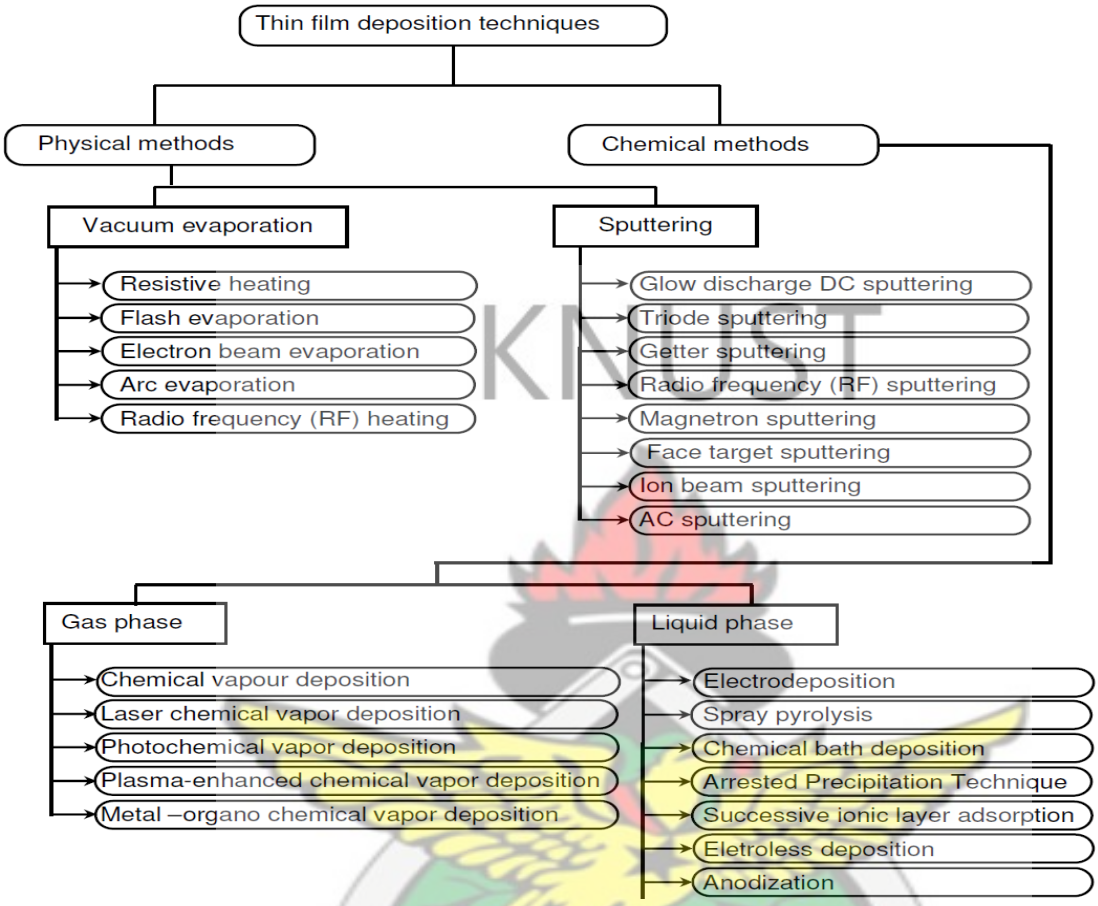

Chemical film fabrication method involves chemical reaction and the precursors are mostly components undergoing reaction at the substrate surface or in the vicinity of the substrate. Under chemical methods we have the gas phase chemical processes such as conventional chemical vapour deposition (CVD), laser CVD, metal organochemical deposition (MOCVD) and plasma enhanced chemical vapour deposition. Liquid phase chemical techniques include electrodeposition, chemical bath deposition, electroless deposition, anodization, successive ionic layer adsorption and reaction (SILAR), spray pyrolysis etc.(Lokhande *et al.*, 2004). In the present work, chemical bath deposition technique is used for preparation of CdSe and PbS_{1-x} Se_x thin films.

2.2.1 Physical Deposition Techniques

I. Physical Sputtering

Sputtering and sputter deposition are widely used techniques for the erosion of surfaces and the deposition of films. Sputter deposition is used for film deposition on semiconductor wafers, on magnetic media and head surfaces, for coating tools and cutting surfaces for wear resistance (this includes, by the way, such tools as shaving razors), for reflective coatings on window glass, for coating the insides of plastic bags and the surfaces of automobile parts, and a number of other wide ranging applications (Seshan, 2002). Sputtering is usually practiced by means of plasmas which generate charged particles which can be accelerated towards a surface electrically. The sputtering process is shown generically in Figure 2.2. The incident particle impacts the surface or near-surface atoms of the solid with sufficient energy to break bonds and dislodge atoms. If, during this process, one or more atoms are removed from the solid, they are considered to be sputtered atoms (Ohring, 1992; Seshan, 2002).

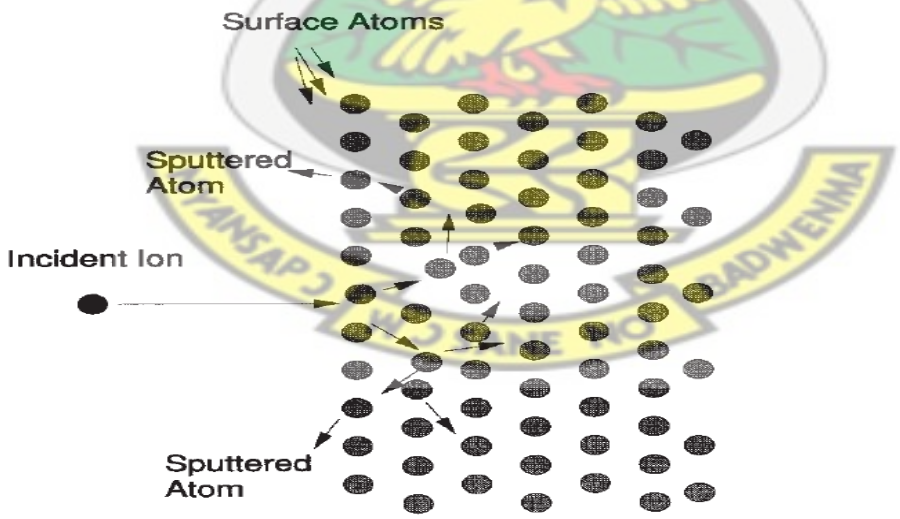

Figure 2.2: Schematic of physical sputtering process (Seshan, 2002)

II. Thermal Evaporation Technique

One of the oldest techniques used for depositing thin films is thermal evaporation or vacuum evaporation and it is widely used in the laboratory and in industry for depositing metal and metal alloys (Mattox, 2010). Thermal evaporation deals with the evaporation of the source materials in a vacuum chamber and condensing the evaporated particles on a substrate. This process is conventionally called vacuum deposition. A thermal evaporator uses an electric resistance heater to melt the material and raise its vapour pressure to a useful range. On heating the material in vacuum, sublimation takes place; the atoms are transported and are deposited on the cleaned substrates. During thermal evaporation, the substrate, crucible and source materials are placed inside the vacuum chamber at room temperature and also at different substrate temperatures to deposit thin films. High-purity films can be deposited from high-purity source material. The possible problems that can be encountered in this technique are the source of material to be vaporized and its purity. Additionally, the line-of-sight trajectory and "limited-area sources" allow the use of masks to define areas of deposition on the substrate and shutters between the source and substrate prevent deposition on non-targeted areas (Mattox, 2010; Seshan, 2002).

2.2.2. Chemical Deposition Techniques

i. Chemical Vapor Deposition

Chemical vapor deposition (CVD) is the process of chemically reacting a volatile compound of a material to be deposited, with other gases, to produce a nonvolatile solid that deposits atomistically on a suitably placed substrate. Among the reasons for the growing adoption of CVD methods is the ability to produce a large variety of films and coatings of metals, semiconductors, and compounds in either crystalline or vitreous form, possessing high purity and desirable properties (Ohring, 1992). Furthermore, the capability of controllably creating films of

widely varying stoichiometry makes CVD unique among deposition techniques. Other advantages include relatively low cost of the equipment and operating expenses, suitability for both batch and semicontinuous operation, and compatibility with other processing steps. However, CVD has a number of disadvantages. One of the primary disadvantages lies in the properties of the precursors. Ideally, the precursors need to be volatile at near-room temperatures. This is non-trivial for a number of elements in the periodic table, although the use of metal-organic precursors has eased this situation (Seshan, 2002).

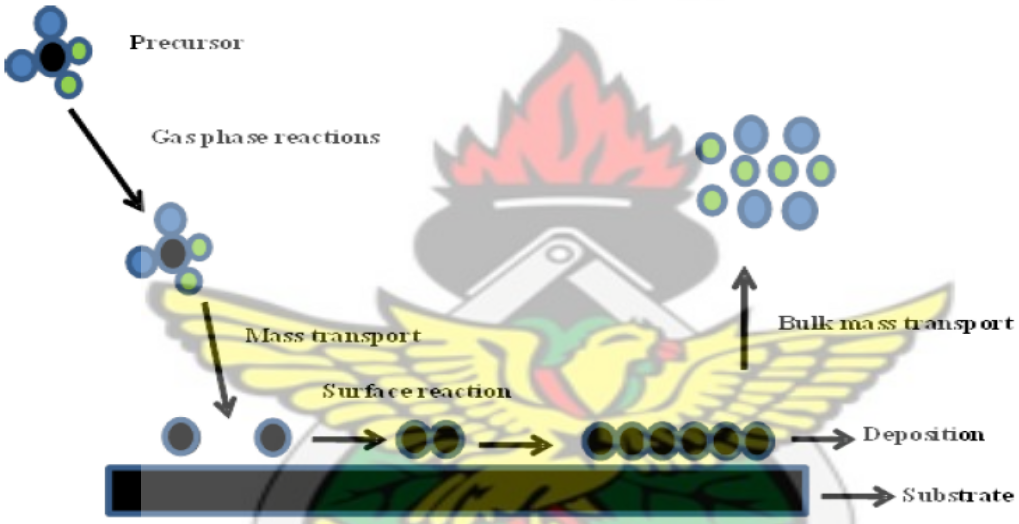

Figure 2.3: Schematic representation of CVD processes (Akhtar, 2013).

CVD precursors can also be highly toxic ($Ni(CO)_4$), explosive (B_2H_6), or corrosive ($SiCl_4$). The byproducts of CVD reactions can also be hazardous (CO, H_2, or HF). Some of these precursors, especially the metal-organic precursors, can also be quite costly. The other major disadvantage is the fact that the films are usually deposited at elevated temperatures. This puts some restrictions on the kind of substrates that can be coated. More importantly, it leads to stresses in films deposited on materials with different thermal expansion coefficients, which can cause mechanical instabilities in the deposited films. Additionally, it requires expensive high

temperature reaction furnace and/or vacuum environment, and expensive high vapor pressure compounds. A schematic diagram involving the steps in the process of CVD is illustrated in Figure 2.3 according to (Akhtar, 2013).

ii. Chemical Bath Deposition

Chemical bath deposition (CBD) has been used as synthesis method for over 130 years (Soga, 2006) and in the recent two decades it has been widely applied successfully, reproducibly, and at low cost, to the synthesis of thin films and other morphologies for solar cells. Many different types of chalcogenide (CdS, CdSe, ZnS, PbS), chalcopyrite ($CuInS_2$, $CuInSe_2$), and oxide (ZnO, TiO_2) materials have been successfully deposited by CBD. The deposition process in CBD uses a controlled chemical reaction or reactions which result in the deposition of a thin film by precipitation (Hodes, 2002; Saeed *et al*., 1995). A ligand or complexing agent acting as a catalyst is usually employed in a bath to control the reaction in a suitable medium as indicated by the pH of deposition solution to obtain crystal growth. Otherwise, spontaneous reaction and sedimentation of materials will be obtained. When a solution of a suitable complexing agent of a metal is mixed with a solution bearing the metal ions, fairly stable complex ions of the metal are formed. Complex ions are formed when a cation or an anion is joined to one or more ligands by dative bonds. Thus an appropriate complexing agent can be chosen so that the concentration of the metal ions is controlled by the concentrations of the complexing agent as well as the solution temperature. This ensures that the cations can be released very slowly from their original compounds in a controlled fashion.

The advantages of CBD technique are several and it is becoming an alternative deposition technique for thin films of compound materials like chalcogenides, oxides and halides. A major success can be found in the recent period with the deposition of semiconducting cadmium sulphide or zinc sulphide buffer or window layers in efficient copper indium diselenide or cadmium telluride thin film solar cells (Barote *et al.*, 2011). However, CBD has some drawbacks: Firstly, in the classical beaker configuration, the material yield during film formation is very low, about a few percent, leading to an unnecessary waste production and increased treatment costs. The reason is that the volume to surface ratio is very high and that only a small part of the solution is contributing to the film formation, the remaining leading to the formation of colloids in the bulk of the solutions (Boyle *et al.*, 2000; Reádigos *et al.*, 2000). Secondly, the formation of particles leads not only to the generation of significant amount of waste but also to the creation of defects in the deposited film (Lokhande and Pathan, 2004). A Brief explanation and deposition principles of CBD process will be given in the next section.

iii. Successive Ionic Layer Adsorption and Reaction (SILAR)

SILAR is aqueous solution technique based on sequential reactions at the substrate solution interface for the deposition of thin films. The SILAR was developed by Nicolau for the deposition of zinc and cadmium chalcogenides thin films (Nicolau, 1985). The adsorption is a surface phenomenon between ions and surface of substrate and is possible due to attraction force between ions in the solution and surface of the substrate. These forces may be cohesive forces or Van der Waals forces or chemical attractive forces. Atoms or molecules of substrate surface possess unbalanced or residual force and hold the substrate particles. Rinsing follows each reaction, which enables heterogeneous reaction between the solid phase and the solvated ions in

the solution (Lokhande and Pathan, 2004). In spite of its simplicity, SILAR has a number of advantages. It is relatively inexpensive, simple and convenient for large area deposition. In principle, it is possible to deposit metal chalcogenide thin films using this method on to variety of substrates (Sartate *et al.*, 2000). The starting materials are commonly available and cheap. As it is a chemical method, a large number of varieties of substrates can be coated. Thus, any insoluble surface to which the solution has free access will be a suitable substrate for the deposition. Figure 2.4 represents the deposition of thin film using SILAR method. It consists of four different steps such as adsorption, rinsing (a and b), reaction and rinsing (c and d) (Lokhande and Pathan, 2004).

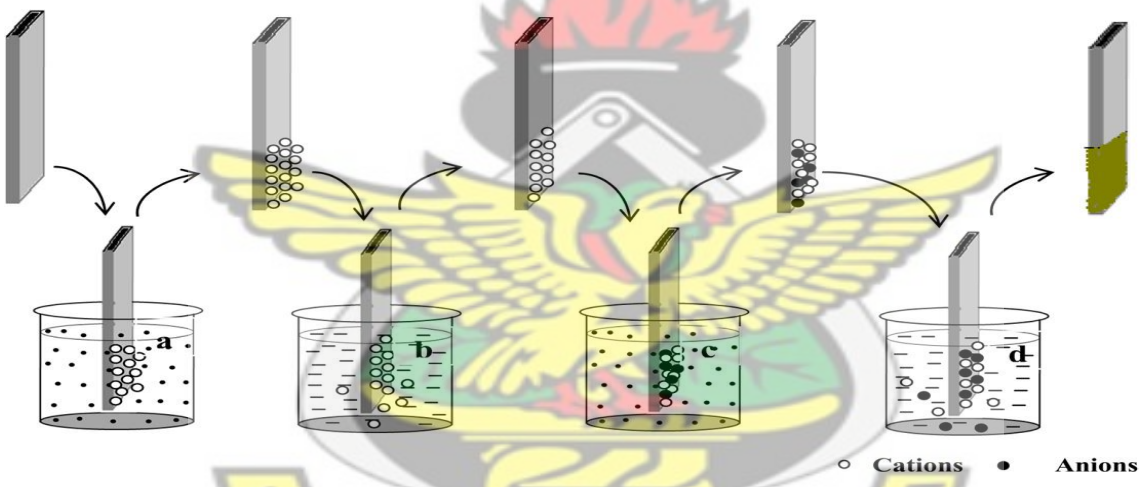

Figure 2.4: Schematic representation of SILAR method (a) cationic precursor and (c) anionic precursor and (b, d) deionised water (Mani *et al.*, 2014).

2.3 CHEMICAL BATH DEPOSITION (CBD) TECHNIQUE

This section begins with a short historical development of the chemical bath deposition followed by an explanation of the basic principles of chemical bath deposition process. Types of nucleation and deposition mechanisms of the chemical bath deposition are presented. Basics of

film formation and factors which affect chemical bath deposition technique discussed in some detail.

2.3.1 Historical Development of CBD

There are many dozens of deposition technologies for material formation; however, thin film deposition technologies are either purely physical, such as evaporative methods, or purely chemical, such as gas and liquid phase chemical processes. A considerable number of processes that are based on glow discharges and reactive sputtering combine both physical and chemical reactions; these overlapping processes can be categorized as physical-chemical methods (Seshan, 2002). Chemical bath deposition (CBD) belongs to purely chemical groups and it has a greater commercial value than either thermal evaporation or sputtering and has attracted the attention of researchers today due to its simplicity, inexpensive, large area scaling and commercial production (Behrnd *et al.*, 1966). In CBD, deposition of thin films takes place from aqueous solutions at low temperatures by a chemical reaction between dissolved precursors, with the help of a complexing agent (or ligand) (Hani *et al.*, 2008). Liebig reported the first chemical solution deposition using silver, the silver mirror deposition in 1835 by chemical solution technique. (Liebig *et al.*, 1835). In general semiconductor thin films are deposited by immersing substrates in diluted solutions containing metal ions and a source of hydroxide, sulphide or selenide ions (Abermann, 2013). The first reported chemical deposition (CD) of a compound semiconductor film appears to be formation of "lüsterfarben" (lustrous colors) on various metals from thiosulphate solutions of lead acetate, copper sulphate, and antimony tartrate, giving films of PbS, CuS or SbS, which possessed "splendid" colors (interference colors resulting from various thicknesses of the deposited films) (Hodes, 2002). PbS was a subject of much attention

during the early studies of CBD. Deposition of PbS films by reaction between thiourea and lead tartrate has been reported (Reynolds, 1884). In 1906, PbS film was deposited for infrared photoconductivity in chemical bath and this application can be considered as the central driving force for successive investigation in chemically deposited lead chalcogenide films. This makes CBD technique vital in making commercial PbS and PbSe infrared detectors during the second world war (Behrnd *et al.*, 1966; Rosenheim *et al.*, 1906).

For a long time, CBD was essentially limited to PbS and PbSe. It was not until the 1960s that deposition of the CBD chalcogenides in particular CdS, was explicitly reported. Moreover, the formation of CdSe and ZnSe were reported in the early 1970s (Nair *et al.*, 1998). As early as; 1982 the first review of Chopra indicated that approximately 20 different non-metallic materials had been synthesized by CBD. The number of known materials now exceeds 50, most of which are semiconductors. There have been many notable books and review articles published over the past decade on chemical bath deposition. The book Chemical Solution Deposition of Semiconductor Films by Hodes (Hodes, 2002) provides an excellent review of the underlying principles governing CBD reactions and offers many recipes to deposit various semiconductor materials. Nair *et al.* (1998) have also published comprehensive review articles on the subject with Nair's work specifically focused on photovoltaic applications for CBD.

The range of materials deposited by CBD was gradually extended and now includes sulphides and selenides of many metals (Ortega-Borges *et al.*, 1993), some oxides, CdTe and also many ternary compounds. Ternary compounds contain either two metals, two chalcogenides or have part of the chalcogenide substituted by a hydroxide group (Kushiya *et al.*, 1996). CBD ternary chalcogenides can be prepared by the combination of all reactants in a single bath or by

preparing bi-layers of two different chalcogenide materials such as Bi_2S_3-Cu_xS, PbS-CdS. The choice of CBD arises from its low cost, ease of handling, possibility of application on a large surface, and simplicity of instruments for deposition (Kanithla *et al.*, 1982). Around 1980, the focus of CBD films slowly turned towards solar energy applications. One of the earlier developments towards this was in solar absorber coatings (Reddy *et al.*, 1987). CBD received an important impetus after CdS films chemically deposited on CdTe and $CuInSe_2$ absorbers were shown to give superior photovoltaic cells compared with the previously evaporated CdS. Nowadays CBD is universally used to form the CdS layer on both CdTe and chalcopyrite thin film photovoltaic cells (Hodes, 2002).

2.3.2 Basic Principle of CBD and Concept of Solubility Product

The basic working principle behind the CBD process is similar to those for all precipitation reactions and it is based on relative solubility of the product. At a given temperature when the ionic product (IP) of reactants exceeds the solubility product (K_{SP}), precipitation occurs. Whereas if the ionic product is less than the solubility product, then the solid phase produced will dissolve back to the solution resulting in no net precipitation (Das and Chopra, 1983). A central concept necessary to understanding the mechanisms of CD is that of the solubility product (*Ksp*).

The solubility product gives the solubility of a sparingly soluble ionic salt (this includes salts normally termed "insoluble"). Sparingly soluble salt, $AB(S)$, when placed in water, a saturated solution containing A^+ and B^- ions in contact with undissolved solid AB is obtained and equilibrium is established between the solid phase and ions in the solution as:

$$AB(S) \rightleftarrows A^+ + B^- \quad (2.1)$$

Applying the law of mass action,

$$K = \frac{[A^+][B^-]}{[AB]} \quad (2.2)$$

where K is stability constant, $[A^+]$, $[B^-]$ and $[AB]$ are concentrations of A^+, B^- and AB in the solution, respectively. The concentration of pure solid is a constant number, i.e.

$$C_{AB}(S) = constant = K^* \quad (2.3)$$

$$K = \frac{[A^+][B^-]}{K^*} \quad (2.4)$$

$$KK^* = [A^+][B^-] \quad (2.5)$$

Since K and K^* are constants, the product of KK^* is also a constant, say K_{SP}, (Mane *et al.*, 2000). Therefore equation (2.5), becomes

$$K_{sp} = [A^+][B^-] \quad (2.6)$$

The constant, K_{SP}, is called solubility product (SP) and $[A^+][B^-]$ is called the ionic product (IP). When the solution is saturated, the ionic product is equal to the solubility product. But when the ionic product exceeds the solubility product ($IP/SP = S > 1$), the solution is supersaturated (where S is degree of supersaturation), precipitation occurs and ions combine on the substrate and in the solution to form nuclei.

There are three main factors which affect the solubility product these are temperature, solvent and particle size (Pietrzyk *et al.*, 1974). The equilibrium between a precipitate and its ions in solution will shift according to whether the heat of solution is endothermic or exothermic (Skoog *et al.*, 1980). Using a solvent of lower dielectric constant, the solubility of moderately insoluble substance in water is reduced by the addition of alcohol or some other water miscible solvent. As particle size decreases, solubility appears to increase.

Solubility constants have been reported by using different methods which includes calorimetric, cation exchange, conductivity, ion exchange, polarography, thermodynamic data, rate of reaction etc. The solubility constants are found to be dependent on temperature, medium and method of measurements and therefore a difference of several orders of magnitudes in solubility constants of a material has been reported in the literature (Sakharam and Lokhande, 2000).

A complexing agent acting as a catalyst is usually employed in a bath to control the reaction otherwise spontaneous reaction and sedimentation of materials will be obtained (Das and Chopra, 1983). The more soluble the salt is, the greater the ion product and the greater the *Ksp*. However, *Ksp* also depends on the number of ions involved, for any formation of thin film there is some minimum number of ions or molecules, which produce a static phase in contact with solution, called nucleus. Nucleation on the substrate of surface starts at local homogeneity. The rate at which nuclei forms on the surface of the substrate, depends on the degree of supersaturation (Lokhande and Pathan, 2004). *Ksp* can be derived theoretically from the free energies of formation of the species involved in the dissolution equilibrium. Thus, for the equilibrium

$$N_a P_b\,(s) \rightleftarrows aN^{c+}(aq) + bP^{d-}(aq) \qquad 2.8$$

where N_a and P_b are sources of cations and anions. The free energy of the dissolution is given by

$$\Delta G^0 = a\Delta G^0\left(aN^{C+}(aq)\right) + b\Delta G^0\left(P^{d-}(aq)\right) - \Delta G^0(N_a P_b\ (s)) \qquad 2.9$$

Since

$$\Delta G^0 = -RTlnK \qquad 2.10$$

Then

$$lnK_{SP} = -\frac{\Delta G^0}{RT} \qquad 2.11$$

Since *Ksp* is a thermodynamic quantity, the ionic product that should result in precipitation may not necessarily do so for kinetic reasons (hence the term used earlier to qualify precipitation: "in principle"). This would be a case of supersaturation. In practice, however, the solubility product does give a fairly good idea of when precipitation will occur in most cases (Hodes, 2002). The preparation of metal sulphides by introducing S^{2-} ions into aqueous solution of metal salt to effect chemical precipitation is well established. In actual fact, in all but highly alkaline solutions most of the sulphur ion will be in the form of HS^- rather than S^{2-}. This is due to the equilibrium between the two species:

$$HS^- \rightleftarrows S^{2-} + H^+ \qquad K_a = 10^{-17.3} \qquad 2.12$$

or alternatively, in terms of hydroxide concentration which is related to the hydrogen ion concentration through the ion product of water:

$$HS^- + OH^- \rightleftarrows S^{2-} + H_2O \qquad K_a = 10^{-3.3} \qquad 2.13$$

Thus at a pH of 11, a common value in chemical deposition (CD), which gives a value for $[OH^-]$ at room temperature of 10^{-3} M, the S^{2-} concentration will be

$$[S^{2-}] = 10^{-3.3}\,[HS^-][OH^-] = 10^{-6.3}[HS^-] \qquad 2.14$$

Therefore the main sulphur ion in solution will be HS^- . Similarly, selenium ions are generated by dissolving inorganic sodium selenosulphate in an alkaline solution as given by the reaction (Sakhare *et al.*, 2012).

$$Na_2SeSO_3 + OH^- \rightarrow Na_2SO_4 + H_2O + Se^{2-} \qquad 2.15$$

If high concentration of S^{2-} or Se^{2-} ions exists locally such that the solubility product is exceeded, localized spontaneous precipitation of a sulphide or selenide may occur as the case may be. This situation can be avoided by generating chalcogen ions slowly and uniformly throughout the volume of the solution. In general the principle of CBD technique is to control the chemical reaction so as to effect the deposition of a thin film by precipitation (Hodes, 2002).

Chemical deposition reactions sometimes proceed via a metal hydroxide intermediate; the concentration of OH^- ions in the solution is particularly important in such cases. Since almost all CD reactions are carried out in aqueous solutions, the pH of the deposition solution will give this concentration. The OH^- concentration increases (decreases) by one order of magnitude for every unit increase (decrease) in pH (Hodes, 2002). This means that the formation of a metal hydroxide (whether as a colloid or as a precipitate) in aqueous solution will be strongly dependent on temperature when the product of the free metal ions and OH^- ions is close to the hydroxide solubility product, although increase in Ksp with temperature may partially offset this effect (Albrecht *et al.*, 2011).

2.3.3 Film Deposition Mechanisms

Chemical bath deposition is one of the solution phase methods useful for the preparation of compound semiconductors on a solid substrate from reaction occurring in a solution, almost always aqueous solutions. It is widely used for the deposition of various metal chalcogenide thin films. It produces good deposits on suitable substrates by the controlled precipitation of the compounds from the solution (Rajaram *et al.*, 1997). The method offers many advantages over other well known vapor phase synthetic routes. It may allow us to easily control the growth factors such as film thickness, deposition rate and quality of crystallites by varying the solution pH, temperature and bath concentration (Kathalinga *et al.*, 2010; Sankapala *et al.*, 2004). The technique is ideally suited for producing uniform films with thickness in the 0.05-0.3 μm range in most cases. Film thickness up to a micron is possible in some cases (Nair *et al.*, 1998). Thin film formation by chemical bath deposition proceeds through various reaction steps at the substrate surface and these different mechanisms have a role in determining the film properties. Thin film deposition mechanisms can be divided into two different major processes: formation of the required compound by ionic reactions involving free anions, and decomposition of metal complexes (Gorer *et al.*, 1995). These two categories can be further divided in two which are complex-decomposition ion-by-ion mechanism and complex-decomposition cluster mechanism. The first two mechanisms involve free chalcogen ion while the last two do not involve formation of free chalcogen ion (Patel, 2012). The two main mechanisms for the compound formation are:

1. **Simple Ion-by-Ion Mechanism**

According to Hodes (2002) and Patel (2012), the conceptually simplest mechanism, often assumed to be the operative one in general, since it occurs by sequential ionic reactions. It is commonly called the ion-by-ion mechanism. If the ionic product exceeds the solubility product,

then there will be a film on the substrate as a solid phase, however, it may not be true under certain circumstances, although a larger ionic product may be required if supersaturation occurs. If the ionic product does not exceed the solubility product, no solid phase will form, except possibly transiently due to local fluctuations in the solution, and the small solid nucleii will redissolve before growing to a stable size. For that reason, the precipitation process is shown as equilibrium rather than as a one-way reaction. In simple ion-by-ion mechanism, first ions diffuse over the substrate which serve as a catalyst and facilitate the nucleation. The nucleation grows as a result of absorption of ions in the solution and nucleation of new crystals occurs. At a further stage the crystals bond with one another by the van der Walls forces forming a film.

For the ion-by-ion growth, the deposition begins only when the negative ion concentrations are high enough to allow nucleation to occur, while the induction time corresponds to build up of negative ion concentration. Growth occurs on these initial nuclei, along with new nucleation, approximately linear region of growth. As the limiting reactant is used up, growth will start to slow down and eventually stop due to depletion of the reactant (Mohammed *et al.*, 2009). It must be pointed out, however, that while it is not very difficult to distinguish between an ion-by-ion and cluster mechanism in most cases, it is much more difficult to distinguish between a simple ion-by-ion and a complex-decomposition ion-by-ion mechanism. Therefore most investigations that conclude an ion-by-ion mechanism is operative, while usually assuming the simple ion-by-ion process, do not distinguish between the simple and complex-decomposition pathways (Gorer *et al.*, 1995; Hodes, 2002).

2. Simple Cluster (hydroxide) Mechanism

CBDs are quite often carried out under conditions where a metal hydroxide (or hydrated oxide) is formed. This might seem to imply that a precipitate is formed at the start of such depositions. In simple cluster mechanism, hydroxide colloidal particles diffuse to the substrate and adhere to it. These hydroxide colloidal particles adsorbed on to the substrate react with free ions in the solution resulting in displacement of hydroxide by the free ions. Such displacement reaction can occur both on the substrate and in the solution and continues until most of the hydroxide converts into sulphide (Araoz, 2009). Yet experiment has shown that the film growth often does not occur for some time (Mohammed *et al.*, 2009; Pawar *et al.*, 2011). It should be repeated at this stage that this mechanism is dependent on a large difference between the solubility products of the hydroxide and chalcogenide of the required metal. It is quite possible that the mechanism will change in the course of the deposition. As the metal is depleted from solution, the complex to metal ratio will increase and may pass the point where no solid hydroxide phase is present in the solution. In this case, the ion-by-ion process will occur if the conditions are suitable. This is most likely if the initial conditions were close to the border between ion-by-ion and cluster mechanisms. The opposite may also occur: initial deposition by an ion-by-ion pathway followed by clusters, which either build up gradually in the solution or change their aggregation properties, in principle both mechanism can in principle coexist (Mehta *et al.*, 2007). This has been shown to occur for CdS deposited from a thiourea bath using a combination of quartz crystal microbalance and electrochemical impedence spectroscopy (Bayer *et al.*, 2002). Change in aggregation properties of the colloids present during the deposition was suggested as the cause of the change in deposition. It is also possible that both mechanisms occur in parallel (Patel, 2012). In complex-decomposition ion-by-ion mechanism and complex-decomposition cluster

mechanism the complex (Cd-Se-L, where L is ligand or part of the S forming species) decomposes to CdSe on the substrate and to a greater or lesser extent also homogeneously in the solution. The CdSe nuclei formed grow by adsorption and decomposition of more complex species until a film of aggregated crystal is formed in a similar manner as for the first two mechanisms. The basis of complex decomposition cluster mechanism is that a solid phase is formed but, instead of reacting directly with the free anion, it forms an intermediate complex with the "anion-forming" reagent (Hodes, 2002; Pawar *et al.*, 2011).

2.3.4 Nucleation and Crystal Growth

2.3.4.1 Nucleation

The formation of solid phase from a solution involves two steps as nucleation and particle growth. The size of particles of a solid phase is independent upon the relative rates at which these two competing processes take place (Kwang-Deog *et al.*, 2005). For any precipitate, there is some minimum number of the ions or molecules required to produce a stable phase in contact with a solution, called as nucleus. The formation of nucleation is necessary for a precipitate formation. The concept of nucleation in solution is that the clusters of molecules formed undergo rapid decomposition and particles combine to grow up to a certain thickness of the film (Mane and Lokhande, 2000). Any formation of film on a foreign substrate starts with a nucleation phase, then followed by a phase in which the nuclei grow further until they form a complete layer. In general, the larger the number of nuclei ('nucleus density') formed during, the nucleation phase, the smaller the grain size in the final layer. On the other hand, if nucleus density is too low, the nuclei are too far from each other and it will take an impractically long

time to reach a complete layer, or total coalescence might not be reached at all. In order to obtain an optimal layer, one can therefore attempt to control nucleation in the early phase of the crystallization or deposition process, aiming at the nucleus density predicted to give the largest grain size in a continuous layer (Poortmans and Arkhipov, 2006). Precipitate will be formed when the ionic product of the concentrations exceeds the solubility product. The solubility product does not provide information on how the particles of the precipitate form nucleation. Nucleation is important in thin films because the grain structure that ultimately develops in a given deposition process is usually strongly influenced by what happens during film nucleation and subsequent growth. Nucleation involves various physical processes, and both thermodynamic and kinetic aspects must be considered. Depending on the deposition mechanism CD can take place either by initial homogeneous nucleation in solution or by heteronucleation on a substrate (Hodes, 2002; Ohring, 1992).

a) Homogeneous Nucleation

Homogeneous nucleation can occur due to local fluctuations in the solution whether in concentration, temperature, or other variables. The first stage in growth is collision between individual ions or molecules to form embryos (embryos are nuclei that are intrinsically unstable against redissolution). Embryos grow by collecting individual species that collide with them (Araoz, 2009). While these species may be ions, atoms, or molecules in general, for CD, adsorption of ions on the embryo seems to be the most probable growth mechanism. They may also grow by collisions between embryos; however, unless the embryo concentration is large, this is less likely. These embryos may redissolve in the solution before they have a chance to grow into stable particles (nuclei). Because of the high surface areas, and therefore high surface

energies of such small nuclei, they are thermodynamically unstable against redissolution. They may, however, be kinetically stabilized by low temperatures, which increase their lifetime, possibly enough for them to grow to a size where they are thermodynamically stable (Hodes, 2002).

b) Heterogeneous Nucleation

In heterogeneous nucleation, subcritical embryos (or even individual ions) can adsorb onto the substrate and particles grow slowly to form a film (Kathalinga *et al.*, 2010). The energy required to form an interface between the embryo and the solid substrate will usually be less than that required for homogeneous nucleation, where no such interface exists. Therefore heterogeneous nucleation is energetically preferred over homogeneous nucleation and can occur near equilibrium saturation conditions, compared with the high degree of supersaturation often required for homogeneous nucleation. These subcritical nuclei can grow, either by surface diffusion or by material addition from solution.

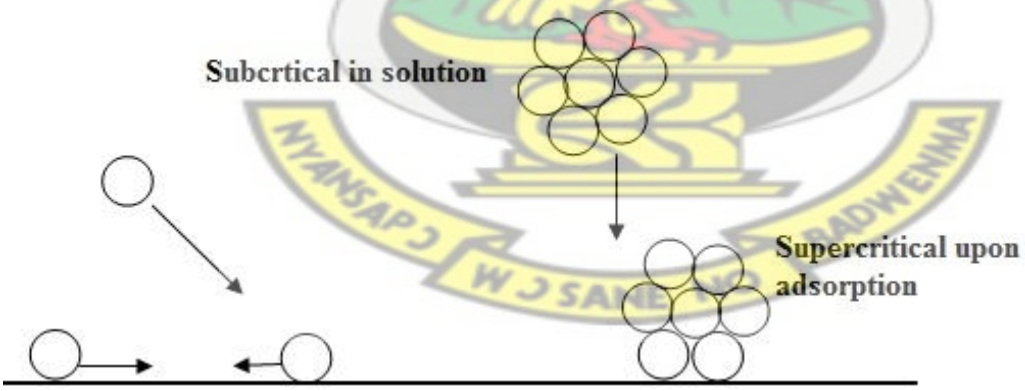

Figure 2.5: Processes involved in heterogeneous nucleation on a surface

It should also be noted that nuclei that are subcritical in solution may be supercritical when adsorbed on a substrate. This is a consequence of reduced contact between nucleus and solution

as well as stabilization of the adsorbed nucleus. These processes are shown schematically in Figure 2.5 (Hodes, 2002). Heterogeneous nucleation of films is a more complicated subject in view of the added interactions between deposit and substrate. The nucleation sites in this case are kinks, ledges, dislocations, etc., which serve to stabilize nuclei of differing size. Suffice it to say that when nucleation rate is high during deposition, many crystallites will nucleate and a fine-grained film results. On the other hand, if nucleation is suppressed, conditions favorable to single-crystal growth are fostered (Hodes, 2002; Ohring, 1992).

Simple models of nucleation are first of all concerned with thermodynamic questions of the energetics of the process of forming a single stable nucleus. Once nucleation is possible, it is usual to try to specify how many such stable nuclei will form within the system per unit volume and per unit time i.e., nucleation rate (NR) (Ohring, 1992). For any precipitate, there is some minimum number of ions or molecules required to produce a stable second phase in contact with a solution called a nucleus. The rate of nuclei formation in a solution is dependent on the degree of supersaturation. The rate of nucleation (RN) increases exponentially in higher supersaturated solution.

$$NR = R_0(C - S)^Y \qquad 2.16$$

Where C is the concentration of solute in solution and Ro and Y are constants and Y > 1. The second step is the growth of particles already present in the solution. This begins when nuclei or other seed particles are present. In the case of ionic solids, the process involves deposition of cation and anion on appropriate sites (Mane and Lokhande, 2000).

$$(AB)_m + A^+ + B^- \rightarrow (AB)_{m+1} \qquad 2.17$$

$$(AB)_{m+1} + A^+ + B^- \rightarrow (AB)_{m+2} \qquad 2.18$$

Where m is the number of A^+ and B^- required for giving stable phase $(AB)_m$.

2.3.4.2 Crystal Growth

There are several ways in which nuclei can increase in size once stable nuclei have formed. One is a continuation of the process of embryo growth i.e adsorption of ionic species from the solution onto the nucleus (Petrov *et al.*, 2003). Crystal growth of this type can be considered a self-assembling process. Figure 2.6 schematically illustrated the processes of nucleation and subsequent growth. When the concentration of solute increases as a function of time, no nucleation would occur even above the equilibrium solubility. The nucleation occurs only when the supersaturation reaches a certain value above the solubility, which corresponds to the energy barrier. After the initial nucleation, the concentration or supersaturation of the growth species decreases.

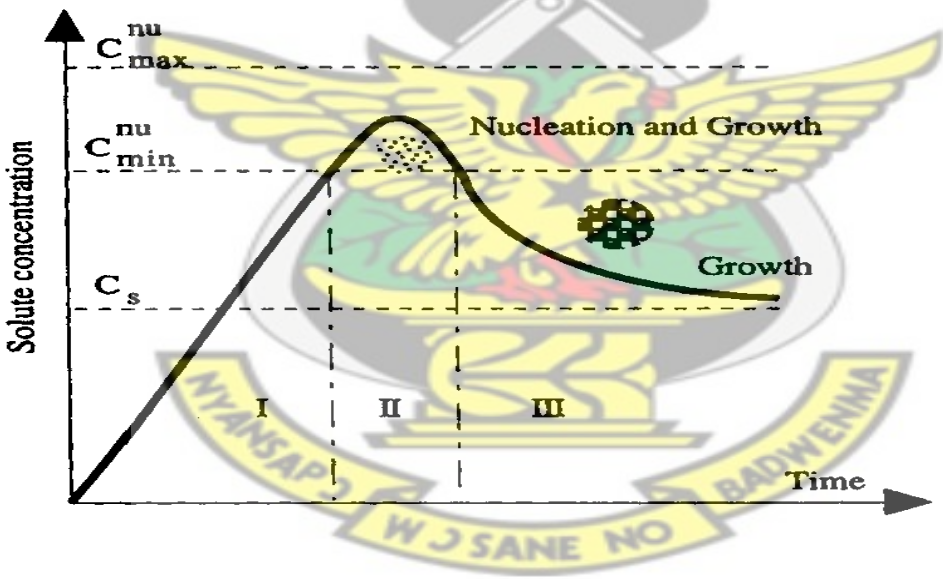

Figure 2.6: Schematic illustrating the processes of nucleation and subsequent growth (Haruta *et al.*, 1986)

When the concentration decreases below this specific concentration, which corresponds to the critical energy, no more nuclei would form, whereas the growth will proceed until the concentration of growth species has attained the equilibrium concentration or solubility.

The next growth step will then be adsorption of the oppositely charged ion to give an additional molecule. This process can continue until either all the ions of any one type are used up or growth is blocked, e.g., by aggregation or by blocking of the crystal surface by a foreign adsorbed species (Hodes, 2002). Also, growth may continue but in a different geometric orientation, giving rise to twinning, polycrystallinity, etc. If a small nucleus or embryo is close to a larger crystal, the ions formed by (partial) dissolution of the smaller, less stable crystal can be incorporated into the larger crystal. This is also another crystal growth mechanism called Ostwald ripening. As the smaller crystal becomes even smaller, its dissolution will become ever more favorable and eventually it will disappear. The result is that the larger crystals grow at the expense of the smaller ones (Hodes, 2002; Viswanatha *et al.*, 2007).

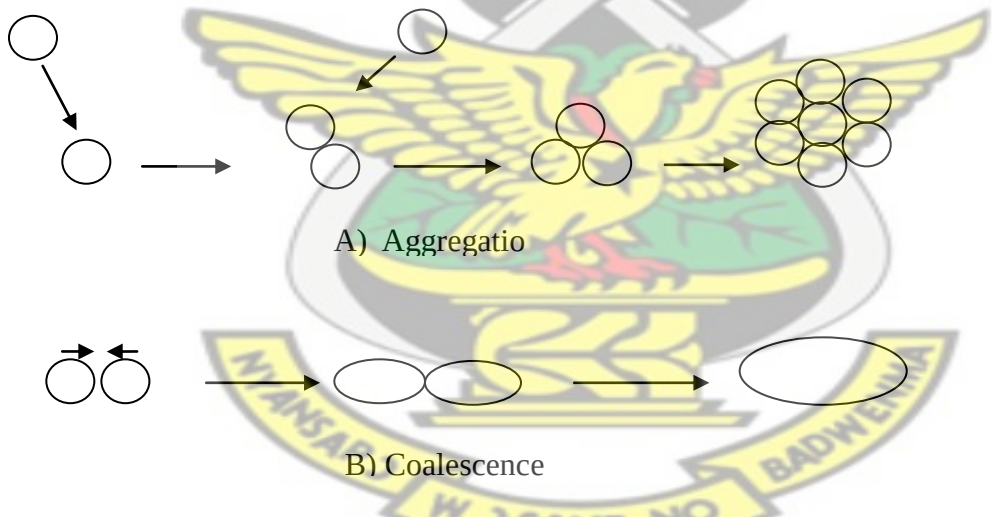

Figure 2.7: A) Aggregation and B) Coalescence of individual particles

In the case of sufficiently high concentration of particles the probability of collisions between these particles becomes high. This can result in either aggregation or coalescence and the process can continue until a large particle has formed (Figure 2.7A). This is the process of aggregation, and the resulting large particle is called an *aggregate.* (In colloidal chemistry, the alternative

terms of *flocculation* and *floc* are often encountered). The properties of the aggregate may be similar to those of the individual particles in some ways (such as X-ray diffraction peak broadening, quantum size effects) and very different in others (e.g., light scattering, sedimentation) (Hodes, 2002).

In an aggregate, there are grain boundaries between individual crystallites. However, in some cases, particularly if the temperature is high enough to allow appreciable diffusion of the crystal atoms, surface diffusion may occur where two (or more) particles have aggregated, resulting in the formation of a neck. This is termed *coalescence*. Coalescence may continue until one large particle is formed from the original two or more particles (Hodes, 2002; Petrov *et al.*, 2003) (Figure 2.7B). The rate of growth (RG) is directly proportional to the supersaturation which is mathematically express as (Mane and Lokhande, 2000):

$$RG = R_0^* b(C - S) \qquad 2.19$$

where b is the surface area of the exposed solid and R_0^* is a constant which is the characteristic of the particular precipitate. If the supersaturation is maintained at low level throughout the chemical reaction, the precipitation process will be occurring. As a result there are great numbers of centers upon which growth process can take place, none of the particles grow very large and a colloidal suspension consists of finely divided solid particles in a liquid phase with diameter of 0.01 to 0.1 mm (Mane and Lokhande, 2000). In general, the growth kinetics of a thin film deposition process is of two types: (i) ion-by-ion growth where deposition process involves the ion-by-ion deposition at nucleation sites on the immersed surfaces and (ii) nucleation takes place by adsorption of the colloidal particles and growth takes place as a result of surface coagulation of these particles, giving thin and adherent film. This is known as cluster-by-cluster growth of

the film (O'Brien *et al.*, 1998). Figure 2.8 schematically shows the relations between the nucleation and growth rates along with the concentration of growth species (Haruta and Delmon, 1986). When the concentration of the growth species increases above the equilibrium concentration, initially there is no nucleation. However, nucleation occurs when the concentration reaches the minimum saturation required to overcome the critical energy barrier, and the nucleation rate increases very rapidly as the concentration increases further.

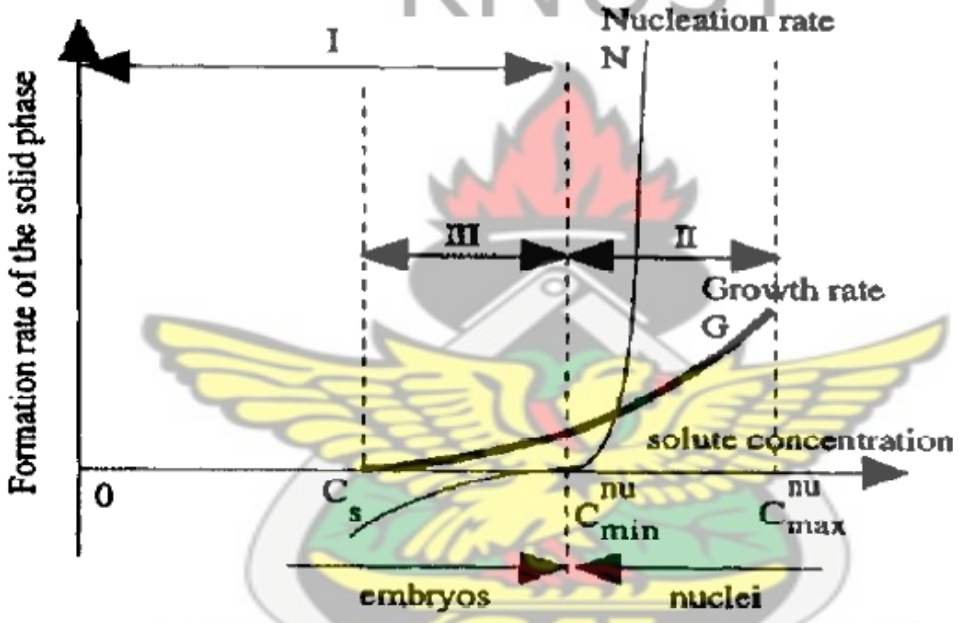

Figure 2.8: Schematic shows the relations between the nucleation and growth rates along with the concentration of growth species (Haruta and Delmon, 1986)

Although growth process cannot proceed when there is no nucleus, growth rate is above zero for a concentration above its equilibrium solubility. Once nuclei are formed, growth occurs simultaneously. Above the minimum concentration, nucleation and growth are inseparable processes; however, these two processes proceed at different speeds. For the synthesis of nanomaterials with uniform size distribution, it is better if all nuclei are formed at the same time.

In this case, all the nuclei are likely to have the same or similar size, since they are formed under the same conditions. In addition, all the nuclei will have the same subsequent growth. Consequently, monosized nanomaterials can be obtained. So it is obvious that it is highly desirable to have nucleation occur in a very short period of time. The size distribution of initial nuclei may increase or decrease depending on the kinetics of the subsequent growth process. The formation of uniformly sized nanomaterials can be achieved if the growth process is appropriately controlled (Haruta and Delmon, 1986). In kinetic studies on the growth of CBD films, there are three definite regimes, induction, growth, and termination (Hodes, 2002).

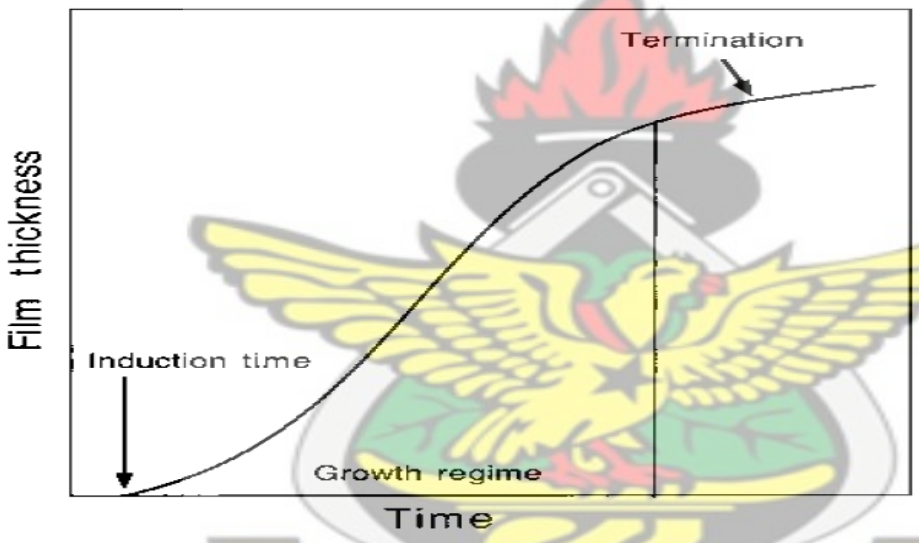

Figure 2.9: Typical shape of the curve reprenting time dependence of film thickness during growth (Hodes, 2002)

An induction regime at the beginning of the process indicates that no clearly observable growth occurs due to initial nuclei in solution and then an approximately linear growth region occurs along with nucleation and sticking formation. In the termination step no further growth occurs; as the limiting reactant is used up, growth will start to slow down and eventually stop due to depletion of the reactants see Figure 2.9.

Kinetics of CBD can vary from one condition to other. For instant, in one study of PbSe deposition from a citrate-complexed selenourea solution containing hydrazine, the rate was proportional to the pH and to the selenourea concentrations but independent of the Pb and citrate concentrations (Lundin *et al.*, 1965). On the other experiment carried out by Kainthla *et al.* (1980), PbSe deposition using citrate as complex for the Pb and selenosulphate as Se precursor, the opposite occurs: The deposition rate decreases with increase in pH.

2.3.5 Factors Affecting Thin Film Deposition Process in CBD

There are several factors which affect thin film deposition process in CBD techniques. For instant the rate of deposition and terminal thickness depend upon the number of nucleation centers, supersaturation of the solution and rate of stirring. The growth kinetics depends on the concentration of ions, their velocities and nucleation and growth processes on immersed substrates. The effect of various deposition conditions on these parameters are discussed below.

2.3.5.1 Effect of Chemical Bath Solution pH

The reaction rate as well as rate of deposition depends on the supersaturation condition and rate of the formation of MX (where M and X is the number of metals and O^-/OH^- ions respectively). If the concentration of OH^- ion in the solution is higher, the M ion concentration will lower and the reaction rate will be slow (Hankare *et al.*, 2006). At a certain pH, the concentration of M ion decreases to a level such that the ionic product of M and X becomes less than the solubility of MX and a film will not be formed. For the growth of good quality thin films, the hydroxy ions in precursor solution are necessary. The thin film formation depends on the pH of the reaction mixture and pH depends on OH^- ions. The decrease in pH results in porous, non-reflecting, powdery and weakly adhered thin films on the substrates. At higher pH metal ion concentration

will be lower and the reaction rate will be slow. With an increase in pH as the metal ion concentration decreases, the rate of film formation decreases (Barote *et al.*, 2011; Hankare *et al.*, 2006).

In most examples of CD from alkaline solution, the deposition rate increases with increase in pH. This is due to both the greater rate of decomposition of the chalcogenide precursor at higher pH (this decomposition usually involves hydroxide ions) and, in many cases, the greater probability of solid hydroxide formation (as long as this is not excessive). The hydrated metal hydroxy complex is a soluble species. However, if the pH is sufficiently high, the metal hydroxide, which is relatively insoluble for most metals (apart from the alkali group metals) will precipitate. (Hodes, 2002).

2.3.5.2 Effect of Complexing Agent

In CBD technique usually a complexing agent is added to control the hydrolysis of the metal ion. The process depends on the slow release of chalcogenide ions into an alkaline/acidic solution in which the free metal ion is buffered at a low concentration (O'Brien and McAleese, 1998). The free metal ion concentration is controlled by the formation of complex species according to the general reaction:

$$M(A)^{+2} \leftrightarrow M^{+2} + A \qquad 2.20$$

Where M is the metallic ion sources and A is the complexing agent; here concentration of the free metal ions at a particular temperature is represented by the relation:

$$K = \frac{[M^{+2}][A]}{[M(A)^{+2}]} \qquad 2.21$$

Where K being the instability constant of the complex ion. The instability constant is different for different complexing agents. As the instability constant increases, more number of ions will

be released. The stability of the complex also depends on temperature and pH of the reaction bath. Increase in temperature of the solution will make the complex less stable; where as an increase in pH generally makes it more stable (Hodes, 2002).

Film formation occurs by combination of released metal ions from complex metal ion source and chalcogen source. It helps to limit the hydrolysis of the metal ion and impart some stability to bath otherwise it undergoes rapid hydrolysis and precipitation (Barote *et al.,* 2011). In general complexing agents usually form complexes with metal ions used to increase the bath stability, control deposition rate and good quality films, it also greatly influence the structural and electro-optical properties of the thin film (Hodes, 2002; Soukup *et al.*, 2010).

Nature of complexing agents may influence the final products. For example, when ammonia is used as a complexing agent for the preparation of ZnS thin film, it is found to result in $ZnO/Zn(OH)_2$ phase rather than ZnS. However when two complexants ammonia and hydrazine are used, the oxide and hydroxide phases could be avoided to a great extent (O'Brien and McAleese, 1998). If a compound containing more than one cation is to be deposited, complexation could be used to offset the difference in *Ksp* between the individual metal compounds. In a general reaction the metal ion concentration decreases with increasing concentration of the complexing ions. Consequently the rate of reaction and precipitation are reduced leading to a larger terminal thickness of the film (Hodes, 2002).

2.3.5.3 Effect of Bath Temperature

The rate of chemical reaction in the bath can also be influenced by the bath temperature. As temperature increases dissociation of the complex increases hence the kinetic energy of the molecules also increases leading to greater interaction between ions and subsequent deposition at volume nucleation centers of the substrate (Al-Jawad *et al.*, 2013). This will result in increase or decrease of terminal thickness, depending on the extent of super saturation of the solution of the bath. Stirring basically brings fresh parts of the solvent into contact with the solute and particles are forced to connect and the presence of temperature assists the entire process for effective desired results (Carrillo-Castillo *et al.*, 2013). Bath temperature has an important effect on crystal size. In most cases higher temperatures allow more grain growth whereas, lower temperatures gives very small nuclei in solution that are thermodynamically unstable. However, if the cluster is smaller than the critical nucleus size, then there is the possibility that the nucleus will redissolve. Srinivasan *et al.* (2012), studied the effect of temperature on the structural and optical properties of PbS thin films. Their result revealed that the crystallinity of films were improved when the temperature was increased from 30 ^{O}C to 60 ^{O}C with the preferred orientation growth along the (200) plane and the band gap energy decreases linearly from 1.2 eV to 0.9 eV.

In most cases chemical bath deposition can be used to carefully control the crystallinity of the thin film semiconductors by adjusting the deposition temperature. The lifetime of the nucleus will then depend on its size and also on the temperature; lower temperatures will slow the redissolution step. Thus lower temperature increases the chance that a subcritical nucleus will eventually grow to a stable size rather than redissolve. In PbS thin film the band gap increases

with increasing temperature, in contrast to the normal semiconductor band gap dependence on temperature (Hodes, 2007; Karthika *et al.*, 2013).

2.3.5.4 Effect of Deposition Time

Deposition time is one of the parameter which affects thin film deposition in CBD method. In most cases it has a great influence on structural, morphological and optical properties of thin films. Fekadu *et al.* (2014), showed that deposition time strongly influenced the preferred orientations of the crystallites as well as structural parameters such as average crystallite size, strain and dislocation density for PbS thin films. In this study the optical band gap of PbS thin films also decreased from 1.32 eV to 1.10 eV with increasing deposition time. O'Brien and Saeed, used ethylenediamine as complexing agent, higher deposition temperatures and glass as a substrate and found that the thickness of the CdS thin film increased linearly with deposition time (Hodes, 2002). In general, the growth of good quality semiconductor thin films by the chemical bath deposition technique proceeds at a slow pace. Higher deposition rates and higher films thicknesses are usually accompanied by powdery deposits and a lack of specular reflection. Nair *et al.* (1998) has studied intensively the effect of deposition period on film thickness by fixing all the other parameters for different semiconductor thin films and for most cases (not always) the film thickness increase with deposition time see Figure 2.10.

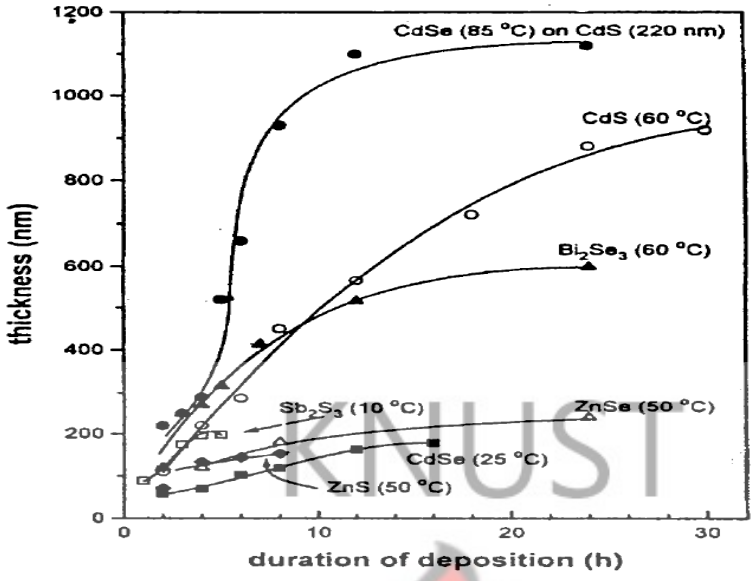

Figure 2.10: Dependency of film thickness on deposition time for some selected semiconductor thin films (Nair *et al.*, 1998).

2.3.5.5 Effect of Concentration of Cation and Anion Sources

It is known that bath composition is critical for synthesis of good quality of thin films. The nature of the reactants influences the whole physical and chemical properties of the deposited thin film. By changing the composition of the reactive solution, competition between the processes of homogeneous and heterogeneous nucleation could be altered to favor thin film growth (Hodes, 2002). The deposition of good quality, adherent, specular and crystalline CdSe has usually been associated with supersaturated bath with respect to the precipitation of cadmium hydroxide species, irrespective of the substrate (Hankare *et al.*, 2006). According to Hankare *et al.* (2006), the growth under these circumstances gives Se^{-2} ions into an alkaline solution, where the free metal ions are buffered. Thus, low concentration of bath ingredients usually favors the nucleation in the first stage. Indeed, the bath concentration plays an important role in the substrate interaction with growing particles. For high concentrations, the films formed were

thicker, indicating stronger interaction. Under these circumstances, the growth process becomes cluster-by-cluster rather than ion-by-ion nucleation. On the other hand, at low concentration, the films formed were too thin and nonuniform. This may be attributed to the fact that the required number of ionic species is not available in the solution to get better quality film. In the preparation of lead sulphide thin films by Preetha *et al.* (2013), using different cationic precursors; it was observed that lead sulphide thin film prepared with lead acetate as cationic precursor was found with very good structural, morphological and optical properties compared to lead sulphide thin films deposited from lead chloride, lead nitrate, and lead sulphate cationic precursors. Liua *et al.* (2013), showed the effect of different thiourea concentrations in bath for ZnS thin film. In this study the surface morphologies of ZnS thin films prepared in baths with a concentration ratio of $ZnSO_4/SC(NH_2)_2$ of 1:1, 1:2, and 1:3 were quite smooth and compact. When the concentration ratio of $ZnSO_4/SC(NH_2)_2$ is 1:4 and 1:5, cracks appeared on the surface of ZnS thin films. Mousa *et al.* (2008), also studied the effect of concentration of lead acetate for PbS thin films. Their result showed that the film thickness goes on decreasing as the concentration of lead acetate increases because this parameter attained a state of higher super saturation earlier, generating precipitate instead of thin film.

2.3.5.6 Nature of Substrates and their Separation

The nature of the substrate is another important factor that plays a major role in the reaction kinetics. Moreover, nucleation and crystal growth also takes place on it during thin film deposition (Kumaran *et al.*, 2013). Substrate should be cleaned properly with a standard procedure before being immersed in the reactant mixture. One of the advantages of CBD is that thin films can be deposited on any surface. Moreover, shape and electrical conductivity of the substrates are usually not important very irregularly shaped substrates can be used. However, the

nature of the substrate is usually important in order to obtain an adherent film (Mane and Lokhande, 2000; Moreno *et al.*, 2011).

Glass is one of the most commonly used substrates in CBD, however, metals make good substrates in general, either because chalcogenides tend to adsorb strongly on many metals, or the non-noble metals are covered with a (hydroxylated in the deposition solution) oxide layer. If the metal in the deposition solution has a sufficiently negative potential, an internal electrochemical reduction may occur (Hodes, 2002). A large variety of CBD thin films have been also deposited on different polymer surfaces. Deposition sometimes is satisfactory on the clean polymer with various activation treatments, such as treatment with permanganate, have been used to improve the adhesion and homogeneity (Pramanik *et al.*, 1987). Apart from adhesion, the crystallographic properties of chemically deposited films are sometimes dependent on the nature of the substrate. One example is epitaxial deposition on a crystallographically-ordered substrate (Furlong *et al.*, 1998).

The kinetics of growth has also been observed to depend sensitively on the nature of the substrate surface. Higher deposition rates and terminal thickness are observed for those substrates whose lattices and lattice parameters match well with those of the deposited material. During deposition of PbSe thin films under similar conditions, higher rates and thickness have been observed on Ge substrate rather than on glass substrate because of better matching of the lattice parameters of PbSe with those of Ge (Kainthla *et al.*, 1979) see Figure 2.11.

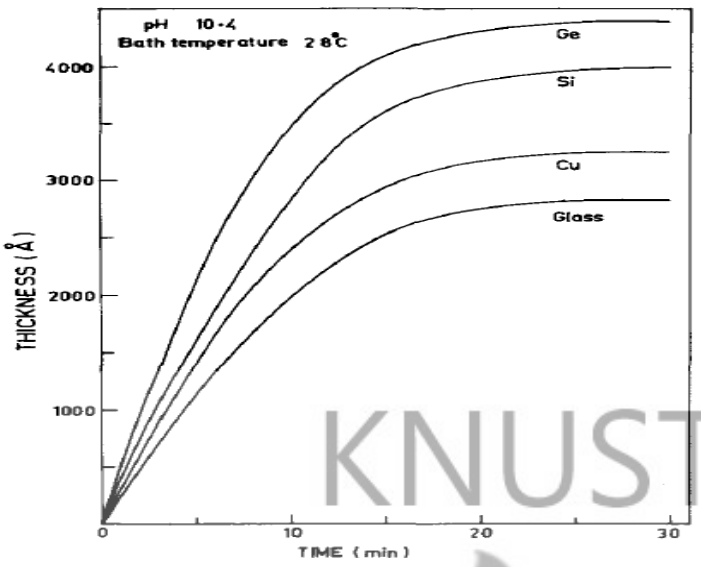

Figure 2.11: Thickness as a function of deposition time for PbSe films grown at 28 °C on different substrate materials (Kainthla *et al.*, 1979)

In addition of substrate cleanness and types, its separation during deposition has significant effect on film thickness. Reádigos *et al.* (2000) explained this phenomenon by considering film thickness as a function of separation between substrates in batch production. They observed that, film thicknesses reach an asymptotic maximum with increase in substrate separation. This behavior is explained on the basis of the existence of a critical layer of solution near the substrate, within which the relevant ionic species have a higher probability of interacting with the thin film layer that contribute to precipitate formation. Actually, the critical layer depends on the solution composition, the temperature of the bath, as well as the duration of deposition. For instant in the case of CdS thin film, this critical layer was found to extend from 0.5 mm to 2.5 mm from the substrate surface depending to deposition (Das and Chopra, 1983).

2.4 CRYSTAL STRUCTURE OF (Cd, Pb) (S, Se) CHALCOGENIDE SEMICONDUCTOR THIN FILMS

Semiconductor materials are always the focus of materials science due to their outstanding optical, electrical and thermal properties and extensively potential application in various devices. Group II–VI and IV-VI chalcogenide semiconductor materials show structural duality, and can be formed as either sphalerite (cubic, zinc blend type) or wurtzite (hexagonal type) (Bouroushian, 2010). The crystal structure of (Cd, Pb) chalcogenide semiconductor is presented in this section for the thin film materials; Cadmium selenide, Lead selenide, Lead sulphide, and Lead sulphur selenide.

2.4.1 Cadmium Selenide (CdSe)

The synthesis of binary metal chalcogenide of group II–VI semiconductors in a nanocrystalline form has been a rapidly growing area of research due to its important non-linear optical properties, luminescent properties, quantum size effect and other important physical and chemical properties (Kissinger *et al.*, 2007). Cadmium selenide (CdSe), one of the binary semiconductor compounds belonging to the II–IV groups of the periodic table, has bright luminescence in the visible range of optical spectra and has shown potential use in nanocrystalline materials. Bulk CdSe has two stable four-coordinated polymorphs, hexagonal wurtzite and cubic sphalerite, that coexist at ambient conditions. Under pressure, they both convert to a denser cubic rocksalt phase at a moderate pressure of 2.5 GPa (Wang *et al.*, 2007). The band gap of CdSe varies among its various structures and the rock salt has the least recording band gap of 0.6 eV at 3 GPa (Zakharov *et al.*, 1995).

Cadmium selenide single crystals crystallizes either as sphalerite (cubic, zinc blende) structure with space group *Fm3m* or as wurtzite (hexagonal) structure with space group $P6_3mc$ and its atomic arrangement is shown in Figure 2.12 (Hotje *et al.*, 2003). The Bohr radius of CdSe is about 5.6 nm (Nirmal *et al.*, 1995). Many workers have reported that chemically deposited CdSe thin films onto the glass substrates are either hexagonal or cubic structure (Dwivedi *et al.*, 2011; Kale *et al.*, 2000).

The Crystal parameters of cadmium selenide for cubic structure is $a = b = c = 6.077\ \dot{A}$ and the hexagonal one has $a = b = 4.299\ \dot{A}$ and $c = 7.010$ Å . In constructing the hexagonal cell of the sphalerite, the cubic [111] direction is taken as hexagonal [001], with hexagonal axes related to the cubic ones as $C_h = \sqrt{3}\,a_c$ and $a_h = 1/\sqrt{2}\,a_c$. As can be seen, the two forms differ essentially for the packing along the ternary axis, which is of the kind fcc (i.e., *ABC*) in the sphalerite and hcp (i.e., *AB*) in the wurtzite (Lehmann *et al.*, 1998).

CdSe single crystals have a specific density of 5.816 g/cm^3, melting point of 1541 K and the microhardness of w-CdSe is about 0.9 GPa and their thermal conductivity is 3.49 $Wm^{-1}K^{-1}$ (Adachi, 2005).

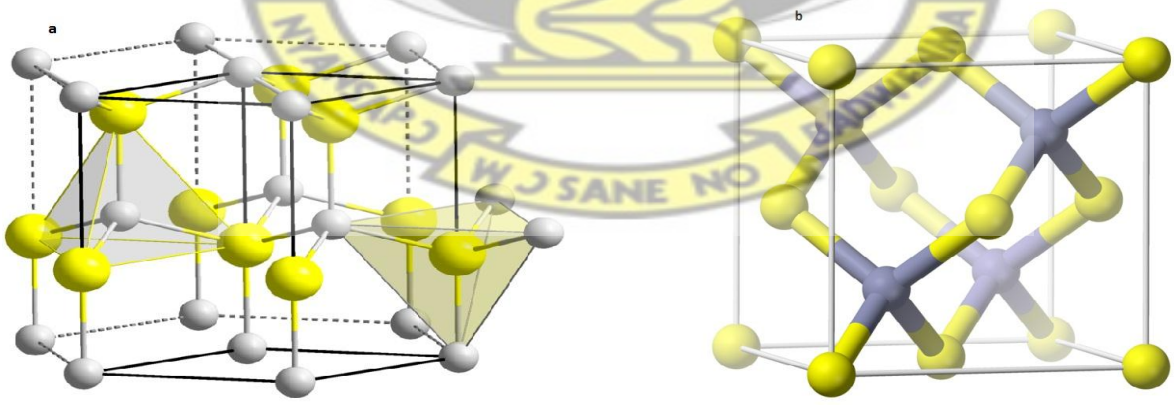

Figure 2.12: Atomic Structure of CdSe (a) Wurtzite and (b) Zincblende

2.4.2 Lead Selenide (PbSe)

Lead selenide (PbSe) belongs to group IV–VI compound semiconductor, possessing excellent optoelectronic properties and its crystal structure is in the six fold-coordinated NaCl type with (B1, space group Fm $\bar{3}m$) (Khokhlov, 2003). The atomic arrangement of PbSe is shown in Figure 2.13(a). Its Lattice constant and melting point are 6.130 Å and 1,078 ^{0}C respectively. The static dielectric constant and density of PbSe are 280 and 8.15 (gcm^{-3}) respectively (Lide, 1995). PbSe has the least band gap of the lead chalcogenides, 0.27 eV at room temperature (Shyju *et al.*, 2012). However, depending on particle size the optical band gap of PbSe films can be tuned to the order of 4.5 eV by changing various preparation conditions. This will pave the way to PbSe films for potential application in solar cells and other optoelectronics devices (Feng-Ling *et al.*, 2008; Shyju *et al.*, 2012).

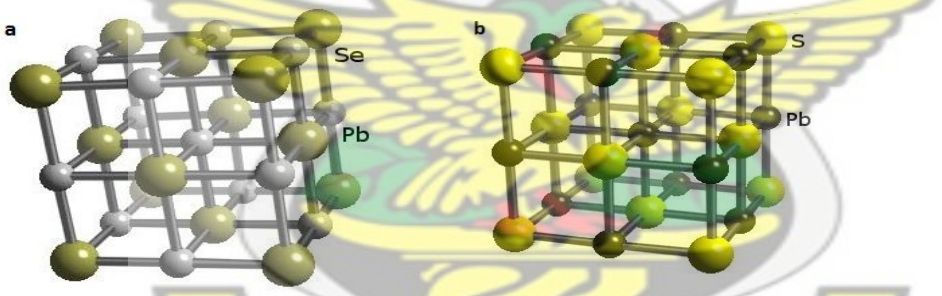

.

Figure 2.13: Atomic structure of (a) PbSe and (b) PbS

2.3.4 Lead Sulphide (PbS)

Historically, lead sulphide was the first compound to be deposited chemically. In 1869, Puscher described a deposition process of PbS from a thiosulphate solution. Emerson-Reynolds reported deposition of PbS films in 1884, while in 1933 Bruckman deposited PbS thin films by the solution growth method (Chattarki *et al.*, 2012). The data on the structure of lead sulphide thin

films are ambiguous. Usually, it is assumed that PbS films have a B1-type cubic (space group No 225 – Fm $\bar{3}m$) structure (Sadovnikov *et al.*, 2013). Bulk PbS is a IV-VI group of semiconductor having face center cubic crystal structure of NaCl type with lattice parameters $a = 5.936\ \AA$, α = β = γ = 90° and a narrow direct band gap of 0.41 eV at room temperature. The atomic position of PbS is shown in Figure 2.13(b). PbS exhibit strong quantum size effects below excitonic Bohr radius of 18 nm, and hence the energy band gap of its nanocrystals can be tuned to anywhere between 0.41 eV (bulk) to 4 eV (Kotadiya *et al.*, 2012; Thielsch *et al.*, 1998; Valenzuela-Jaureguia *et al.*, 2003). Lead sulphide (PbS) thin film is obtained by the reaction of Pb^{2+} and S^{2-} ions, which form covalent bonds. The size of the ions is: Pb^{+2} = 1.21 Å, S^{-2} = 1.84 Å. The K_{PS} = 1.3 × 10^{-28}; enthalpy of formation: $\Delta H_{f\ solid}^{0}$ = - 98.32 kJ/mol, entropy: $S°_{\ solid}$ = 91.34 J·mol^{-1} K^{-1} and its optical density: n_{D20} = 3.921 (Moreno *et al.*, 2011). The static dielectric constant and density of PbS is 161 and 7.61 (g/cm^{-3}) respectively (Lide, 1995).

2.4.5 Lead Sulphur Selenide ($PbS_{1-x}Se_x$)

Chemical bath deposition method has been widely used in the past to make binary polycrystalline thin films such as PbSe, ZnSe, CdS, CdSe, Bi_2S_3, Ag_2S, PbS, etc; (Jamal *et al.*, 2014; Rajaram and Dnyandev, 1997). Recently CBD technique becomes very popular to synthesis ternary compounds/alloys for different optoelectronic application. Ternary alloys prepared out of binary semiconductors can be grouped as a class of semiconductors in which the lattice parameter, energy band gap and other operational parameters could be continuously varied as per requirement by selecting binary constituents and their relative concentrations suitably (Adachi, 2009). $PbS_{1-x}Se_x$ is an alloy of the two lead chalcogenides binary compounds of PbS and PbSe. The interest in lead chalcogenides (PbS, PbSe and PbTe) and their alloys stems

from their important applications, in crystalline and polycrystalline forms (Obaid *et al.*, 2012). Lead chalcogenides (PbS, PbSe and PbTe) have many special characteristics as compared to other semiconductors. Their band gaps are smaller at lower temperatures, i.e the temperature coefficients of the band gap are positive while they are negative for all other elemental or compound semiconductors. In addition, the lattice structure may be very unstoichiometeric. The vacancies and interstitials control the conductivity type, an excess of Pb causes n-type conductivity and excess of chalcogenide causes p-type conductivity (Kothiyal *et al.*, 1990).

In recent years, there has been considerable interest in lead chalcogenides and their alloys due to their demanding applications as detectors of infrared radiation, photoresistors, lasers, solar cells, optoelectronic devices, thermoelectric devices, and more recently, as infrared emitters and solar control coatings. There have been many theoretical and experimental studies on lead chalcogenides (PbS, PbSe, and PbTe) (Barros *et al.*, 2006; Bencherif *et al.*, 2011). These chalcogenides are narrow, direct bandgap semiconductors (IV-VI groups) and crystallize at ambient condition in the cubic NaCl structure. They possess ten valence electrons instead of eight for common zinc blende and wurtzite group III-V and II-VI compounds. They also exhibit some unusual physical properties, such as anomalous order of band gaps, high carrier mobility, and high dielectric constants. All these unique properties of these semiconductors have inculcated great interest in the fundamental studies of these materials (Aghamkar *et al.*, 2009; Alvi and Khan, 2013).

2.5 REVIEW OF CADMIUM SELENIDE (CdSe) THIN FILM PREPARED BY CBD METHOD

Recently, extensive research has been devoted to study the fabrication and characterization of chalcogenide compounds in the form of thin films (Choi *et al.*, 2012; Cyrus *et al.*, 2009). Among the metal chalcogenides, synthesis of binary semiconductors of group II-VI attracts many researchers attention for their great experimental and applied interests (Alvi and Khan, 2013; Baban *et al.*, 2003). CdSe is one of the most interesting group II-VI semiconductors owing to its interesting optical, electrical and optoelectronic properties and applications (Patil *et al.*, 2013; Yukselici *et al.*, 2013). A variety of physical and chemical techniques have been used for the deposition of cadmium selenide thin films. Among these techniques chemical bath deposition is one of the most suitable technique relatively at low temperature for chalcogenides thin films synthesis because it is simple and inexpensive method for large area deposition. Moreover, it yields stable, adherent, uniform and hard films with good reproducibility (Bhushan *et al.*, 2002). In this section a review of some works done by different scholars to synthesize CdSe thin films using CBD is presented.

Kanithla *et al.* (1982) prepared CdSe thin films on glass substrates by a solution growth technique from cadmium acetate, ammonia and sodium selenosulphate. Spectral distribution of refractive index (n) and absorption coefficient (α) have been calculated. The films had a direct energy gap of 1.74 eV. These films have been sensitized by heating in air, and maximum value of light to dark current ratio found to be 2 X $l0^3$ at 50 mW-cm^{-2}. The maximum peak of spectral sensitivity was at 0.7 μm. Trap density was found to be in the range of 10^{17} - 10^{18} traps cm^3 eV

in the energy range of 0.21 - 0.26 eV had been estimated. Properties of the sensitizing centers have been studied and were observed to be similar to those of single crystals.

Effect of annealing temperature on the crystalline quality of chemically deposited CdSe films was studied by (Calzadilla *et al.*, 2002). The CdSe films were deposited from an aqueous solution of 0.027 M Na_2SeSO_3, 0.027 M $CdCl_2$ and 50 ml NH_3 30% as complexing agent. The pH of the solution was adjusted by the NH_3 and the deposition carried out at 50 ^{0}C for 72 hrs. Chemically deposited CdSe thin films have been studied to their crystalline quality with the variation of annealing time and temperature. It was found that the as-grown films had cubic structure. These samples maintain their cubic structure if the annealing temperature does not exceed the temperature of phase transition. The analysis made by X-ray diffraction and Raman dispersion showed that the samples annealed at temperature less than the transition temperature increase their crystalline quality.

Lokhande *et al.* (2005), used chemical bath deposition method for the preparation of cadmium selenide thin films on a glass substrate at room temperature. The films were deposited using cadmium acetate as a Cd^{2+} ion source, sodium selenosulfate as a Se^{2-} ion source and ammonia as complexing agent and to adjust the pH of the bath. The CdSe thin films were deposited by an aqueous alkaline medium at room temperature and grown with nanocrystalline cubic phase, with energy band gap of 2.3 eV and electrical resistivity of the order of 10^6 ohm cm. The films were annealed in air at 673 K for 4 hrs. Thermal annealing was found to increase the crystallites of films along with a recrystallization process that changes the metastable nancocrytalline cubic (zinc-blende type) phase of CdSe into the stable polycrystalline hexagonal (wurtzite type) phase.

The elemental analysis was carried out only for Cd and Se; the average atomic percentage of Cd:Se was 50.5:49.5, showing that the sample was slightly Se^{2-} deficient. The SEM study revealed that when the film annealed at 673 K, all the nanorods are strongly oriented in the plane perpendicular to the substrate surface. They were united together at the base, but separate when coming out from the substrate. They form the cauliflower-like structure that looks like it has grown and/or originated from the surface of substrate. Due to air annealing, the crystallite size of particle increases from 45 Å to 180 Å that resulted in a decrease in electrical resistivity. The average crystallite size and residual strain were found to be 45 Å, -1.428×10^{-4} and 180 Å, 1.36 $\times 10^{-4}$ for cubic and hexagonal phase, respectively. The increase in crystallite size showed the improvement in crystallinity that decreases the grain boundary discontinuities. The negative and positive values of residual strain revealed the presence of both the compressive and tensile strain.

Kwang-Deog *et al.* (2005), deposited cadmium selenide thin films on titanium, nickel, and ITO coated glass substrates by chemical bath method, without addition of ammonia for the pH adjustment. Sodium citrate ($Na_3C_6H_5O_7 \cdot 3H_2O$) was used as a complexing agent and to adjust the pH of the bath (7 to 9). Cadmium sulphate and sodium selenosulphate were the precursors for Cd^{2+} and Se^{2-} ions sources respectively. The solution was heated to 65 ^{0}C using thermostatic arrangement for 120 min. The film thickness was between 50 to 300 nm, depending upon deposition time and temperature. X-ray diffraction, scanning electron microscopy, optical absorption techniques were used to characterize the CdSe films. The photoactivity of CdSe film was tested by forming photoelectrochemical cell using polysulphide electrolyte. The CdSe films showed hexagonal crystal structure irrespective of type of substrate. The CdSe films were photoactive. At high SEM magnification, round shaped grains were observed for ITO substrate.

For titanium and nickel substrates, well connected elongated grains were seen. The films had a direct energy gap of 1.80 eV and the dark current was nearly equal to zero. Under the intensity of illumination of 100 $mWcm^{-2}$, the photocurrent and photovoltage obtained were of the order of 1–2 $mAcm^{-2}$ and 0.5 V, respectively.

Esparza-Ponce *et al.* (2009), synthesized CdSe thin films from ammonia free bath on glass substrate. The materials used in the chemical bath were cadmium chloride complexed with sodium citrate and sodium selenosulphate. The films thickness was in the range of 400 – 500 nm with a growing time of 4 hrs. The material obtained was characterized by optical absorption, SEM with the energy dispersive X-ray analysis (EDX) and X-ray diffraction. The films obtained at bath temperatures of 70 ^{0}C and 80 ^{0}C had the hexagonal structure (of wurtzite type), with crystallite size of about 20 nm. Room temperature deposition results in films with the cubic structure and crystallite size of about 4 nm. From optical transmission data, an energy gap was found to be 1.88 eV.

Hankare *et al.* (2006), has deposited crystalline CdSe thin film from solution containing cadmium sulphate octahydrate, tartaric acid, potassium hydroxide, ammonia and sodium selenosulphate at room temperature for 3 hrs. Cadmium sulphate octahydrate, complexed with tartaric acid and the pH of the bath was adjusted to 12.1 by using ammonia and KOH solution. The 'asdeposited' CdSe thin film was found to be red in color, specularly reflective and well adherent to the glass substrate. The crystalline phase of the deposited sample was hexagonal wurtzite-type with average grain size of 230 Å. The compositional analysis of the sample gave 49.4% cadmium and 50.6% selenium, showing that the samples were cadmium deficient and the

film had a direct band gap of 2.01 eV. The electrical resistivity of CdSe thin film was found to the order of 10^6 Ωcm.

Dhanam *et al.* (2008) deposited CdSe polycrystalline thin films onto glass substrates by chemical bath deposition at 70 ^{0}C. The precursors were 6ml of Cadmium sulphate (1 M), sodium selenosulphite (0.25N), 3ml of triethanolamine (1N) and aqueous ammonia (14N) was added to vary the pH value from 9 to 11. The XRD results revealed that the deposited CdSe thin films were polycrystalline in nature with cubic structure having the (111) plane as the preferred orientation. The structural parameters such as the lattice constant, crystallite size, dislocation density, number of crystallites per unit area and strain were calculated for the films and it was found that the estimated structural parameters are better compared with those of vacuum based hot wall deposited CdSe thin films. The EDX pattern confirms the presence of cadmium and selenium and the proportion of constitutive elements measured were 67% Cd and 33% Se. This result indicated that the deposited films were non-stoichiometric in composition: $Cd_{1.3}$ $Se_{0.7}$. The calculated absorption coefficients were found to be high of the order of 10^6 m^{-1} in the CdSe thin films of different thicknesses. The band gap energies obtained for the CdSe films of different thicknesses were in the range of 1.72–1.80 eV. Various optical parameters such as absorption coefficient and extinction coefficient of the films were also evaluated. The thickness dependence of structural and optical parameters has been discussed in detail. The high temperature conductivity mechanism has been found to be due to the grain boundary scattering contribution and the evaluated high temperature electrical parameters strongly confirm the semiconducting nature of CdSe thin films.

Gopakumar *et al.* (2010), synthesized CdSe thin films by CBD from the bath constituted 0.2 M solutions of Cadmium chloride ($CdCl_2$), 20 ml sodium selenosulphate, few drops of triethanolamine and 30% NH_4. The pH of the solution was adjusted to 10 by adding excess ammonia. The thickness of the film in a single dipping estimated by gravimetric method and thickness prolifometry was 0.34 and 0.4 µm, respectively. The SEM micrograph of CdSe thin films for as-deposited sample was nonuniform with two layers and agglomeration of microcrystallites. The estimated average grain size was about 0.45 µm. The uniformity of film increased with annealing and grain size improved to about 1 µm. Structural analysis using XRD showed single phase film crystallized in cubic structure with preferred growth in the (111) direction. The energy band gap calculated from the absorption spectra of unannealed CdSe thin films about 1.80 eV and absorption coefficient near band edge (α) was 0.58 x 10^5 cm^{-1}. The sample annealed at 250 ^{0}C had the lowest band gap of 1.38 eV. CdSe film annealed at 150 ^{0}C showed an additional phase $Cd_{1-x}Se_x$. The conductivity of CdSe thin film was found to be n-type.

Khomanea *et al.* (2010), synthesized CdSe thin films by chemical bath deposition method on glass substrate at room temperature for 24 hrs. For the deposition of CdSe thin films they used cadmium chloride and sodium slenosulphate as source of Cd^{2+} and Se^{2-} ions respectively. Malonic acid was used as a complexing agent in the synthesis of CdSe thin films. The pH of reaction mixture was 7.5. The SEM micrograph of annealed CdSe thin films at 450 ^{0}C showed smooth and uniform surface without cracks and well adherent to the glass substrate. The annealed sample showed total conversion into nanorods. The X-ray diffraction analysis revealed that the film samples were in cubic crystal structure. The optical band gap energy (Eg) was found to be 1.70 eV.

Shyju *et al.* (2010), studied the effects of annealing on cadmium selenide nanocrystalline thin films prepared by chemical bath deposition at 80 ^{0}C using cadmium acetate and sodium selenosulphate as source materials and ethylene diamine tetra acetic acid (EDTA) as a chelating agent with concentrations 0.025, 0.075 and 0.1 M. The thickness of the film was found to be 0.6 μm using interferometery technique. The as-deposited film exhibited the cubic structure and the 350 ^{0}C annealed film changed from cubic to hexagonal phase. Annealing of the film increased the crystallite size and decreased the dislocation density. The optical study revealed the direct transition band gaps and found to be 2.10 eV and 1.84 eV for the as deposited and the annealed CdSe films respectively. The optical transmittance of the film reduced after annealing at 350 ^{0}C. From the photoluminescence analysis, it was inferred that the deposited samples had direct band transition and also red shift was observed after annealing. This shows that CdSe is a potential candidate for solar cell fabrication. The homogeneous formations of crystalline grains were observed from SEM as well as AFM images. The as-deposited and annealed CdSe films had negative Hall coefficient which confirms the n-type conductivity. The Hall mobility of the as deposited CdSe film was found to be 0.2154 cm^2/Vs, resistivity (2.023×10^7 Ωcm), carrier concentration ($\eta = 1.223\times10^{12}$ $/cm^3$) and conductivity (7.308×10^{-7} /Ωcm). The Hall mobility of the annealed CdSe film was found to be (3.3×10^3 cm^2/Vs), resistivity (8.21×10^4 Ωcm), carrier concentration (2.356×10^{10} $/cm^3$) and conductivity (1.21×10^{-5} /Ωcm).

Singh *et al.* (2011), used CBD to deposit CdSe semiconductor films on glass substrates. The precursors were 1M cadmium acetate, triethanolamine (TEA), sodium selenosulphate and 30% aqueous ammonia. TEA was used as a complexing agent and the deposition was carried out for 60 min at 60 ^{0}C. The SEM studies showed spherical type structures with approximate grain size

ranging between 4 nm and 8 nm with voids on uniform background. The film crystallized in the wurtzite phase and presents a preferential orientation along the c-axis. The highest texture coefficient was observed in the (002) plane for CdSe thin film and the energy band gap obtained was in the range of 1.77 eV to 1.89 eV. Optical constants such as refractive index and extinction coefficient were determined from transmittance spectrum in the ultraviolet-visible (UV-VIS) regions using envelope methods. Absorption coefficient and the thickness of the film were calculated from interference of transmittance spectra. Optical excitation spectra showed maximum excitation at 389 nm. The photoluminescence (PL) emission spectra under this excitation consisted of two peaks at 485 nm and 531 nm wavelengths, which were attributed to the presence of one deep trapping site and electron hole recombination via trap state or imperfection site. The blue shift observed in the PL emission spectra corresponds to the nanocrystalline effect.

Deshpande *et al.* (2013), prepared cadmium selenide thin films by chemical bath deposition on glass substrates at different temperatures (25 ^{0}C to 80 ^{0}C) from an aqueous alkaline medium using a precursor solution containing cadmium acetate, triethanolamine (TEA), ammonia and sodium selenosulphate. The pH of bath was kept constant around 10.50 ± 0.10. Energy dispersive analysis of X-rays confirmed that all the films reveal nearly desired stoichiometry up to 60 ^{0}C. The average atomic percentage of deposited films at 70 ^{0}C and 80 ^{0}C showed that the films were slightly rich in selenium. From the SEM and AFM studies, it was found that the entire surface area of the substrate was covered by the large number of grains which are densely packed with irregular shapes and sizes. Also some flaws, voids, pinholes or cracks were seen at few places on the micrographs. The X-ray peak broadening was used to evaluate the crystallite size

and lattice strain by the Williamson–Hall plots. The XRD pattern of the deposited films indicated the presence of crystalline cubic phase with the (111) plane as preferred orientation and revealed that the deposited films were under compressive and tensile strain. Dislocation density and strain decreased with increased deposition temperature while crystallite size and lattice parameter were increased. From PL analysis it was observed that deposited CdSe thin films were luminescent in nature (under 465 nm excitation), exhibiting blue shift and having narrow emission peak.

The effect of annealing on CdSe thin film was investigated by Sachin *et al.* (2013). They synthesized CdSe thin films by CBD at 70 ^{0}C for 8 hrs using cadmium sulphate as a precursor for Cd^{+2}, 25 vol% NH_4OH as a complexing agent and freshly prepared sodium selenosulphate (Na_2SeSO_3-Selenourea) for Se^{2-} source. Soda-lime glass and F: SnO2 (FTO) were substrates for deposition. The as-deposited films were annealed at temperatures of 100, 200, 300 and 400 ^{0}C respectively for 1 hr in ambient air. The optical band gap energy was found to decrease from 1.97 to 1.71 eV with increased in annealing temperature and exhibited a red shift. The XRD patterns showed the formation of amorphous CdSe for as-deposited thin films. Annealing the samples leads to the transition of crystal structure from amorphous to cubic and cubic to hexagonal. FESEM images showed the formation of CdSe pebbles with average size of the order of 2.16 µm. The size of the pebble decreased from 2.4 to 1.8 µm with increasing annealing temperature. Photoluminescence spectra of all the samples of CdSe thin films showed an undefined trend in intensity with respect to increasing annealing temperature. The maximum current density of 3.90 mA/cm^2 for the sample annealed at 300 ^{0}C was observed with the highest power conversion efficiency of 2.08%.

All the above reviewed literatures revealed that only few works have been done so far to synthesis CdSe thin films using tartaric acid as a complexing agent. This knowledge gap motivated me. Hence, in the present study CdSe thin film is synthesized by CBD method using tartaric acid as a complexing agent, at a bath temperature of 85 ^{0}C, a pH of 9.5 and a deposition time of ninety minutes.

2.6 REVIEW OF LEAD SULPHUR SELENIDE ($PbS_{1-x}Se_x$) THIN FILMS BY DIFFERENT DEPOSITION TECHNIQUES

Ternary semiconductor thin films are considered to be an important technological material due to their specific physical properties like high efficiency, high optical absorbance and direct band gap, are considered to be potential materials in respect for a wide spectrum of optoelectronic applications (Barote *et al.*, 2011; Deshmukh *et al.*, 1994; Razykov, 1988). Thin film semiconductor compounds, especially lead chalcogenide, and their alloys have drawn a lot of attention due to their technological importance and future prospects in various electronic and optoelectronic devices (Alvi and Khan, 2013).

Isoelectronic alloys of compounds, e.g. $Cd_{1-x}Zn_xSe$, $Cd_{1-x}Zn_xS$, $Cd_{1-x}Zn_xTe$, $Cd_{1-x}Pb_xS$ have been studied extensively in electronic and optical devices with major emphasis related to photoelectrochemical solar cell performance (Ashokkumar *et al.*, 2013; Barote *et al.*, 2011). The synthesis of ternary PbS_xSe_{1-x} nanocrystals thin films remains underdeveloped compared to the widely studied cadmium chalcogenides alloy (Wanli *et al.*, 2009). Only few works have been done so far by chemical bath deposition and other deposition techniques to synthesize $PbS_{1-x}Se_x$ thin films. In the present section attempt is being made to review some of the works done by different researchers.

Sarma *et al.* (1982), reported on solution growth technique for depositing of PbS_xSe_{1-x} thin films at room temperature. In order to prepared PbS_xSe_{1-x} thin films with x varying from 0 to 1, the following typical procedure was used: 5 ml of lead nitrate solution was mixed with 25 ml of NaOH with constant stirring and was diluted with about 65 ml of water; to this, various quantities of solutions of thiourea and sodium selenosulphate were added. The solution was then transferred to a beaker containing a well-cleaned substrate. After some time, depending on x, a mirror-like film began to deposit onto the sides of the beaker and the substrate. Films of various thicknesses were obtained by keeping the substrates in the solution for different times. Thicker films were obtained by repeated deposition. The thicknesses of these films were measured by the Fizeau interferometric method. The films deposited onto the lower side of the substrates were more uniform and more adherent.

Debye-Scherrer photographs of the film material scraped off from the substrate, taken with a camera 11.46 cm in diameter using nickel-filtered Cu Kα radiation, were analyzed to identify and to characterize the material. The study showed that in all cases the material of the films were a single phase fcc of PbS_xSe_{1-x}. The value of the lattice parameters calculated by the extrapolation method from Vegard's law and it varies from 6.110 Å to 5.935 Å as "x" goes from 0 to 1. The surface morphology of a film was depends on its composition, in general; the films consist of spherical shaped clusters with dimensions of the order of microns.

The spatial uniformity of the films on glass substrates were investigated by scanning the film surface with a focused spot of light from a microdensitometer (Enraf Nonius Delft,model II) along the length of the film (6 cm), the distance between successive scans being 5 mm. The result showed that, except near the edge, the transmission of the entire film was almost the same,

which revealed the uniformity of the deposited thin films. In contrast to the case for Cd and Zn, Se was preferentially deposited. (Small selenosulphate concentrations in solution resulted in much larger Se concentrations in the film. For example, from a solution containing 0.5 mM selenosulphate and 500 mM thiourea, the film composition was ca. $PbS_{0.75}$ $Se_{0.25}$). This was explained by the large difference in solubility products of PbS and PbSe.

Majeed *et al.* (2004), deposited polycrystalline PbS_xSe_{1-x} thin films with composition ranges ($0 \leq x \leq 1$) onto ultra clean glass substrates by vacuum evaporation technique keeping the substrates at room temperature in a vacuum of 10^{-6} Torr. The deposited films were annealed in the same vacuum chamber at about 80 ^{0}C for 2 hrs. The films were kept inside the vacuum chamber for 24 hrs to attain metastable equilibrium. The thicknesses of the films were measured using quartz crystal thickness monitor. The thicknesses of all these films were in the range of 5000 Å. The post-deposition annealing resulted in a reduction of lattice defect density with little increase in average grain size in the range of film thickness investigated. All the films of the PbS_xSe_{1-x} system were found to be polycrystalline in nature as confirmed by X-ray diffraction patterns and had a predominantly rock salt (NaCl) structure. As the composition x of PbS_xSe_{1-x} alloys decreased, diffraction angle (2θ) increased slightly for each plane and the corresponding values of inter planar spacing d(Å) and lattice constant a(Å) were decreased slightly. For each composition of these alloys of lead chalcogenides, a preferential orientation was along the [200] direction. The lattice parameters of each composition of ternary alloys of PbS_xSe_{1-x} followed the Vegard`s law meaning that within the experimental errors, the lattice parameter of these ternary alloys of concentration "x" can be linearly interpolated from the lattice constants of the corresponding lead salts. It has been observed that the dc conductivity increased as "x" increased from 0 to 1 for PbS_xSe_{1-x} alloys. The activation energy of different compositions of this system

was in the order of 10^{-1} eV. The band gap changes from 0.42 eV to 0.29 eV and the absorption edge was shifted towards the longer wavelength as x increases from 0 to 1.

Kumar *et al.* (2010), deposited thin films of the solid solutions of PbS_xSe_{1-x} by flash evaporation of the fused material (i.e. lead, sulphur and selenium in their elemental form) in an evacuated quartz ampoule placed in a furnace at sufficiently high temperature of 700 ^{0}C on the glass substrate at room temperature and then cooled slowly resulting in small crystallites. During the flash evaporation process, the pressure was maintained at 10^{-5} Torr and the substrate (glass slide) was kept at room temperature. The distance between the substrate and the source was kept constant i.e. 15 cm. Here the evaporation rate was maintained at 10 Å /s. The energy gap of the alloy films becomes narrower gradually on replacing the sulphur by selenium. The forbidden band width of lead sulphide was 0.40 eV while that of PbSe was 0.29 eV. The band gaps of the ternary compounds were supposed to be in between the two. The presences of sharp structural peaks in the XRD patterns evinced the polycrystalline nature of the samples. For PbS and $PbS_{0.8}Se_{0.2}$ the preferred orientation was along the [111] direction while for $PbS_{0.4}4Se_{0.6}$, $PbS_{0.5}Se_{0.5}$, $PbS_{0.2}Se_{0.8}$ and PbSe alloy it was found to be along the [200] direction. This indicated that variation in stoichiometry of anion atoms (S and Se) of the series PbS_xSe_{1-x} were changed only the direction of preferred orientations but did not cause any structural phase transition. Excess of selenium was also observed in the XRD patterns in the form of small peaks originating from Se crystals. The resistivity of the films were decreased continuously with increasing sulphur content except for a selenium concentration (x = 0.8). The resistivity of the alloy films lied in between the resistivity of PbS and that of PbSe. The resistivity of PbSe had the lowest value. The successive decreased in resistivity on partial substitution of sulfur by selenium

was accounted for the increased grain size. This phenomenon had also been supported by the SEM photograph. At higher Se concentrations the carrier density decreased and becomes highest when all the sulphur was replaced by selenium. On still higher concentration of Se, the gradual fall in mobility might be attributed to the increased in carrier-carrier scattering which plays an important role at room temperature.

Al-Fawade *et al.* (2013), synthesized $PbS_{1-x}Se_x$ films by thermal evaporation technique under lower pressure of about 10^{-6} mbar with (0.3 ± 0.04) μm thickness. The weighting of the required amount of precursors were placed into molybdenum boat. The deposition process was carried out by instantaneous evaporation of the material with minimum possible time of contact. The structure of the $PbS_{1-x}Se_x$ alloys as bulks and thin films had been examined by XRD with Cu Kα wavelength (λ) 1.5405 Å, at room temperature (RT) with "x" content (0, 0.1, 0.15, 0.3, 0.4, 1). The X-ray diffraction study revealed that the structures of polycrystalline with cubic structure with preferential orientation in the [200] direction for alloy and films. The intensity of preferential orientation as bulks and films increased with increasing of sulphide (*S*) content. A little shifting toward higher diffraction angle (2θ) was observed for preferential orientation plane with increasing "x" content. The grain size and lattice constant of the alloys and films were determined by using the Scherrer formula. The optical properties of $PbS_{1-x}Se_x$ films with different "x" content (0, 0.1, 0.15, 0.3, 0.4, 1) at RT were calculated from FTIR transmittance spectra in the region of 3,100 - 4,200 nm on silicon substrates. It was observed that increasing (*S*) content shifts the peak of transmittance spectrum to a shorter wavelength for (x = 0, 0.1, 0.15, 0.4, 1) alloys. The shift in the film's peak position may be attributed to the crystallite of the film structure by increasing the grain size. Moreover, the transmittance decreased with increasing S

content except at (x = 0.3) value which has increased and shifted to a higher wavelength and then decreased for (x = 0.4, 1). Also the value of absorption coefficient decreased with increasing *S* content. The value of optical energy gap increased with increasing S content except x = 0.3 and the range of energy gap was from 0.296 eV to 0.445 eV. The refractive index decreased slightly with increasing *S* content. This behavior was due to increase in the energy gap which causes to expand the crystal lattice and grow the grain size and decreased the defects. The value of refractive index ranged from 3.842 to 4.239 for $PbS_{1-x}Se_x$. The extinction coefficient also decreased with increasing composition for all films except (x = 0.3).

The same group, Nasir *et al.* (2013), studied the influence of sulphur on structural and electrical properties of PbS_xSe_{1-x} films with different "x" content where x = 0, 0.1,0.15,0.3,0.4,1. The PbS_xSe_{1-x} films have been prepared by thermal evaporation technique under lower pressure of about 10^{-6} mbar with 0.3 μm thickness. The X-ray diffraction for PbS_xSe_{1-x} films with "x" content (0, 0.1, 0.15, 0.3, 0.4, 1), showed that these films were polycrystalline of face centered cubic structure and the intensity increased with increasing sulphide S content. This increase was more significant at higher S concentration indicating that the [200] direction was the preferred plane for the crystal growth. The variation of grain size reported from 29.53 to 82.10 nm with S content, shows that the crystallinity of PbS_xSe_{1-x} films increased with "x" content. The conductivity of the film decreased continuously with increasing sulphur content except for a sulphur concentration (x = 0.3). The conductivity of the alloy films lied in between the conductivity of PbS and that of PbSe. The successive decreased in resistivity on partial substitution of selenium by sulphur was accounted for the increase in grain size. The rise in resistivity at higher S contents may also be attributed to the surface scattering effects due to

imperfect matching of the various areas of the grown films. The direct current conductivity of PbS_xSe_{1-x} decreased with increasing S content. This decreased means a negative coefficient of resistance. The electrical activation energy increased in the temperature range of 498 K with increasing S content. Hall measurement showed that the films of (x = 0, 0. 1, 0.3, and 0.4) were n-type and the films of (x = 1) was p-type. The carrier concentration decreased with increasing S content except of (x = 0.3). Hall mobility increased with increasing S content while it decreased for (x = 0.3).

Literature review showed that $PbS_{1-x}Se_x$ thin films have been synthesized mainly by physical deposition techniques which are required sophisticated technology and big investment. But, one of the attractive features of the CBD approach is ease with which the alloys can be synthesize without the use of any sophisticated instrumentation and process control. Hence, in this work the synthesis and characterization of $PbS_{1-x}Se_x$ thin films deposited by chemical bath deposition technique on glass substrate will be reported. The deposition was carried out over the entire composition range of ($0 \leq x \leq 1$) from chemical baths containing lead acetate, thiourea, sodium hydroxide, ammonia and sodium selenosulphate.

Chapter 3

3. PHYSICS OF SEMICONDUCTOR THEORY

3.1 INTRODUCTION

It is well known that the electrical and optical properties of semiconductors are understood with the help of energy band structures. The energy states or energy band structures of electrons in crystals reflect the periodic potential of the crystals and they can be calculated when we know the exact shape and the magnitude of the crystal potentials (Hamaguchi, 2010). The shape and the magnitude of the potential are not determined directly from any experimental methods, and thus we have to calculate or estimate the energy bands by using the assumed potentials. One important outcome of the band theory of solids is the concept of a conduction band, valence band, and an energy band gap separating the two bands. Semiconductors are a class of materials that display such an energy band characteristics. The conductivity of these materials can be modified by the introduction of controlled amounts of certain impurities (Bhattacharya *et al.*, 2010).

In this chapter the basic theories of different electron models and the concept of allowed and forbidden energy bands in a single-solid crystal will be discussed in some detail. Electron and hole concentrations at equilibrium will be introduced including statistical characteristics of electrons in a crystal. Quantum size effects for selected semiconductor thin films are also presented.

3.2 ENERGY BAND STRUCTURES OF SEMICONDUCTORS

3.2.1 Free – Electron Model

A free electron model is the simplest way to represent the electronic structure of metals. Although the free electron model is a great oversimplification of the reality, surprisingly in many cases it works pretty well, so that it is able to describe many important properties of conducting materials. Free electron model, proposed by Drude and Lorentz near 1900 (Balaguru *et al.*, 2012) well before quantum mechanics was developed, can qualitatively explain the DC electrical conductivity, AC electrical conductivity, Hall effect, and magnetoresistance. Later inclusion of Fermi-Dirac distribution (as opposed to Boltzmann distribution) helps to explain the thermal conductivity and specific heat of electrons. However, many properties still need a full quantum mechanical explanation (Kittel, 2005). In this model a metal is assumed to be consisting of two parts: one is the fixed positive charges and the other is free electrons.

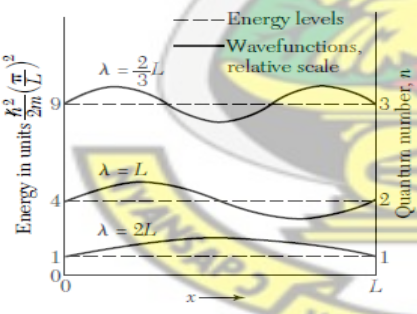

Figure 3.1: First three energy levels and wave functions of a free electron of mass *m* confined to a line of length L. The energy levels are labeled according to the quantum number n which gives the number of half-wavelengths in the wave function. The wavelengths are indicated on the wave functions (Kittel, 2005)

According to this model, the conduction electrons are free to move anywhere in the sample except for rare reflection from the surface and resembles much like molecules of an ideal gas. Consider a free electron in one dimension, taking account of quantum theory and of the Pauli principle (see Figure 3.1).

An electron of mass m is confined to a length L by infinite barriers represented by the wave function ψ(x) can be equated as:

$$H\psi = E\psi \qquad 3.1$$

Where H is Hamiltonian and E is total energy (sum of potential and kinetic energy) also it is the allowed eigen values (energies) of the electron in the orbital (i.e., here the study is for a system of single electron and the orbital model is valid only when there are no interactions between electrons). Since we can assume that the potential lies at zero, the Hamiltonian H comprises only the kinetic energy so that equation (3.1), takes the form

$$H = \frac{p^2}{2m} \qquad 3.2$$

where P is the momentum and in quantum mechanics it can be express as:

$$P = -i\hbar \frac{d}{dx} \qquad 3.3$$

The time independent schrodinger equation can be written for potential energy zero as follow:

$$H\Psi_n = -\frac{\hbar^2}{2m}\frac{d^2\Psi_n}{dx^2} = E_n\Psi_n \qquad 3.4$$

where E_n, is the energy of the electron in the orbital. We use the term orbital to denote a solution of the wave equation for a system of only one electron. Note that this is a one-electron equation, which means that we neglect the electron-electron interactions. The boundary conditions are $\Psi_n(0) = 0$ and $\Psi_n(L) = 0$, as imposed by the infinite potential energy barriers i.e the electron present inside the box of dimension L. The general solution of equation (3.4) is:

$$\Psi_n(x) = Ae^{ikx} + Be^{-ikx} \quad 3.5$$

where

$$k^2 = \frac{2m}{\hbar^2} E_n \quad 3.6$$

A = -B obtained by substituting the first boundary condition $\psi_n = 0$ and this shows that the wave function takes the sine like shape. Applying the second boundary condition $\psi(L) = 0$, yields $sinkL = 0$

where $k = n\pi/L$

On substituting in equation (3.6), yields E_n

$$E_n = \frac{\hbar^2}{2m}\left(\frac{n\pi}{L}\right)^2 \quad 3.7$$

And their corresponding wave function representation is

$$\Psi_n = Asin\left(\frac{n\pi x}{L}\right) \quad 3.8$$

We want to accommodate N electrons on the line. According to the Pauli Exclusion Principle, no two electrons can have all their quantum numbers identical. That is, each orbital can be occupied by at most one electron. This applies to electrons in atoms, molecules, or solids (Kittel, 2005). This model is frequently used when analyzing metals. However, this model does not work well for semiconductors since the effect of the periodic potential due to the atoms in the crystal has been ignored.

3.2.2 Allowed and Forbidden Energy Bands

3.2.2.1 Formation of Energy Bands

Figure 3.2a, shows the radial probability density function for the lowest electron energy state of the single, non-interacting hydrogen atom, and Figure 3.2b, shows the same probability curves for two atoms that are in close proximity to each other. The wave functions of the two atom electrons overlap, which means that the two electrons will interact.

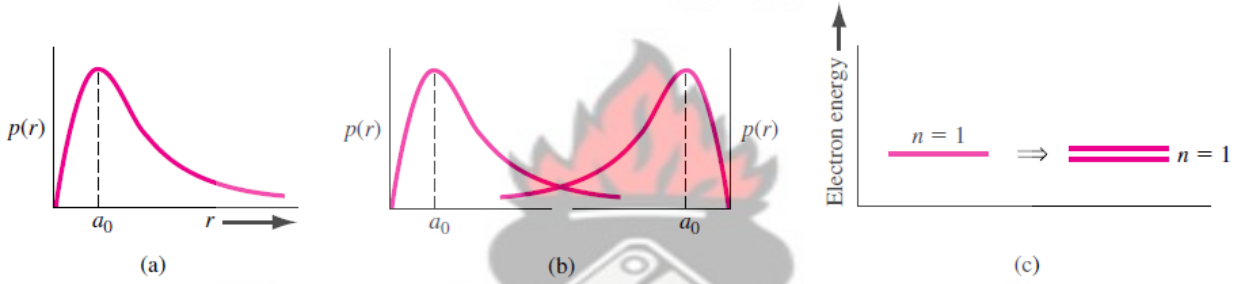

Figure 3.2: (a) Probability density function of an isolated hydrogen atom. (b) Overlapping probability density functions of two adjacent hydrogen atoms. (c) The splitting of the $n = 1$ state (Neamen, 2001).

This interaction or perturbation results in the discrete quantized energy level splitting into two discrete energy levels, schematically shown in Figure 3.2c. The splitting of the discrete state into two states is consistent with the Pauli Exclusion Principle (Neamen, 2001). Consider again a regular periodic arrangement of atoms, in which each atom now contains more than one electron. Suppose the atom in this imaginary crystal contains electrons up through the $n = 3$ energy level. If the atoms are initially very far apart (their nuclei are sufficiently far apart and do not influence each other), the electrons in adjacent atoms will not interact and will occupy the discrete energy levels. If these atoms are brought closer together, the outermost electrons in the $n = 3$ energy

shell will begin to interact initially, so that this discrete energy level will split into a band of allowed energies.

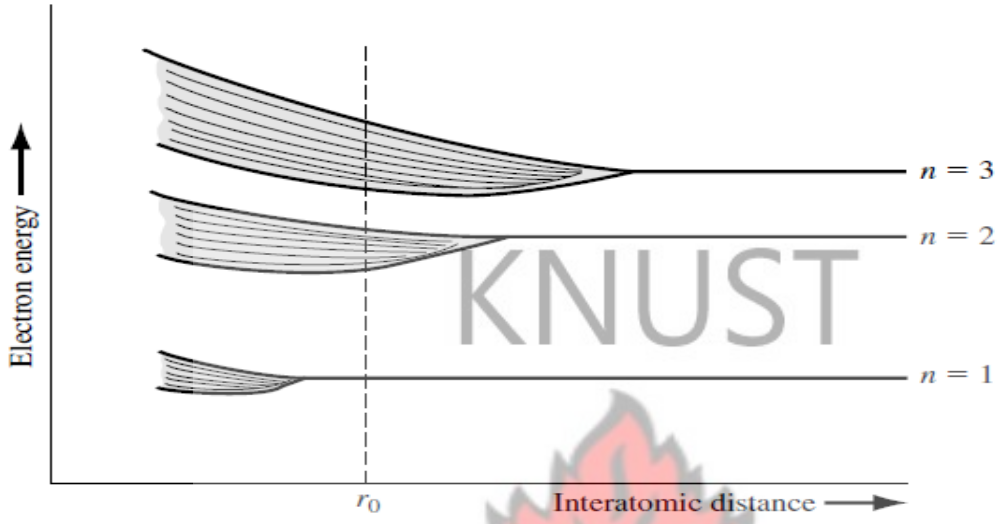

Figure 3.3: Schematic showing the splitting of three energy states into allowed bands of energies (Bhattacharya and Bhaskaran, 2010)

If the atoms continue to move closer together, the electrons in the $n = 2$ shell may begin to interact and will also split into a band of allowed energies. Finally, if the atoms become sufficiently close together, the innermost electrons in the $n = 1$ level may interact, so that this energy level may also split into a band of allowed energies (Bhattacharya and Bhaskaran, 2010; Neamen, 2001). The splitting of these discrete energy levels is qualitatively shown in Figure 3.3. If the equilibrium interatomic distance is r_0, then we have bands of allowed energies that the electrons may occupy separated by bands of forbidden energies. This energy-band splitting and the formation of allowed and forbidden bands is the energy-band theory of single-crystal materials. The actual band splitting in a crystal is much more complicated than indicated in Figure 3.3 (Altmann, 1994).

3.2.2.2 The Kronig -Penney Model

In the previous section splitting of allowed electron energies was discussed as atoms are brought together to form a crystal. The concept of allowed and forbidden energy bands can be developed more rigorously by considering quantum mechanics and Schrodinger's wave equation (Neamen, 2001). The potential function of a single, noninteracting, one-electron atom is shown in Figure 3.4a. Also indicated on the figure are the discrete energy levels allowed for the electron. Figure 3.4b, shows the same type of potential function for the case when several atoms are in close proximity arranged in a one-dimensional array. The potential functions of adjacent atoms overlap, and the net potential function for this case is shown in Figure 3.4c. It is this potential function we would need to use in Schrodinger's wave equation to model a one-dimensional single crystal material (Bhattacharya and Bhaskaran, 2010). The solution to Schrodinger's wave equation, for this one-dimensional single crystal lattice, is made more tractable by considering a simpler potential function.

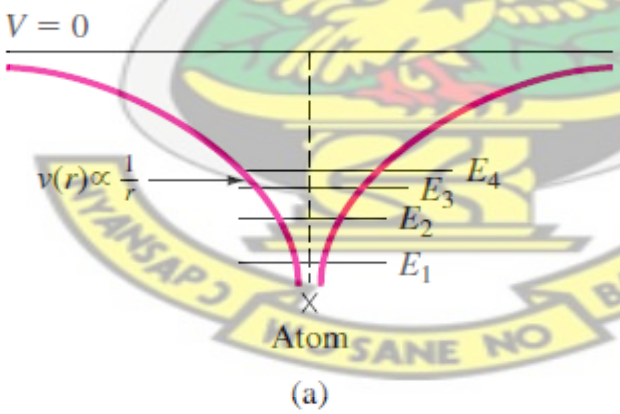

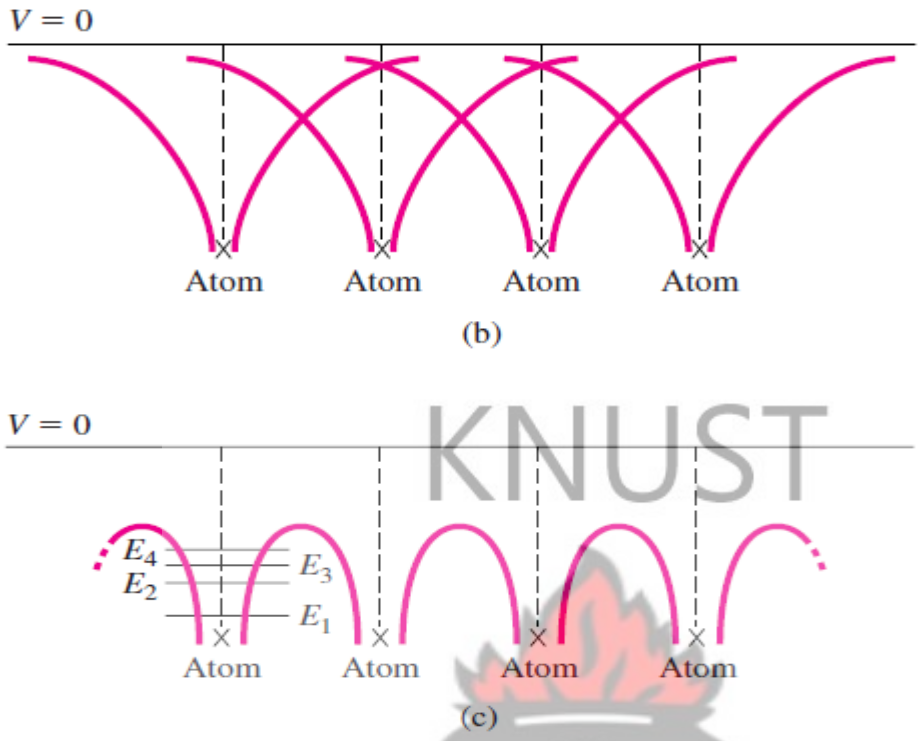

Figure 3.4: (a) Potential function of a single isolated atom. (b) Overlapping potential functions of adjacent atoms. (c) Net potential function of a one-dimensional single crystal (Neamen, 2001)

Figure 3.5 is the one-dimensional Kronig–Penney model of the periodic potential function, which is used to represent a one-dimensional single-crystal lattice.

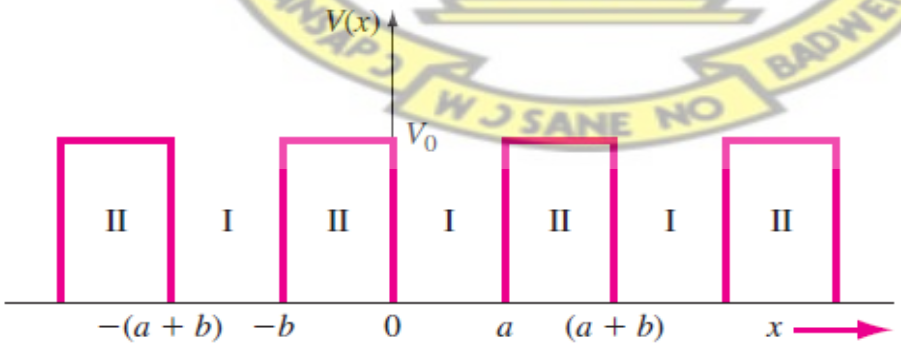

Figure 3.5: The one-dimensional periodic potential function of the Kronig–Penney model

Schrodinger's wave equation should solve in each region. As with previous quantum mechanical problems, the more interesting solution occurs for the case when $E < V_0$, which corresponds to a particle being bound within the crystal. The electrons are contained in the potential wells, but we have the possibility of tunneling between wells. The Kronig–Penney model is an idealized periodic potential representing a one-dimensional single crystal, but the results will illustrate many of the important features of the quantum behavior of electrons in a periodic lattice. To obtain the solution to Schrodinger's wave equation, let us apply Bloch theorem. The theorem states that all one-electron wave functions, for problems involving periodically varying potential energy functions, must be of the form

$$\psi(x) = u(x)e^{jkx} \tag{3.9}$$

The parameter *k* is called a constant of motion and the function *u(x)* is a periodic function with period *(a + b).* The total solution to the wave equation is the product of the time-independent solution and the time-dependent solution i.e.

$$\Psi(x,t) = \psi(x)\phi(t) = u(x)e^{jkx}.e^{-j(E/\hbar)t} \tag{3.10}$$

which may be written as

$$\Psi(x,t) = u(x)e^{j[kx-(E/\hbar)t]} \tag{3.11}$$

This traveling-wave solution represents the motion of an electron in a single-crystal material. The amplitude of the traveling wave is a periodic function and the parameter *k* is also referred to as a wave number. We can now begin to determine a relation between the parameter *k*, the total energy *E*, and the potential V_0. If we consider region I in Figure 3.5, (0 < x < a) in which *V(x)* =

0, take the second derivative of equation (3.9), and substitute this result into the time-independent Schrodinger's wave equation and yield the relation

$$\frac{d^2u_1(x)}{dx^2} + 2jk\frac{du_1(x)}{dx} - (k^2 - \alpha^2)u_1(x) = 0 \qquad 3.12$$

The function $u_1(x)$ is the amplitude of the wave function in region I and the parameter α is defined as

$$\alpha^2 = \frac{2mE}{\hbar^2} \qquad 3.13$$

Consider now a specific region II, $-b < x < 0$, in which $V(x) = V_0$, and apply Schrodinger's wave equation then we obtain the relation

$$\frac{d^2u_2(x)}{dx^2} + 2jk\frac{du_2(x)}{dx} - \left(k^2 - \alpha^2 + \frac{2mV_0}{\hbar^2}\right)u_2(x) = 0 \qquad 3.14$$

where $u_2(x)$ is the amplitude of the wave function in region II. We may define

$$\frac{2m}{\hbar^2}(E - V_0) = \alpha^2 - \frac{2mV_0}{\hbar^2} = \beta^2 \qquad 3.15$$

so that equation (3.14) may be written as

$$\frac{d^2u_2(x)}{dx^2} + 2jk\frac{du_2(x)}{dx} - (k^2 - \beta^2)u_2(x) = 0 \qquad 3.16$$

Note that from equation (3.15), if $E > V_0$, the parameter β is real, whereas if $E < V_0$, then β is imaginary. The solution to equation (3.12), for region I, is of the form

$$u_1(x) = Ae^{j(\alpha-k)x} + Be^{-j(\alpha+k)x} \qquad for\ 0 < x < a \qquad 3.17$$

and the solution to equation (3.16), for region II, is of the form

$$u_2(x) = Ce^{j(\beta-k)x} + De^{-j(\beta+k)x} \qquad for\ -b < x < 0 \qquad 3.18$$

Since the potential function $V(x)$ is everywhere finite, both the wave functions $\psi(x)$ and its first derivative $\partial\psi(x)/\partial x$ must be continuous. This continuity condition implies that the wave

amplitude function $u(x)$ and its first derivative $\partial u(x)/\partial x$ must also be continuous. If we consider the boundary at $x = 0$ and apply the continuity condition to the wave amplitude, we have

$$u_1(0) = u_2(0) \tag{3.19}$$

Substituting equations (3.17), and (3.18), into equation (3.19), to obtain

$$A + B - C - D = 0 \tag{3.20}$$

Now applying the condition that

$$\frac{du_1}{dx} = \frac{du_2}{dx} \quad at\ x = 0 \tag{3.21}$$

It yield

$$(\alpha - k)A - (\alpha + k)B - (\beta - k)C + (\beta + k)D = 0 \tag{3.22}$$

Let us considered region I as $0 < x < a$ and region II as $-b < x < 0$. The periodicity and the continuity condition mean that the function u_1, as $x \rightarrow a$, is equal to the function u_2, as $x \rightarrow -b$. This condition may be written as

$$u_1(a) = u_2(-b) \tag{3.23}$$

Applying the solutions for $u_1(x)$ and $u_2(x)$ to the boundary condition in equation (3.23), yields

$$Ae^{j(\alpha-k)a} + Be^{-j(\alpha+k)a} - Ce^{-j(\beta-k)b} - De^{j(\beta+k)b} = 0 \tag{3.24}$$

The last boundary condition is

$$\frac{du_1}{dx} = \frac{du_2}{dx} \tag{3.25}$$

In equation (3.24), x = a for first derivative and x = -b for second derivative, then it gives

$$(\alpha - k)Ae^{j(\alpha-k)a} + (\alpha + k)Be^{-j(\alpha+k)a} - (\beta - k)Ce^{-j(\beta-k)b} + (\beta + k)De^{j(\beta+k)b} = 0 \tag{3.26}$$

We now have four homogeneous equations, equations (3.20), (3.22), (3.24), and (3.26), with four unknowns as a result of applying the four boundary conditions. In a set of simultaneous, linear, homogeneous equations, there is a nontrivial solution if, and only if, the determinant of the

coefficients is zero. In our case, the coefficients in question are the coefficients of the parameters *A*, *B*, *C*, and *D*. The evaluation of this determinant is extremely laborious and will not be considered in detail. The result is

$$\frac{-(\alpha^2+\beta^2)}{2\alpha\beta}(sin\alpha a)(sin\beta b)+(cos\alpha a)(cos\beta b)=cosk(a+b) \qquad 3.27$$

Equation (3.27), relates the parameter *k* to the total energy *E* (through the parameter α) and the potential function V_0 (through the parameter β). As mentioned earlier, the more interesting solutions occur for $E < V_0$, which applies to the electron bound within the crystal. From equation (3.15), the parameter β is an imaginary quantity and define as:

$$\beta = j\gamma \qquad 3.28$$

where γ is a real quantity. Equation (3.27), can be written in terms of γ as

$$\frac{\gamma^2-\alpha^2}{2\alpha\gamma}(sin\alpha a)(sinh\gamma b)+(cos\alpha a)(cosh\gamma b)=cosk(a+b) \qquad 3.29$$

Equation (3.29) does not lend itself to an analytical solution, but must be solved using numerical or graphical techniques to obtain the relation between *k*, *E*, and V_0. The solution of Schrodinger's wave equation for a single bound particle resulted in discrete allowed energies. The solution of equation (3.29) will result in a band of allowed energies.

To obtain an equation that is more susceptible to a graphical solution and thus will illustrate the nature of the results, let the potential barrier width $b \rightarrow 0$ and the barrier height $V_0 \rightarrow \infty$, but such that the product bV_0 remains finite. Equation (3.29), then reduces to

$$\left(\frac{mV_0ba}{\hbar^2}\right)\frac{sin\alpha a}{\alpha a}+cos\alpha a=coska \qquad 3.30$$

We may define a parameter $\boldsymbol{P'}$as

$$\boldsymbol{P'}=\frac{mV_0ba}{\hbar^2} \qquad 3.31$$

Then, finally, the following relation is obtained

$$P' \frac{sin\alpha a}{\alpha a} + cos\alpha a = coska \qquad 3.32$$

Equation (3.32), again gives the relation between the parameter k, total energy E (through the parameter α), and the potential barrier bV_0. We may note that equation (3.32) is not a solution of Schrodinger's wave equation but gives the conditions for which Schrodinger's wave equation will have a solution. If we assume the crystal is infinitely large, then k in equation (3.32), can assume a continuum of values and must be real (Neamen, 2001).

3.2.2.3 The K-Space Diagram

To begin to understand the nature of the solution, initially consider the special case for which $V_0 = 0$. In this case $P' = 0$, which corresponds to a free particle since there are no potential barriers. From equation (3.32), we have that

$$cos\alpha a = coska \qquad 3.33$$

or

$$\alpha = k \qquad 3.34$$

Since the potential is equal to zero, the total energy E is equal to the kinetic energy, so that, equation (3.13), and equation (3.34), may be written as

$$\alpha = \sqrt{\frac{2mE}{\hbar^2}} = \sqrt{\frac{2m(1/2mV^2)}{\hbar^2}} = \frac{P}{\hbar} = k \qquad 3.35$$

where p is the particle momentum. The constant of the motion parameter k is related to the particle momentum for the free electron. The parameter k is also referred to as a wave number. Energy and momentum can also relate as

$$E = \frac{p^2}{2m} = \frac{k^2\hbar^2}{2m} \qquad 3.36$$

Figure 3.6, shows the parabolic relation of equation (3.36), between the energy E and momentum P for the free particle. Since the momentum and wave number are linearly related, Figure 3.6 is

also the *E* versus *k* curve for the free particle. We now want to consider the relation between *E* and *k* from equation (3.32), for the particle in the single-crystal lattice. As the parameter $\boldsymbol{P'}$ increases, the particle becomes more tightly bound to the potential well or atom. The left side of equation (3.32), may be define to be a function *f (αa)*, so that

$$f(\alpha a) = \boldsymbol{P'}\frac{\sin\alpha a}{\alpha a} + \cos\alpha a \qquad 3.37$$

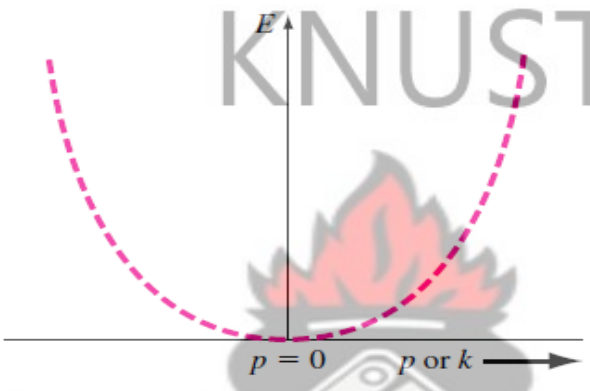

Figure 3.6: The parabolic *E* versus *k* curve for the free electron

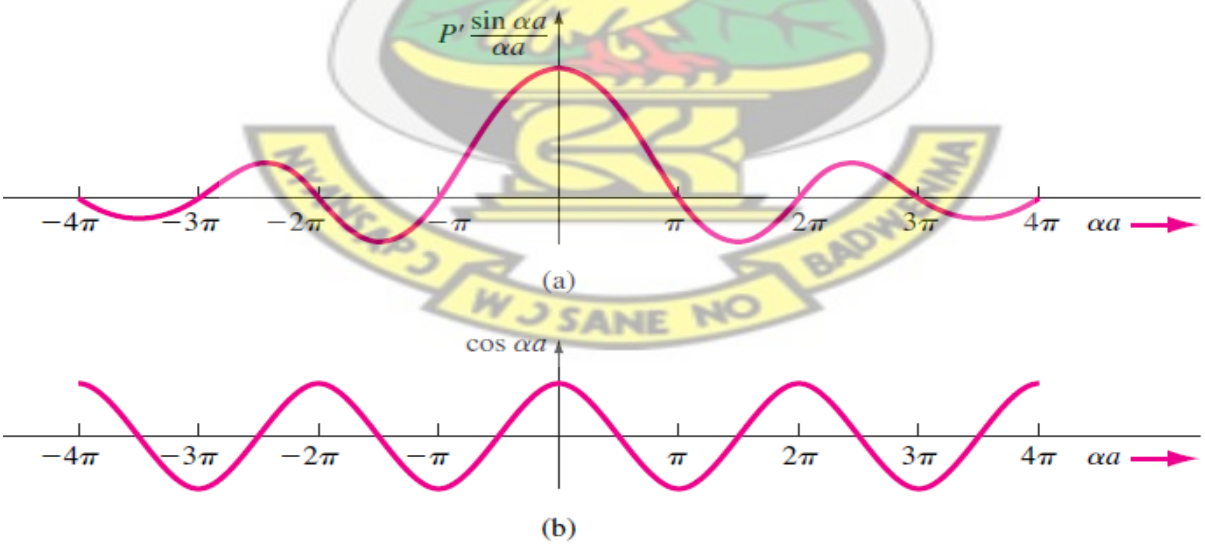

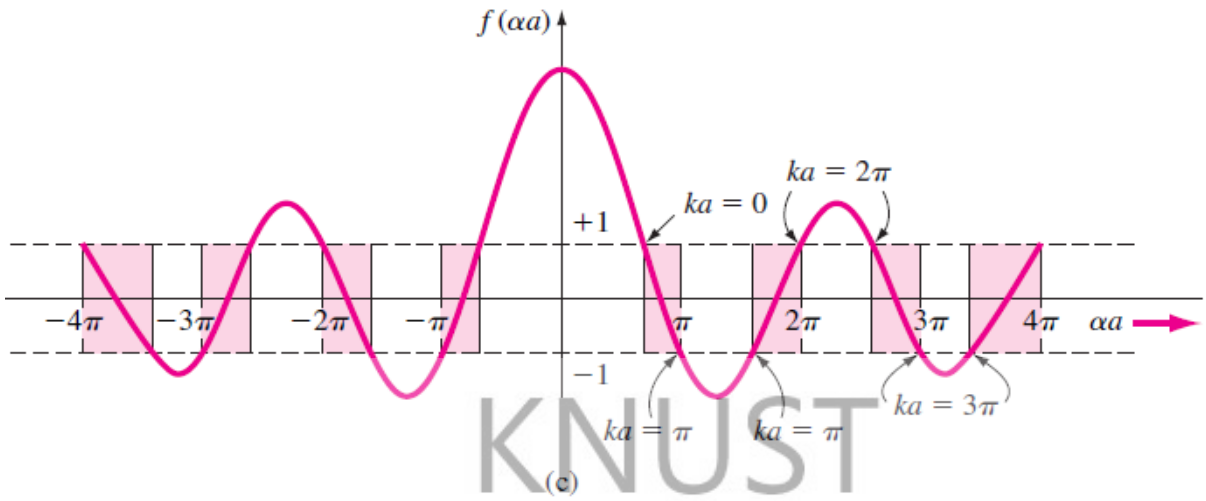

Figure 3.7: A plot of (a) the first term in equation (3.37), (b) the second term in equation (3.37), and (c) the entire *f (αa)* function. The shaded areas show the allowed values of *(αa)* corresponding to real values of *k* (Neamen, 2001)

Figure 3.7a, is a plot of the first term of equation (3.29), versus *αa*. Figure 3.7b, shows a plot of the cos *αa* term and Figure 3.7c, is the sum of the two terms, or *f (αa)*. Now from equation (3.32), we also have that

$$f(\alpha a) = coska \qquad 3.38$$

For equation (3.38), to be valid, the allowed values of the *f (αa)* function must be bounded between +1 and −1 (Grundmann, 2010). Figure 3.7c, shows the allowed values of *f (αa)* and the allowed values of *αa* in the shaded areas. Also shown on the figure are the values of *ka* from the right side of equation (3.38), which correspond to the allowed values of *f (αa)*.The parameter α is related to the total energy *E* of the particle through equation (3.13), which is $\alpha^2 = 2mE/\hbar^2$. A plot of the energy *E* of the particle as a function of the wave number *k* can be generated from Figure 3.7c. Figure 3.8, shows this plot and shows the concept of allowed energy bands for the particle

propagating in the crystal lattice. Since the energy E has discontinuities, we also have the concept of forbidden energies for the particles in the crystal.

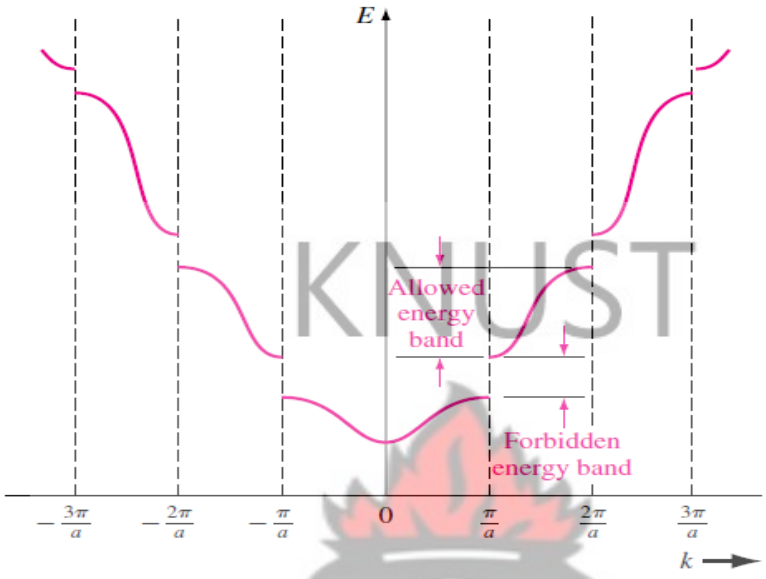

Figure 3.8: The E versus k diagram generated from Figure 3.7. The allowed energy bands and forbidden energy band gaps are indicated (Neamen, 2001)

Consider again the right side of equation (3.32), which is the function cos ka. The cosine function is periodic so that

$$\cos ka = \cos(ka + 2n\pi) = \cos(ka - 2n\pi) \qquad 3.39$$

where n is a positive integer. Let us consider Figure 3.8, and displace portions of the curve by 2π. Mathematically, equation (3.32) is still satisfied. Figure 3.9a shows how various segments of the curve can be displaced by the 2π factor. Figure 3.9b, shows the case in which the entire E versus k plot is contained within $-\pi/a < k < \pi/a$. This plot is referred to as a reduced k-space diagram, or a reduced-zero representation. We noted in equation (3.35), that for a free electron, the particle momentum and the wave number k are related by $p = \hbar k$. Given the similarity between

the free electron solution and the results of the single crystal shown in Figure 3.8, the parameter $\hbar k$ in a single crystal is referred to as the crystal momentum.

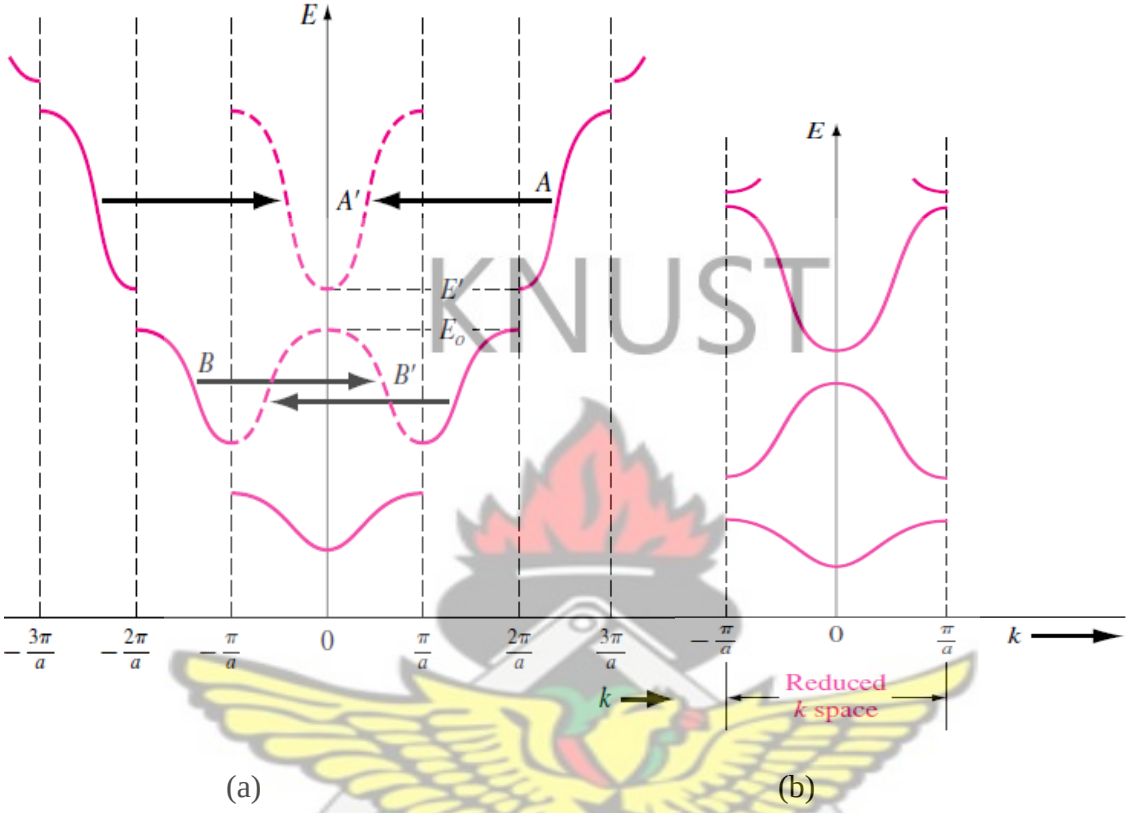

Figure 3.9: (a) The *E* versus *k* diagram showing 2π displacements of several sections of allowed energy bands (b) The *E* versus *k* diagram in the reduced-zone representation (Bhattacharya and Bhaskaran, 2010).

This parameter is not the actual momentum of the electron in the crystal, but it is a constant of the motion that includes the crystal interaction (Bhattacharya and Bhaskaran, 2010; Neamen, 2001).

Kronig–Penney model, which is a one dimensional periodic potential function used to model a single-crystal lattice. The principle result of this analysis, so far, is that electrons in the crystal occupy certain allowed energy bands and are excluded from the forbidden energy bands. For real three-dimensional single-crystal materials, a similar energy-band theory exists (Neamen, 2001).

Although the Kronig-Penney model presented here shows clearly the existence of allowed and forbidden energy bands and at the same time gives us a mathematical expression with which to find the *E* versus *k* curves, it does not give much physical insight for the existence of these bands. Moreover, as presented here, it does not answer a question that will be important in the understanding of the difference between conductors, insulators, and semiconductors. The question is: *How many energy states are allowed within a given band?* The answer so far seems to be an infinite number because within a band *y* can vary continuously. It would seem, therefore, that *E* can take an infinite, continuous range of values within an allowed band. The reason for this result is that in the periodic potential model we have assumed that the periodicity is infinitely long (Altmann, 1994).

3.3 FERMI LEVEL AND CARRIER CONCENTRATION

3.3.1 Fermi-Dirac Function

Electrons in solids obey Fermi-Dirac statistics in the development of this type of statistics; one must consider the indistinguishability of the electrons, their wave nature, and the Pauli Exclusion Principle. The rather simple result of these statistical arguments is that the distribution of electrons over a range of allowed energy levels at thermal equilibrium is

$$f(E) = \frac{1}{1+e^{(E-E_F)/kT}} \qquad 3.40$$

Where *k* is Boltzmann's constant (k = 8.62 x 10^{-5} eV/K = 1.38 X 10^{-23} J/K). The function $f(E)$ is called Fermi-Dirac distribution function which gives the probability that an available energy state at *E* will be occupied by an electron at absolute temperature *T*. The quantity E_F is called the Fermi level, and it represents an important quantity in the analysis of semiconductor behavior. For an energy *E* equal to the Fermi level energy E_F, the occupation probability is

$$f(E) = [1 + e^{(E_F - E_F)/kT}]^{-1} = \frac{1}{2} \quad 3.41$$

Thus an energy state at the Fermi level has a probability of ½ of being occupied by an electron. A closer examination of $f(E)$ indicates that at 0 K the distribution takes the simple rectangular form shown in Figure 3.10. With $T = 0$ in the denominator of the exponent, $f(E)$ is $1/(1 + 0) = 1$ when the exponent is negative $(E < E_F)$, and is $1/(1 + \infty) = 0$ when the exponent is positive $(E > E_F)$. This rectangular distribution implies that at 0 K every available energy state up to E_F is filled with electrons, and all states above E_F are empty. At temperatures higher than 0 K, some probability exists for states above the Fermi level to be filled. For example, at $T = T_1$ in Figure 3.10, there is some probability $f(E)$ that states above E_F are filled, and there is a corresponding probability $[1 - f(E)]$ that states below E_F are empty.

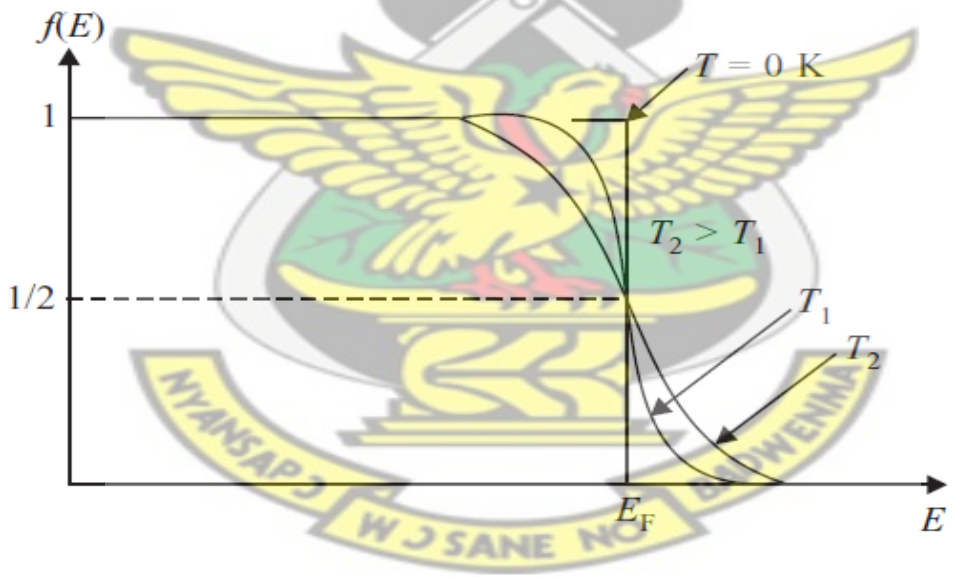

Figure 3.10: The Fermi-Dirac distribution function

In applying the Fermi-Dirac distribution to semiconductors, we must recall that $f(E)$ is the probability of occupancy of an *available* state at *E*. Thus if there is no available state at *E* (e.g., in the band gap of a semiconductor), there is no possibility of finding an electron there. We can

best visualize the relation between $f(E)$ and the band structure by turning the E verses $f(E)$ diagram on its side so that the E scale corresponds to the energies of the band diagram see Figure 3.11. For intrinsic material it is know that the concentration of holes in the valence band is equal to the concentration of electrons in the conduction band. Therefore, the Fermi level E_F must lie at the middle of the band gap in intrinsic material see Figure 3.11a. In n-type material there is a high concentration of electrons in the conduction band compared with the hole concentration in the valence band. Thus in n-type material the distribution function $f(E)$ must lie above its intrinsic position on the energy scale (Figure 3.11b) (Streetman and Banerjee, 2006). Since $f(E)$ retains its shape for a particular temperature, the larger concentration of electrons at E_c in n-type material implies a correspondingly smaller hole concentration at E_v. It is noticed that the value of $f(E)$ for each energy level in the conduction band (and therefore the total electron concentration n_0) increases as E_F moves closer to E_c, thus the energy difference (E_c - E_F) gives a measure of n.

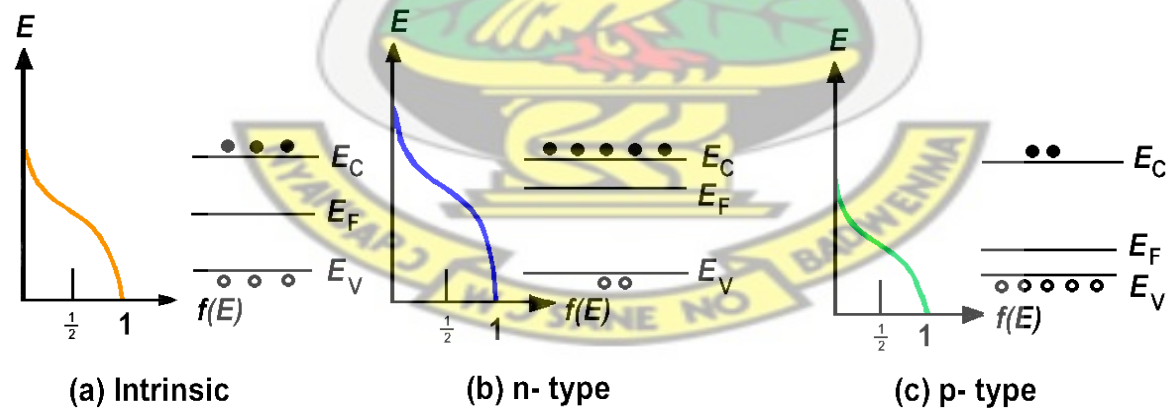

Figure 3.11: The Fermi distribution function applied to semiconductors: (a) intrinsic material; (b) n-type material; (c) p-type material

For p-type material the Fermi level lies near the valence band (Figure 3.11c), such that the [1 - $f(E)$] tail below E_v is larger than the $f(E)$ tail above E_c. The value of $(E_F - Ev)$ indicates how strongly p-type the material is (Kwok *et al.*, 2007; Streetman and Banerjee, 2006).

3.3.2 Electron and Hole Concentrations at Equilibrium

The Fermi distribution function can be used to calculate the concentrations of electrons and holes in a semiconductor, if the densities of available states in the valence and conduction bands are known. For example, the concentration of electrons in the conduction band is

$$n_0 = \int_{E_c}^{\infty} N(E) f(E) dE \qquad 3.42$$

where $N(E)dE$ is the density of states (cm^{-3}) in the energy range dE. The subscript 0 used with the electron and hole concentration symbols (n_0, p_0) indicates equilibrium conditions. The number of electrons per unit volume in the energy range dE is the product of the density of states and the probability of occupancy $f(E)$. Thus the total electron concentration is the integral over the entire conduction band, as in equation (3.42). Since $N(E)$ is proportional to $E^{1/2}$, the density of states in the conduction band increases with electron energy. On the other hand, the Fermi function becomes extremely small for large energies. The result is that the product $f(E)N(E)$ decreases rapidly above E_c, and very few electrons occupy energy states far above the conduction band edge. Similarly, the probability of finding an empty state (hole) in the valence band [1 - $f(E)$] decreases rapidly below E_v, and most holes occupy states near the top of the valence band (Kwok and Sze, 2007).

This effect is demonstrated in Figure 3.12, which shows the density of available states, the Fermi function, and the resulting number of electrons and holes occupying available energy states in the conduction and valence bands at thermal equilibrium (i.e., with no excitations except thermal

energy). For holes, increasing energy points down in Figure 3.12, since the E scale refers to electron energy. The result of the integration of equation (3.42) is the same as that obtained if we represent all of the distributed electron states in the conduction band by an effective density of states N_c located at the conduction band edge E_c. Therefore, the conduction band electron concentration is simply the effective density of states at E_c times the probability of occupancy at E_c.

$$n_0 = N_c f(E_c) \qquad 3.43$$

In this expression we assume the Fermi level E_F lies at least several kT below the conduction band. Then the exponential term is large compared with unity, and the Fermi function $f(E_c)$ can be simplified as

$$f(E_c) = \frac{1}{1+e^{(E_c - E_F)/kT}} \cong e^{-(E_c - E_F)/kT} \qquad 3.44$$

Since kT at room temperature is only 0.026 eV, this is generally a good approximation. For this condition the thermal-equilibrium electron concentration in the conduction band can be written as:

$$n_0 = N_c\, e^{-(E_c - E_F)/kT} \qquad 3.45$$

The parameter N_c, is called the effective density of states function in the conduction band

$$N_c = 2\left(\frac{2\pi m_n^* kT}{h^2}\right)^{3/2} \qquad 3.46$$

By similar arguments, the thermal-equilibrium concentration of holes in the valence band is found as:

$$p_0 = N_v[1 - f(E_v)] \qquad 3.47$$

Where N_v is the effective density of states in the valence band. The probability of finding an empty state at E_v is

$$1 - f(E_v) = 1 - \frac{1}{1 + e^{(E_v - E_F)/KT}} \cong e^{-(E_c - E_F)/kT} \qquad 3.48$$

for E_F larger than E_v by several kT. From these equations, the thermal-equilibrium concentration of holes in the valence band may now be written as

$$p_0 = N_v e^{-(E_F - E_v)/kT} \qquad 3.49$$

The effective density of states in the valence band reduced to the band edge is

$$N_v = 2\left(\frac{2\pi m_p^* kT}{h^2}\right)^{3/2} \qquad 3.50$$

The magnitude of N_c is also on the order of 10^{19} cm^{-3} at T = 300 K for most semiconductors. The electron and hole concentrations predicted by equations (3.45) and (3.49) are valid whether the material is intrinsic or doped, provided thermal equilibrium is maintained (Kwok and Sze, 2007; Streetman and Banerjee, 2006; Sze, 1981).

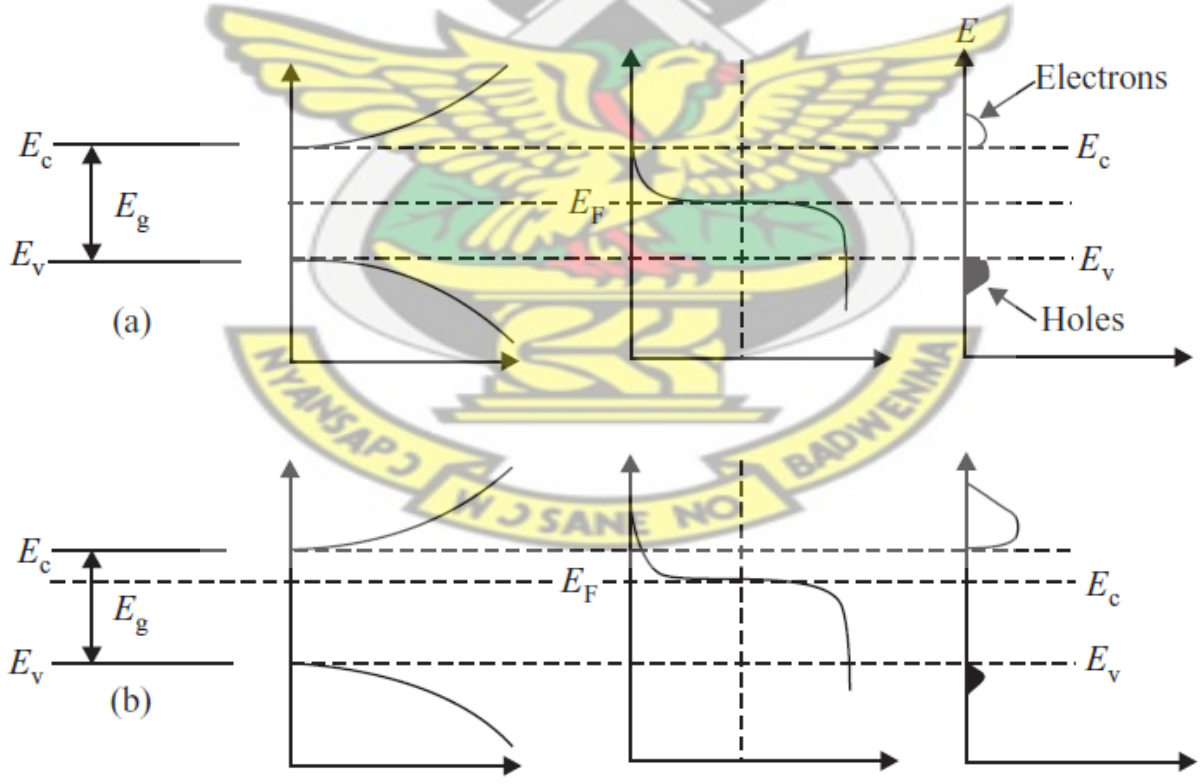

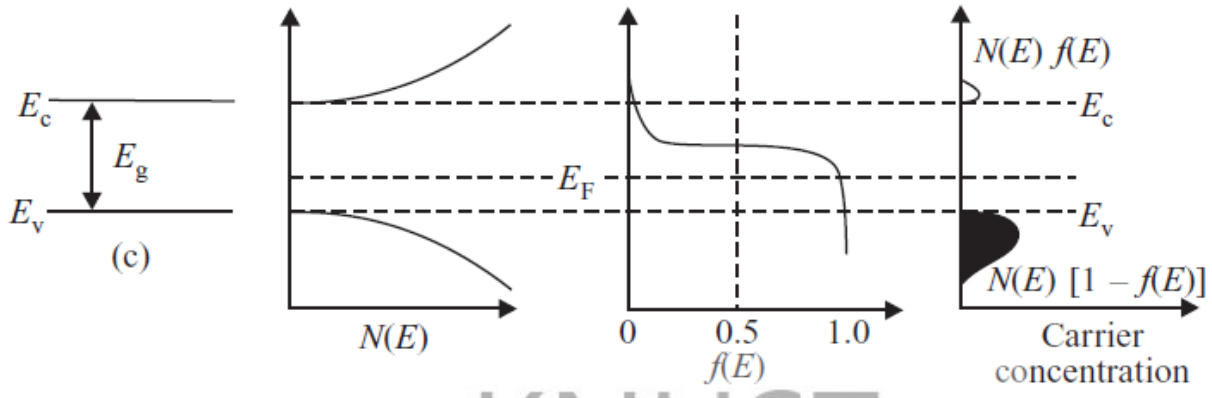

Figure 3.12: Thermal equilibrium band diagram, density of states, Fermi–Dirac distribution, and the carrier concentration for (a) intrinsic, (b) n-type, and (c) p-type semiconductors at thermal equilibrium (Bhattacharya and Bhaskaran, 2010)

3.3.3 The Intrinsic Carrier Concentration

For an intrinsic semiconductor, the concentration of electrons in the conduction band is equal to the concentration of holes in the valence band. We may denote n_i and p_i as the electron and hole concentrations, respectively, in the intrinsic semiconductor. These parameters are usually referred to as the intrinsic electron concentration and intrinsic hole concentration. Thus for intrinsic material, E_F lies at some intrinsic level E_i near the middle of the band gap and the intrinsic electron and hole concentrations are

$$n_i = N_c\, e^{-(E_c - E_i)/kT} \text{ and } p_i = N_v\, e^{-(E_i - E_v)/kT} \qquad 3.51$$

The product of n_0 and p_0 at equilibrium is a constant for a particular material and temperature, even if the doping is varied:

$$n_0 p_0 = (N_c\, e^{-(E_c - E_F)/kT})\,(N_v\, e^{-(E_F - E_v)/kT}) = N_c N_v\, e^{-(E_c - E_v)/kT}) \qquad 3.52a$$

$$= N_c N_v e^{-E_g/kT}$$

$$n_i p_i = (N_c\, e^{-(E_c - E_i)/kT})\,(N_v\, e^{-(E_i - E_v)/kT}) = N_c N_v e^{-E_g/kT} \qquad 3.52b$$

where E_g is the band gap energy. For a given semiconductor material at a constant temperature, the value of E_g, is a constant, and independent of the Fermi energy. The intrinsic electron and hole concentrations are equal (since the carriers are created in pairs), $n_i = p_i$ thus the intrinsic concentration is:

$$n_i = \sqrt{N_c N_v} e^{-E_g/2kT} \qquad 3.53$$

The constant product of electron and hole concentrations in equation (3.44), can be written conveniently as:

$$n_0 p_0 = n_i^2 \qquad 3.54$$

Comparing equations (3.51) and (3.52), we note that the intrinsic level E_i is the middle of the band gap *(E_c - E_i = Eg/2)*, if the effective densities of states N_c and N_v are equal (Colinge and Colinge, 2002; Sze, 1981).

3.3.4 Extrinsic Semiconductor

An extrinsic semiconductor is defined as a semiconductor in which controlled amounts of specific dopant or impurity atoms have been added so that the thermal-equilibrium electron and hole concentrations are different from the intrinsic carrier concentration. One type of carrier will predominate in an extrinsic semiconductor (Bhattacharya and Bhaskaran, 2010).

When the concept of doping was introduced, we assumed the material contained either N_d donors or N_a acceptors, so that the extrinsic majority carrier concentrations were $n_0 = N_d$ or $p_0 = N_a$ respectively, for the n-type or p-type material. It often happens, however, that a semiconductor contains both donors and acceptors. A semiconductor containing donor impurities is called an *N-type semiconductor,* since most of the carriers have a negative charge, and a semiconductor

containing acceptor impurities is called a *P-type semiconductor*, since most of the carriers have a positive charge. For example, Figure 3.13, illustrates a semiconductor for which both donors and acceptors are present, but $N_d > N_a$. The predominance of donors makes the material n-type. In fact, the filling of the E_a states occurs at the expense of the donated conduction band electrons. The mechanism can be visualized as follows: Assume an acceptor state is filled with a valence band electron with a hole resulting in the valence band.

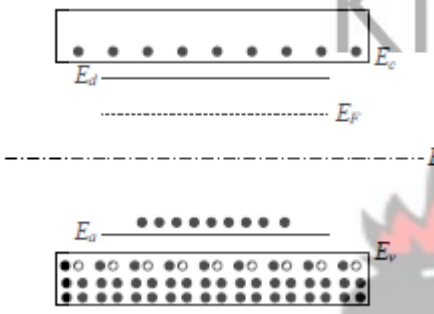

Figure 3.13: Compensation in an n-type semiconductor *($N_d > N_a$)* (Streetman and Banerjee, 2006)

This hole is then filled by recombination with one of the conduction band electrons. Extending this logic to all the acceptor atoms, we expect the resultant concentration of electrons in the conduction band to be N_d - N_a instead of the total N_d. This process is called *compensation.* By this process it is possible to begin with an *n-type* semiconductor and add acceptors until $N_a = N_d$ and no donated electrons remain in the conduction band. In such compensated material, $n_0 = n_i = p_0$ and intrinsic conduction is obtained. With further acceptor doping the semiconductor becomes p-type with a hole concentration of essentially $Na - N_d$ (Colinge and Colinge, 2002; Kwok and Sze, 2007).

3.4 OPTICAL ENERGY BAND GAP VARIATION WITH COMPOSITION IN ALLOY SEMICONDUCTORS

Semiconductor alloys, which are solid solutions of two or more semiconducting elements, have important technological applications. One of the easiest ways to change artificially the electronic and optical properties of semiconductors is by forming their alloy (Labidi *et al.*, 2009).

In alloy semiconductors, the size of the band gap and the character of the band gap will depend on the composition. The dependence of the band gap on the ternary composition is mostly nonlinear (Swafford *et al.*, 2006) and can usually be expressed with a bowing parameter *b* that is mostly positive. For a compound $A_xB_{1-x}C$ the band gap is written as

$$E_g(A_xB_{1-x}C) = E_g(BC) + x\left[E_g(AC) - E_g(BC)\right] - bx(1-x) \qquad 3.55$$

The Si_xGe_{1-x} alloy has diamond structure for all concentrations and the position of the conduction band minimum in **k**-space switches from L to X at about $x = 0.15$ (Figure 3.14a). However, for all concentrations the band structure is indirect. The $In_xGa_{1-x}As$ alloy has zincblende structure for all compositions. The band gap is direct and decreases with a bowing parameter of $b = 0.6$ eV (Figure 3.14b). This means that for $x = 0.5$ the band gap is 0.15 eV smaller than expected from a linear interpolation between GaAs and InAs, as reported by various authors (Grundmann, 2010).

If one binary end component has a direct band structure and the other is indirect, a transition occurs from direct to indirect at certain composition. An example is $Al_xGa_{1-x}As$ where GaAs is direct and AlAs is indirect. For all concentrations the crystal has zincblende structure. In Figure 3.14c, the Γ, L and X conduction band minima for ternary $Al_xGa_{1-x}As$ are shown. Up to an aluminum concentration of $x = 0.4$ the band structure is direct. Above this value the band structure is indirect with the conduction band minimum being at the X point. The particularity of

Al_xGa_{1-x} As is that the lattice constant is almost independent of *x*. If the two binary end components have different crystal structure, a phase transition occurs at a certain composition (range). An example is Mg_xZn_{1-x} O, where ZnO has wurtzite structure and MgO has rocksalt structure. The band gap is shown in Figure 3.14d. In this case, each phase has its own bowing parameter. All alloys of Figure 3.14b – d, have mixed cations. The band gap also varies upon anion substitution in a similar way as shown in Figure 3.15, for ternary alloys with the cation Zn and the chalcogenides S, Se, Te and O (Grundmann, 2010; Merita *et al.*, 2006).

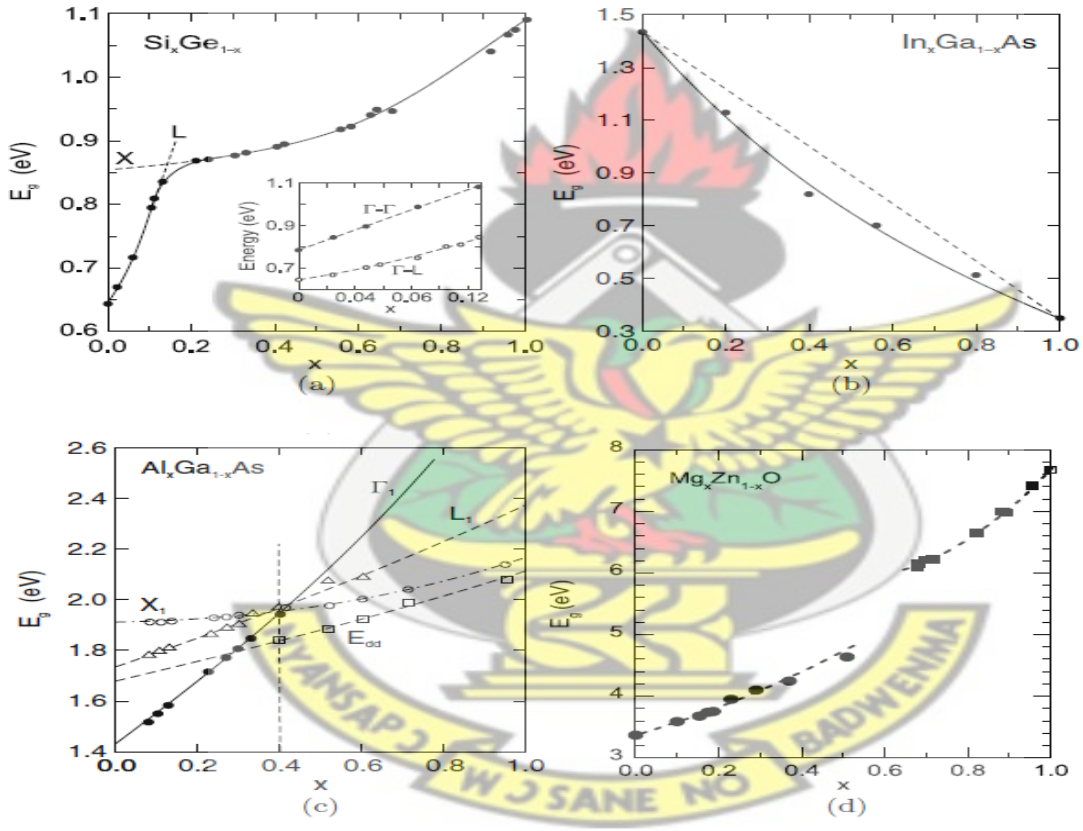

Figure 3.14: (a) Band gap of Si_xGe_{1-x} alloy (T = 296 K) with a change from the conduction band minimum at L (Ge-rich) to X. The *inset* depicts the transition energy of the indirect (Γ–L) and direct (Γ–Γ) absorption edge for low Si content. (b) Band gap (at room temperature) of In_xGa_{1-x} As. The *solid line* is an interpolation with bowing (b = 0.6 eV) and the *dashed line* is the linear interpolation. (c) Band gap (at room temperature) in the ternary system Al*x*Ga1−*x*As. For *x* <

0.4 the alloy is a direct, for $x > 0.4$ an indirect, semiconductor. E_{dd} denotes the energy position of a deep donor. (d) Band gap (at room temperature) in the ternary system $Mg_xZn_{1-x}O$. Data are for hexagonal wurtzite phase (*circles*), and Mg-rich cubic rocksalt phase (*squares*). *Dashed lines* are fits to data with a different bowing parameter for each phase (Grundmann, 2010)

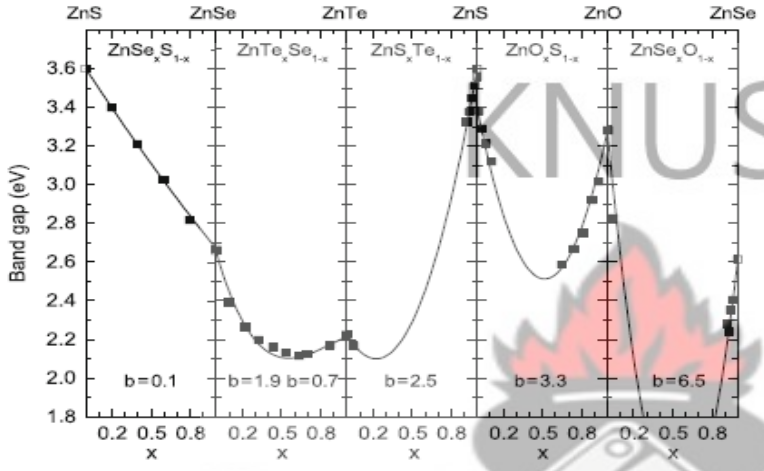

Figure 3.15: Band gap of various Zn-based alloys the bowing parameter *b* is labeled (Grundmann 2010)

3.5 QUANTUM SIZE EFFICTS

When we move from bulk material toward smaller and smaller aggregates, we realize that reaching certain dimensions one begins to enter a new regime where the particles start to experience changes in their properties compared to the bulk material (Mehta *et al.*, 2008). The nanomaterial domain is a bridge in between the two, implying that their properties lie between those of the bulk and the isolated molecules. From elemental quantum mechanics we know that, when the electronic particles or charge carriers (electrons and holes) are confined in a volume limited by potential barriers that are comparable or smaller than the de Broglie wavelength of the particle, their allowed energy states become discrete (quantized) rather than continuous as in the

bulk material (Margaret, 2009). Nanocrystalline semiconductors exhibit changes in the energy band structure, resulting in quantum size effects. Since the energy levels are confined to potential wells of small dimensions, the spacing between the energy levels increase as the crystal becomes smaller (Mark *et al.*, 1999). Therefore, the quantum size effects are dependent on the effective mass of the charge carriers. An analytical approximation for the lowest excited 1s state is given by

$$E^* \approx E_g + \frac{h^2}{8r^2}\left(\frac{1}{m_e} + \frac{1}{m_h}\right) - \frac{1.8q^2}{\varepsilon r} \qquad 3.56$$

where r is the crystal radius, m_e an effective mass of electrons and m_h an effective mass of holes. The second term shifts E^* to higher energy as r^2, and the third term shifts E^* to lower energy as r^{-1}. Thus, E^* always increases for small r. Other than the increase of the effective band gap, the discrete electronic states are created in the valence and conduction bands (Soga, 2006).

In semiconductor materials, the electric current is carried by electrons and holes. There is an energy gap or band gap (Figure 3.16) between the allowed energies of the electrons in the material that separates the normally filled energy levels of the valence band (where missing electrons behave like positively charged current carriers called "holes") and the conduction band (where electrons behave like a gas of free negatively charged carriers). The band gap width in between the two bands depends on the nature of the material, but also on temperature and pressure (Alivisatos, 1996). In bulk semiconductors, the two charge carriers are separated by the energy of the band gap. At low temperature, these two charge carriers form a weak coupled pair, which is called **exciton**. The energy of the exciton lies below the energy of the band gap of the semiconductor crystal because of the electrostatic Coulomb interaction (Alivisatos, 1996; Rhee *et al.*, 2013).

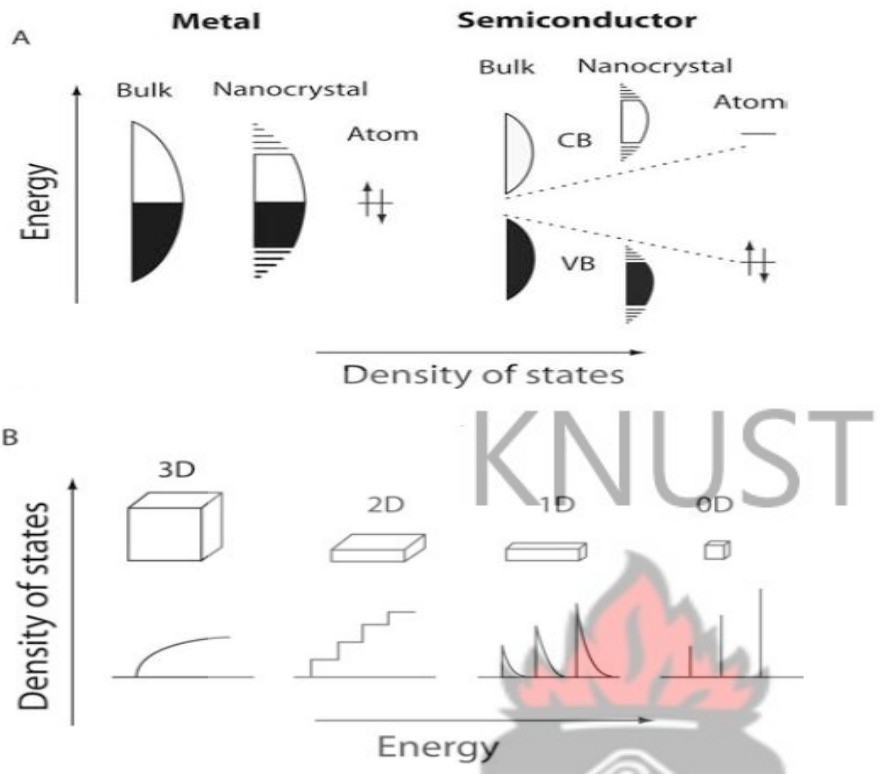

Figure 3.16: A) Schematic illustration of the density of states in metal and semiconductor clusters. For semiconductors, the dashed lines are showing the increasing band gap separations for bulk toward molecule, between valence band (VB) and conduction band (CB). B) Density of states in one band of a semiconductor as a function of the dimensional freedom. 3D represents the bulk, 2D quantum films, 1D quantum wires or fibers and 0D the zero dimensional quantum dots (Alivisatos, 1996)

Quantization depends on spatial confinement and can be classified in three different regimes: confinement in one, two or three dimensions. Confinement in one dimension produces quantum films, in two dimensions quantum wires and confinement in three dimensions produces quantum particles, often referred to as quantum dots, nanoparticles or nanocrystals. Fundamental differences exist between the three different quantization regimes, for example the density of states (DOS) as a function of the energy is quite different for each quantum system (Figure 3.16

B). For quantum films the DOS is a step function while for the quantum dots it is a series of discrete values resembling that of a molecule or an atom. Quantum wires have a DOS distribution that is intermediate between the quantum films and the quantum dots (Alivisatos, 1996). When the size of the bulk material is reduced in all 3 dimensions and approaches the value of the Bohr radius (a_B) of the bulk material, zero-dimension electronic system will appear (Grundmann, 2010).

3.6 SIZE QUANTIZATION OF CdSe AND PbSe COMPOUNDS

The size of the crystals formed in CD films is often small enough that quantum- size effects become apparent. The terms quantum size effect and size quantization are normally used to describe a material whose energy structure differs from that of the bulk material (Andersen *et al.*, 2002). CdSe nanocrystals and films are useful in understanding the phenomenon of quantum confinement effect (Hodes, 2002; Mehta *et al.*, 2007). The most easily observable effect is the blue shift of the optical absorption and emission of the semiconductor quantum dot with decreasing size resulting from the increasing band gap. For example, bulk CdSe has a band gap of 1.74 eV or 714 nm (Kanithla *et al.*, 1982), but when it is produced as quantum dots with average diameter of 1, 2 or 3 nm absorption onset will become 400, 480 or 540 nm (3.10, 2.58 or 2.29 eV) respectively, and emission spectra will be similarly shifted. Relation between optical band gap and wavelength in semiconductor materials is given as:

$$E(eV) = \frac{1.2398\,x\,10^3}{\lambda(nm)} \qquad 3.57$$

In chemically deposited CdSe films with grain sizes 5 < nm, optical band gap of up to 0.7 eV higher than the bulk value (of 1.74 eV) has been reported (Nair *et al.*, 1998). It is observed that

there is a certain critical ratio between the complexing agent and Cd ions concentration in the bath used for preparation of CdSe film, below certain concentration there was a pronounced blue shift. This observation was interrelated with decrease in crystal size (Gorer *et al.*, 1994).

PbSe nanocrystal also exhibit size quantization at relatively large crystal size (smaller than ca. 70 nm) due mainly to the small reduced effective electron/hole mass and, to a lesser extent, to the high dielectric constant which screens the electron/hole Coulomb interaction (this interaction opposes the charge localization) (Sarkar *et al.*, 2007). PbSe should show very low values of electron and hole effective masses (average electron, hole and reduced effective masses are 0.047, 0.041 and 0.022 respectively) for a crystalline size less than Bohrs diameter and increase in effective band gap due to size quantization and blue shifts in photoconductivity spectral response of evaporated PbTe and PbSe were attributed to small crystal size (Jadhav *et al.*, 2012). Since PbSe has a large exciton Bohr radius (46 nm), it offers the opportunity to achieve strong size quantization at relatively large crystal size and stronger quantum confinement with respect to II-VI and III-V semiconductor materials when they are in a similar nanoscale regime (Zhang *et al.*, 2011). Gorer *et al.* (1995), had studied quantum size effects in chemically deposited lead selenide films. They reported variation in band gap energies in the range from 0.55 to 1.55 eV and they showed that a wide range of different optical properties can be obtained with values of Eg ranging from 0.55 to 1.55 eV. Vorobiev *et al.* (2012) in their study observed the following blue shift values relative to the bulk material data in all cases: 0.06 eV for CdS, 0.15eV for CdSe and 0.1 to 0.4eV for different samples of PbS. An illustration of the size quantization effect is shown for a range of cluster sizes for different semiconductor particles in Figure 3.17 (Welle, 2004).

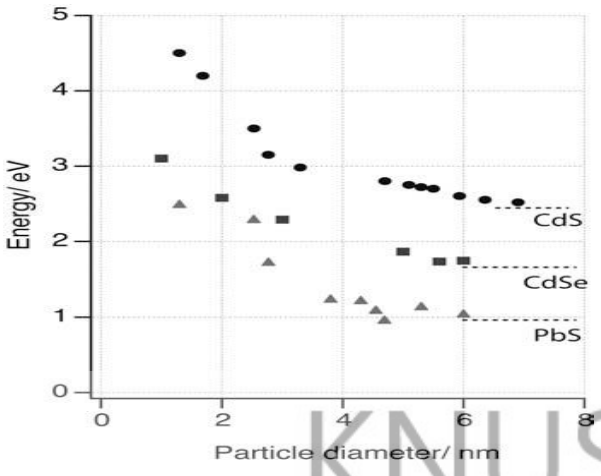

Figure 3.17: Illustration of the band gap energy changes in function of semiconductor nanoparticle diameter for PbS (triangles) and CdS (circles), and calculated for CdSe (squares) (Geissuhler, 2005)

3.6 TYPES OF SOLIDS

A crystalline solid is distinguished by the fact that the atoms making up the crystal are arranged in a periodic fashion. That is, there is some basic arrangement of atoms that is repeated throughout the entire solid. Thus the crystal appears exactly the same at one point as it does at a series of other equivalent points, once the basic periodicity is discovered. However, not all solids are crystals (Streetman and Banerjee, 2006). The periodicity in a crystal is defined in terms of a symmetric array of points in space called the lattice. We can add atoms at each lattice point in an arrangement called a basis, which can be one atom or a group of atoms having the same spatial arrangement, to get a crystal. In every case, the lattice contains a volume or cell that represents the entire lattice and is regularly repeated throughout the crystal. Amorphous, polycrystalline, and single crystal are the three general types of solids. Each type is characterized by the size of an ordered region within the material. An ordered region is a spatial volume in which atoms or

molecules have a regular geometric arrangement or periodicity amorphous materials have order only within a few atomic or molecular dimensions (Neamen, 2001), while polycrystalline materials have a high degree of order over many atomic or molecular dimensions. An important parameter is the grain size and its distribution (Streetman and Banerjee, 2006). It can be influenced via processing steps such as annealing. Polycrystalline semiconductors are used in cheap, large-area applications such as solar cells (e.g. polysilicon, $CuInSe_2$) or thin film transistors (poly-Si) or as n-conducting contact material in MOS diodes (poly-Si). Polycrystalline material can be fabricated from amorphous material using annealing procedures (Grundmann, 2010).

The single crystal regions are called grains and are separated from one another by grain boundaries. Single crystal materials, ideally, have a high degree of order, or regular geometric periodicity, throughout the entire volume of the material. The advantage of a single crystal material is that, in general, its electrical properties are superior to those of a non single crystal material, since grain boundaries tend to degrade the electrical characteristics (Neamen, 2001). Two-dimensional representations of amorphous, polycrystalline, and single crystal materials are shown in Figure 3.18.

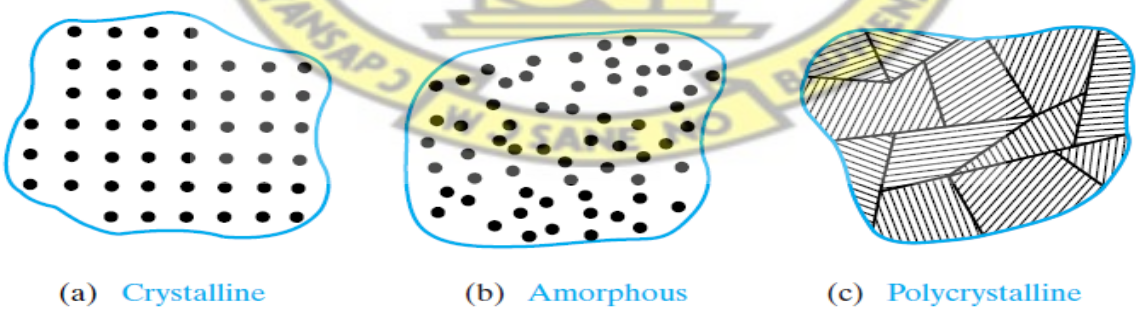

Figure 3.18: (a) crystalline and (b) amorphous materials are illustrated by microscopic views of the atoms, whereas (c) polycrystalline structure is illustrated by a more macroscopic view of adjacent single crystalline regions, such as (a) (Streetman and Banerjee, 2006)

Chapter 4

4. THIN FILM CHARACTERIZATION METHODS

4.1 INTRODUCTION

Scientific disciplines are identified and differentiated by the experimental equipment and measurement techniques they employ. The same is true for thin film science and technology. Characterization is an important step in the development of superior materials. The complete characterization of any material consists of phase analysis, compositional characterization, structural elucidation, micro-structural analysis and surface characterization, which have strong bearing on the properties of materials. This has led to the emergence of a variety of advanced techniques in the field of thin film technology. This chapter gives a short summary of commonly used characterization techniques in thin film technology. It is not intended to provide a complete discussion of the methods. Further information on the techniques can be found in standard text books.

4.2 STRUCTURAL ANALYSIS

The analysis of crystal structure is of great importance in the description of materials; such an analysis is typically performed by employing X-ray diffraction techniques (Other techniques include electron and neutron diffraction method). X-rays were discovered in 1895 by the German physicist Roentgen and were so named because their nature was unknown at the time. Unlike ordinary light, these rays were invisible, but they travelled in straight lines and affected photographic film in the same way as light (Cullity, 1978). They were much more penetrating

than light and could easily pass through the human body, wood, quite thick pieces of metal, and other "opaque" objects. X-rays have wavelengths on the order of a few Angstroms (1 Angstrom = 0.1 nm). This is the typical inter-atomic distance in crystalline solids, making X-rays the correct order of magnitude for diffraction of atoms of crystalline materials (Simon *et al.*, 2008).

A crystal may be defined as a solid composed of atoms arranged in a pattern periodic in three dimensions. About 95% of all solid materials can be described as crystalline. Today about 50,000 inorganic and 25,000 organic single component, crystalline phases, diffraction patterns have been collected and stored on magnetic or optical media as standards. Joint Committee on Powder Diffraction Standards (JCPDS) or formerly known as International Center Diffraction Data (ICDD) is the organization that maintains the data base of inorganic and organic spectra (Sharma *et al.*, 2012). The main use of powder diffraction is to identify components in a sample by a search/match procedure. Furthermore, the areas under the peak are related to the amount of each phase present in the sample (Ermrich *et al.*, 2013).

4.2.1 Powder Diffraction Method

The powder diffraction method, by using conventional X-ray sources, was devised independently in 1916 by Debye and Scherrer in Germany and in 1917 by Hull in the United States. The technique developed steadily and, half a century later, the 'traditional' applications, such as phase identification, the determination of accurate unit cell dimensions and the analysis of structural imperfections, were well established (Langfordy *et al.*, 1996). Powder data have been used for the identification of unknown materials or mixtures of phases since the late 1930s. This is achieved by comparison of experimental data with standard data in crystallographic databases (Ermrich and Opper, 2013). The technique has benefited substantially from the revolution in the

development of storage media during the last decade and from the introduction of fast search/match algorithms. Phase identification sometimes precedes a quantitative analysis of compounds present in a sample and powder diffraction is frequently the only approach available to the analyst for this purpose (Ermrich and Opper, 2013; Langfordy and Louer, 1996). A major advance in recent years has occurred in the determination of crystal structures *ab initio* from powder diffraction data, in cases where suitable single crystals are not available. This is a consequence of progress made in the successive stages involved in structure solution, e.g. the development of computer based methods for determining the crystal system, cell dimensions and symmetry (indexing) and for extracting the intensities of Bragg reflections, the introduction of high resolution instruments and the treatment of line-profile overlap by means of the Rietveld method (Simon and Dinnebier, 2008). There has been spectacular progress in characterizing the microstructural properties which arise from various types of structural imperfection. The principal advance has been the 3-dimensional reconstruction of 'anisotropic' (direction- or *hkl*-dependent) features or properties of polycrystalline materials. These include the shape of diffracting domains and the distribution of the size, structural 'mistakes' induced during the formation or subsequent treatment of a sample and dislocations or other forms of lattice distortion. The main innovation here has been a comparison of experimental data with those derived from a physical model based on data from other techniques or from prior knowledge of the behaviour of the material (Langfordy and Louer, 1996).

4.2.2 Diffractometery

4.2.2.1 The Debye-Scherrer Geometry / Classic Transmission Geometry

The Debye-Scherrer diffraction method has been well known for a long time. It is used for the study of crystalline powders or polycrystalline samples (Artemiev *et al.*, 2013). This geometry employs a parallel beam, and the sample has a roughly cylindrical symmetry. The sample is contained in a tube (neutrons) or capillary (X-rays), and is uniformly illuminated by the incident beam. The detector(s) are placed on a "detection cylinder" (Figure 4.1) generally covering only a small portion of the cylinder, near the scattering plane.

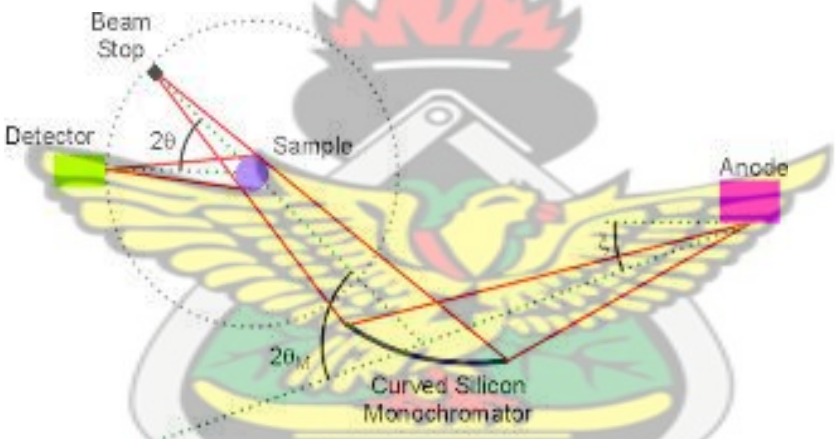

Figure 4.1: The Debye-Scherrer powder diffraction geometry

A convergent beam strikes the sample and the intensity as a function of diffraction angle, 2θ is measured, and it enables the collection of all the reflections corresponding to various (*hkl)* planes. The width generated in a peak which known as full width at half maximum (FWHM) can be used to calculate the mean crystallites sizes in a direction perpendicular to the respective (*hkl*) planes by using Debye-Scherrer equation. As the crystallite size decreases, the width of the diffraction pattern increases (Cullity, 1978). The Debye-Scherrer formula is derived assuming

that a diffraction peak is associated with a family of crystal planes in a size limited crystal (Hall *et al.*, 2000). The Debye-Scherrer formula is mathematically given as:

$$D = \frac{K\,\lambda}{\beta_{2\theta} Cos\theta} \qquad 4.1$$

where D is the crystallite size

λ is the wavelength of the X-rays

θ is the Bragg angle in radian

β is the FWHM of the peak corrected for instrumental broadening

The main advantage of this geometry is that it is easy to rotate the sample around its axis, there by obtaining a good powder average and eliminating at least part of the non randomness of the real powder sample (preferred orientation). Also, geometrical aberrations on the Bragg peak positions can be reduced or eliminated by employing Soller slits. Therefore, the Debye-Scherrer geometry is generally employed to obtain quantitative intensity measurements (Hall *et al.*, 2000). Another advantage of this geometry is that it is easy to use many detectors simultaneously. There are several variants of the Debye-Scherrer geometry, differing mainly by the degree and type of collimation, the type of monochromator and the detector technology. An important class of instruments, for both X-rays and neutrons, employs a linear position sensitive detector (PSD) without scattered-beam collimation. This results in a very large increase of count rates, at the expense of introducing some aberrations (Parrish *et al.*, 1959).

4.2.2.2 Bragg-Brentano Focusing Geometry

The Bragg-Brentano or parafocusing geometry has widely been applied to the commercial X-ray diffractometers and it is almost the technical standard for X-ray diffractometry. In the Bragg-Brentano geometry, an X-ray source and a receiving slit are placed on the diffractometer circle arc and they slew around the specimen with keeping the relation so that the X-ray incident angle to the specimen and the exit angle from the specimen to the receiving slit become the same (Takeyoshi, 2006). In this method, the angular resolution is defined by the width of the receiving slit that is placed in front of a point detector, such as a scintillation counter or proportional counter. A receiving slit of a few tens of a millimeter is usually used. Thus only a small portion of the diffracted beam is utilized and scan speed like 5°2θ/min is usually applied to obtain decent signal to noise ratio (Simon and Dinnebier, 2008; Takeyoshi, 2006). In this configuration a focusing circle is defined as positioned tangentially to the sample surface see Figure 4.2.

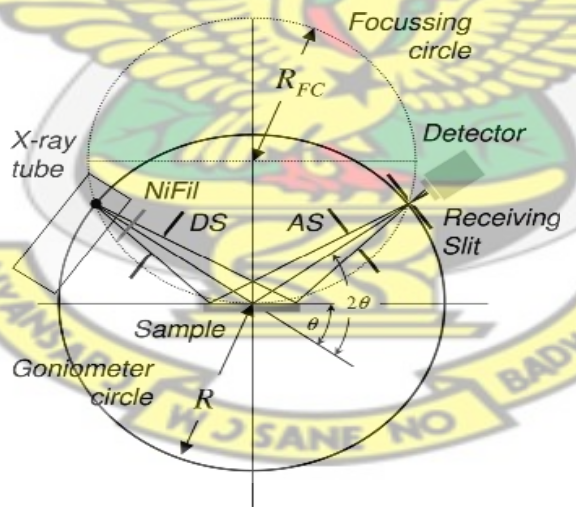

Figure 4.2: Schematic representation of θ/2θ diffraction in Bragg–Brentano geometry (Birkholz, 2006)

The focusing condition in the Bragg–Brentano geometry is obeyed when the X-ray source and detector are positioned on the goniometer circle where it intersects the focusing circle. True

focusing would indeed occur only for a sample that is bent to the radius of the focusing circle. Since focusing circle differs for various scattering angles 2θ, true focusing cannot be obtained in a θ/2θ scan and the arrangement is thus termed parafocusing geometry (Birkholz, 2006).

4.2.3 Bragg's Law

Diffraction can occur when any electromagnetic radiation interacts with a periodic structure. The repeat distance of the periodic structure must be about the same wavelength of the radiation. To express Bragg law mathematically let us consider a crystal as made out of parallel planes of ions, spaced a distance d apart (Figure 4.3). The conditions for a sharp peak in the intensity of the scattered radiation are:

1. That the X-rays should be specularly reflected by the ions in any one plane and
2. The reflected rays from successive planes should interfere constructively. Path difference between two rays reflected from adjoining planes is:

$$2dsin\theta \qquad 4.2$$

For the rays to interfere constructively, this path difference must be an integral number of wavelength λ.

$$n\lambda = 2dsin\theta \qquad 4.3$$

The possible d-spacing defined by the indices h, k, l are determined by the shape of the unit cell. Rewriting Bragg's law we get:

$$sin\theta_{hkl} = \lambda/2\,d_{hkl} \qquad 4.4$$

Therefore the possible 2θ values where we can have reflections are determined by the unit cell dimensions. However, the intensities of the reflections are determined by the distribution of the electrons in the unit cell. The highest electron density is found around atoms. Therefore, the intensities depend on what kind of atoms we have and where in the unit cell they are located. Planes going through areas with high electron density will reflect strongly, planes with low electron density will give weak intensities.

Figure 4.3: X-ray diffraction from plane

Experimentally, the Bragg law can be utilized in two ways. By using X-rays of known wavelength λ and measuring θ, we can determine the spacing d of various planes in a crystal. Alternatively, we can use a crystal with planes of known spacing d, measure θ, and thus determine the wavelength λ of the radiation used: this is X-ray spectroscopy (Cullity, 1978 ; Ermrich and Opper, 2013).

4.3 CRYSTAL DEFICIT

4.3.1 Strain and Dislocation

A perfect crystal is an idealization; there is no such thing in nature. Atom arrangements in real materials do not follow perfect crystalline patterns. Nonetheless, most of the materials that are useful in engineering are crystalline to a very good approximation. The XRD method is used to analyze structural parameters such as microstrain, crystallite size and dislocation density. The knowledge of such parameters especially for new materials are important prior to their technical applications (Bushroa *et al.*, 2012).

One of the characteristics of XRD signature is line broadening. The line broadening can be observed due to changes in the lattice structure of the thin films. It is known that the line broadening is a result of small crystallite size in the growth direction of the coating, strains, stacking faults, dislocations and point defects. The broadening due to crystallite size is caused by the finite size components diffracting incoherently with respect to one another. The broadening due to strain is caused by the non-uniform displacements of the atoms with respect to their reference lattice positions (Birkholz, 2006; Deshpande *et al.*, 2013).

During film deposition and post-deposition treatments, there is always a possibility of the development of strain (stress), which affects the mechanical properties of the films such as the stability of the microstructure, the adhesion between the film and the substrate and the opto-electronic properties of the deposited films. Strain (stress) in a film can be intrinsic, caused by the conditions prevailing during deposition (temperature, pH of solutions, deposition rate, concentration, impurities, etc). On the other hand, strain (stress) can be extrinsic to the film, but intrinsic to the composite film substrate system, caused by the difference in thermal expansion

coefficients (Lokhande and Kale, 2005). A mechanical strain (or equivalently stress) causes changes in the bond lengths. Accordingly, the band structure is affected. For small strain, typically $\varepsilon \leq 0.01$ the shift of the band edges is linear with the strain, for large strain it becomes nonlinear (Christensen, 1984). The origin of strain is related to lattice 'misfit' which in turn depends upon the growing conditions of the films (Sarmah *et al.*, 2008). In thin crystalline films the presence of defects not only serves to disrupt the geometric regularity of the lattice on a microscopic level, it also significantly influences many film properties, such as chemical reactivity, electrical conduction, and mechanical behavior. Dislocations are important because they have provided a model to help explain a great variety of mechanical phenomena and properties in all classes of crystalline solids (Ohring, 1992). The density of dislocations is the number of dislocation lines that intersect a unit area in the crystal. The density ranges from well below 10^2 dislocations/cm^2 in the best germanium and silicon crystals to 10^{11} or 10^{12} dislocations/ cm^2 in heavily deformed metal crystals (Kittel, 2005).

It is useful to classify crystal lattice defects by their dimension. The 0-dimensional defects affect isolated sites in the crystal structure and are hence called point defects. An example is a solute or impurity atom, which alters the crystal pattern at a single point. The 1-dimensional defects are called dislocations. They are lines along which the crystal pattern is broken. The 2-dimensional defects are surfaces, such as the external surface and the grain boundaries along which distinct crystallites are joined together. The 3-dimensional defects change the crystal pattern over a finite volume. They include precipitates, which are small volumes of different crystal structure, and also include large voids or inclusions of second-phase particles (Grundmann, 2010; Kittel, 2005). The dislocation density δ is the measure of the defects in the crystalline (Rajashree *et al.*, 2014).

4.3.2 Texture Coefficient

Crystallographic texture in thin films, i.e. the preferred orientation of particular crystal planes relative to the film substrate, is a common and frequently useful phenomenon. Important materials properties, such as polarization, dielectric constant and elastic modulus, are typically anisotropic, and the most effective use of anisotropic materials in thin film applications often involves controlling the texture of the film. The texture coefficient (*TC*) represents the texture of the particular plane, deviation of which from unity implies the preferred growth (Ilican *et al.*, 2007).

The degree of preferred orientation σ of the sample as a whole can be assessed by estimating the standard deviation of all the TC(hkl) values calculated from the sample

$$\sigma = \sqrt{\frac{\sum_{i=1}^{N}(TC_{hkl} - TC_i)^2}{N}} \qquad 4.5$$

Where TC_i is the texture coefficient of powder sample and its value is always unity. The value of σ is an indicator of the degree of orientation of a sample and can be used to compare different samples. A value of zero for σ indicates that the sample is completely randomly oriented and the sample with a higher value of σ has a preferred orientation (Gupta *et al.*, 2014).

X-ray diffraction is the most convenient tool for crystallographic structural analysis like phase identification, phase quantification and lattice parameter refinement. In the present work this technique is applied as a major analytical tool for phase identification and lattice parameter refinement of the cadmium selenide and $PbS_{1-x}Se_x$ thin films. The effect of Se/S doping on nature of diffraction, peaks position and crystalline sizes were evaluated in $PbS_{1-x}Se_x$ thin films. PANalytical Empyrean Series 2 powder X-ray diffractometer with a Cu-k_α radiation ($\lambda_{\alpha 1}$ = 1.5406 Å and $\lambda_{\alpha 2}$ = 1.54439 Å) was used to analyze the samples (see Figure 4.4).

Figure 4.4: Empyrean Series 2 powder X-ray diffractometer

The machine was operated at 40 mA and 45 kV for phase analysis using the Bragg-Brentano geometry. Total analysis time per samples was around 35 minutes with a scan step of 0.02° in 2θ. XRD data treatment and analysis were carried out using high score plus four software packages. The peaks were identified by comparing the *d*-spacing values obtained from the XRD patterns with Joint Committee on Powder Diffraction Standards (JCPDS) data.

4.4. OPTICAL ANALYSIS

Optical properties of a material change or affect the characteristics of light passing through it by modifying its propagation vector or intensity. Measurement of the absorption of light is one of the most important techniques for optical measurements in solids. In optical absorption spectroscopy, electromagnetic radiation in the near-ultraviolet, visible or near-infrared regions are used to excite transitions between the electronic states. Optical measurements have many unique and attractive features for studying and characterizing semiconductor properties. They are

contactless, nondestructive, and compatible with any transparent ambient including high-vacuum environments.

4.4.1 Optical Properties of Semiconductors

Rapid advances in semiconductor manufacturing and associated technologies have increased the need for optical characterization techniques for materials analysis and in-situ monitoring or control applications (Seiler *et al.*, 2009). The optical properties of a semiconductor can be defined as any property that involves the interaction between electromagnetic radiation or light and the semiconductor, including absorption, diffraction, polarization, reflection, refraction and scattering effects. The electromagnetic spectrum is an important vehicle for giving an overview of the types of measurements and physical processes characteristic of various regions of interest involving the optical properties of semiconductors (Bass, 1995).

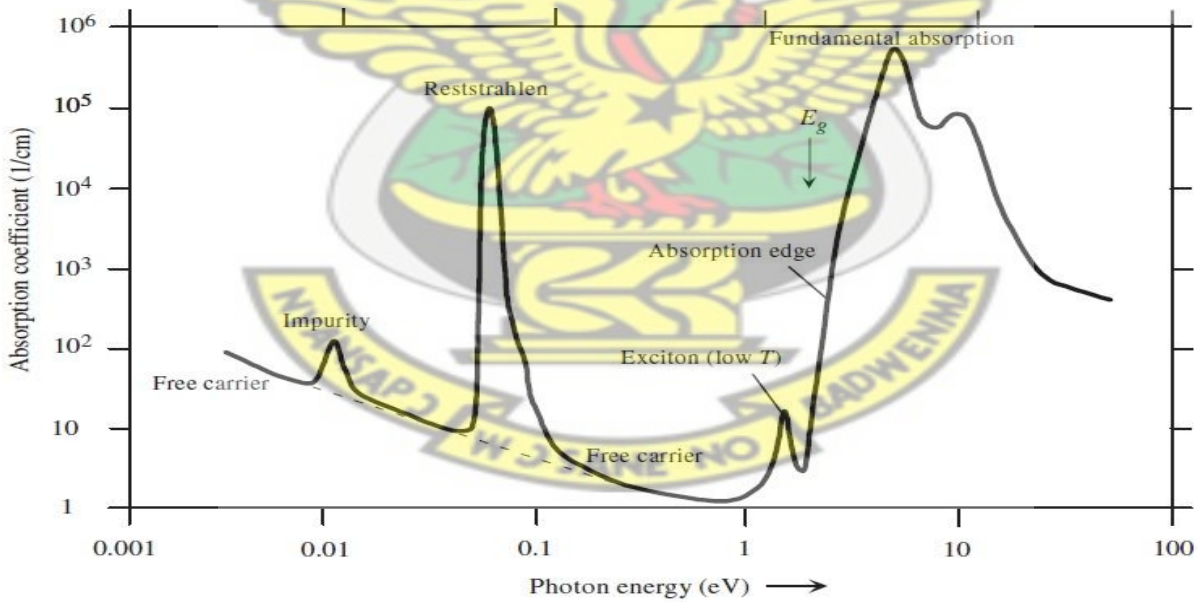

Figure 4.5: Absorption coefficient is plotted as a function of the photon energy in a typical semiconductor to illustrate various possible absorption processes (Jai, 2006)

Optical properties of semiconductors typically consist of their refractive index *n* and extinction coefficient *K* or absorption coefficient α (or equivalently the real and imaginary parts of the relative permittivity) and their dispersion relations, that is their dependence on the wavelength, λ, of the electromagnetic radiation or photon energy *hν*. A typical relationship between the absorption coefficient and photon energy observed in a crystalline semiconductor is shown in Figure 4.5, where various possible absorption processes are illustrated.

The important features in the α verses *hν* behavior as the photon energy increases can be classified in the following types of absorptions (see Figure 4.5): (a) Reststrahlen or lattice absorption in which the radiation is absorbed by vibrations of the crystal ions, (b) Free-carrier absorption due to the presence of free electrons and holes, an effect that decreases with increasing photon energy, (c) An impurity absorption band (usually narrow) due the various dopants, (d) Exciton absorption peaks that are usually observed at low temperatures and are close to the fundamental absorption edge, and (e) Band-to-band or fundamental absorption of photons, which excites an electron from the valence to the conduction band. The type (e) absorption has a large absorption coefficient and occurs when the photon energy reaches the band gap energy *Eg* (Jai, 2006).

4.4.2 UV/VIS Spectrophotometer

UV/VIS spectrometers collect the data over the required range and generate the spectrum of the compound under analysis as a graph representing the transmittance (or the absorbance) as a function of wavelength along the abscissa, given in nanometres, the recommended unit in this region. This region of the spectrum is conventionally divided into three sub-domains termed near UV (185–400 nm), visible (400–700 nm) and very near infrared (700 – 1100 nm) (Rouessac *et al.*, 2007). One of the defining features of a semiconductor is the band gap, which separates the

conduction and valence bands. Upon absorption of light, an electron is promoted from the valence to the conduction band. The wavelength of light absorbed and emitted from this material is determined by the width of the band gap. The UV-VIS absorption spectroscopy is frequently used to characterize semiconductors thin films and to determine the band gap of the nanostructure materials and also to understand the quantum confinement of the nanoparticles (Pradeep, 2008).

In the present study, optical characterization was carried out to determine the nature of absorption and energy band gap of CdSe and PbS_{1-x} Se_x thin films. These properties have dependence on grain size and chemical composition of the thin films. During this study the optical absorption measurement was carried out in the wavelength range from 200 nm to 1100 nm by using a Shimadzu UV/VIS mini-1240 spectrophotometer at room temperature. A clean glass substrate was used for baseline correction. Figure 4.6 shows UV/VIS spectrometer used for this research.

Figure 4.6: Shimadzu UV/VIS mini-1240 Spectrophotometer

4.4.3 Energy band gap calculation from the absorbance spectra

On the basis of their optical properties there are two types of optical transition that can occur at the fundamental edge of crystalline semiconductors: direct and indirect transitions. Both involve the interaction of an electromagnetic wave with an electron in the valance band, which is raised across the band gap to the conduction band. However, indirect transitions also involve simultaneous interaction with lattice vibrations (see Fig 4.7b). Thus the wave vector of the electron can change in the optical transition, the momentum change being taken or given up by the phonons (Kim *et al.*, 2000). Phonons are quantum of lattice vibration having a small amount of energy and a large amount of momentum, and one or more phonons can take part in the transition process if they have the required amount of momentum and energy (Lancry *et al.*, 2011).

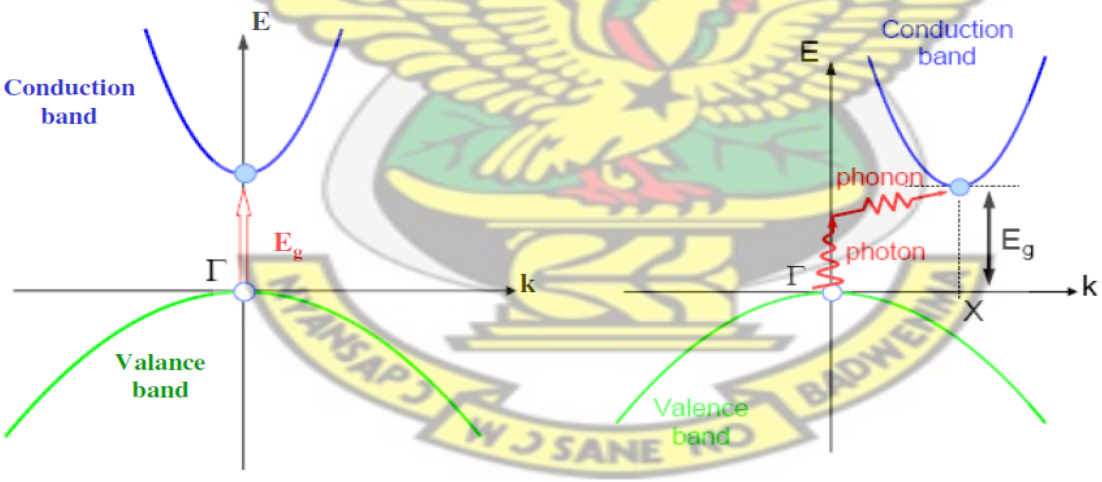

Figure 4.7: E-K diagrams showing (a) direct and (b) indirect inter-band transition.

The direct inter-band optical transition involves a vertical transition of electrons from the valence band to the conduction band such that there is no change in the momentum of the electrons and energy is conserved as shown in Figure 4.7a. Hence the wave vector k for electron remains

unchanged in E-K space. The optical transition is denoted by a vertical upward narrow (Streetman and Banerjee, 2006).

The energy band gap and transition type can be determine from mathematical treatment of data obtained from optical absorbance versus wavelength, with the Stern (1963), relationship of near-edge absorption which is given as (Anuar *et al.*, 2010):

$$A = \frac{[K(h\nu - E_g)]^{n/2}}{h\nu} \qquad 4.6$$

Where A is absorbance, hν is the incident photon energy, K is a constant, and the exponent "n" assumes the values 1, 4 ,3 and 6 for allowed direct, allowed indirect, forbidden direct and forbidden transitions, respectively. The energy band gap can be obtained by extrapolating the linear portion of $(Ahv)^2$ versus hv to the energy axis at $(Ahv)^2 = 0$.

4.5 ELEMENTAL AND MORPHOLOGICAL ANALYSIS

Photovoltaic thin films are highly nonhomogenous at the micron and submicron scale, involving layers of different composition, polycrystallinity, point and extended defects. Spatially resolved characterization at high resolution is therefore adequate to resolve the properties of these different parts and their effect on the device properties, without averaging over the entire material. With the increasingly interdisciplinary nature of applications, new demands for film characterization and other property measurements arise.

4.5.1 Energy Dispersive X-ray analysis (EDX)

EDX makes use of the X-ray spectrum emitted by a solid sample bombarded with a focused beam of electrons to obtain a localized chemical analysis. All elements from atomic number 4 (Be) to 92 (U) can be detected in principle, though not all instruments are equipped for 'light' elements (Z < 10) (Russ, 1984). Most energy-dispersive X-ray analysis systems are interfaced to SEMs, where the electron beam serves to excite characteristic X-rays from the area of the specimen being probed (Ohring, 1992). An EDX system comprises three basic components that must be designed to work together to achieve optimum results: the X-ray detector or spectrum, the pulse processor, and the analyzer (NanoAnalysis, 2013). The process of X-ray emission is shown schematically in Figure 4.8.

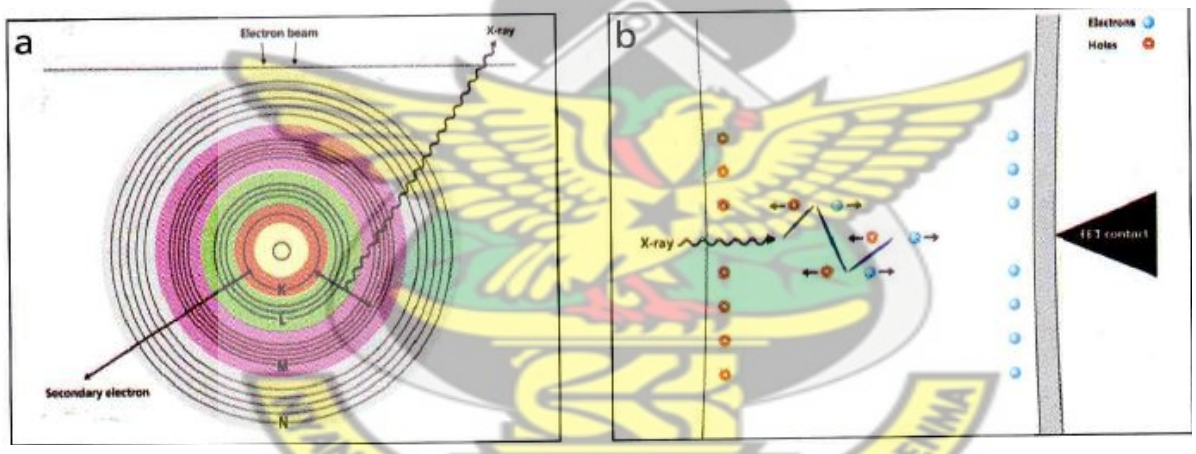

Figure 4.8: Conversion of X-ray signals into a voltage ramps by the EDX detector. (a) Generation of a characteristic X-ray in a sample by electron bombardment (b) Generation and measurement of electron-hole pairs in the crystal (NanoAnalysis, 2013)

First, an electron from, say, a scanning electron microscope, ejects an electron from an inner shell of a sample atom. The resulting vacancy is then filled by an electron from a higher energy shell in the atom. Since this energy difference is fairly large for inner shells, the radiation appears

as X-rays. To complicate matters a bit, there are many energy levels therefore many potential vacancy filling mechanisms within every atom.

As a consequence, even a sample of pure iron will emit X-rays at much energy. Nonetheless, the principle is a simple one: When excited by electrons of sufficient energy, every element in a sample will emit a unique and characteristic pattern of X-rays. Furthermore, under a given analysis conditions, the number of X-rays emitted by each element bears a more or less direct relationship to the concentration of that element. Converting these X-ray emissions to analyzable data is the job of a series of electronic components (see Figure 4.9), which, in the end, produce a digital spectrum of the emitted radiation.

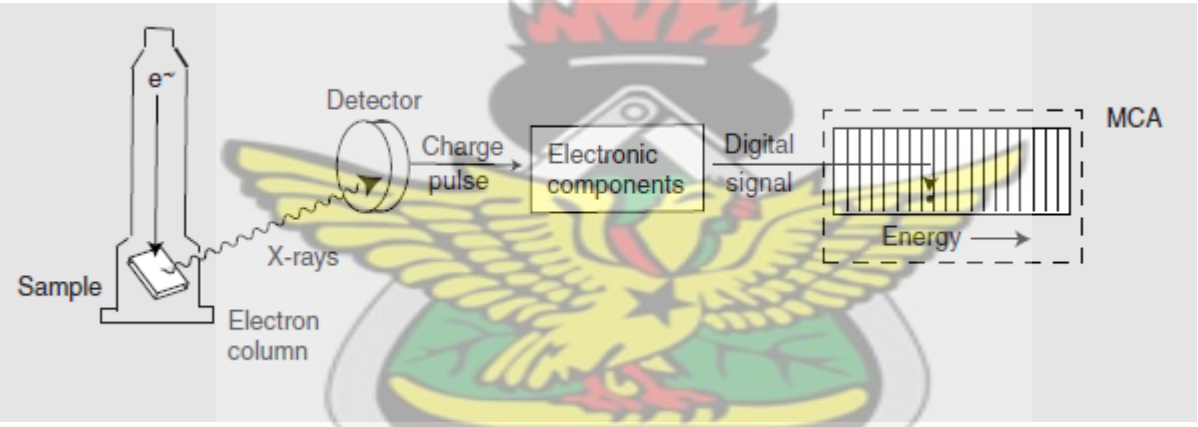

Figure 4.9: Energy dispersive microanalysis, each emitted X-ray produces a charge pulse in a semiconductor detector. This tiny and short-lived current is converted first into a voltage pulse, then into a digital signal reflecting the energy of the original X-ray. The digital signal, in turn, adds a single count to the appropriate channel of a multichannel analyzer (Vaughan, 1999).

4.5.2 Scanning Electron Microscopy (SEM)

The scanning electron microscope (SEM) is one of the most promising technique for generating particle distribution profiles as well as surface characteristics with the possibility to visually re-

evaluate the data by re-assessing the particle. The technique holds promise for characterization of the size and shape of unknown products with relatively wide distribution profiles from the nanometer to the micron range (Sahoo *et al.*, 2011). Also very frequently, scanning electron microscopes are equipped with energy-dispersive X-ray (EDX) detectors, which are used for analyzing local elemental compositions in thin films. However, the possibilities of analysis in SEM go far beyond imaging and compositional analysis. It will be shown that imaging is divided into that making use of secondary electrons (SE) and of backscattered electrons (BSEs), resulting in different contrasts in the images and thus providing information on compositions, microstructures, and surface potentials. Also, it will be demonstrated how important it is to combine various techniques on identical sample positions, in order to enhance the interpretation of the results obtained from applying individual SEM techniques (Abou-Ras *et al.*, 2011).

The schematic of scanning electron microscope is shown in Figure 4.10. The principle of operation of SEM consists of scanning a fine beam of electrons across the sample surface. The electron beam interacts with the sample and generates characteristic X-rays and secondary electrons. The detectors collect these signals and form an image of the sample which is displayed on the screen. Each element in the sample produces its own characteristic X-rays having different energies, thus the chemical composition and the percentage of each element in the sample may be determined. The average surface composition is obtained by scanning several small areas of the sample. Normal SEM operation requires quite low pressure (2 Torr or less), inside the sample chamber, so samples must be in solid form. The sample used for SEM analysis should be conductive. If the sample is non-conductive then it is coated with a thin layer of some conducting material (Abou-Ras *et al.*, 2011).

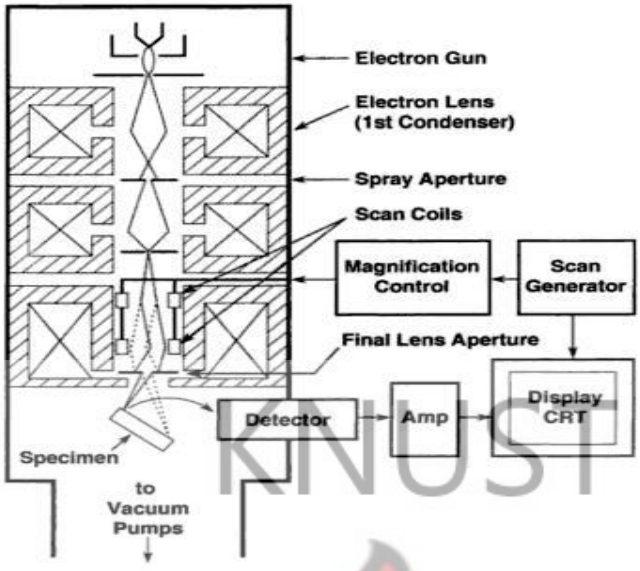

Figure 4.10: Diagram of an SEM column showing the arrangement of the magnetic lenses used to focus the beam (Goldstein *et al.*, 2003)

In general SEM is nicely applicable to evaluate grain size, surface roughness, porosity, particle size distributions and material homogeneity. Surface morphology and atomic percentage compositions for the present study were done by using high resolution Zeiss 1550 VP scanning electron microscope (SEM) attached with Energy dispersive X-ray analyzer (EDX). The equipment was operating with an accelerating voltage of 20 kV and working distance of 6.7 mm which was chosen as most suitable for observing grains in the as-prepared thin films. From this morphology study, it was possible to understand the effect of varying the relative concentration of selenium in $PbS_{1-x}Se_x$ thin films on the grain size and surface morphology. Shape and distribution of the crystallites of both the as-deposited and annealed CdSe thin films were also studied from SEM.

Chapter 5

5. DEPOSITION AND CHARACTERIZATION OF NANOCRYSTALLINE CdSe THIN FILMS BY CBD TECHNIQUE

5.1 INTRODUCTION

Development and designing of next generation solar cells begins with the semiconductor nanocrystals CdSe, PbS, PbSe (Kamat, 2008; Sachin *et al.*, 2013). The unique physical properties of semiconductor nanocrystals such as size-dependent electronic structure, large extinction coefficients and multiple exciton generation make them attractive candidates for photon harvesters. The synthesis and characterization of binary metal chalcogenide semiconductors in a nanocrystalline form has been a rapidly growing area of research (Sachin *et al.*, 2013).

Group II -VI compounds have been found to be interesting for a number of technical applications because of their wide range of chemical, structural, electrical and optical properties. Therefore, rigorous investigations have been carried out to form this compound in single crystal and thin film form (Cyrus *et al.*, 2009; Lee *et al.*, 2000). Among these compounds, cadmium selenide is one of the group II-VI semiconductors considered as a promising material for the development of many interesting applications such as nanosensors, biomedical imaging device, solar cells, photoelectrochemical, optoelectronic devices, electron-beam pumped lasers, light emitting diodes, electroluminescent devices, etc (Ajaya *et al.*, 2011; Mansour *et al.*, 2014; Patil *et al.*, 2013; Toda *et al.*, 2011). CdSe often possesses *n*-type conductivity in bulk as well as in thin film

form (Kalita *et al.*, 2003) with a direct band gap of 1.74 eV and a dielectric constant of 10.2 at 300 K. It has high efficiency of radioactive recombination, high absorption coefficient, high photosensitivity, and direct band gap corresponding to a wide spectrum of wavelengths from ultraviolet to infrared regions (Kanithla *et al.*, 1982; Sutrave *et al.*, 2000) and quantum size effects (Deshpande *et al.*, 2013). Bulk CdSe has two stable four-coordinated polymorphs, hexagonal and cubic structure. Usually the cubic modification exists in thin layers, while the bulk CdSe has the hexagonal structure (Zakharov *et al.*, 1995). Semiconductor devices based on CdSe thin films strongly depend on the structural and optical properties of the films obtained from various experimental conditions (Chandrasekaran *et al.*, 2009; Sarmah *et al.*, 2009).

There exists a wide variety of techniques available for the deposition of CdSe thin films, which originate from purely physical or purely chemical processes, such as thermal evaporation (Pal *et al.*, 2008; Shaha *et al.*, 2008), successive ionic layer adsorption and reaction (SILAR) (Pathan *et al.*, 2002), physical vapor deposition (David *et al.*, 2013), electrochemical (Chowdhury *et al.*, 2012), photochemical (Ichimura *et al.*, 2001), metal oxide chemical vapor deposition (MOCVD) (Chae *et al.*, 2006), photoelectrochemical (Moholkar *et al.*, 2006), electron beam evaporation (Kissinger *et al.*, 2010) and chemical bath deposition (CBD) (Calzadilla *et al.*, 2002; Lokhande and Kale, 2005). Among these techniques, chemical bath deposition (CBD) is becoming an important deposition technique for thin films of compound materials like chalcogenides (Hodes, 2002). The basic principles behind the CBD process are similar to those for all precipitation reactions and are based on relative solubility of the product (Trojanek *et al.*, 2000).

Chemical bath deposition is traditionally performed in a batch reactor, requiring only a substrate to be immersed in a supersaturated solution of aqueous precursors such as metal salts,

complexing agents, and pH buffers. The complexing agent is used to control the speciation of the metal ion (Li *et al.*, 2010). The process is sensitive to precursor concentrations and to the substrate used (Elisabetha *et al.*, 2004). The characteristics of chemical bath deposited CdSe thin films depend strongly on the growth condition; by changing the deposition key parameters, one can control thickness, size of the nanoparticles, and the energy band gap of the obtained thin films (Ghobadi *et al.*, 2013). Highlights of CBD include low cost, operation at low temperature and atmospheric pressure, and scalability to large area substrates (Kanithla *et al.*, 1982).

A survey of available literatures on chemical bath deposited CdSe thin films shows that, most researchers use complexing agents such as; ammonia, triethylamine, sodium hydroxide, trisodium citrate, among others. There are very few reports on the use of tartaric acid as a complexing agent for the deposition of CdSe thin films. The few available reports such as (Hankare *et al.*, 2006), indicates that the deposition was carried out at room temperature and at a pH of 12.1. In the present study CBD technique used to synthesis nanocrystalline CdSe thin films from chemical bath containing cadmium acetate, tartaric acid, ammonia and sodium selenosulphate, at bath temperature of 85 ^{0}C, a pH of 9.5 and deposition time of one and half hours.

5.2 EXPERIMENTAL PROCEDURES

5.2.1 Substrate Cleaning

Substrate cleaning is very important in the deposition of thin films. In principle, most clean surfaces can be used as substrates, although the degree of adhesion can vary greatly from one material to another. Glass is one of the most commonly used substrates in CBD. In spite of the

fact that glass is a relatively inert material, the surface of glass can be very reactive towards species in solution. Procedure for cleaning the substrate is important, as it is one of the factors determining the composition and grain size of the film. One can opt for various cleaning methods depending on the nature of the substrate, type of contaminants and the extent of cleanliness required for thin film deposition. In this work, ordinary commercially available soda lime glass of dimension 75 mm × 25 mm × 2 mm were used as substrates for the deposition of CdSe and $PbS_{1-x}Se_x$ thin films. Before deposition the microscope glass slides were degreased in nitric acid over night and subsequently kept in ethanol for about an hour, after that, ultrasonically cleaned with distilled water and dried under ambient conditions.

5.2.2 Preparation of Sodium Selenosulphite Solution

Ordinarily selenium is not soluble in water at room temperature. In order to create a selenium ion source in the form of sodium selenosulphite (Na_2SeSO_3), selenium granules of 99 % purity were grind to fine powder. Sodium sulphite was dissolved in water and selenium powder was added to the sodium sulphite solution and vigorously stirred using a magnetic stirrer until all the selenium powder had dissolved in the solution. Sodium selenosulphite (Na_2SeSO_3) was prepared by refluxing appropriate amount of selenium powder with 15.275 gm of anhydrous sodium sulphite (Na_2SO_3) of 96 % purity in a three round bottom flask containing distilled water for 6 hours at 80 ^{0}C. Selenosulphate is produced according to the following reaction (Shikha *et al.*, 2014):

$$Na_2SO_3 + Se \rightarrow Na_2SeSO_3$$

Undissolved selenium particles were filtered out after the solution was cooled to room temperature. The resultant product yielded clear sodium selenosulphate solution. This solution is relatively unstable and it is noted that the age of the sodium selenosulphate solution is often important in $CdSe/PbS_{1-x}Se_x$ deposition. Fresh selenosulphate often results in rapid precipitation

of CdSe/$PbS_{1-x}Se_x$ when the selenosulphate solution is added. It was found to be more reproducible and controllable to use a sodium selenosulphate solution which has been prepared and left for about 2 to 5 days. Similar observation has been reported by (Sarkar *et al.*, 2007).

5.2.3 Synthesize of CdSe Thin Films

The preparation conditions of CdSe thin films were optimized by adjusting concentration of dissolved chemicals, bath temperature, and bath solution pH as well as deposition time to obtain homogeneous films with good adherence to the substrate. The chemical bath contained cadmium acetate dihydrate [$Cd(CH3COO)_2.2H_2O$] of 99 % purity and freshly prepared sodium selenosulphite [Na_2SeSO_3] which provided cadmium ions and selenide ions respectively, while tartaric acid [$(CHOH{\cdot}COOH)_2$] of 99 % purity was used as a complexing agent and ammonia (NH_3) to adjust the pH of the aqueous solutions. All the solutions were prepared using deionized water and all the chemicals used were analytical graded without further purification. The complexing agent in the chemical bath deposition technique prevents spontaneous precipitation and reduces the concentration of free metal ions (Anuar *et al.*, 2010; Prabukanthan *et al.*, 2010). The tartarate complex has a lower value of stability constant so that complexed metal ion can be made free in alkaline medium of high pH value (Hankare *et al.*, 2006).

The following procedures were used for the deposition of cadmium selenide thin films: 10 ml of cadmium acetate [$Cd\ (CH3COO)_2.\ 2H_2O$] was poured into a 100 ml beaker and complexed with tartaric acid [$(CHOH{\cdot}COOH)_2$], enough amount of (30%) ammonia solution was added slowly to adjust the pH of the bath . A Mettler Toledo InteLab@Expert Pro pH meter with temperature compensation and glass electrodes (calibrated against standard pH 4.01, 7.00 and 9.21 buffers) was used to record the pH of the solution, after which 10 ml of sodium selenosulphate [Na_2SeSO_3] and some distilled water was added to obtain a final volume of 65 ml. The reaction

mixture was stirred and maintained at a temperature of 85 ^{0}C for deposition. Glass slides were immersed in the reaction bath, and held vertically using a special holder made in our laboratory.

Figure 5.1: Color changes of CdSe chemical bath during CdSe thin film depotion

Initially the solution was colorless then slowly changed to yellow and became orange in color. Subsequently the color of the solution changed from orange to red, which indicates the formation of CdSe (See Figure 5.1). The coated substrates were removed after one and a half hours, washed several times with distilled water and allowed to dry under ambient conditions before film characterization. As-deposited thin films were redishe in color, well adherent and specularly reflective.

5.2.4 Reaction Mechanism

Deposition of cadmium selenide thin film involves controlled release of cadmium ions from the cadmium tartaric acid complex and its reaction with Se^{2-} ions of Na_2SeSO_3 present in the reaction bath. The formation of CdSe involves the following steps: in the anionic precursor solution, the hydrolysis of sodium selenosulphite releases selenide ions as:

$$Na_2SeSO_3 + OH^- \leftrightarrow Na_2SO_4 + HSe^- \quad 5.1$$

$$HSe^- + OH^- \leftrightarrow H_2O + Se^{2-} \quad 5.2$$

The cationic precursor solution releases Cd^{2+} ions from complexed $[Cd(\text{tartaric acid})]^{2+}$ as

$$[Cd(\text{tartaric acid})]^{2+} \rightarrow Cd^{2+} + \text{tartaric acid} \quad 5.3$$

Tartaric acid was used to limit the hydrolysis of the metal ion and impart some stability to the bath. When glass substrate is immersed in the solution, Cd^{2+} and Se^{2-} ions are adsorbed on it when the ionic product of Cd^{2+} and Se^{2-} ions exceeds the solubility product of CdSe (K_{sp} CdSe) = 10^{-33} then deposition of CdSe thin film takes place (Delekar *et al.*, 2005; Pathan *et al.*, 2002).

$$Cd^{2+} + Se^{2-} \rightarrow CdSe + \text{tartaric acid} \quad 5.4$$

5.3 SAMPLE CHARACTERZATION

Preparation and characterization of any material are two equally important aspects. In the case of thin films, appropriate characterization often widens the scope of applications. However characterizing of thin films with precision is a challenging activity. In the present study the crystallographic structure of the films were analyzed by a PANalytical Empyrean Series 2 powder X-ray diffractometer with a Cu-K_α radiation ($\lambda_{\alpha 1}$ = 1.5406 Å) source. The machine was operated at 40 mA and 45 kV. Scanning electron microscopy measurements were conducted using Zeiss 1550 VP (SEM) machine which was operating at an accelerating voltage of 20 kV and working distance of 6.7 mm. The elemental composition of the samples were determined using an energy dispersive X-ray analysis (EDX) attached to the scanning electron microscope. Optical properties were measured at room temperature by using a Shimadzu UV/VIS mini-1240 Spectrophotometer within the wavelength range of 200 nm – 1100 nm.

5.4 RESULTS AND DISCUSSION

5.4.1 Structural Characterization

Analysis of an XRD pattern often relies substantially on prior knowledge about the likely composition of a sample; with this knowledge, however, the process of analysis is relatively simple. Joint Council for Powder Diffraction standards (JCPDS) provides a database of powder diffraction files (PDFs) which are incorporated into many of the available analysis programs that exist. Regardless of the software used, the basic principle is the same; the diffraction pattern obtained experimentally is compared to the standard patterns of the likely elements and compounds present in the sample. Based on this comparison conclusions can be drawn about crystal structure and orientation of the sample. Figure 5.2 shows the X-ray diffraction pattern of the as-deposited CdSe thin films analyzed over the diffraction angle 2θ between 5^{O} and 80^{O}.

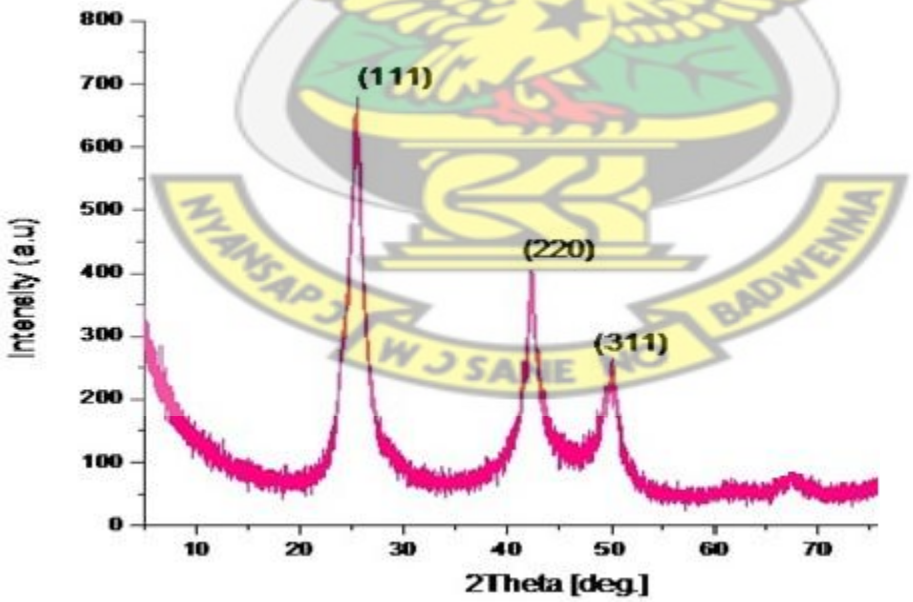

Figure 5.2: XRD pattern of as-deposited CdSe thin film

From Figure 5.2, the XRD pattern shows three well defined peaks at 2θ position 25.46^0, 42.33^0 and 49.77^0 which can be indexed as reflections from the (111), (220) and (311) planes respectively. The peaks are in good agreement with the standard JCPDS data file reference code: 00-019-0191 of the cubic (zinc blend) structure. The intensity of the peak at position 25.46^0 indicates that the grains have a preferred orientation along the (111) plane. The XRD analysis agreed well with earlier reports (Khomanea and Hankare, 2010; Park, 2011). The lattice parameters for cubic phase structure (hkl) is given by equation (5.5) (Sarmah *et al.*, 2009).

$$a_{hkl} = d_{hkl}\sqrt{h^2 + k^2 + l^2} \qquad 5.5$$

The average crystalline size (D) was obtained from the X-ray diffraction pattern, using the Scherrer (1918), formula which is given as:

$$D = \frac{K\lambda}{\beta_{2\theta}\cos\theta} \qquad 5.6$$

where, θ is the diffraction angle, β is the full width at half maximum in radians, K is the constant known as the shape factor, taken as 0.94 by assuming the crystallites to be spherical in shape (Deshpande *et al.*, 2013) and λ is the wave length of the X-ray radiation . The average grain size was estimated to be 4.02 nm. Similar result was reported by (Esparza-Ponce *et al.*, 2009).

Table 5-1: Comparison of crystallographic parameters of as-deposited CdSe thin film obtained from XRD analysis with standard JCPDS data file number 00-019-0191

2θ in degree	hkl Planes	d-space in Å		Cell parameter (a) in Å		Intensity (counts)		Crystalline size (D_{hkl}) (nm)	Average Crystalline size D_{hkl} (nm)
		standard	Observed	standard	Calculated	standard	Observed		
25.460	111	3.510	3.4956	6.077	6.053	100	100	4.37	4.02
42.339	220	2.149	2.1330			55	51	3.82	
49.772	311	1.833	1.8304			25	30	3.86	

From Table 1, the calculated lattice constant deviates from the standard bulk value. This shows that the crystallites may be under some strain (Choudhury *et al.*, 2011). A perfect crystal would extend infinitely in all directions; therefore, no crystals are perfect due to their finite size. This deviation from perfect crystallinity leads to a broadening of the diffraction peaks. The two main properties extracted from peak width analysis are the crystallite size and lattice strain (Zak *et al.*, 2011). Crystallite size is a measure of the size of coherently diffracting domains. The crystallite size of the particles is not generally the same as the particle size due to the formation of polycrystalline aggregates. Lattice strain is a measure of the distribution of lattice constants arising from crystal imperfections, such as lattice dislocations. Other sources of strain include the grain boundary triple junction, contact or sinter stresses, stacking faults and coherency stresses (Xu *et al.*, 2006). Crystallite size and lattice strain affect the Bragg peak in different ways. Both these effects increase the peak width and intensity and shift the 2θ peak position accordingly.

Strain-induced broadening arising from crystal imperfections and distortion are related by $\varepsilon \approx \beta/\tan\theta$ (Zak *et al.*, 2011). It is confirmed that the peak width from crystallite size varies as $1/\cos\theta$

and strain varies as tanθ. Depending on different θ positions the separation of size and strain broadening analysis is done using Williamson and Hall function. Assuming that the particle size and strain contributions to line broadening are independent to each other and both have a Cauchy-like profile (Mote *et al.*, 2012), the observed line breadth is simply the sum of the Scherrer equation and $\varepsilon \approx \beta/\tan\theta$ which results in the following equation:

$$\beta_{hkl} = \frac{K\lambda}{D\cos\theta} + 4\varepsilon \tan\theta \qquad 5.7$$

By rearranging the above equation, we get

$$\beta_{hkl} \cos\theta = \frac{K\lambda}{D} + 4\varepsilon \sin\theta \qquad 5.8$$

where K, λ, θ, β_{hkl} and D are defined in equation (5.6), and ε is the lattice strain for nanocrystalline CdSe thin film. If the size and strain broadening are present simultaneously then the crystallite size and lattice strain can be obtained from Williamson-Hall (W–H) plot using equation (5.8) (Mehta *et al.*, 2007). A plot is drawn with $4\sin\theta$ along the x-axis and $\beta_{hkl}\cos\theta$ along the y-axis. Equation (5.8) represents the uniform deformation model (UDM), where the strain was assumed to be uniform in all crystallographic directions, thus considering the isotropic nature of the crystal, where the material properties are independent of the direction along which they are measured (Mote *et al.*, 2012; Prabhu *et al.*, 2014).

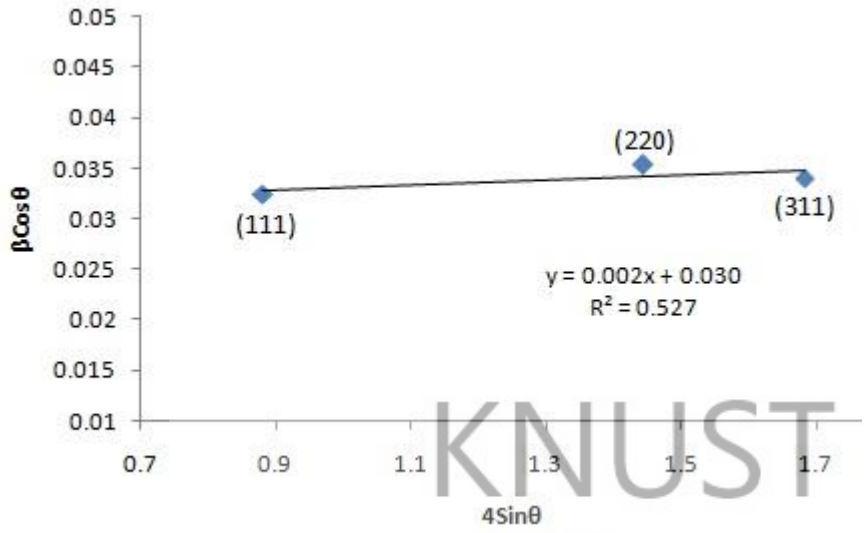

Figure 5.3: Williamson–Hall plot for as-deposited CdSe thin film

Figure 5.3 represents a plot of 4sinθ versus βcosθ for CdSe thin film. The slope of the plot gives the amount of lattice strain, which turns out to be 2×10^{-3} for CdSe thin film. The reciprocal of the intercept on the βcosθ axis gives the average crystallite size as 4.83 nm. The average crystallite size estimated is in close agreement with the value obtained from the Debye-Scherrer formula.

5.4.2 Elemental Analysis and Morphological Studies

Elemental analysis for the as-deposited CdSe thin film was carried out using Energy-Dispersive X-ray (EDX) attached to the SEM. The elemental analysis was carried out only for Cd and Se elements.

Figure 5.4: Energy-Dispersive X-ray spectrum of the as-deposited CdSe thin film

Figure 5.4 shows the EDX spectrum of the as-deposited CdSe thin film, which is consistent with the formation of the binary compound. The atomic percentage of Cd:Se is 49.4:50.6, which is nearly 1:1 indicating that the thin film had the desired stoichiometric ratio. This is comparable to results reported by (Chate *et al.*, 2013; Hankare *et al.*, 2006). Figures 5.5a, 5.5b and 5.5c show the SEM micrographs of the as-deposited CdSe thin films taken at different magnifications. The surface morphology is composed of largely spherically shaped grains with different grain sizes and uniformly distributed over a smooth homogenous background without visible defects such as cracks, peeling or pinholes. Some of the micrographs also show the presence of pockets of clusters of spherically shaped grains. Similar observations were reported by (Ajaya *et al.*, 2011; Metin *et al.*, 2008).

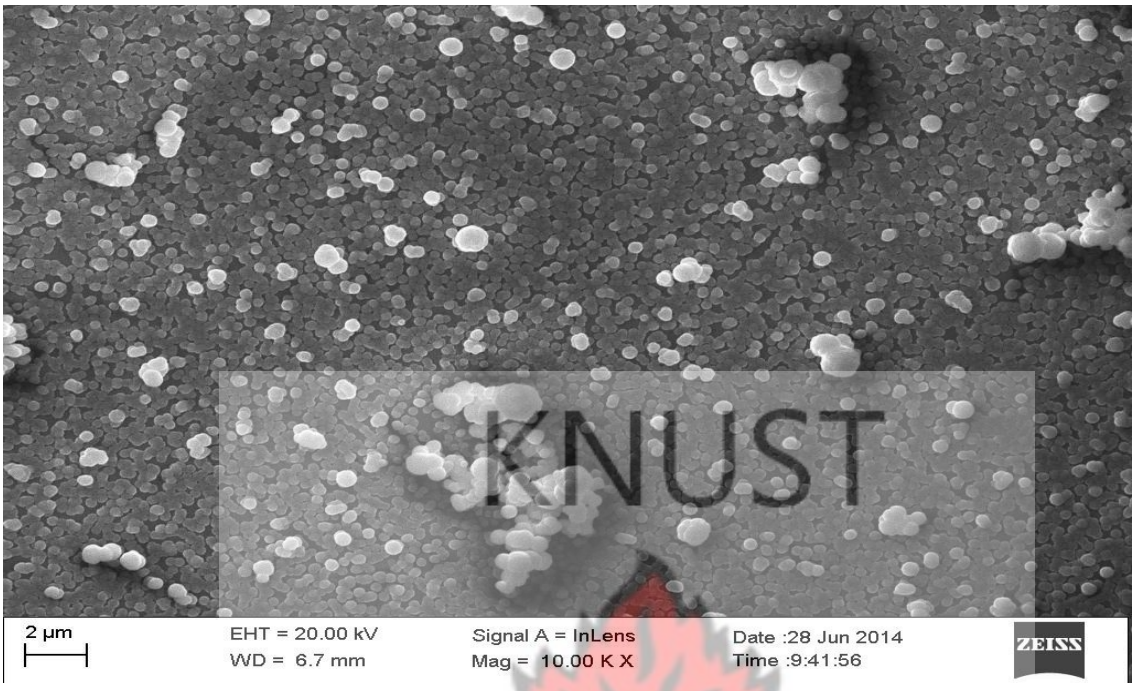

Figure 5.5 (a): The SEM micrograph of as-deposited CdSe thin film (magnification 10 KX)

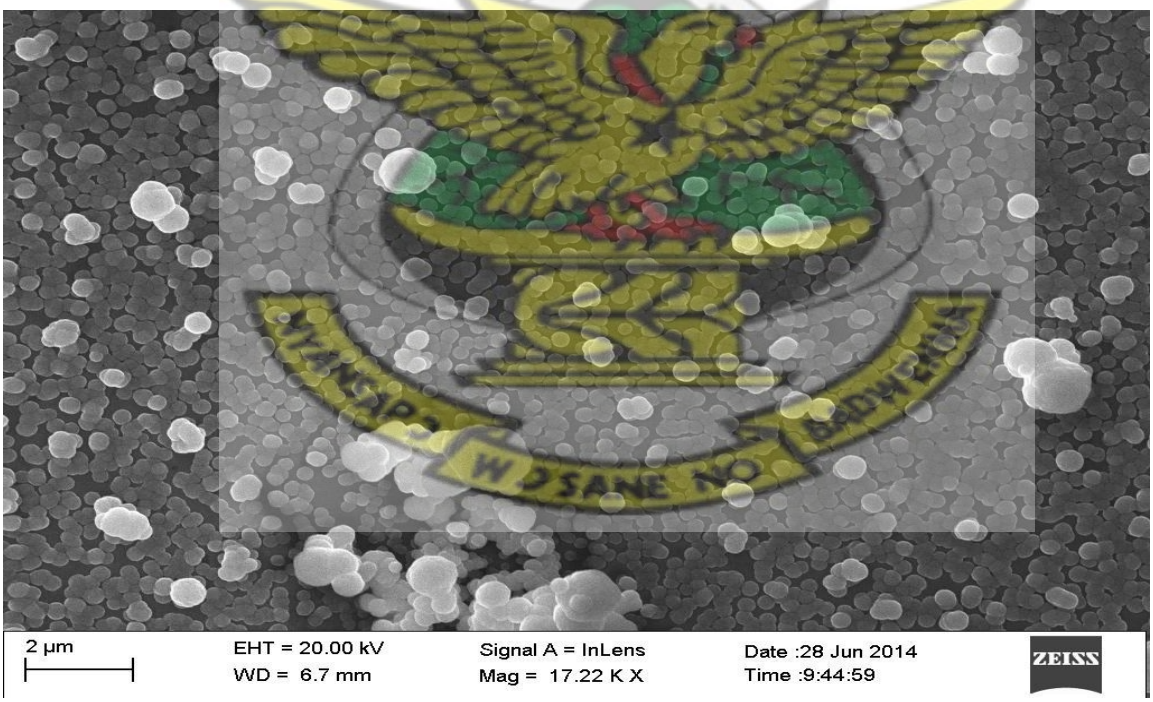

Figure 5.5 (b): The SEM micrograph of as-deposited CdSe thin film (magnification 17.22 KX)

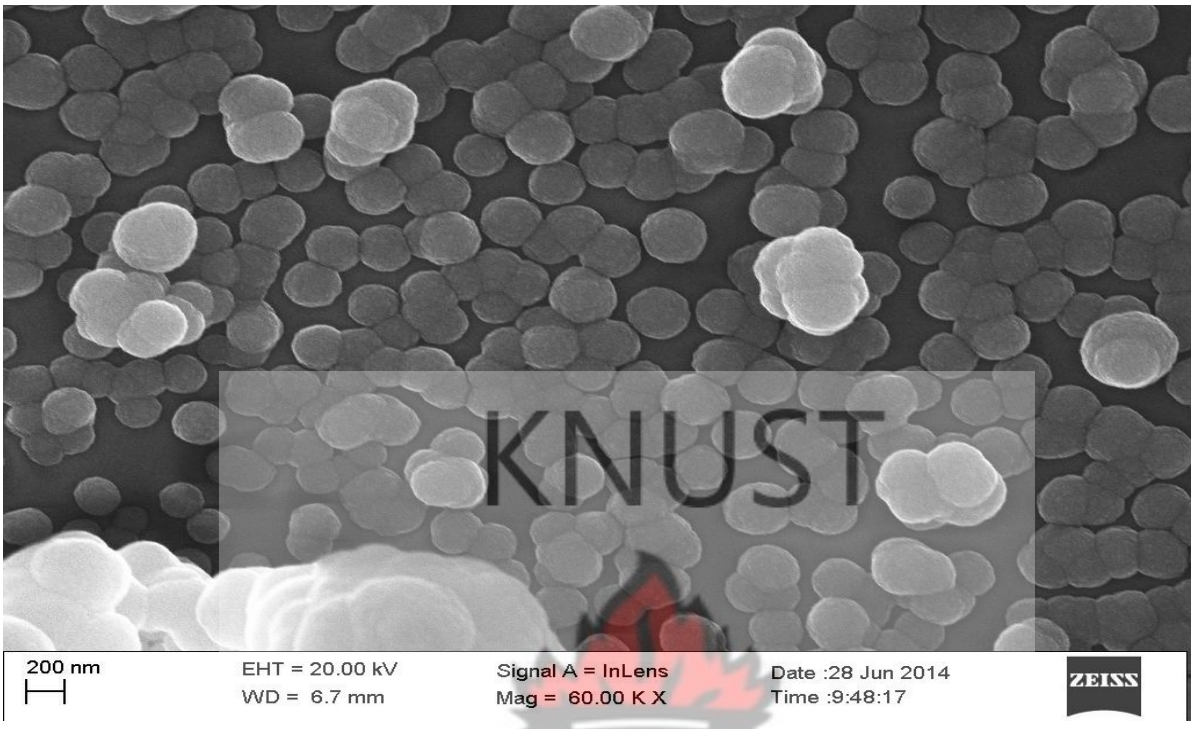

Figure 5.5 (c): The SEM micrograph of as-deposited CdSe thin film (magnification 60 KX)

5.4.3 Determination of the Optical Band gap

The energy band gap and transition type was derived from mathematical treatment of data obtained from optical absorbance versus wavelength with the Stern (1963), relationship of near-edge absorption which is given in Equation 4.6 as:

$$A = \frac{\left[K(h\nu - E_g)\right]^{n/2}}{h\nu} \qquad 5.9$$

where v is the frequency of the photon, h is the Planck's constant, K is a constant while n carries the value of either 1 or 4. The value of n carries either 1 for direct transition or 4 for indirect. Since CdSe is a direct band gap material, thus n is taken as 1. The band gap energy is obtained by extrapolating the linear portion of $(Ahv)^2$ versus hv to the energy axis at $(Ahv)^2 = 0$ (see Figure 5.6). The optical band gap for CdSe thin film was found to be 1.86 eV, which is in good

agreement with earlier reports (Esparza-Ponce *et al.*, 2009; Zhao *et al.*, 2013). The variation of $(Ahv)^2$ versus hν shown in Figure 5.6 was linear at the absorption edge, which confirmed that CdSe is a semiconductor with a direct band gap (Kwang-Deog *et al.*, 2005).

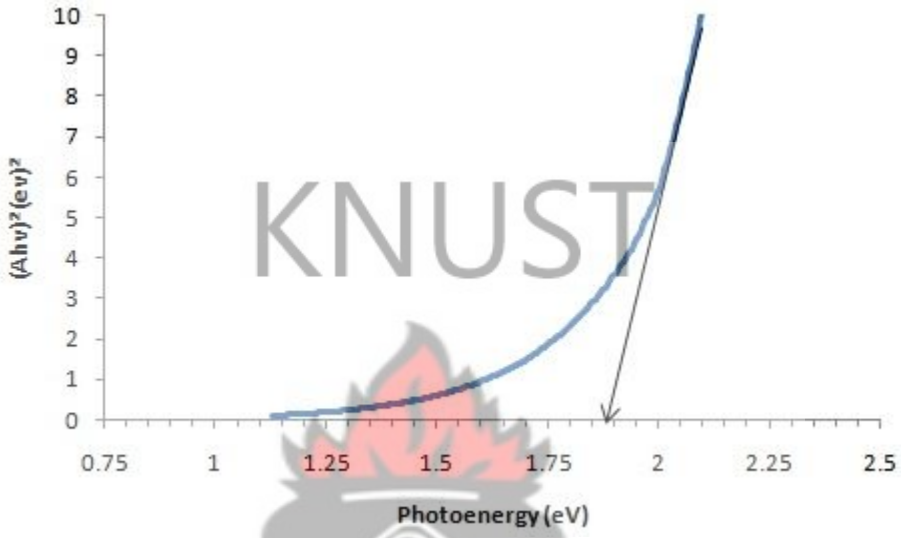

Figure 5.6: A graph of $(Ahv)^2$ plotted as a function of the photon energy($h\upsilon$) for as-deposited CdSe thin film

The value of the band gap determined for the CdSe thin film shown in Figure 5.6 is slightly higher when compared to the reported bulk value of 1.74 eV (Kanithla *et al.*, 1982). It is known that such blue shift to higher optical band gaps arises from very small grain sizes and the resulting quantum confinement of electronic states in the thin films (Kale and Lokhande, 2000). For example, in chemically deposited CdSe thin films with grain sizes less than 5 nm, optical band gap of up to 0.70 eV higher than the bulk value of 1.74 eV has been reported by (Nair *et al.*, 1998). In the synthesized sample the average grain size estimated from the XRD measurements was 4 nm, and this explains the slightly larger band gap when compared to the bulk value.

5.5 EFFECT OF ANNEALING ON STRUCTURAL, MORPHOLOGICAL AND OPTICAL PROPERTIES OF CdSe THIN FILM

Annealing is an important process; it provides the base for the solid state processing of all metals and semiconductors (Humphreys *et al.*, 2004). Annealing can be defined as heat treatment of materials at elevated temperature to investigate or improve their properties (Ampong, 2012). Annealing leads to significant changes in structural, electrical and optical properties of semiconductor thin films (Nair *et al.*, 1998). Material annealing can lead to phase transitions, recrystallization, homogenization, relaxation of internal stresses and rearrangement of defects and so on. The results of annealing depend significantly on its kinetics, the rate of heating and cooling and the time of exposure at a given temperature (Lokhande and Kale, 2005). Annealing semiconductor thin films would enhance their characteristics in different applications, including photoelectrochemical cell study. This is because annealing is assumed to enhance grain size and eliminate grain boundaries between them. In addition, annealing should remove imperfections within the microcrystal of the thin film (Sachin *et al.*, 2013).

In the present study both CdSe thin film and its precipitates collected from the bottom of the deposition vessel were annealed at a temperature of 350 ^{0}C for one hour in carbolite furnace after which the furnace was switched off and allowed to cool to room temperature. The samples were then removed and characterized to investigate the effect of annealing on structural, morphological and optical properties of the CdSe thin film. The as-deposited films were redish while the annealed films were dark grey in color as shown in Figure 5.7.

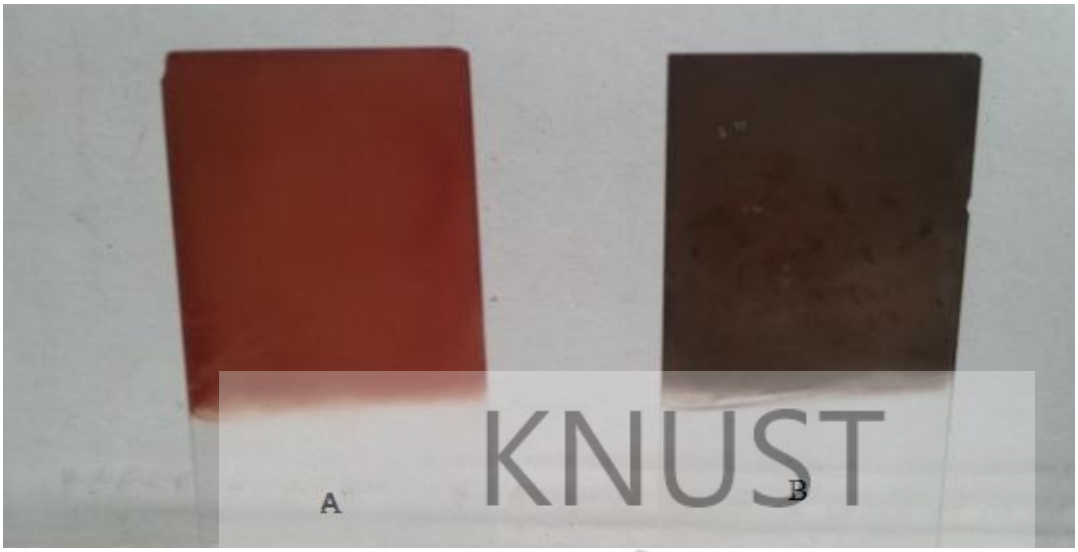

Figure 5.7: Color of CdSe thin films before annealing (A) and after annealing (B)

5.5.1Structural Analysis

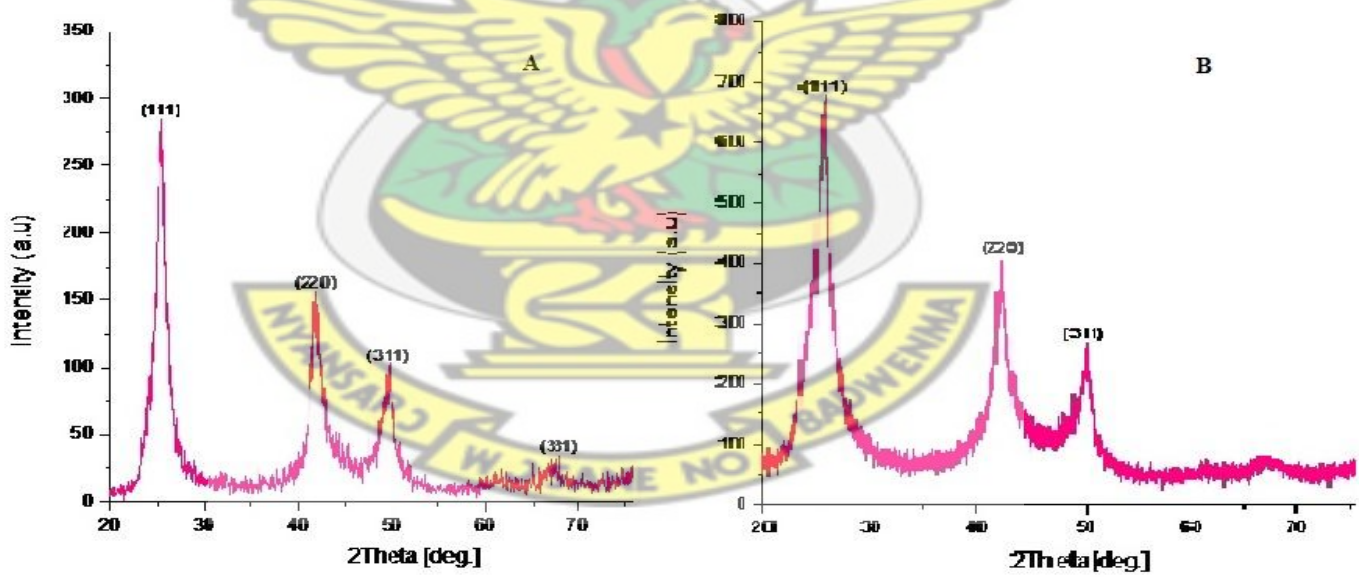

Figure 5.8: XRD patterns of CdSe samples: (A) annealed at 350 ^{0}C for 1 hour and (B) as-deposited

The X-ray diffraction spectra for the annealed crystalline CdSe thin film in Figure 5.8 (A) indicate that the intensity of all the peaks corresponding to the (111), (220), (311) planes

increased and became more pronounced as compared to the as-deposited film. This result is in agreement with earlier reports (Khomane, 2011; Mattoussi *et al.*, 1998). In addition a new peak is observed at 67.1^0 and indexed the (331) plane. It was also noticed that the peak positions shifted slightly towards lower 2θ positions (see Table 5.2). This indicates that the crystallinity of the films increased after annealing (Cao *et al.*, 2007). It is also noticeable from Figure 5.8 that the width of the prominent peaks of the annealed film is smaller than that of the as-deposited film which implies a reduction in strain within the film and improvement in crystallinity (Gokul *et al.*, 2013). The observed d-values (distance between the diffracting planes) and respective prominent peaks for both as-deposited and annealed CdSe samples obtained from the XRD studies were in good agreement with JCPDS data file number 00-019-0191 for cubic zinc blend structure. No phase change was observed after annealing. Below the critical annealing temperature for CdSe thin film the cubic phase is retained (Calzadilla *et al.*, 2002).

Lattice constant a(Å) for cubic phase structure and the crystallites size D_{hkl} in a direction perpendicular to the respective planes (hkl) were calculated using the Debye–Scherrer equation (5.6). Mathematically, the micro strain value ε was evaluated by using the following formula (Bhuiyan *et al.*, 2011; Gokul *et al.*, 2013):

$$\varepsilon = \frac{\beta \cos\theta}{4} \qquad 5.10$$

where θ is the Bragg angle in radian. The dislocation density δ which is a measure of the defects in the crystallite (Rajashree *et al.*, 2014), has been calculated by using Williamson and Smallman's formula (Williamson *et al.*, 1956):

$$\delta = \frac{n}{D^2} \qquad 5.11$$

where n is a factor, which equals unity giving minimum dislocation density and D is the crystallite size (Sarmah *et al.*, 2008). All these parameters obtained from XRD data for both as-deposited and annealed CdSe samples are compared with standard data and are presented in Table 5.2. Strain and dislocation density were calculated from the highest intense peak of the X-ray diffraction pattern for both as-deposited and annealed CdSe.

Table 5-2: Different parameters calculated from XRD

CdSe Samples			d-space in Å		Cell parameter in Å		Intensity counted		Crystalline size (D_{hkl})(Å)	Strain ε $lines^{-2}m^{-4}$	Dislocation density (δ) lines/ m^2
	2θ in degree	hkl	standard	observed	standard	observed	standard	observed			
As deposited	25.460	111	3.510	3.496	6.077	6.053	100	100	43.68	8.29×10^{-3}	5.24×10^{16}
	42.339	220	2.149	2.133			55	51	38.24		
	49.772	311	1.833	1.830			25	15	38.62		
Annealed	25.32	111	3.510	3.515	6.077	6.083	100	100	65.24	5.55×10^{-3}	2.35×10^{16}
	42.09	220	2.149	2.145			55	49	47.75		
	49.47	311	1.833	1.840			25	15.69	46.12		
	67.10	331	1.394	1.394			4	3.2	20.75		

From Table 5.2, it is observed that annealing of the film increased the crystallite size and decreased the dislocation density, similar observation was reported by (Shyju *et al.*, 2010). Dislocation density and strain are the manifestation of dislocation network in the films, the decrease in dislocation density indicates the formation of high quality films (Bhuiyan *et al.*, 2011) the same phenomena were reported by (Bhuiyan *et al.*, 2011; Gokul *et al.*, 2013). The strain in CdSe thin film also decreased after annealing indicating the release of intrinsic film stress due to annealing thereby reducing the imperfections within the crystalline lattice.

It was also found that the value of the lattice constant a (Å) of the film deviates from its bulk value of 6.077 Å for both as-deposited and annealed CdSe samples. There are several possible sources of error like divergences of X-ray beams, refraction and absorption of X-rays by the specimen etc in the measurement of θ and d-values (Simon and Dinnebier, 2008). So accuracy in the determination of lattice constant is dependent upon the accuracy of their measurements. The most accurate value of lattice parameter was estimated from the Nelson-Riley function (Ubale *et al.*, 2007).

$$f(\theta) = \frac{1}{2}\left(\frac{cos^2\theta}{sin\theta} + \frac{cos^2\theta}{\theta}\right) \qquad 5.12$$

where θ is the Bragg angle and f (θ) is an error function. The Nelson-Riley plot is obtained by plotting the calculated 'a_{hkl}' for each plane against the corresponding error function. The intersection at $f(\theta) = 0$ gives the corrected value of the lattice parameter which is more or less free from systematic errors as shown in Figure 5.9 and Figure 5.10.

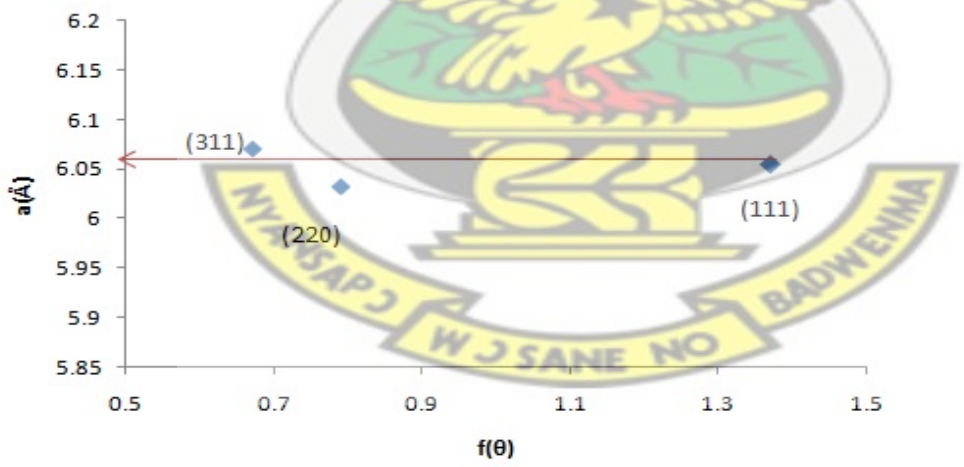

Figure 5.9: Nelson-Riley plot for as-deposited CdSe thin film

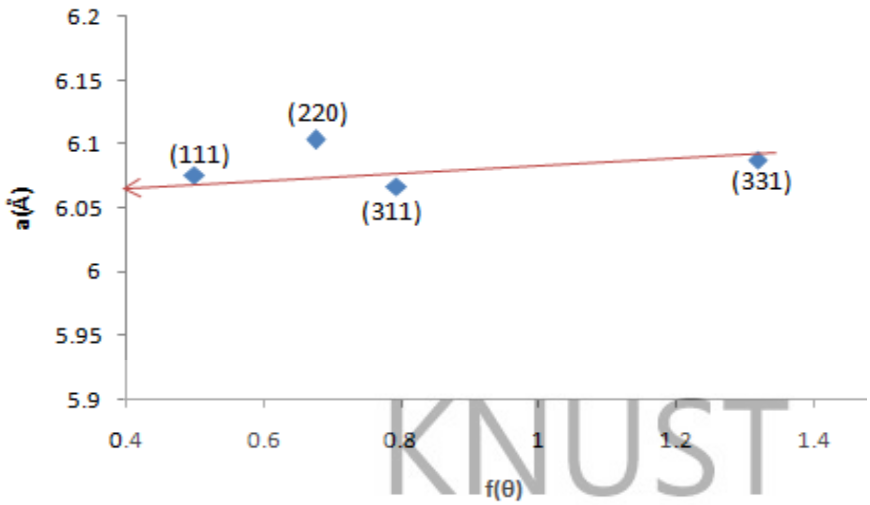

Figure 5.10: Nelson-Riley plot for annealed CdSe thin film

The corrected value of lattice parameter from Nelson–Riley plots for both as-deposited and annealed CdSe samples was estimated to be $a = 6.074$ Å, which is very close to the JCPDS card number 00-019-0191 of cubic CdSe compound. The lattice parameter is independent of post-deposition annealing (Al-Azad *et al.*, 2008).

The texture coefficient (*TC*) represents the texture of the particular plane, deviation of which from unity implies the preferred growth. Quantitative information concerning the preferential crystallite orientation was obtained from the texture coefficient TC(hkl) defined as (Caglar *et al.*, 2006; Thanikaikarasan *et al.*, 2010).

$$TC(hkl) = \frac{I(hkl)/I_0(hkl)}{N^{-1}\sum_N I(hkl)/I_0(hkl)} \qquad 5.13$$

where *I(hkl)* is the measured relative intensity of a plane *(hkl)*, $I_o(hkl)$ is the standard intensity of the plane *(hkl)* taken from the JCPDS data, N is the number of diffraction peaks. The value *TC*(*hkl*) = 1 represents films with randomly oriented crystallites, while higher values indicate the abundance of grains oriented in a given (*hkl*) direction (Ilican *et al.*, 2007; Mahdi *et al.*, 2012).

The calculated texture coefficients are presented in Table 5.3. From the result it was observed that the crystallites are oriented in the (111) plane for both as-deposited and annealed CdSe thin films. But larger abundance of crystallites orientation was noticed for annealed CdSe thin films in the (111) plane comparing to the as-deposited CdSe.

Table 5-3: The texture coefficients of both as-deposited and annealed CdSe samples

CdSe samples	2θ in degree	hkl Planes	d-space (Å) observed	I/I_0	TC
As-deposited	25.460	111	3.4956	1	1.20
	42.339	220	2.1330	0.927	1.10
	49.772	311	1.8304	0.6	0.71
Annealed	25.32	111	3.515	1	1.35
	42.09	220	2.145	0.891	1.20
	49.47	311	1.840	0.6276	0.85
	67.1	331	1.394	0.8	1.08

5.5.2 Surface Morphology studies

The surface morphology of the annealed samples were determined using high resolution JEOL JSM-7600F scanning electron microscope operating at an accelerating voltage of 15 kV and average working distance of 7.9 mm. The SEM micrographs of the annealed CdSe thin films at 350 ^{0}C are shown in Figure 5.11 with two different magnifications. From the SEM micrographs, it is observed that the grains are nearly spherical in shape and uniformly distributed over the

surface of the substrate without cracks and pinholes. Comparing to the as-deposited films, most of the annealed grains are interconnected to each other and cover the entire surface of the substrate without pores. In addition, the SEM micrographs of the annealed film showed a slight improvement in crystallinity. This is also consistent with the XRD result. The improvement of crystallinity after annealing may be due to coalesce of smaller nanoclusters into larger clusters (Musetafa *et al.*, 2012).

Figure 5.11: The SEM micrographs of annealed CdSe thin film at 350 ^{0}C for 1 hour: (a) 5 KX magnification (b) 25 KX magnification

5.5.3 Optical studies

The energy band gap and transition type was derived from mathematical treatment of data obtained from optical absorbance versus wavelength with the Stern (1963) relationship of near-edge absorption (see Equation 4.6). The optical band gap is found to be 1.86 eV and 1.74 eV for the as-deposited and the annealed CdSe films respectively (see Figure 5.12). The energy band gap decreased after the films were annealed for 1 hour. These conditions revealed that the grain size increase gradually with annealing which agreed well with XRD results. The observed decrease in energy band gap in the annealed film can be attributed to an increase in crystallite size of the material as compared to the as-deposited thin film. This phenomena is in good agreement with early report by (Shyju *et al.*, 2012).

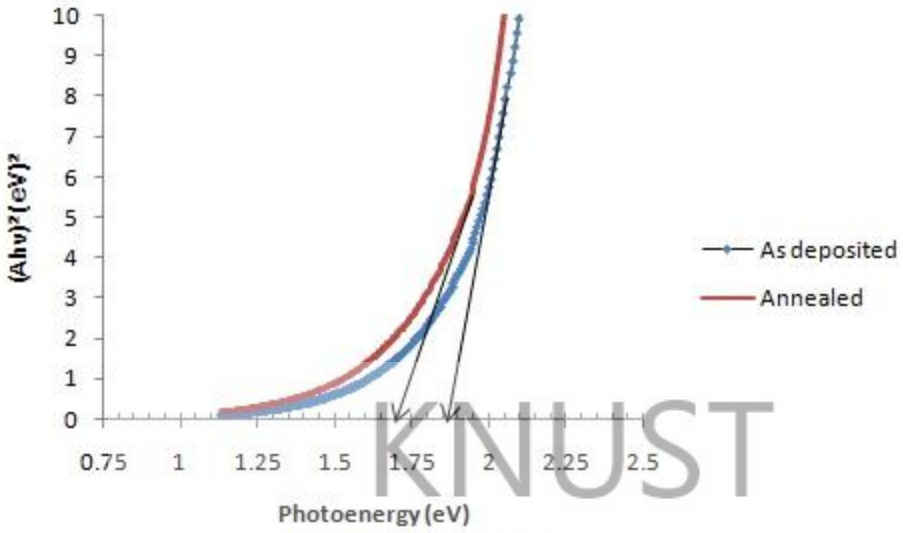

Figure 5.12: A graph of $(Ahv)^2$ plotted as a function of the photon energy($h\upsilon$) for as-deposited and annealed CdSe thin films

5.6 CONCLUSION

A well adherent cadmium selenide nanocrystalline thin film has been successfully deposited on glass substrate by chemical bath deposition technique using tartaric acid as complexing agent at a bath temperature of 85 ^{0}C. Powder X-ray diffraction revealed a cubic phase of nanocrystalline CdSe thin films. The intensities corresponding to the cubic reflections indicate that the film is oriented along the (111) plane. The average crystallite size of CdSe film was obtained from the X-ray diffraction patterns using the Debye-Scherrer equation and was found to be 40 Å. The SEM micrographs showed homogeneous surface morphology composed of largely spherically shaped grains without visible defects such as, cracks, peeling or pinholes. Energy dispersive X-ray spectroscopy confirmed that the as-deposited thin film had the desired stoichiometric ratio 1:1. The optical band gap determined from optical absorption was found to be 1.86 eV and exhibiting blue shift. Annealing effect on the structural, morphological and optical properties of the CdSe thin films has been also studied. From the XRD analysis it was observed that the deposited films mainly consisted of cubic CdSe phase. No phase change was observed after annealing. However, a new peak was observed at 67.1^0 and it was also noticed that the peak positions shifted slightly towards lower 2θ angle. This revealed that the crystallite size improved by annealing. The average crystallite size was found to increase from 40 Å for as-deposited to 45 Å whereas the dislocation density and microstrain decreased after annealing. The decrease in dislocation density and microstrain indicates the formation of high quality thin film by reducing the imperfections within the crystalline lattice. Texture coefficent results revealed that the crystallites are oriented in the (111) plane for both as-deposited and annealed CdSe thin films. But larger abundance of crystallites orientation was noticed for annealed CdSe thin film in the (111) plane compared to the as-deposited one. The SEM micrographs of the annealed film

showed a slight improvement in crystallinity and the grains are interconnected to each other and cover the entire surface of the substrate without pores. The optical study revealed that the deposited samples have direct band transition and decreased from 1.86 eV to 1.74 eV after annealing. The variation of optical band gap is due to the change in the crystallite size.

Chapter 6

6. SYNTHESIS AND CHARACTERIZATION OF LEAD SULPHUR SELENIDE ($PbS_{1-x}Se_x$) THIN FILMS BY CHEMICAL BATH DEPOSITION TECHNIQUE

6.1 INTRODUCTION

In the last few years considerable interest has been shown in the synthesis of semiconducting thin films, due to variety of applications (Guitierrez *et al.*, 1989). Lead chalcogenides (PbX, X = S, Se, Te) are a special class of group IV–VI narrow band gap (0.2 – 0.41 eV) semiconductors. These materials have been studied for many decades, but they still reveal some interesting physical properties (Khokhlov, 2003). These include ferroelectricity, large optical dielectric constant, and a narrow fundamental energy gap whose temperature co-efficient dEg/dT is positive (Al-Fawade *et al.*, 2013; Delin *et al.*, 1998).

Thin solid films of these materials have always been a subject of interest mainly because of their possible application in the manufacture of large area photodiode arrays, solar selective coatings, solar cells, photoconductors, sensors and, so forth (Khanlary *et al.*, 2012). One of the easiest ways to change artificially the electronic and optical properties of semiconductors is by forming their alloy (Labidi *et al.*, 2009). The method commonly adopted to grow ternary semiconductors is by mixing suitable binary semiconductors under appropriate solid solubility conditions. The ternary semiconductor thin films are considered to be an important technological material due to their prime applications in various optoelectronics devices (Mohammad *et al.*, 2014). Criteria governing choice of binary constituents are their operational characteristics, chemical bonding and structural compatibility, which could provide smooth restructuring of energy bands and

continuous variation of characteristics with variation of relative concentration of constituents in resulting materials. Ternary alloys prepared out of binary semiconductors can thus be grouped as a class of semiconductors in which lattice parameter, energy band gap and other operational parameters could be continuously varied as per requirement by selecting binary constituents and their relative concentrations suitably (Majeed *et al.*, 2004). Group IV–VI semiconductors and their heterostructures are well-known to form ternary and quaternary alloys with a direct fundamental band gap over most of the alloy composition range with high absorption coefficients, which can be used as materials for fabricating thin film heterojunction photovoltaic (PV) devices and photo-electrochemical cells. Photovoltaic devices made using ternary $PbS_{1-x}Se_x$ nanoparticles are more efficient than either pure PbS or pure PbSe based nanocrystal devices (Wanli *et al.*, 2009). Lead salts from group IV-VI semiconductors are in common use in infrared optoelectronics. Typical mixed crystals of this material family like the ternaries $PbS_{1-x}Se_x$, cover a band gap range with a corresponding wavelength range of roughly 3 μm to 8 μm (Abbas *et al.*, 2008). Among various semiconducting materials the two compounds PbS and PbSe, which are direct gap semiconductors at the L point of the Brillouin zone, form a continuous series of alloys denoted by $PbS_{1-x}Se_x$, where "x" is the mole fraction of PbSe in the alloy. The properties of PbS and PbSe lead to an ideal substitutional alloy because their atomic anion radii are within 15% of each other and the lattice mismatch factor is only 2% between PbS and PbSe (Wanli *et al.*, 2009). Besides, these semiconductors have a simple cubic crystal structure with nearly identical lattice constants 5.93 Å for PbS and 6.13 Å for PbSe at 300 K, respectively, which facilitates the formation of solid solution.

$PbS_{1-x}Se_x$ alloys in the bulk and film form at room temperature appear as polycrystalline with face centered cubic (fcc) structure and their lattice parameters vary according to the value of "x" (Meradji *et al.*, 2011; Nill *et al.*, 1971). The formation of solid solutions in semiconductors is of interest, because of the possibility of manipulating the material characteristics as per requirement of the device. The continuous variation of electrical and optical properties of ternary alloy semiconductors with relative concentration of constituents is of utmost utility in development of solid state technology (EL-Nahas, 1992; Kumar *et al.*, 2010). Continuous variation of discrete structural, optical and electronic properties, if achieved in semiconducting materials in a controlled manner, could enhance their employability in the fabrication of devices with predetermined characteristics (Majeed *et al.*, 2004).

The band structures, optical properties and crystal structures of both PbS and PbSe are very similar and therefore the system $PbS_{1-x}Se_x$ cannot only have a feasibly graded energy gap of a broad spectral sensitivity but many more material characteristics can perhaps be altered and very well controlled via system composition "x". The carrier concentration in lead chalcogenides can be controlled by adjusting the lead:chalcogen ratio of a pure material. It is possible to obtain controlled n-type and p-type films by controlling the quantity of excess metal or chalcogen (Majeed *et al.*, 2004). Lead sulphure selenide ternary compound in thin film form can be deposited by various methods, such as thermal evaporation (Al-Fawade *et al.*, 2013; Nasir *et al.*, 2013), flash evaporation (Kumar *et al.*, 2010), vacuum evaporation (Majeed *et al.*, 2004) and chemical bath deposition (Sarma *et al.*, 1982).

Amongst the various methods available for the synthesis of chalcogenide thin films, the chemical bath deposition (CBD) method is found to be one of the most popular and commonly used

techniques. It is relatively inexpensive, simple and convenient for large area deposition with better homogeneity and easier control over composition (Sachin *et al.*, 2013). One of the attractive features of the chemical bath deposition process is that, alloy compounds can be easily synthesized without the use of any sophisticated instrumentation and process control (Seghaier *et al.*, 2006). A lot of reports are available for ternary thin film materials such as; $Cd_{1-x}Zn_xS$, $Cd_{1-x}Pb_xS$, $Hg_{1-x}Cd_xTe$, $Cd_{1-x}Zn_xTe$, and $CdS_{1-x}Se_x$ synthesized by chemical bath deposition. But the synthesis of ternary $PbS_{1-x}Se_x$ nanocrystals thin films by CBD remains underdeveloped compared to the widely studied cadmium chalcogenides alloys (Wanli *et al.*, 2009).

Many researchers have been using physical deposition techniques to synthesize $PbS_{1-x}Se_x$ thin films but only few reports are available by chemical bath deposition (Sarma *et al.*, 1982). In the present study $PbS_{1-x}Se_x$ thin films were synthesized by simple chemical bath deposition technique on glass substrate. Their optical, structural and morphological properties have been investigated. The deposition were carried out over the entire composition range of ($0 \leq x \leq 1$) from chemical bath containing lead acetate, thiourea, sodium hydroxide, ammonia and sodium selenosulphate, at a bath temperature of 90 ^{0}C and deposition time of 45 min. To the best of my knowledge, the deposition conditions and combination of reactants are being reported for the first time.

6.2 SYNTHESIS OF $PbS_{1-x}Se_x$ TERNARY THIN FILMS

The preparation conditions were optimized by adjusting concentration of dissolved precursors, temperature, pH value as well as deposition time to obtain homogeneous stoichiometric films. The chemical bath contained lead acetate $[Pb(CH_3COO)_2{\cdot}3H_2O]$ of 99 % purity, freshly prepared

sodium selenosulphite [Na_2SeSO_3] and thiourea [$CS(NH_2)_3$] of 99 % purity which provided lead ions, selenide ions and sulphur ions respectively, while sodium hydroxide (NaOH) was used as a complexing agent and ammonia (NH_3) used to adjust the pH of the aqueous solutions. All the solutions were prepared using deionized water.

A typical $PbS_{0.8}Se_{0.2}$ thin film was deposited in a reactive solution by mixing 5 ml lead acetate [$Pb(CH_3COO)_2{\cdot}3H_2O$] with 10 ml NaOH in a 100 ml beaker. The pH of the resulting solution was adjusted by drop wise addition of ammonia (30%). A Mettler Toledo InteLab@Expert Pro pH meter with temperature compensation and glass electrodes was used to record the pH of the solution. Thiourea $CS(NH_2)_3$ and 1 ml of sodium selenosulphate [Na_2SeSO_3] and some distilled water were added to obtain a final volume of 70 ml. Sodium selenosulphate was prepared by the same procedures explained in section 5.2.2. All chemicals used were of analytical grade. Well cleaned non-conducting glass slide substrates were introduced into the solution vertically with the help of a suitably designed substrate holder. The detail of the substrate cleaning process was discussed in section 5.2.1. The solution in the vessel was stirred continuously with a magnetic stirrer for homogeneous concentration in the entire solution and maintained at a temperature of 90 ^{0}C. The prepared solution was clear and colorless initially but turned yellowish after a few minutes. Depending on "x", a mirror like film began to deposit onto the sides of the beaker and the substrate this confirms the formation of $PbS_{1-x}Se_x$ thin films. After a deposition time, samples were removed from the solution, rinsed ultrasonically with distilled water and dried under ambient conditions before film characterization. Well adherent and mirror-like grey thin film surfaces were obtained. A similar procedure was adopted to prepare $PbS_{1-x}Se_x$ thin films in the range of ($0.04 \leq x \leq 0.96$). The solutions of lead acetate, thiourea and sodium selenosulphate were mixed in the required stoichiometric ratio of 1: $(1 - x)$: x and the reactive solution was

found to exhibit pH in the range of 12 to 12.5. The composition parameter "x" was obtained by adjusting the volume concentrations of S^{2-} and Se^{2-} ions sources in the reaction container.

The deposition process is based on the controlled formation of precipitates by slow release of S^{2-} and Se^{2-} ions. The reaction process for the formation of $PbS_{1-x}Se_x$ thin films may be described by the following steps. In an alkaline solution, thiourea decomposition is described by the following reaction (Xie *et al.*, 2014):

$$SC(NH_2) + 3OH^- \rightarrow CN_2^{2-} + HS^- + 3H_2O$$

$$HS^- + OH^- \rightarrow S^{2-} + H_2O \qquad 6.1$$

Similarly, sodium selenosulphate hydrolyzes in alkaline medium to give Se^{2-} ions as (Rajaram and Dnyandev, 1997):

$$Na_2SeSO_3 + OH^- \rightarrow Na_2SO_4 + HSe^-$$

$$HSe^- + OH^- \rightarrow Se^{2-} + H_2O \qquad 6.2$$

In the presence of Pb^{2+} ions in the bath, $PbS_{1-x}Se_x$ thin films will be formed if the ionic product of Pb^{2+}, S^{2-} and Se^{2-} exceeds the solubility product of $PbS_{1-x}Se_x$. The overall reaction in the presence of metal ions Pb^{2+} will be as follows:

$$Pb^{2+} + (1-x)S^{2-} + xSe^{2-} \rightarrow PbS_{1-x}Se_x \qquad 6.3$$

6.3 CHARACTERIZATION OF THE THIN FILMS

The crystallographic structure of the films were analyzed with a PANalytical Empyrean Series 2 powder X-ray diffractometer with a Cu-k_α radiation ($\lambda_{\alpha 1}$ = 1.5406 Å and $\lambda_{\alpha 2}$ = 1.5443 Å) source over the diffraction angle 2θ between 5^O to 80^O. The machine was operated at 40 mA and 45 kV. Scanning electron microscopy measurements were conducted using high resolution Zeiss 1550 VP SEM machine and operating at an accelerating voltage of 20 kV. The elemental compositions of the samples were determined using an energy dispersive X-ray analysis (EDX). Optical properties were measured at room temperature using a Shimadzu UV/VIS mini-1240 Spectrophotometer within the wavelength range of 200 nm – 1100 nm.

6.4 RESULTS AND DISCUSSION

6.4.1 Structural characterization

X-ray diffraction is an extremely important technique in the field of material characterization to obtain information on an atomic scale from both crystalline and non crystalline (amorphous) materials. It can be used to determine the phase content in many minerals and materials. It requires no elaborate sample preparation and is essentially non-destructive (Mathew, 2009). In this study the X-ray diffraction traces of all samples were taken at room temperature. The horizontal axis of the graph is 2θ, twice the Bragg angle and the vertical axis is the intensity count rate.

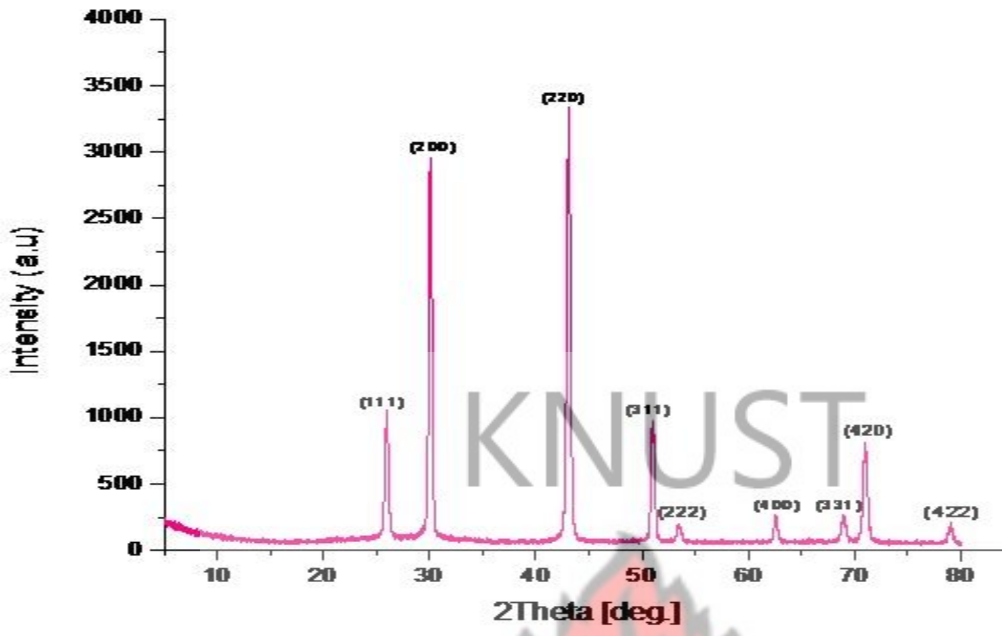

Figure 6.1: X-ray diffraction pattern of PbS thin film

Figure 6.1 shows the X-ray diffraction pattern of pure PbS thin film. The diffractogram shows well defined peaks corresponding to reflection from the (111), (200), (220), (311), (222), (400), (331), (420) and (422) planes with preferential orientation along the (220) plane. The diffraction pattern was well matched with standard [Galena, JCPDS data file reference code: 00-005-0592]. It can be noticed from the XRD pattern that a pair of peaks is followed by a single peak, which is again followed by a pair. This is a typical characteristic observation of a face centered cubic structure (Hankare *et al.*, 2003).

Figure 6.2: X-ray diffraction pattern of $PbS_{0.96}Se_{0.04}$ thin film

Figure 6.3: X-ray diffraction pattern of $PbS_{0.94}Se_{0.06}$ thin film

Figure 6.4: X-ray diffraction pattern of $PbS_{0.9}Se_{0.1}$ thin film

Figures 6.2 to 6.4, shows the X-ray diffraction patterns of $PbS_{1-x}Se_x$ thin films with composition, x = 0.04, 0.06 and 0.10. From the XRD studies it can be observed that addition of Se in PbS shifted the peak positions slightly towards smaller 2θ angles. Correspondingly, the values of d-spacing increased (see Appendix-1). This indicates the possibility of formation of solid solution (Mariappan *et al.*, 2012). Besides, it is important to note that no reflections corresponding to PbSe have been observed in this range. This also strengthens the possibility of solid solution formation (Shahane *et al.*, 2001; Swafford *et al.*, 2006). It is also observed that the addition of Se modified the intensities of reflections and changed the preferred orientation from the (220) plane of pure PbS to the (200) plane. Such variation of preferred orientations with stoichiometry of anion atoms S and Se was also reported by (Kumar *et al.*, 2010).

Figure 6.5: X-ray diffraction pattern of $PbS_{0.8}Se_{0.2}$ thin film

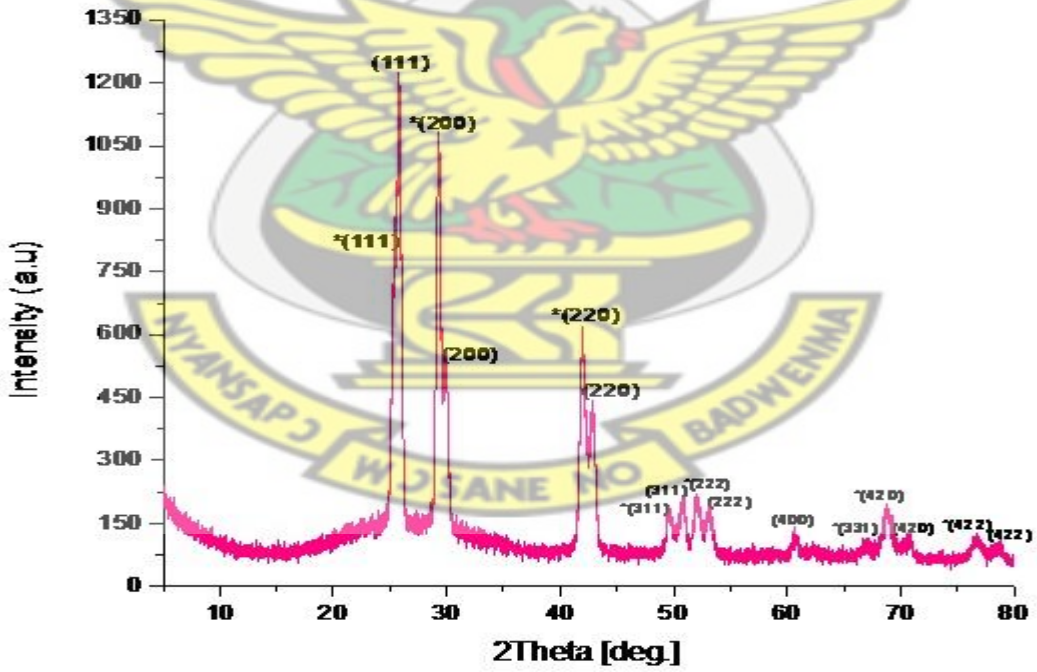

Figure 6.6: X-ray diffraction pattern of $PbS_{0.5}Se_{0.5}$ thin film

For the range of $0.2 \leq x < 0.8$, shown in Figures 6.5 and 6.6, it can be noticed that the number of peaks and intensity of peaks corresponding to PbS decreases whereas that of PbSe begins to appear and increases. This clearly shows that $PbS_{1-x}Se_x$ composites are the admixture of the PbS and PbSe phases (see Appendix-1). Of course, possibility of negligibly small amount of solid solution in this region cannot be ruled out. In this range ($0.2 \leq x < 0.8$) the preferential orientation of the films were along the (111) plane. In Figures 6.5 and 6.6, the peaks labeled by an asterisks (*) correspond to PbSe thin film and matched with the JCPDS data file reference number 01-078-1903.

Figure 6.7: X-ray diffraction pattern of $PbS_{0.2}Se_{0.8}$ thin film

Figure 6.8: X-ray diffraction pattern of $PbS_{0.06}Se_{0.94}$ thin film

Figure 6.9: X-ray diffraction pattern of $PbS_{0.04}Se_{0.96}$ thin film

Figure 6.10: X-ray diffraction pattern of PbSe thin film

For Se-dominated films ($0.8 \leq x \leq 1$), displayed from Figure 6.7 to Figure 6.10, it can be observed that addition of Se varied the intensities of reflections and a small peak shift towards lower 2θ angles, which indicates that the crystals obtained are not a simple mixture of PbS and PbSe, but a $PbS_{1-x}Se_x$ solid solution (Xie *et al.*, 2014). Likewise, the values of d-spacing increased (see Appendix-1). This indicates the possibility of formation of solid solution (Mariappan *et al.*, 2012). Furthermore, it is important to note that no reflections corresponding to PbS have been observed; this also strengthens the possibility of solid solution formation (Shahane *et al.*, 2001; Swafford *et al.*, 2006). It was also observed that further addition of Se in this region changed the preferred orientation from the (111) plane for x= 0.8 to the (200) plane of PbSe thin film. Figure 6.10 shows the X-ray diffraction pattern of undoped PbSe thin film. Well defined peaks observed correspond to reflection from the (111), (200), (220), (311), (222), (400), (331), (420) and (422) planes with preferred orientation along the (200) plane. The peaks are in

good agreement with the standard [JCPDS data file reference code: 01-077-0245] of the face centered cubic structure. A small peak at 11.93^0 in the undoped PbSe thin film could be as a result of impurities in the as-deposited thin film. The observed small hump with 2θ range of 20^0 to 34^0 in some of the XRD patterns may be due to the amorphous glass substrate (Lokhande and Kale, 2005; Sagadevan *et al.*, 2014).

From the X-ray diffraction analyses of $PbS_{1-x}Se_x$ samples it was observed that the preferred orientation changed from the (220) plane for $x = 0$ to the (200) plane for the range of $0.04 \leq x \leq 0.1$ then to the (111) plane for $(0.2 \leq x \leq 0.8)$ and finally to the (200) plane for the range of $0.8 < x \leq 1$. This indicates that the orientation of the grain growth for $PbS_{1-x}Se_x$ thin films prepared at different Se concentration is along different directions. Similar observation was reported by (Begum *et al.*, 2012). The presence of sharp and large number of peaks in all the XRD patterns can be attributed to the highly crystalline nature of the samples (Fekadu *et al.*, 2014; Pérez *et al.*, 2013). The lattice parameters for the cubic phase structure were determined from Equation 5.5 for selected values of "x" in the entire range of $(0 \leq x \leq 1)$ and listed in Appendix-1.

$$a_{hkl} = d_{hkl}\sqrt{h^2 + k^2 + l^2}$$

The crystallite size (D) was obtained from the X-ray diffraction pattern, using the Scherrer (1918) formula (see Equation 4.1). All parameters obtained from the XRD data for $PbS_{1-x}Se_x$ thin films are compared with the standard and are presented in Appendix-1. The lattice parameters have been determined for all $PbS_{1-x}Se_x$ thin films. From Appendix-1, it can be easily observed that the average lattice parameter increased from 5.932 Å for pure PbS to 6.130 Å for pure PbSe with increasing Se concentration. Beside, the average crystalline size was also found to increase from 25.60 nm to 39.54 nm as S was substituted by Se in $PbS_{1-x}Se_x$ thin films. Similar observation has been reported by (Al-Fawade *et al.*, 2013).

6.4.2 Variation of Lattice Parameters with Selenium ion Concentrations

The interplanar spacing d_{hkl} (Å) between the different lattice planes is characterized by Miller indices (hkl) (Ermrich and Opper, 2013). The interplanar distance d_{hkl} (Å) for PbS_{1-x} Se_x thin films have been plotted as a function of selenium ion concentration for the (111), (200) and (220) planes, where d_{hkl} (Å) was calculated from the Bragg diffraction law (Kittel, 2005).

$$2d_{hkl}\sin\theta_{hkl} = n\lambda \qquad 6.4$$

where *n* is the reflection order normally equal to unit, θ_{hkl} is the Bragg angle corresponding to hkl planes and λ = 1.5406 Å. Hence, the lattice parameter d_{hkl} (Å) for the peak positions of the (111), (200) and (220) planes are determined as:

$$d_{hkl} = \frac{1.5406\ \text{Å}}{2\sin\theta_{hkl}} \qquad 6.5$$

The variation of interplanar distance with increasing selenium mole ratio in PbS_{1-x} Se_x thin films are shown in Figure 6.11, Figure 6.12 and Figure 6.13.

Figure 6.11: Variation of interplanar distance d_{111} with increasing selenium ion concentration

Figure 6.12: Variation of interplanar distance d_{200} with increasing selenium ion concentration

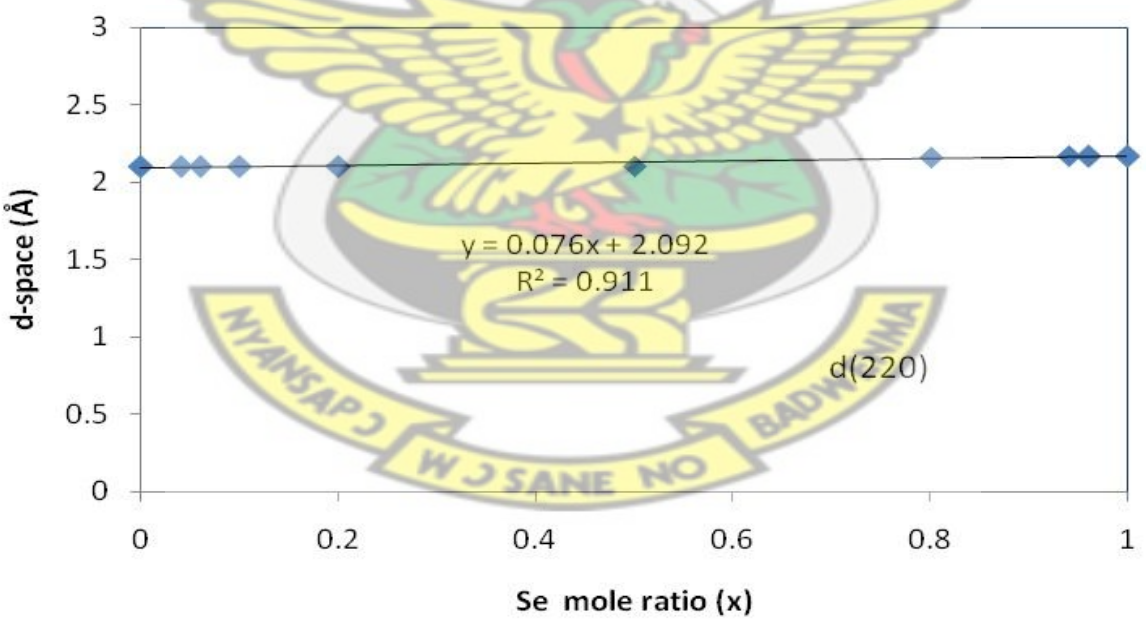

Figure 6.13: Variation of interplanar distance d_{220} with increasing selenium ion concentration

From Figure 6.11 to Figure 6.13, it can be easily observed that the interplanar distance d (Å) varies linearly with selenium ion concentration for the entire composition range of ($0 \leq x \leq 1$). This linear variation can be explained on the basis of Vergard`s law which states that: The crystallographic parameters of a continuous substitutional solid solution vary linearly with concentration at constant temperature when the nature of the bonding is similar in the constituent phases (Vegard, 1921).

The lattice parameter a (Å) for the cubic phase structure is mathematically related to the d-space by the following equation:

$$a = d\sqrt{h^2 + k^2 + l^2}$$

Miller indices and the d-space values can be obtained from X-ray diffraction spectrum; hence the lattice parameter a (Å) can be easily calculated from the above mathematical relation. The variation of lattice parameter a (Å) with selenium ion concentration is shown in Figure 6.14.

Figure 6.14: Lattice constant a (Å) versus increasing selenium ion concentration for PbS_{1-x} Se_x thin films

From Figure 6.14, a linear increase in lattice parameter is observed with the gradual addition of selenium. The linear relation between the lattice parameter and selenium mole ratio over the entire compositional range of ($0 \leq x \leq 1$) for PbS_{1-x} Se_x thin films suggest the formation of a substitutional solid solution. Since the ionic radius of the Se^{2-} ion is greater than the S^{2-} ion (EL-Nahas, 1992), addition of Se in PbS gradually expands the cell uniformly. This result is consistent with the well known approximate empirical rule called Vegard's law (Vegard, 1921). According to this rule, at constant temperature, a linear dependence is realized between the crystal lattice parameter of an alloy and the concentrations of the constituent elements (Kharchenko *et al.*, 2013). Usually, in the treatment of alloy problems, it is assumed that the atoms are located at ideal lattice sites and the lattice constants of alloys should vary linearly with composition "x" according to Vegard's law (Meradji *et al.*, 2011).

6.4.3 Elemental Analysis

Elemental analyses of the $PbS_{1-x}Se_x$ thin films were carried out by using the EDX (Energy-Dispersive X-ray) technique to study the stoichiometry of the films. The elemental analysis was carried out only for Pb, S and Se elements. The typical EDX spectrums of PbS, $PbS_{0.94}Se_{0.06}$, $PbS_{0.5}Se_{0.5}$ and PbSe are displayed from Figure 6.15 to Figure 6.18 and the other EDX data are presented in Table 6.1.

Figure 6.15: Energy-Dispersive X-ray spectrum of PbS thin film

Figure 6.16: Energy-Dispersive X-ray spectrum of $PbS_{0.94}Se_{0.06}$ thin film

Figure 6.17: Energy-Dispersive X-ray spectrum of $PbS_{0.5}Se_{0.5}$ thin film

Figure 6.18: Energy-Dispersive X-ray spectrum of PbSe thin film

All the EDX spectrums from Figure 6.15 to Figure 6.18 revealed that the deposited films are consistent with the formation of $PbS_{1-x}Se_x$ thin films on the glass substrate.

Table 6-1: Comparison of initial atomic percentage in bath solution of the films and elemental composition of $PbS_{1-x}Se_x$ thin films from EDX analyses

Table 6.1, shows that the atomic percentage of the elements in all investigated films are in close agreement with the volumetric ratio of the elemental precursor chemical solutions in the bath during deposition, which indicate that the samples are nearly stoichiometric. This result supports the possibility of preparing a complete range of solid solutions of $PbS_{1-x}Se_x$ by using CBD technique.

Figure 6.19 shows the relationship between the molar percentages of Se in $PbS_{1-x}Se_x$ thin films and in chemical bath solutions.

Figure 6.19: The relationship between the molar percentages of Se in $PbS_{1-x}Se_x$ thin films and in bath solutions

From Figure 6.19, it is observed that the molar percentages of Se in $PbS_{1-x}Se_x$ thin films and in the chemical bath solutions are almost linear. This linear relation suggests the great convenience to control the thin film composition as desired.

6.4.4 Surface Morphology Studies

Surface morphology of the ternary $PbS_{1-x}Se_x$ thin films were carried out using high resolution Zeiss 1550 VP scanning electron microscopy (SEM) with average working distance of 8.8 mm.

Figure 6.20 (a): SEM micrograph of PbS thin film (magnification 17.22 KX)

Figure 6.20 (b): SEM micrograph of PbS thin film (magnification 60 KX)

Figure 6.21 (a): SEM micrograph of $PbS_{0.8}Se_{0.2}$ thin film (magnification 17.22 KX)

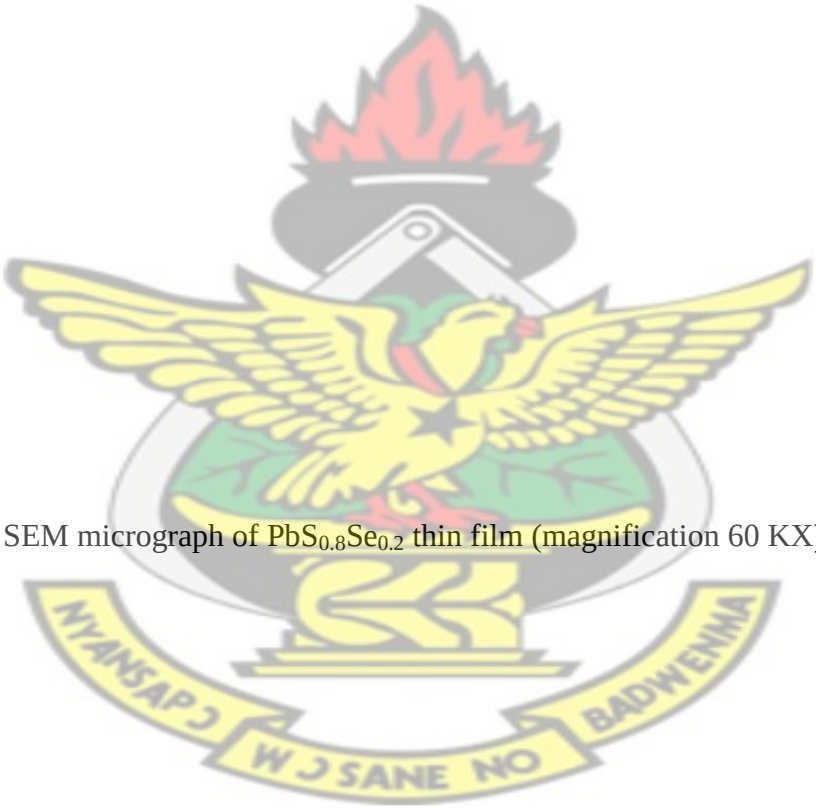

Figure 6.21 (b): SEM micrograph of $PbS_{0.8}Se_{0.2}$ thin film (magnification 60 KX)

Figure 6.22 (a): SEM micrograph of $PbS_{0.5}Se_{0.5}$ thin film (magnification 17.22 KX)

Figure 6.22 (b): SEM micrograph of $PbS_{0.5}Se_{0.5}$ thin film (magnification 60 KX)

Figure 6.23 (a): SEM micrograph of $PbS_{0.06}Se_{0.94}$thin film (magnification 17.22 KX)

Figure 6.23 (b): SEM micrograph of $PbS_{0.06}Se_{0.94}$thin film (magnification 60 KX)

Figure 6.24 (a): SEM micrograph of PbSe thin film (magnification 17.22 KX)

Figure 6.24 (b): SEM micrograph of PbSe thin film (magnification 60 KX)

Figures 6.20 to 6.24 show the SEM micrographs of $PbS_{1-x}Se_x$ thin films for x = 0, 0.2, 0.5, 0.94 and 1 respectively with two different magnifications (17.22 KX and 60 KX). The SEM micrograph of all the films shows uniform surface morphology over the entire glass substrates. Nearly all the films are composed of well defined cubic shaped grains, with different grain sizes

and uniformly distributed over a smooth homogenous background without defects like cracks, peeling or pinholes. Most of the nanocubes are interconnected to each other and quite compact without pores. The sharp jagged edges of the grains shown in almost all the SEM micrographs are characteristic signatures of crystals (Ampong, 2012). Those some large particles on some of the micrographs are quite likely colloidal particles formed in the solution and adsorbed on the substrate during the growth of the films (Chaudhari *et al.*, 2008). The micrograph of undoped PbS thin film shows plate like structure. Similar observation was reported by (Altıokka *et al.*, 2013).

6.4.5 Optical Analysis

6.4.5.1 Optical Absorbance

The most direct and perhaps the simplest method for probing the band structure of semiconductors is to measure the absorption spectrum (Majeed *et al.*, 2004). Optical measurements have many unique and attractive features for studying and characterizing semiconductors. They are contactless, nondestructive, and compatible with any transparent ambient including high-vacuum environments (Bass, 1995; Seiler *et al.*, 2009).

Optical properties of a material change or affect the characteristics of light passing through it by modifying its propagation vector or intensity. In optical absorption spectroscopy, electromagnetic radiation in the near-ultraviolet, visible or near-infrared regions are used to excite transitions between the electronic states (Bass, 1995). Any changes in the electronic structure of the material would be reflected in its optical behavior (Chopra, 1969). In the present study, optical characterization was carried out to study the nature of the absorption spectra and energy band gap of $PbS_{1-x}Se_x$ thin films. These properties have dependence on crystallite size

and chemical composition of the thin films. Therefore it is logical to study the optical properties in correlation with the above mentioned factors. The optical absorbance spectra of the $PbS_{1-x}Se_x$ thin films were recorded within the wavelength range of 200 -1100 nm. The optical absorbance spectrum of $PbS_{1-x}Se_x$ thin films for the entire range of ($0 \leq x \leq 1$) is shown in Figure 6.25.

Figure 6.25: Optical absorbance verses wavelenght of $PbS_{1-x}Se_x$ thin films with increasing Se concentration for the entier range of ($0 \leq x \leq 1$)

The vertical axis is absorbance of the materials and the horizontal axis is the wavelength of the incident photons. Although, the absorbance measurements were taken within the wavelength range of 200 nm to 1100 nm, the axis has been formatted to show the absorbance within the visible to NIR rang i.e 500 nm to 1100 nm. This is because the band gap of $PbS_{1-x}Se_x$ ($0 \leq x \leq 1$), thin films lies within this range. The films show a gradual increase in absorbance as Se concentration increases. Similar phenomena was observed by (Al-Fawade *et al.*, 2013). This may be attributed to crystalline size variation with Se concentration.

The samples exhibit a strong and broad absorption edge in the range of 500 nm to 900 nm as shown in Figure 6.25. In addition, from the optical absorption spectra it is observed that the

absorption edge shifts towards higher wavelength region with an increase in Se concentration. This red shift in absorption edge with increasing Se concentration indicates a decrease in optical band gap. One way to achieve effective harvesting of sunlight for solar energy is through the use of nanostructured thin films like PbS, PbSe or their ternary, which have absorption edges that can be tuned through the near-infrared range (Fritz *et al.*, 2008).

6.4.5.2 Optical Band gap Determination

The absorbance data were analyzed to determine the optical band gap of the samples using the classical Stern relation (see Equation 4.6) for near edge optical absorption of semiconductors. The band gap energy is obtained by extrapolating the linear portion of $(Ahv)^2$ versus hv to the energy axis at $(Ahv)^2 = 0$. Figure 6.26, shows the optical band gap of PbS thin film.

Figure 6.26: A graph of $(Ahv)^2$ plotted as a function of the photon energy(hv) for PbS thin film

From Figure 6.26 the estimated optical band gap is about 1.32 eV. This value is consistent with earlier reports (Sadovnikov and Gusev, 2013; Tohidi *et al.*, 2013). The estimated band gap for PbS thin film in the present work is slightly higher when compared to the reported bulk value of 0.41 eV (Thangavel *et al.*, 2010), this may be attributed to quantum size effects induced by the nanocrystallites in the thin film (Kotadiya *et al.*, 2012; Tohidi *et al.*, 2013).

Figure 6.27: A graph of $(Ahv)^2$ plotted as a function of the photon energy(hv) for $PbS_{0.5}Se_{0.5}$ thin film

Figure 6.27, shows a plot of $(Ahv)^2$ verses photon energy for $PbS_{0.5}Se_{0.5}$ thin film. Extrapolation of the linear portion of the curve to $(Ahv)^2 = 0$ gives the band gap energy. The estimated band gap is 1.18 eV, which clearly shows that the optical band gap decreased from pure PbS due to doping of Se. Figure 6.28, shows a plot of $(Ahv)^2$ versus photon energy for undoped PbSe thin film.

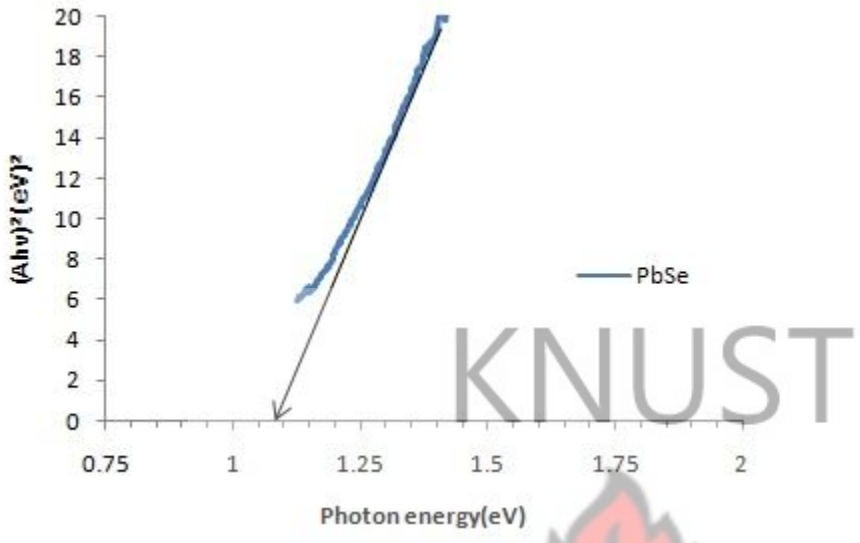

Figure 6.28: A graph of $(A h\nu)^2$ plotted as a function of the photon energy($h\upsilon$) for PbSe thin film

The estimated optical band gap from the extrapolation of best fit line between $(A h\nu)^2$ and photon energy to intercept the photon energy axis at $(A h\nu)^2 = 0$ is 1.08 eV. This value is in good agreement with already published results. Shandalov *et al.* (2007), reported the band gap of chemically deposited PbSe thin films varies from 1.09 eV to 0.86 eV on increasing the deposition time. Optical band gap of 1.10 eV for PbSe nanocrystal is also reported by (Zhu *et al.*, 2000). The estimated band gap for PbSe thin film in this work is slightly higher when compared to the reported bulk value of 0.27 eV at room temperature (Shyju *et al.*, 2012).

The increase of band gap is indicative of size quantization. For a crystallite size less than the Bohr diameter (≈ 80 nm for PbSe), an increase in the effective band gap due to size quantization should begin to be apparent (Sartale *et al.*, 2006; Zhu *et al.*, 2000).

The linear nature of the plot of $(Ahv)^2$ versus hν at the absorption edge shown in Figure 6.26, Figure 6.27 and Figure 6.28 indicate the presence of a direct transition (Lokhande and Kale, 2005). In general the obtained band gaps in this work compare favorably well with the reported values of PbS and PbSe thin films. The other compositions have in between those values. The summary of the estimated optical band gap for PbS_{1-x} Se_x thin films with selenium mole concentration for the entire composition range is tabulated in Table 6.2.

Table 6-2: Summary of band gap variation in $PbS_{1-x}Se_x$ thin films with selenium mole concentration

From Table 6.2, it is observed that the optical band gap of PbS_{1-x} Se_x thin films decreased from PbS (1.32 eV) to PbSe (1.08 eV) with increasing Se concentration. The variation of optical band gap with Se mole concentration "x" is shown in Figure 6.29.

Figure 6.29: Optical band gap of $PbS_{1-x}Se_x$ thin films verses Se mole concentration "x"

From Figure 6.29, it can be easily observed that the optical band gap of ternary $PbS_{1-x}Se_x$ thin films decreased as Se concentration increased. Similar observations were reported earlier by (Kumar *et al.*, 2010; Majeed *et al.*, 2004). In addition, it is clearly observed that the variation of band gap with Se concentration is almost linear indicating the formation of a continuous series of solid solution (Ampong, 2012). It is worth noting here that the structural, optical, morphological and electrical characteristics depend on the method of preparation (Sartale *et al.*, 2006).

Since the optical properties of alloys vary with composition, it is possible to tune the spectrum while maintaining a small size. Thus, by varying composition, we can get a second tool for altering physical and optical properties. Both size and composition may be tuned to select multiple desirable qualities simultaneously (Swafford *et al.*, 2006). The band gap of material should be compatible with the available solar spectrum for use in solar cell applications. Therefore, materials having only specific optical band energy are used (Dhankhar *et al.*, 2014).

The possibility for optical band gap variation in $PbS_{1-x}Se_x$ thin films presents the opportunity for the design of solar cells application. It is worth mentioning that the semiconductors with optical band gap within the range of 1–1.5 eV are suitable for achieving high energy conversion efficiency (30%) when used as absorber material in optoelectronic devices (Barrios-Salgado *et al.*, 2011; Shyju *et al.*, 2012). The optical band gap of $PbS_{1-x}Se_x$ thin films can be controlled in an optimal region of (1-1.5 eV) for photovoltaic application. This tunable band gap property of ternary $PbS_{1-x}Se_x$ thin film makes it an appropriate material for solar cell applications.

6.5 CONCLUSION

Well adherent nanocrystalline $PbS_{1-x}Se_x$ thin films were successfully synthesized by chemical bath deposition technique for the entire compositional range of $0 \leq x \leq 1$. The thin films were deposited from chemical baths containing lead acetate, thiourea, sodium hydroxide, ammonia and sodium selenosulphate, at a bath temperature of 90 ^{0}C. The deposited $PbS_{1-x}Se_x$ thin films were smooth and mirror-like grey in color. The films were characterized using a variety of

techniques. The X-ray diffraction analyses revealed that all $PbS_{1-x}Se_x$ thin films were polycrystalline in nature and it also showed that Se^{-2} has three important roles depending on its concentration when incorporated into the lattice of $PbS_{1-x}Se_x$ thin films. Addition of Se in PbS shifted the peak positions slightly towards smaller 2θ angles and modified the intensities of reflections and d-spacing. From the X-ray diffraction analysis of $PbS_{1-x}Se_x$ samples it was also observed that the preferred orientation changed from the (220) plane for $x = 0$ to (200) plane for the range of $0.04 \leq x \leq 0.1$ then to the (111) plane for $(0.2 \leq x \leq 0.8)$ and finally to the (200) plane for the range of $0.8 < x \leq 1$. The average crystallite size measured from FWHM was found to increase from 25.60 nm to 39.54 nm with increasing Se content. The lattice parameter a (Å) and inter planer distance d (Å) increased linearly with the gradual addition of Se, this result is consistent with the well known Vegard's law and supports the formation of a continuous series of solid solution.

The EDX analyses confirmed that the films were consistent with the formation of binary and ternary compounds on silica glass slide. It was also observed that the relations between molar percentages of Se in PbS_{1-x} Se_x thin films and in the chemical bath solutions are almost linear. This linear relation suggests a great convenience to control the thin film compositions as desired for different optoelectronic applications.

The SEM micrographs of all the films showed uniform surface morphology over the entire glass substrates and highly adhered films. Nearly all films were composed of well defined cubic shaped grains, with different grain sizes and uniformly distributed over a smooth homogenous background without defects like cracks, peeling or pinholes. Most of the grains were interconnected to each other and quite compact without pores. The sharp jagged edges of the grains shown in almost all SEM micrographs are characteristic signatures of crystals.

All the films showed a gradual increase in absorbance as Se concentration increased. The samples exhibited a strong and broad absorption edge in the range of 500 nm to 900 nm. In addition, the absorption edge shifted towards the higher wavelength region with an increase in Se concentration. This red shift in the absorption edge indicates band gap narrowing.

The optical band gap, calculated from optical absorption of ternary $PbS_{1-x}Se_x$ samples decreased almost linearly from PbS (1.32 eV) to PbSe (1.08 eV) as Se concentration increased. This linear variation of the band gap with composition parameter "x" ($0 \leq x \leq 1$), provides a lot of control in selecting a particular spectral sensitivity for a specific application.

Chapter 7

7. GENERAL CONCLUSION AND RECOMMENDATION

7.1 GENERAL CONCLUSION

Cadmium selenide thin films were successfully deposited on glass substrate using tartaric acid as a complexing agent, at a bath temperature of 85 ^{0}C. To the best of the author`s knowledge, this is the first time cadmium acetate is being used as the source of cadmium ions in combination with tartaric acid as complexing agent for the chemical bath deposition of CdSe thin films. The CdSe

thin films were annealed in air for 1 hour at 350 ^{0}C. The XRD analyses of both as-deposited and annealed CdSe thin films revealed that a uniform cubic phase of CdSe nanocrystalline thin films with preferred orientation along the (111) plane were deposited. The SEM micrographs showed the film surfaces were composed of spherically shaped grains. After annealing new peak at 67.1^0 position appeared. Annealing also caused the peak positions to shift towards smaller 2θ values. The average crystallite sizes were found to increase from 4 nm for as-deposited to 4.5 nm. After annealing other structural parameters such as dislocation density and micro-strain were decreased. The optical study revealed that the deposited samples have a direct band gap which decreased from 1.86 eV to 1.74 eV after annealing. The reactants, bath temperature, pH and deposition time used for this work, provide another set of deposition conditions for the growth of quality CdSe thin films by CBD technique.

$PbS_{1-x}Se_x$ ternary thin films have been successfully deposited for the entier range of ($0 \leq x \leq 1$) using the chemical bath deposition technique. Stractural analyses established that all the films had the face centered cubic structure and incorporation of Se into PbS had the effect of varying the preffered orientation and the growth direction of the grains. The variation of lattice parameter with Se ion composition were in good agreement with Vegard's law. Optical absorption measurements showed that the deposited samples have direct band gaps and varied linearly from 1.32 eV for PbS to 1.08 eV for PbSe as Se ion concentration increased. The SEM studies showed that most of the grains were interconnected to each other and quite compact without pores. The EDX analyses confirmed that the films were consistent with the desired stoichiometric ratio. These results support the possibility of preparing a complete range of solid solutions of $PbS_{1-x}Se_x$ thin films by using simple and cost effective chemical bath deposition technique.

7.2 RECOMMENDATION FOR FUTURE WORK

Further studies are needed:

1. To investigate the effect of annealing in an inert gas for both CdSe and $PbS_{1-x}Se_x$ thin films at various temperatures which may be considered to improve the quality and optoelectronic properties.
2. Hall Effect measurements to determine Hall coefficient, types of carrier concentration and mobility of the carriers.
3. To study the variation of conductivity and resistivity of $PbS_{1-x}Se_x$ thin films with increasing selenium concentrations and temperatures.
4. To carryout photoluminescence and photoconductivity measurements for both CdSe and $PbS_{1-x}Se_x$ thin films.
5. To apply FTIR Spectrophotometer measurement for $PbS_{1-x}Se_x$ thin films in the range of 400 - 4,200 nm wavelength to carry out the transmittance and absorbance. These will be helpful in determining other optical constants such as absorption coefficient, refractive index, extinction coefficient and optical dielectric constants.
6. To deposit the quaternary $Pb_{1-y}Cd_y$ (S, Se) thin films and investigate their optical, structural, morphological and electrical properties.

REFERENCES

Abbas, N., Al-Ansari, R., and Kadhum, K. (2008). Preparing PbS thin films doped with Cu and studying their structural properties. *Journal of Baghdad for Sciences, 5*(4), 522-533.

Abdin, Z., Alim, M. A., Saidur, R., Islam, M. R., Rashmi, W., Mekhilef, S., and Wadi, A. (2013). Solar energy harvesting with the application of nanotechnology. *Renewable and Sustainable Energy Reviews, 26,* 837-852.

Aberle, A. (2007). Recent Advances in Solar Cells *Advances in OptoElectronics 2007*, 1-2.

Abermann, S. (2013). Non-vacuum processed next generation thin film photovoltaics: Towards marketable efficiency and production of CZTS based solar cells. *Solar Energy, 94*, 37-70.

Abou-Ras, D., Kirchartz, T., and Uwe Rau. (2011). Advanced Characterization Techniques for Thin Film Solar Cells, Wiley-VCH, Germany, ISBN 978-3-527-41003-3.

Adachi, S. (2005). Properties of Group-IV, III-V and II-VI semiconductors, John Wiley and Sons Ltd., USA, ISBN 978-0-470-09032-9.

Adachi, S. (2009). Properties of Semiconductor Alloys: Group-IV, III–V and II–VI Semiconductors, John Wiley and Sons Ltd., United Kingdom, ISBN 978-0-470-74369-0.

Aghamkar, P., Kumar, S., Lal, B., and Husain, M. (2009). Influence of sulfur, selenium and tellurium doping on optical, electrical and structural properties of thin films of lead salts. *J. Alloys Compd., 488*.

Ajaya, K. S., Deo, S. R., Thool, G. S., Singh, R. S., Katre, Y. R., and Gupta, A. (2011). Synthesis and Characterization of Chemically Deposited Nanocrystalline CdSe Thin Film. *Synth. React. Inorg. Met.Org. Chem., 41*, 1346 -1350.

Akhtar, M. (2013). *Synthesis of Iron Chalcogenide Nanocrystals and Deposition of Thin Films from Single Source Precursors.* PhD Thesis, The University of Manchester, UK.

Al-Azad, M. A., Bhuiyan, M. R., and Hasan, S. M. F. (2008). Valance-band characterization of $AgGaSe_2$. *Journal of Physics D: Applied Physisc, 41*, 235108.

Al-Fawade, E., Abbas, N., and Alatya, S. (2013). Structure and Optical Investigations of PbS_xSe_{1-x} Alloy and Films. *Journal of Materials Science and Engineering A, 3*(2), 82-92.

Al-Jawad, S. M. H. and H.Alioy, F. (2013). Kinetics of Growth and Structural Characterization of Cd_{1-X} Zn_xS Thin Films Synthesized By CBD Method. *Eng. & Tech. Journal . 31*(4), 505-519.

Albrecht, T. W. J., Addai-Mensah, J., and Fornasiero, D. (2011). Effect of pH, Concentration and Temperature on Copper and Zinc Hydroxide Formation/Precipitation in Solution. *conference.net.au*, 477-487.

Alivisatos, A. P. (1996). Semiconductor Clusters, Nanocrystals and Quantum Dots. *Science, 271*(5251), 933-937.

Altıokka, B., Baykul, M. C., and Altıokka, M. R. (2013). Some physical effects of reaction rate on PbS thin films obtained by chemical bath deposition. *Journal of Crystal Growth, 384*, 50-54.

Altmann, S. L. (1994). Band Theory of Solids: An Introduction from the Point of View of Symmetry, Oxford University Press, UK, ISBN 978-0-198-55866-8.

Alvi, M. A. and Khan, Z. H. (2013). Synthesis and characterization of nanoparticle thin films of a-$(PbSe)_{100-x}Cd_x$ lead chalcogenides. *Nanoscale Research Letters, 148*(8), 1-10.

Ampong, F. K. (2012). *Synthesis and Characterization of Cadmium zinc sulphide ($Cd_{1-x}Zn_xS$) thin films from acidic chemical baths.* PhD Thesis, Kwame Nkrumah Universty of Science and Technology

Andersen, K. E., Fong, C. Y., and Pickett, W. E. (2002). Quantum confinement in CdSe nanocrystallites. *Journal of Non-Crystalline Solids, 299-302*, 1105-1110.

Anuar, K., Tan, W., Kuang, A. D., Mohd, S. A., Min, H. S., Siew, G. Y., and Saravanan, N. (2010). Preparation and characterization of iron sulphide thin films by chemical bath deposition method. *Indonesian Journal of Chemistry, 10*(1), 8-11.

Araoz, R. S. (2009). *Chemical bath deposition of Zn(S,O) buffer layers and application in Cd-free chalcopyrite-based thin-film solar cells and modules.* PhD Dissertation, Freien Universität Berlin, Helmholtz-Zentrum Berlin für Materialien und Energie.

Artemiev, A. N., Belyaev, A. D., Artemiev, N. A., Demkiv, A. A., Maevsky, A. G., Gorobtsov, O. Y., . . . Shalyapin, V. N. (2013). X-Ray, Synchrotron and Neutron Techniques. *Journal of surface Investigation, 7*(5).

Ashokkumar, M. and Muthukumaran, S. (2013). Size dependent structural and optical properties of $Cd_{0.9}$ $Zn_{0.1}S$ thin films. *Physics Procedia, 49*.

Asim, N., Sopian, K., Ahmadi, S., Saeedfar, K., Alghoul, M. A., Saadatian, O., and Zaidi, S. H. (2012). A review on the role of materials science in solar cells. *Renewable and Sustainable Energy Reviews, 16*, 5834-5847.

Baban, C. and Rusu, G. I. (2003). *Applied surface science 211*, 6-12.

Balaguru, R. J. B. and Jeyaprakash, B. G. (2012). Kronig–Penney Model - Free-Electron / Quasifree-Electron Approximation: Density of States Function

Barote, M. A., Yadav, A. A., and Masumdar, E. U. (2011). Effect of deposition parameters on growth and characterization of chemically deposited $Cd_{1-x}Pb_xS$ thin films. *Chalcogenide Letters, 8*(2), 129-138.

Barrios-Salgado, E., Nair, M. T. S., Nair, P. K., and Zingaro, R. A. (2011). Chemically deposited thin films of PbSe as an absorber component in solar cell structures. *Thin Solid Films, 519*, 7432-7437.

Barros, A. S., Abramof, E., and Rappl, P. H. O. (2006). Electrical and optical properties of PbTe p-n junction infrared sensors. *Jounal of Applied Physics 99*.

Bass, M. (1995). Hand book of Optics: Devices, Measurements and Properties Vol. II, McGraw-Hill, Inc., United States of America, ISBN 0-07-04797-7.

Bayer, A., Boylea, D. S., and O'Brien, P. (2002). In situ kinetic studies of the chemical bath deposition of zinc sulfide from acidic solutions. *J. Mater. Chem., 12*, 2940-2944.

Begum, A., Hussain, A., and Rahman, A. (2012). Effect of deposition temperature on the structural and optical properties of chemically prepared nanocrystalline lead selenide thin films. *Beilstein J. Nanotechnol., 3*, 438-443.

Behrnd, K. H., R. W. Hoffman, Bode, D. E., Maissel, L. I., and Vecht, L. V. G. A. (1966). Physics of Thin Films: Advances in Research and Development Vol. 3, Academic Press Inc., New York.

Bencherif, Y., Boukra, A., Zaoui, A., and Ferhat, M. (2011). Lattice dynamics study of lead chalcogenides. *Infrared Phys. Tech. , 54*, 39.

Bhattacharya, D. K. and Bhaskaran, A. (2010). Engineering Physics, Oxford University Press, UK, ISBN 978-0-19-806542-5.

Bhuiyan, M. R. A., Azad, M. A. A., and Hasan, S. M. F. (2011). Annealing effect on structural and electrical properties of $AgGaSe_2$ thin films *Indian Journal of pure and Applied Physics, 49*, 180-185.

Bhushan, S., Mukherjee, M., and Bose, P. (2002). Electro-optical studies in chemically deposited La/Nd doped (Cd-Pb) S films. *Journal of Materials Science: Materials in Electronics, 13*(10), 581-584.

Birkholz, M. (2006). Thin Film Analysis by X-ray Scattering, Wiley-VCH, Germany, ISBN 978-3-527-31052-4.

Bouroushian, M. (2010). Electrochemistry of Metal Chalcogenides, Springer, Verlag Berlin Heidelberg, ISBN 978-3-642-03966-9.

Boyle, D. S., Bayer, A., Heinrich, M. R., Robbe, O., and O'Brien, P. (2000). Novel approach to the chemical bath deposition of chalcogenide semiconductors. *Thin Solid Films, 61*, 150-154.

Bushroa, A. R., Rahbari, R. G., Masjuki, H. H., and Muhamad, M. R. (2012). Approximation of crystallite size and microstrain via XRD line broadening analysis in TiSiN thin films. *Vacuum, 86*, 1107 - 1112.

Caglar, M., Ilican, S., and Caglar, Y. (2006). The determination of the thickness and optical constants of the ZnO crystalline thin film by using envelope method. *Journal of optoelectronics and advanced materials, 8*(4), 1410-1413.

Calnan, S. (2014). Applications of Oxide Coatings in Photovoltaic Devices. *Coatings, 4*, 162-202.

Calzadilla, O., Zapata-Torres, M., Narvaez, L., Jiménez, S., and Rábago, F. (2002). Effect of annealing temperature on the crystalline quality of chemically deposited CdSe films. *Superficies y Vacío, 14*, 35-37.

Cao, L. Z., Meng, Q. D., Fu, W. Y., Wang, S. F., Leia, M., Cheng, B. L., . . . Chen, Z. H. (2007). Effect of annealing on the crystal structure and dielectric properties of $Ba_{0.6}Sr_{0.4}TiO_3$ thick films. *Physica B, 393*, 175-178.

Carrillo-Castillo, A., Lazaro, R. C. A., Ojeda, E. M. L., Perez, C. A. M., Quevedo-Lopez, M. A., and Aguirre-Tostado, F. S. (2013). Characterization of CdS thin films deposited by CBD using novel-complexing agents. *Chalcogenide Letters, 10*(10), 421.

Chae, D. Y., Seo, K. W., Lee, S. S., Yoon, S. H., and Shim, W. (2006). CdSe Thin Films Grown by MOCVD Method Using New Single-source Precursors. *Bull. Korean Chem. Soc, 27*(5), 762-764.

Chandrasekaran, J., Mohan, S. M., Thirumalairajan, S., and Girija, K. (2009). Structural and Optical Characteristics of CdSe Thin Films Prepared by Chemical Bath Deposition Technique. *Iraqi Journal of Applied Physice Letters, 2*(4).

Chate, P. A., Sathe, D. J., Hankare, P. P., Lakade, S. D., and Bhabad, V. D. (2013). Synthesis and characterization of cubic cadmium selenide by chemical route. *Journal of Alloys and Compounds, 552*, 40-43.

Chattarki, A. N., Kamble, S. S., and Deshmukh, L. P. (2012). Role of pH in aqueous alkaline chemical bath deposition of lead sulfide thin films. *Materials Letters, 67*, 39-41.

Chaudhari, J. B., Deshpande, N. G., Gudage, Y. G., Ghosh, A., Huse, V. B., and Sharma, R. (2008). Studies on growth and characterization of ternary $CdS_{1-x}Se_x$ alloy thin films deposited by chemical bath deposition technique. *Applied Surface Science, 254*, 6810-6816.

Choi, M., Hu, S. G., Abdallah, J., Limpinsel, L. S., Zhang, M., Zollner, Y. N., . . . Law, R. Q. (2012). Pseudodielectric function and critical-point energies of iron pyrite. *Physical Review B, 86*(11), 115-207.

Chopra, K. L. (1969). Thin-Film Phenomena, McGraw-Hill, New York.

Choudhury, N. and Sarma, B. K. (2011). Structural analysis of chemically deposited nanocrystalline PbS films. *Thin Solid Films, 519*, 2132-2134.

Chowdhury, R. I., Islam, M. S., Sabeth, F., Mustafa, G., Farhad, S. F. U., Saha, D. K., . . . Islam, A. B. M. O. (2012). Characterization of Electrodeposited Cadmium Selenide Thin Films. *Dhaka Univ. J. Sci., 60*(1), 137-140.

Christensen, N. E. (1984). Electronic structure of GaAs under strain. *Phys. Rev. B 30*.

Colinge, J. P. and Colinge, C. A. (2002). Physics of Semiconductor Devices, Kluwer Academic, Dordrecht, ISBN 0-306-47622-3.

Commission, E. (2003). World energy, technology and climate policy outlook 2030 — WETO (pp. 137).

Cullity, B. D. (1978). Elements of X-Ray Diffraction, Addison Wesley, USA, ISBN 56-10137.

Cyrus, W., Alivisatos, A. P., and Kammen, D. M. (2009). Materials availability expands the opportunity for large-scale photovoltaics deployment. *Environ. Sci. Technol., 43*(6), 2072-2077.

Das, S. R. and Chopra, K. L. (1983). Thin film Solar Cells, Plenum Press, New York, ISBN-10: 0306411415.

David, M. K. and Devadason, S. (2013). A Comparative Study on the Optical Properties of Multilayer CdSe / CdTe Thin Film with Single Layer CdTe and CdSe Films. *Jounal of Nano-and Electronic Physics, 5*(3), 1-4.

Delekar, S. D., Hankare, P. P., Chate, P. A., Sabane, S. D., Garadkar, K. M., and Bhuse, V. M. (2005). A novel route to synthesize Cd_{1-x} Pb_xSe thin films from solution phase. *Semiconductor Science and Technology, 20*, 257-264.

Delin, A., Ravindran, P., Eriksson, O., and Wills, J. M. (1998). Full-Potential Optical Calculations of Lead Chalcogenides. *Int J Quant Chem, 69*, 349-358.

Deshmukh, L. P., More, B. M., Holikatti, S. G., and Hankare, P. P. (1994). Preparation and properties of $(CdS)_x$ -$(PbS)_{1-x}$ thin-film composites. *Bulletin of Materials Science, 17*(5), 455-463.

Deshpande, M. P., Garg, N., Bhatt, S. V., Sakariya, P., and Chaki, S. H. (2013). Characterization of CdSe thin films deposited by chemical bath solutions containing triethanolamine. *Materials Sciencein Semiconductor Processing, 16*, 915-922.

Dhanam, M., Prabhu, R. R., and Manoj, P. K. (2008). Investigations on chemical bath deposited cadmium selenide thin films. *Materials Chemistry and Physics, 107*, 289-296.

Dhankhar, M., Singh, O. P., and V.N.Singh. (2014). Physical principles of losses in thin film solar cells and efficiency enhancement methods. *Renewable and Sustainable Energy Reviews, 40*, 214-223.

Dragoman, D. and Mircea, D. (2010). Advanced optoelectronic devices, Springer series, Germany, ISBN 1-03-642-08435-4.

Dwivedi, D. K., Kumara, V., Dubey, M., and Pathak, H. P. (2011). Structural, Electrical and Optical investigation of CdSe Nanoparticles. *Chalcogenide Letters, 8*(9), 521-527.

EL-Nahas, M. M. (1992). Structural and electrical properties of cadmium-sulpho-selenide solid solutions. *Jounal of materials science:Mater.Electron, 3*(1), 71-76.

Elisabetha, S., Zilbermann, I., Maimon, E., Nahmani, Y., Cohen, H., Adarc, E., and Meyerstein, D. (2004). Radical catalyzed debromination of bromo-alkanes by formate in aqueous solutions via a hydrogen atom transfer mechanism. *Tetrahedron Letters, 45*, 989-992.

Ermrich, M. and Opper, D. (2013). X-Ray Powder Diffraction for Anslyst: Getting aquainted with the Principles, PANalytical Gmb, Nurnberger, ISBN 978-90-809086-0-4.

Eser, E. and Birkmire, R. W. (1997). Polycrystaline thin film solar cells: Present Status and Future Potential. *Annu. Rev. Mater. Sci., 27*(53), 625-648.

Esparza-Ponce, H. E., Hernández-Borja, J., Reyes-Rojas, A., Cervantes-Sánchez, M., Vorobiev, Y. V., Ramírez-Bon, R., . . . González-Hernández, J. (2009). Growth technology, X-ray and optical properties of CdSe thin films. *Materials Chemistry and Physics, 113*, 824-828.

Evans, R. L. (2007). Fueling Our Future: An Introduction to Sustainable Energy, Cambridge University Press, UK, ISBN 978-0-511-28943-9.

Fanchi, J. R. (2004). Energy:Technology and Diractions for Future, Cambridge University Press, UK, ISBN 978-0-511-28943-9.

Fekadu, H. G., Ampong, F. K., Abza, T., Nkrumah, I., Nkum, R. K., and Boakye, F. (2014). Investigating the effect of deposition time on the morphology, structure and optical band gap of PbS thin films synthesized by CBD technique. *Elixir Thin Film Tech., 76*, 28432-28437.

Feng-Ling, Z., Xiao-Min, L., Xiang-Dong, G., and Ji-Jun, Q. (2008). Low cost Preparation and Photoelectric Property Study of PbSe Nanocrystalline Films. *Journal of Inorganic Materials*, 11-21.

Fritz, K. P., Guenes, S., Luther, J., Kumar, S., Sariciftci, N. S., and Scholes, G. D. (2008). IV–VI Nanocrystal–polymer solar cells. *Journal of Photochemistry and Photobiology A: Chemistry, 195*, 39-46.

Furlong, M. J., Froment, M., Bernard, M. C., Cortés, R., Tiwari, A. N., Krejci, M., . . . Lincot, D. (1998). Aqueous solution epitaxy of CdS layers on $CuInSe_2$. *Jounal of crystal growth, 193*.

Geissuhler, I. (2005). *Cadmium selenide nanocrystals for specific interaction with biomolecules.* . PhD Thesis, Éole Polytechnique Federale De Lausanne, , Lausanne.

George, J. (1992). Preparation of Thin Films, Marcel Dekker, Inc., New York.

Ghobadi, N. and Moradian, R. (2013). Strong localization of the charge carriers in CdSe nanostructural films. *International Nano Letters, 3*(47), 1-5.

Gokul, B., Matheswaran, P., and Sathyamoorthy, R. (2013). Influence of Annealing on Physical Properties of CdO Thin Films Prepared by SILAR Method. *J. Mater. Sci. Technol., 29*(1), 17-21.

Goldstein, D.E.Newbury, Joy, D. C., C.E.Lyman, Echlin, P., E.Lifshin, . . . J.R.Michael. (2003). Scanning electron microscopy and X-ray microanalysis, 3rd Ed., Springer, ISBN 978-1-4615-0215-9.

Gopakumar, N., Anjana, P. S., and Pillai, P. K. V. (2010). Chemical bath deposition and characterization of CdSe thin films for optoelectronic applications. *J Mater Sci., 45*, 6653-6656.

Gorer, S., Albu-Yaron, A., and Hodes, G. (1995). Quantum size effects in chemically deposited, nanocrystalline Lead Selenide films. *J. Phys. Chem., 99*(44), 16442-16448.

Gorer, S. and Hodes, G. (1994). Quantum size effects in the study of chemical solution deposition mechanisms of semiconductor films. *J.Phys.Chem., 98*(20), 5338-5346.

Graham-Rowe, D. (2007). Solar cells get flexible. *Nature Photonics, 1*(8), 433-435.

Grundmann, M. (2010). The Physics of Semiconductors: An Introduction Including Nanophysics and Applications, 2nd Ed., Springer-Verlag, Berlin Heidelberg, ISBN 978-3-642-13883-6.

Guitierrez, M. T. and Ortega, J. (1989). *Sol. Ener. Mater., 19*.

Gupta, S. and Munirathnam, K. (2014). Synthesis and characterization of sputtered $Cd_{1-x}Mg_xTe$ alloy and their applications in solar cells. *Indian Journal of pure and Applied Physics, 52*, 44-52.

Hall, B. D., Zanchetb, D., and Ugarte, D. (2000). Estimating nanoparticle size from diffraction measurements. *J. Appl. Cryst., 33*, 1335-1341.

Hamaguchi, C. (2010). Basic Semiconductor Physics, Springer-Verlag, Berlin Heidelberg, ISBN 978-3-642-03302-5.

Hani, K., Isaiah, O., and Lee, C. (2008). Optimization of chemical bath deposited CdS thin films using nitrilotriacetic acid as a complexing agent. *Thin Solid Films, 516*(18), 5967-5973.

Hankare, P. P., Delekar, S. D., Asabe, M. R., Chate, P. A., Bhuse, V. M., Khomane, A. S., . . . Sarwade, B. D. (2006). Synthesis of Cadmium Selenide thin films at low-temperature by simple Chemical route and their Characterization. *Journal of Physics and Chemistry of Solids, 67*(12), 2506-2511.

Hankare, P. P., Delekar, S. D., Bhuse, V. M., Garadkar, K. M., Sabane, S. D., and Gavali, L. V. (2003). Synthesis and characterization of chemically deposited lead selenide thin films. *Materials Chemistry and Physics, 82*, 505-508.

Haruta, M. and Delmon, B. (1986). Preparation of homodisperse solids. *J. Chem. Phys., 83*.

Hersch, P. and Zweibel, K. (1982). Basic Photovoltaic Principles and Methods, Solar Energy Research Institute for the U.S. Department of Energy, USA.

Hodes, G. (2002). Chemical solution deposition of semiconductor films, Marcel Dekker, Inc., New York, ISBN 0-8247-0851-2.

Hodes, G. (2007). Semiconductor and ceramic nanoparticle films deposited by chemical bath deposition. *Physical Chemistry Chemical Physics, 9*(18), 2181-2196.

Horowitz, G. (1990). Organic semiconductors for new electronics. *Advanced Materials 2*.

Hotje, U., Rose, C., and Binnewies, M. (2003). Lattice constants and molar volume in the system ZnS, ZnSe, CdS and CdSe. *Solid State Sciences, 5*, 1259-1262.

Humphreys, J. and Hatherly, M. (2004). Recrystallization and Related Annealing Phenomena, Elsevier, ISBN 978-0-08-044164-1.

Ichimura, M., Kumaresan, R., Sato, N., and Arai, E. (2001). *Photochemical deposition and Elrctrochemical deposition of semiconductors for solar cell*. Paper presented at the 4th International Conference on Mechanical Engineering, Dhaka, Bangladesh.

Ilican, S., Caglar, M., and Caglar, Y. (2007). Determination of the thickness and optical constants of transparent indium-doped ZnO thin films by the envelope method. *Materials Science-Poland, 25*(3), 709-718.

Jadhav, S. R. and Khairnar, U. P. (2012). Study of Optical Properties of Co-evaporated PbSe Thin Films. *Archives of Applied Science Research, 4*(1), 169-177.

Jager-Waldau, A. (2011). Progress in chalcopyrite compound semiconductor research for photovoltaic applications and transfer of results into actual solar cell production. *Solar Energy Materials & Solar Cells, 95*, 1509-1517.

Jai, S. (2006). Optical Properties of Condensed Matter and Applications, John Wiley and Sons Ltd., England, ISBN 13 978-0-470-02192-7.

Jamal, M., Al-jumaili, H. S., and Antar, F. H. (2014). Effect of Cadmium Sources on Structural and Optical Properties of Nanocrystalline CdS Thin Films Prepared by CBD Technique. *International Journal of Application or Innovation in Engineering and Management, 3*(5), 196-199.

Johnston, S. (2012). *Output Performance and Payback Analysis of a Residential Photovoltaic System in Colorado*. Paper presented at the IEEE Photovoltaic Specialists Conference, Austin, Texas.

Kaelin, M., Rudmann, D., and Tiwari, A. N. (2004). Low cost processing of CIGS thin film solar cells. *Solar Energy, 77*(6), 749-756.

Kainthla, R. C., Pandya, D. K., and Chopra, K. L. (1980). Solution Growth of CdSe and PbSe Films. *Jounal of the Electrochemical Society, 127*(2), 277-283.

Kainthla, R. C., Sharma, N. C., Pandya, D. K., and Chopra, K. L. (1979). Electroless Deposition of Semiconductor Films. *Thin Solid Films, 60*.

Kale, S. S. and Lokhande, C. D. (2000). Thickness-dependent properties of chemically deposited CdSe thin film. *Materials Chemistry and Physics 62*, 103-108.

Kalita, P. K., Sarma, B. K., and Das, H. L. (2003). Space charge limited conduction in CdSe thin films. *Bull. Mater. Sci., 26*(6), 613-617.

Kamat, P. V. (2008). Quantum Dot Solar Cells. Semiconductor Nanocrystals as Light Harvesters. *J. Phys. Chem. C, 112*, 18737-18753.

Kanithla, R. C., Pandya, D. K., and Chopra, K. L. (1982). Photo-Electronic Properties of Solution-Grown CdSe Films. *Solid-State Electronics, 25*(1), 73-76.

Karim, M. U. (2007). Solar Revolution: The Economic Transformation of the Global Energy Industry. *Electronic Green Journal, 1*(25).

Karthika, P. C., Ratnakar, A., Balasubramaniam, N., Sahatiya, P., Teja, K., and Mohan, A. (2013). Synthesis and Characterization of Lead-Cadmium Selenide Nanoparticles by Polyol Method for Semiconductor based Applications. *Asian Journal of Chemistry, 25*, 381-383.

Kathalinga, A., Ambika, N., Kim, M. R., Elanchezhiyan, J., Chae, Y. S., and Rhee, J. K. (2010). Chemical bath deposition and characterization of nanocrystalline ZnO thin films. *Materials Science-Poland, 28*(2), 513-522.

Kemell, M., Ritala, M., and Leskel, M. (2005). Thin Film Deposition Methods for $CuInSe_2$ Solar Cells. *Critical Reviews in Solid State and Materials Sciences, 30*, 1-31.

Khanlary, M. R. and Salavati, E. (2012). Optical Properties and Characterization of Prepared Sn-Doped PbSe Thin Film. *Advances in Condensed Matter Physics*, 1-4.

Kharchenko, V. O. and Kharchenko1, D. O. (2013). Ab-initio calculations for structural properties of Zr–Nb alloys. *Condensed Matter Physics, 16*(1), 13801: 13801–13808.

Khokhlov, D. (2003). Lead Chalcogenides: Physics and Applications, Taylor and Francis Books, Inc., New York, ISBN 1-56032-916-5.

Khomane, A. S. (2011). Structural and optical characterizations of chemically deposited cadmium selenide thin films. *Materials Research Bulletin, 46*, 1600-1603.

Khomanea, A. S. and Hankare, P. P. (2010). Structural, optical and electrical characterization of chemically deposited CdSe thin films. *Journal of Alloys and Compounds, 489*, 605-608.

Kim, E., Jiang, Z.-T., and No, K. (2000). Measurement and calculation of optical band gap of chromium aluminum oxide films. *Jpn. J. Appl. Phys. , 39*, 4820-4825.

Kissinger, N. J. S., Jayachandran, M., Perumal, K., and Raja, C. S. (2007). Structural and optical properties of electron beam evaporated CdSe thin films *Bull. Mater. Sci., 30*(6), 547-551.

Kissinger, N. J. S., Suthagar, J., Kumar, B. S., Balasubramaniam, T., and Perumal, K. (2010). Effect of Substrate Temperature on the Structural and Optical Properties of Nanocrystalline Cadmium Selenide Thin Films Prepared by Electron Beam Evaporation Technique. *Acta Physica Polonica A, 118*(4).

Kittel, C. (2005). Introduction to Solid state Physics, Vol. 8th, John Wiley and Sons, Inc., USA, ISBN 0-471-41526-X.

Knapp, K. E. and Jester, T. L. (2000). *An Empirical Perspective on the Energy Payback Time for Photovoltaic Modules*. Paper presented at the Solar 2000 Conference, Madison, Wisconsin.

Kotadiya, N. B., Kothari, A. J., Tiwari, D., and Chaudhuri, T. K. (2012). Photoconducting nanocrystalline lead sulphide thin films obtained by chemical bath deposition. *Appl. Phys. A, 108*, 819-824.

Kothiyal, G. P. and Ghosh, B. (1990). On conductivity in lead chalcogenides. *Prog.Cryst. Growth Charact., 20*(4), 313-332.

Krylova, V., Milbrat, A., Embrechts, A., and Baltrusaitis, J. (2014). Ag_2S deposited on oxidized polypropylene as composite material forsolar light absorption. *Applied Surface Science, 301*, 134-141.

Kumar, R., Jain, G., Saini, R., and Agarwal, P. (2010). Compositional Effects on Properties of PbS_{1-x} Se_x Thin films. *Chalcogenide Letters, 7*(4), 233-240.

Kumaran, T. S. and Banu, S. P. (2013). Investigation on structural and optical properties of chemically deposited PbS thin films *International Journal of Recent Scientific Research, 4*(11), 1685-1687.

Kushiya, K., Nii, T., Sugiyama, I., Sato, Y., Inamori, Y., and Takeshita, H. (1996). *Japan J. Appl. Phys., 35*(4383).

Kwang-Deog, J., Lokhande, C. D., Lee, E.H., and Joo, O.-S. (2005). Ammonia-free chemical bath method for deposition of microcrystalline cadmium selenide films. *Materials Chemistry and Physics, 91*, 200-204.

Kwok, K. N. and Sze, S. M. (2007). Physics of Semiconductor Devices, 3rd Ed., John Wiley and Sons, Inc., New Jersey, ISBN 978-0-47 1-1 4323-9.

Labidi, S., Meradji, H., Labidi, M., Ghemid, S., Drabliaa, S., and Hassanb, F. E. H. (2009). First principles calculations of structural, electronic and thermodynamic properties of SrS, SrSe, SrTe compounds and $SrS_{1-x}Se_x$ alloy. *Physics Procedia, 2*, 1205-1212.

Lancry, O., Farvacque, J. L., Pichonat, E., and Gaquiere, C. (2011). Indirect interband transition in hexagonal GaN. *J. Phys. D: Appl. Phys., 44*, 1-4.

Langfordy, J. I. and Louer, D. (1996). Powder diffraction. *Rep. Prog. Phys., 59*, 131-234.

Lee, S.C. and Lee, M. J. (2000). Effects of multi-energetic grain-boundary trapping states on the electrical characteristics of poly-CdSe thin film transistors. *Journal of Applied Physics, 88*(4), 1999-2004.

Lehmann, A. G., Bionducci, M., and Buffa, F. (1998). Effect of mechanical grinding on the hexagonal structure of CdSe. *Physical Review B, 58*, 5282.

Li, Z. Q. S., Liu, J. H., Wang, Q. Q., Z. A., S., Z. , and Huang, S. M. (2010). Effect of [Zn]/[S] ratios on the properties of chemical bath deposited zinc sulfide thin films. *Applied Surface Science 257*, 122-126.

Lide, D. R. (1995). Handbook of Chemistry and Physics, 76th Ed., CRC Press, United Kingdom, ISBN 9780849304767.

Liebig, J. and Pharma, A. (1835). Ueber die Producte der Oxydation des Alkohols. *Annalen der Chemie, 14*(2), 133.

Liua, W.L., Yangb, C.S., Hsieha, S.H., Chenb, W.J., and Fernb, C.L. (2013). Effect of deposition variables on properties of CBD ZnS thin films prepared in chemical bath of $ZnSO_4/SC(NH_2)_2/Na_3C_3H_5O_7/NH_4OH$. *Applied Surface Science, 264*, 213-218.

Lokhande, C. D. and Kale, R. B. (2005). Band gap shift, structural characterization and phase transformation of CdSe thin films from nanocrystalline cubic to nanorod hexagonal on air annealing. *Semicond. Sci. Technol. , 20*, 1-9.

Lokhande, C. D. and Pathan, H. M. (2004). Deposition of metal chalcogenide thin films by successive ionic layer adsorption and reaction (SILAR) method. *Bulletin of Materials Science, 27*(2), 85-111.

Lundin, A. B., Kitaev, G. A., and Nauk, I. A. (1965). *Inorg. Mater.,, 1*, 2107-2112.

Lynn, P. A. (2010). Electricity from Sunlight: An Introduction to Photovoltaics, John Wiley and Sons, Ltd., United Kingdom, ISBN 978-0-470-74560-1.

Mahdi, M. A., Obaid, A. S., Dihe, A. A., and Hassan, Z. (2012). Effect of Deposition Time on the PbS Thin films Prepared using Microwave-Assisted Chemical Bath Deposition: Structure and Optical Characterization. *International Conference on Education, Applied Sciences and Management*, 1-4.

Majeed, K. A., Kumar, S., Khan, S. A., and Husain, M. (2004). Studies on vacuum evaporated $PbS_{1-x}Se_x$ thin films. *Optical Materials, 25*, 25-32.

Mane, R. S. and Lokhande, C. D. (2000). Chemical deposition method for metal chalcogenide thin films. *Materials Chemistry and Physics, 65*, 1-31.

Mani, P., Manikandan, K., Ramya, A. J., seelan, A. I., Zahirullah, S. S., hameed, M. S., and prince, J. J. (2014). Influence of Molar Concentrations on Optical Properties of Copper Sulphide Thin Films by SILAR Method. *Int.J. ChemTech Res.*, *6*(7), 3573-3578.

Mansour, H. L., Mishjil, K. A., Habubi, N. F., and Chiad, S. S. (2014). Structural and Optical Properties of $Cd_{0.4}$ $Se_{0.6}$ Thin Films Prepared by CBD. *Int. J.Thin Films Sci. Tec., 3*(2), 57-60.

Margaret, V. H. (2009). *Optical and Material Properties of Colloidal Semiconductor Nanocrystals.* PhD Thesis PhD University of Toronto, Toronto.

Mariappan, R., Ponnuswamy, V., and Ragavendarb, M. (2012). Characterization of CdS_{1-x} Se_x thin films by chemical bath deposition technique. *Optik, 123*, 1196-1200.

Mark, G. and O'Brien, P. (1999). Recent advances in the preparation of semiconductors as isolated nanometric particles: new routes to quantum dots. *Chem. Commun.*, 2235-2241.

Mascaro, D. J. and Dimitrakopoulos, C. D. (2001). Organic thin-film transistors: A review of recent advances. *IBM Journal of Research and Development 45*(1), 11-28.

Mathew, M. (2009). *Engineering the Properties of Indium Sulfide for Thin Film Solar Cells by Doping.* PhD Thesis, Cochin University of Science and Technology.

Mattoussi, H., Radzilowski, L. H., Dabbousi, B. O., Thomas, E. L., and, M. G. B., and Rubner, M. F. (1998). *J. Appl. Phys. , 83*, 7965.

Mattox, D. M. (2010). Handbook of Physical Vapor Deposition (PVD) Processing, 2nd Ed., Elsevier/ William Andrew, ISBN 978-0815520375.

Mehta, C., Abbas, J. M., Saini, G. S. S., and Tripathi, S. K. (2007). Effect of deposition parameters on the optical and electrical properties of nanocrystalline CdSe. *Chalcogenide Letters, 4*(11), 133-138.

Mehta, C., Abbas, J. M., Saini, G. S. S., and Tripathi, S. K. (2008). Preparation and Characterization of Self-Assembled n-ZnS Thin Films. *Iraqi Journal of Applied Physics, 4*(4), 31-34.

Meradji, H., Labidi, M., Ghemid, S., and Labidi, S. (2011). Structural, Electronic, Optical and Thermodynamic Properties of PbS, PbSe and Their Ternary Alloy $PbS_{1-x}Se_x$. *Modern Physics Letters B, 25*(7), 473-486.

Merita, S., Kramer, T., Mogwitz, B., Franz, B., Polity, A., and Meyer, B. K. (2006). *Phys.Stat. Sol. (C), 3*.

Metin, H., Erat, S., Ari, M., and Bozoklu, M. (2008). Characterization of CdSe films prepared by chemical bath deposition method. *Optoelectronics and Advanced Materials 2*(2), 92-98.

Mohamed, H. A. (2014). Theoretical study of the efficiency of CdS/PbS thin film solar cells. *Solar Energy, 108*, 360-369.

Mohammad, J. F. and Al-jumaili, H. S. (2014). Structural and optical properties of Nanocrystalline $Zn_xCd_{1-x}S$ thin films deposited by chemical bath technique. *International Journal of Application or Innovation in Engineering & Management, 3*(5), 204-210.

Mohammed, S., Al-Jawad, H., and J.Alogili, H. K. (2009). Growth Kinetics of Chemically Deposited CdO Thin Films. *Eng. & Tech. Journal, 27*(11).

Moholkar, A. V., Pawar, S. M., Rajpure, K. Y., and Bhosale, C. H. (2006). Electrosynthesis and characterization of CdSe thin films: Optimization of preparative parameters by photoelectrochemical technique. *Journal of Physics and Chemistry of Solids, 67*(11), 2386-2391.

Moreno, O. P., Avila, G. A., Cerna, J. R., Tecorralco, J. H., Portillo, M. C., Juárez, J. M., . . . Ángel, O. Z. (2011). Characterization of Chemical Bath Deposited CdS, CdSe and PbS. *Journal of Materials Science and Engineering A, 1*, 692-704.

Mote, V. D., Purushotham, Y., and Dole, N. (2012). Williamson-Hall analysis in estimation of lattice strain in nanometer-sized ZnO particles. *Journal of Theoretical and Applied Physics, 6*(6), 1-8.

Mousa, A. M. and Ali, S. B. (2008). Effects of Deposition Parameters on Chemically Deposited PbS Thin Films. *Iraqi Journal of Applied Physics Letters, 4*(4), 1-7.

Munteha, P. (2011). *Electrodeposition of Nickel Sulphied for photovoltaic applications and its thermal oxidation.* The University of Texas at Arlington, Texas.

Musetafa, G., Chowdhury, R. I., D. K. Saha, S. H., and Islam, O. (2012). Annealing Effects on the Properties of Chemically Deposited CdS Thin Films at Ambient Condition. *Dhaka Univ. J. Sci., 60*(2), 283-288.

Nain, C. K. and Maini, K. A. (2010). Thin films and their application in military and and civil sectors, DRDO, New Delhi.

Nair, P. K., Nair, M. T. S., Garcıa, V. M., L.Arenas, O., Pen, Y., Castillo, A., . . . Rinco, M. E. (1998). Semiconductor thin films by chemical bath deposition for solar energy related ap plications. *Solar Energy Materials and solar cells 52*, 313-344.

NanoAnalysis, O. I. (2013). An Introduction to Energy-Dispersive and Wavelength-Dispersive X-Ray Microanalysis. *Microscopy and Analysis*.

Nasir, E. M., N.K.Abas, and S.J.Alatya. (2013). Influence of Sulfur on structural and electrical properties of PbS_xSe_{1-x} films. *International Journal of Thin Films Science and Technology, 2*(2), 133-142.

Neamen, D. A. (2001). Semiconductor physics and devices: Basic principles, 3rd Ed., McGraw-Hill, Inc., New York, ISBN 0-07-232 107-5.

Nelson, J. (2007). The Physics of Solar Cells, Imperial College Press, UK.

Nicolau, Y. F. (1985). Solution deposition of thin solid compound films by a successive ionic-layer adsorption and reaction process. *Applications of Surface Science, 22/23*, 1061–1074.

Nill, K. W., Blum, F. A., Galawa, A. R., and Harman, T. C. (1971). *Appl. Phys. Lett. , 19*.

Nirmal, M., Norris, D. J., Kuno, M., Bawendi, M. G., Efros, A. L., and Rosen, M. (1995). Observation of the "Dark Exciton" in CdSe Quantum Dots. *Physical Review Letters, 75*.

O'Brien, P. and McAleese, J. (1998). Developing an understanding of the processes controlling the chemical bath deposition of ZnS and CdS. *J. Mater. Chem., 8*(11), 2309-2314.

Obaid, A. S., Mahdi, M. A., Ramizy, A., and Hassan, Z. (2012). Structural Properties of Nanocrystalline PbS Thin Films Prepared by Chemical Bath Deposition Method. *Advanced Materials Research, 364*, 60-64.

Ohring, M. (1992). The materials science of thin films, Academic Press, California, ISBN 0-12-524990-X.

Ortega-Borges, R. and Lincot, D. (1993). Mechanism of chemical bath deposition of cadmium sulfied thin films in the ammonia-therioa system *J.Electrochem.Soc., 140*.

Pal, U., Zaldivar, M. H., Sathyamoorthy, R., Manjuladevi, V., Sudhagar, P., Mohan, S. C., and Senthilarasu, S. (2008). Nanocrystalline CdSe Thin Films of Different Morphologies in Thermal Evaporation Process. *Journal of Nanoscince Nanotechnology 8*(11), 1-7.

Parida, B., Iniyanb, S., and Goic, R. (2011). A review of solar photovoltaic technologies. *Renewable and Sustainable Energy Reviews, 15,* 1625-1636.

Park, W. D. (2011). Structural, Optical and Photoconductive Properties of Chemically Deposited Nanocrystalline CdS Thin Films. *Trans. Electr. Electron. Mater., 12*(4), 164-168.

Parrish, W. and Lowitzsch, K. (1959). Geometery, alignment and angular calibration of X-ray diffractometers. *The American Minerologst 44*, 765-787.

Patel, T. H. (2012). Influence of Deposition Time on Structural and Optical Properties of Chemically Deposited SnS Thin Films. *The Open Surface Science Journal, 4*, 6-13.

Pathan, H. M., Sankapal, B. R., Desai, J. D., and Lokhande, C. D. (2002). Preparation and characterization of nanocrystalline CdSe thin films deposited by SILAR method. *Materials Chemistry and Physics, 78*, 11-14.

Patil, V. T., Joshi, V. P., Tayade, D. A., Dhanvij, J. V., and Gujarathi, D. N. (2013). Surface morphological and optical properties of CdSe thin films by closed space sublimation technique *Chalcogenide Letters, 10*(7), 239-247.

Paulson, P. D., Chopra, K. L., and Dutta, V. (2004). Thin-film solar cells: an overview. *Progress in Photovoltaics: Research and Applications, 12*, 69-92.

Pawar, S. M., Kim, J. H., Pawar, B. S., Joo, O.-S., and Lokhande, C. D. (2011). Recent status of chemical bath deposited metal chalcogenide and metal oxide thin films. *Current Applied Physics, 11*, 117-161.

Pérez, R. G., Téllez, G. H., Rosas, U. P., Torres, A. M., Hernández, J., Tecorralco, . . . Moreno, O. P. (2013). Growth of PbS Nanocrystals Thin Films by Chemical Bath. *Journal of Materials Science and Engineering A 3*(1), 1-13.

Petrov, I., Barna, P. B., Hultman, L., and Greene, J. E. (2003). Microstructural evolution during film growth. *J. Vac. Sci. Technol. A, 21*(5), S117-S128.

Pietrzyk, D. J. and Frank, C. W. (1974). Analytical Chemistry: An Introduction, Academic Press, New York.

Poortmans, J. and Arkhipov, V. (2006). Thin Film Solar Cells: Fabrication, Characterization and Applications, John Wiley and Sons, Ltd., USA, ISBN 978-04700-9128-9.

Prabhu, Y. T., Rao, K. V., Kumar, V. S. S., and Kumari, B. S. (2014). X-Ray Analysis by Williamson-Hall and Size-Strain Plot Methods of ZnO Nanoparticles with Fuel Variation. *World Journal of Nano Science and Engineering, 4*.

Prabukanthan, P., Soukup, R., Ianno, N., Sarkar, A., Kment, S., Kmentova, H., . . . Darveau, S. (2010). *Chemical bath deposition (CBD) of iron sulfide thin films for photovoltaic applications, crystallographic and optical properties.* Paper presented at the Photovoltaic Specialists Conference (PVSC), 2010 35th IEEE.

Pradeep, T. (2008). Nano: The Essentials, 1st Ed., McGraw-Hill, ISBN 0-071-54829-7.

Pramanik, P. and Bhattacharya, S. (1987). *Jounal of materials science letters, 6*.

Preetha, K. C., Murali, K. V., Ragina, A. J., Deepa, K., Dhanya, A. C., and Remadevi, T. L. (2013). The role of cationic precursors in structural, morphological and optical properties of PbS thin films *IOP Conf. Series: Materials Science and Engineering, 43*, 1-7.

Price, S. and Margolis, R. (2010). 2008 Solar Technologies Market Report (pp. 1-132). California: Lawrence Berkeley National Laboratory.

Rajaram, M. S. and Dnyandev, L. C. (1997). Studies on chemically deposited cadmium sulphoselenide (CdSSe) films. *Thin Solid Films, 304*(1-2), 56-60.

Rajashree, C., Balu, A. R., and Nagarethinam, V. S. (2014). Substrate Temperature effect on the Physical properties of Spray deposited Lead sulfide Thin Films suitable for Solar control coatings. *Int.J. ChemTech Res., 6*(1), 347-360.

Randolph, J. and Masters, G. M. (2008). Energy for Sustainability: Technology, Planning, Policy, Island Press, United States of America, ISBN 978-1-59726-103-6.

Razykov, T. M. (1988). Physical properties of II-VI binary and multi-component compound films and heterostructures fabricated by chemical vapour deposition. *Thin Solid Films, 164(c),* 301-308.

Razykov, T. M., Ferekides, C. S., Morel, D., Stefanakos, E., Ullal, H. S., and Upadhyaya, H. M. (2011). Solar photovoltaic electricity: Current status and future prospects. *Solar Energy, 85*, 1580-1608.

Reádigos, A. A.-C., García, V. M., Gomezdaza, O., Campos, J., Nair, M. T. S., and Nair, P. K. (2000). Substrate spacing and thin-film yield in chemical bath deposition of semiconductor thin films. *Semicond. Sci. Technol., 15*(11), 1022-1029.

Reddy, G. B., Dutta, V., Pandya, D. K., and Chopra, K. L. (1987). Solution grown $(PbS)_{1-x}(Cds)_x$ composite selective surfaces. *Solar Energy Materials 15*(5), 383-390.

Reynolds, J. E. (1884). Deposition of lead sulphide as a specular film. *Jounal of chemical society, 45*, 162-165.

Rhee, J. H., Chung, C.-C., and Diau, E. W.-G. (2013). A perspective of mesoscopic solar cells based on metal chalcogenide quantum dots and organometal-halide perovskites. *NPG Asia Materials, 5*, 1-17.

Richard, W. M. and Hu, C. (1983). Solar Cells: From Basics to Advanced Systems, McGraw-Hill, Inc., United States of America, ISBN 0-07-030745-8.

Rosenheim, G., Stadler, W., Mayer, V. J., and Anorg, Z. (1906). *chemisitry, 49*(13).

Rouessac, F. and Annick, R. (2007). Chemical Analysis: Modern Instrumentation Methods and Techniques 2nd (Ed.)

Russ, J. C. (1984). Fundamentals of Energy Dispersive X-Ray Analysis (Monographs in Materials), Butterworth-Heinemann, ISBN 978-0408110310.

Sachin, P. A., Devan, R. S., Patil, D. S., Moholkar, A. V., Gang, M. G., Ma, Y.-R., . . . Patil, P. S. (2013). Improved solar cell performance of chemosynthesized cadmium selenide pebbles. *Electrochimica Acta, 98*, 244-254.

Sadovnikov, S. I. and Gusev, A. I. (2013). Structure and properties of PbS films. *Journal of Alloys and Compounds, 573*, 65-75.

Saeed, T. and O'Brien, P. (1995). Deposition and characterisation of ZnO thin films grown by chemical bath deposition. *Thin Solid Films, 271*, 35-38.

Sagadevan, S. and Sundaram, A. S. (2014). Dielectric Properties of Lead Sulfied thin films for solar cell applications. *Chalcogenide Letters, 11*(3), 159-165.

Sahoo, S., Chakraborti, C. K., Mishra, S. C., and Nanda, U. N. (2011). Scanning Electron Microscopy as an analytical tool for particle size distribution and aspect ratio analysis of Ciprofloxacin Mucoadhesive Polymeric suspension. *IJRRAS 6*(1), 94-100.

Sakharam, M. R. and Lokhande, C. D. (2000). Review Chemical deposition method for metal chalcogenide thin films. *Materials Chemistry and Physics, 65*, 1-31.

Sakhare, Y. S. and Ubale, A. U. (2012). Optical properties of FeSe thin films deposited by chemicalbath deposition technique: Effect of molar concentration of Fe $(NO_3)_3.9H_2O$. *Archives of Physics Research, 3*(6), 452-458.

Sankapala, B. R., Sartalea, S. D., Lokhandeb, C. D., and Ennaoui, A. (2004). Chemical synthesis of Cd-free wide band gap materials for solar cells. *Solar Energy Materials and Solar Cells, 83*(4), 447-458.

Sarkar, S. K., Kababya, S., Vega, S., Cohen, H., Woicik, J. C., Frenkel, A. I., and Hodes, G. (2007). Effects of Solution pH and Surface Chemistry on the Postdeposition Growth of Chemical Bath Deposited PbSe Nanocrystalline Films. *Chem. Mater., 19*(4), 879-888.

Sarma, Y. S., Acharya, H. N., and Misra, N. K. (1982). A solution growth technique for depositing PbS_xSe_{1-x} thin films. *Thin Solid Films, 90*, L43-L47.

Sarmah, K., Sarma, R., and Das, H. L. (2008). Structural Characterization of Thermally Evaporated CdSe thin films. *Chalcogenide Letters, 5*(8), 153-163.

Sarmah, K., Sarma, R., and Das, H. L. (2009). Correlative assessment of structural and photoelectrical properties of thermally evaporated CdSe thin films. *Journal of Non-Oxide Glasses, 1*(2), 143-156.

Sartale, S. D., Kale, R. B., Ganesan, V., Lokhande, C. D., Lin, Y.-F., and Lu, S.-Y. (2006). Room temperature chemical synthesis of lead selenide thin films with preferred orientation. *Applied Surface Science, 253*, 930-936.

Sartate, S. D. and Lokhande, C. D. (2000). Deposition of cobalt sulphide thin films by SILAR methods and their characterization. *Indian Journal of pure and Applied Physics, 38*, 48-52.

Seghaier, S., Kamoun, N., Brini, R., and Amara, A. B. (2006). Structural and optical properties of PbS thin films deposited by chemical bath deposition. *Materials Chemistry and Physics, 97*, 71-80.

Seiler, D. G., Zollner, S., Diebold, A. C., and Amirtharaj, P. (2009). Optical Properties of Semiconductors. *NIST*.

Seshan, K. (2002). Hand Books of Thin Film Deposition Processes and Techniques, Principles, Methods, Equipment and Applications, 2nd Ed., Noyes Publications, United States of America, ISBN 0-8155-1442-5.

Shaha, R. K., Patel, K. D., Makhija, D. L., Pathak, V. M., and Srivastava, R. (2008). Chemical and structural characterization of CdSe thin films. *Journal of Ovonic Research, 4*(6), 129-139.

Shahane, G. S., Mulik, R. N., Sutrave, D. S., and Deshmukh, L. P. (2001). Studies on pseudobinary Cd_{1-x} Pb_xSe thin films. *Proceedings of SPIE, 4413,* 21-26.

Shandalov, M., Makai, J. P., Balazs, J., Horvath, Z. s. J., Gutman, N., Sa'ar, A., and Golan, Y. (2007). Optical properties of size quantized PbSe films chemically deposited on GaAs. *Eur. Phys. J. Appl. Phys.*, 1-6.

Sharma, R., Bisen, D. P., Shukla, U., and Sharma4, B. G. (2012). X-ray diffraction: a powerful method of characterizing nanomaterials. *Recent Research in Science and Technology, 4*(8), 77-79.

Shikha, D., J.K.Sharma, and Sharma, J. (2014). Review on Effect of Deposition Parameters and Annealing on Structural Properties of Nanocrystalline MSe Thin Films by Chemical bath Deposition. *Sch. J. Eng. Tech., 2*(5B), 761-768.

Shyju, T. S., Anandhi, S., Indirajith, R., and Gopalakrishnan, R. (2010). Effects of annealing on cadmium selenide nanocrystalline thin films prepared by chemical bath deposition. *Journal of Alloys and Compounds, 506,* 892-897.

Shyju, T. S., S.Anandhi, R.Sivakumar, S.K.Garg, and R.Gopalakrishnan. (2012). Investigation on structural, optical, morphological and electrical properties of thermally deposited lead selenide (PbSe) nanocrystalline thin films. *Journal of Crystal Growth, 353*, 47-54.

Simon, B. J. L. and Dinnebier, R. E. (2008). Powder Diffraction Theory and Practice, The Royal Society of Chemistry, UK, ISBN 978-0-85404-231-9.

Singh, R. S., Bhushan, S., Singh, A. K., and Deo, S. R. (2011). Characterization and optical properties of CdSe Nanocrystalline thin films. *Digest Journal of Nanomaterials and Biostructures, 6*(2), 403-412.

Skoog, D. A. and West, D. M. (1980). Fundamentals of Analytical Chemistry, 2nd Ed., Holt, Rinehart and Winston, New York.

Soga, T. (2006). Nanostructured Materials for Solar Energy Conversion, Elsevier, The Netherlands, ISBN 978-0-444-52844-5.

Soukup, R. J., Prabukanthan, P., lanno, N. J., sarffr, A., Kment, S., Kmentova, H., . . . Oarveau, S. A. (2010). Chemical bath deposition (CBD) of iron sulfide thin films for photovoltaic applications, crystallographic and optical properties. *IEEE*, 002965- 002969.

Srinivasan, P. and Rajesh, P. (2012). Effect of temperature on the structural and optical properties of chemically deposited PbS thin films. *Elixir Thin Film Techecnology, 42*, 6206-6208.

Stolle, C. J., Harvey, T. B., and Korgel, B. A. (2013). Nanocrystal photovoltaics: a review of recent progress. *Current Opinion in Chemical Engineering, 2*, 160-167.

Streetman, B. G. and Banerjee, S. K. (2006). Solid state Electronic Devices, 6th Ed., Prentice-Hall, Inc., New Delhi, ISBN 978-81 -203-3020-7.

Sushil, K., Hussain, M., P.Thaneshwar, S., and Mushahid, H. (2003). Characterization of $PbS_{1-x}Te_x$ thin films *Jounal of Physics and Chemistry Solids, 64*(3), 367-376.

Sutrave, D. S., Shahane, G. S., Patil, V. B., and Deshmukh, L. P. (2000). Micro-crystallographic and optical studies on Cd< sub> $_{1-x}$</sub> Zn< sub> $_x$</sub> Se thin films. *Materials chemistry and physics, 65*(3), 298-305.

Swafford, L. A., Weigand, L. A., II, M. J. B., McBride, J. R., Rapaport, J. L., Watt, T. L., . . . Rosenthal, S. J. (2006). Homogeneously Alloyed CdS_xSe_{1-x} Nanocrystals: Synthesis, Characterization, and Composition/Size-Dependent Band Gap. *J. Am. Chem. Soc., 128*, 12299-12306.

Sze, S. M. (1981). Physics of Semiconductor Devices, 2nd Ed., John Wiley and Sons, Inc., New York, ISBN 0-471-09837-X.

Takeyoshi, T. (2006). A new area detector for high-speed and high-sensitivity X-ray diffraction analysis, JCPDS, ISBN 1097-0002.

Thangavel, S., Ganesan, S., Chandramohan, S., Sudhagar, P., Kangd, Y. S., and Hong, C. H. (2010). Band gap engineering in PbS nanostructured thin films from near-infrared down to visible range by in situ Cd-doping. *Journal of Alloys and Compounds, 495*, 234-237.

Thanikaikarasan, S., Sundaram, K., Mahalingam, T., Velumani, S., and Rhee, J. K. (2010). Electrodeposition and characterization of Fe doped CdSe thin films from aqueous solution. *Materials Science and Engineering B, 174*, 242-248.

Thielsch, R., Hull, R., Bohme, J. M., Reiche, R., Schalfer, D., Bauer, D. H., and Bottcher, H. (1998). Quantum-size effects of PbS nanocrystallites in evaporated composite films. *Nanostruct. Mater., 10,* 131-149.

Toda, Y. R., Chaudhari, K. S., Jain, A. B., and Gujarathi, D. N. (2011). Structural and Optical Properties of CdSe Thine Films Deposted by Chemical bath deposition Technique. *Asian J. Chem. and Envi. Res., 4*(1), 40-43.

Tohidi, T., Jamshidi-Ghaleh, K., Namdar, A., and Abdi-Ghaleh, R. (2013). Comparative studies on the structural, morphological ,optical and electrical properties of nanocrystalline PbS thin films grown by chemical bath deposition using two different bath compositions. *Materials Sciencein Semiconductor Processing*.

Trojanek, F., Cingolani, R., Cannoletta, D., Mikes, D., Nemec, P., Uhlirova, E., . . . Maly, P. (2000). *J. Crystal Growth, 209*, 695.

Trykozko, R. (1997). Principles of photovoltaic conversion of solar energy. *Opto-Electr. Rev., 5*(4), 271-277.

Tyagi, V. V., Rahim, N. A. A., Rahim, N. A., and Selvaraj, J. A. L. (2013). Progress in solar PV technology: Research and achievement. *Renewable and Sustainable Energy Reviews, 20*, 443-461.

Ubale, A. U., Junghare, A. R., Wadibhasme, N. A., Daryapurkar, A. S., Mankar, R. B., and Sangawar, V. S. (2007). Thickness Dependent Structural, Electrical and Optical Properties of Chemically Deposited Nanopartical PbS Thin Films. *Turk J. Phys., 31*, 279-286.

Udai, S. P. and Patra, S. P. (2010). Progress in Polycrystalline Thin-Film Cu(In,Ga)Se_2 Solar Cells. *International Journal of Photoenergy*, 1-19.

Valenzuela-Jaureguia, J. J., Ramirez-Bon, R., Mendoza-Galvan, A., and Sotelo-Lermab, M. (2003). Optical properties of PbS thin films chemically deposited at different temperatures. *Thin Solid Films, 441,* 104-110.

Vaughan, D. (1999). Energy-Dispersive X-ray Microanalysis: An Introduction, NORAN Instruments, USA.

Vegard, L. (1921). The constitution of the mixed crystals and the space filling of the atoms. *Z. Phys., 5*, 17.

Velumani, S., Mathew, X., Sebastian, P. J., Narayandass, S. K., and Mangalaraj, D. (2003). Structural and optical properties of hot wall deposited CdSe thin films. *Solar energy materials and solar cells, 76*, 347-358.

Velumania, S., Narayandassb, S. K., and Mangalarajb, D. (1998). Structural characterization hot wall deposited cadmium selenide thin films. *Semiconductor Science and Technology 13*.

Viswanatha, R. and Sarma, D. D. (2007). Nanomaterials Chemistry, Wiley-Vch Verlag GmbH and Co., ISBN 978-3-527-31664-9.

Vorobiev, Y. V., Horley, P. P., Hernández-Borja, J., Esparza-Ponce, H. E., Ramírez-Bon, R., Vorobiev, P., . . . González-Hernández, J. (2012). The effects of porosity on optical properties of semiconductor chalcogenide films obtained by the chemical bath deposition. *Nanoscale Res Lett., 7*(1).

Wang, Z. and Finkelstein, K. (2007). Structure stability, fracture, and tuning mechanism of CdSe nanobelts. *Applied Physics Latters 90*.

Wanli, M., Luther, J. M., Zheng, H., Wu, Y., and Alivisatos, A. P. (2009). Photovoltaic Devices Employing Ternary PbS_xSe_{1-x} Nanocrystals. *Nano letters 9*(4), 1699-1703.

Wasa, K., Kitabatake, M., and Adachi, H. (2004). Thin film materials technology : sputtering of compound materials, William Andrew, Inc., USA, ISBN 0-8155-1483-2.

Welle, H. (2004). Quantized Semiconductor Particles: A novel state of matter for materials science. *Advanced Materials, 5*(2), 88-95.

West, A. R. (2003). Solid State Chemistry, John Willey and Sons, Singapore.

Williamson, G. K. and Smallman, R. E. (1956). Dislocation Densities in Some Annealed and Cold-Worked Metals from Measurements on the X-Ray Debye-Scherrer Spectrum. *Philosophical Magazine, 1*(1), 34-45.

Xie, R., Su, J., Liu, Y., and Guo, L. (2014). Optical, structural and photoelectrochemical properties of $CdS_{1-x}Se_x$ semiconductor films produced by chemical bath deposition. *International Journal of hydrogen energy 39*, 3517-3527.

Xu, K. W., Zhang, J., Zhang, Y., and Ji, V. (2006). General compliance transformation relation and applications for anisotropic hexagonal metals. *Solid state communications, 139*(3), 87-91.

Yafei, Z., Geng, H., Zhou, Z., Wu, J., Wang, Z., Zhang, Y., . . . Hwang, H. L. (2012). Development of Inorganic Solar Cells by Nanotechnology. *Nano-Micro Lett., 4*(2), 124-134.

Yukselici, M. H., Bozkurt, A. A. k., and Omur, B. C. (2013). A detailed examination of the growth of CdSe thin films through structural and optical characterization. *Materials Research Bulletin, 48*, 2442-2449.

Zak, A. K., Majid, W. H. A., Abrishami, M. E., and Yousefi, R. (2011). X-ray analysis of ZnO nanoparticles by WilliamsoneHall and sizeestrain plot methods. *Solid State Sciences, 13*, 251-256.

Zakharov, O., Rubio, A., and Cohen, M. L. (1995). Calculated structural and electronic properties of CdSe under pressure. *Physical Review B, 51*(8), 4926-4930.

Zhang, Y., Dai, Q., Li, X., Liang, J., Colvin, V. L., Wang, Y., and Yu, W. W. (2011). PbSe/CdSe and PbSe/CdSe/ZnSe Hierarchical Nanocrystals and Their Photoluminescence. *Langmuir, 27*(15), 9583–9587.

Zhao, Y., Yan, Z., Liu, J., and Wei, A. (2013). Synthesis and characterization of CdSe nanocrystalline thin films deposited by chemical bath deposition. *Materials Sciencein Semiconductor Processing, 16*, 1592-1598.

Zhu, J., Aruna, S. T., Koltypin, Y., and Gedanken, A. (2000). A Novel Method for the Preparation of Lead Selenide: Pulse Sonoelectrochemical Synthesis of Lead Selenide Nanoparticles. *Chem. Mater., 12*, 143-147.